Université de Montréal

Étude de l'évolution spectrale des étoiles naines blanches riches en hélium et le problème de l'origine de l'hydrogène dans les hybrides de type DBA

par

Benoit Rolland

Département de physique

Faculté des arts et des sciences

Thèse présentée à la Faculté des études supérieures

en vue de l'obtention du grade de

PhilosohiæDoctor (Ph. D.)

en physique

Mai, 2019

Université de Montréal

Faculté des études supérieures

Cette thèse intitulée:

Étude de l'évolution spectrale des étoiles naines blanches riches en hélium et le problème de l'origine de l'hydrogène dans les hybrides de type DBA

présentée par:

Benoit Rolland

a été évaluée par un jury composé des personnes suivantes:

Björn Benneke,	président-rapporteur
Pierre Bergeron,	directeur de recherche
Gilles Fontaine,	codirecteur de recherche
Paul Charbonneau,	membre du jury
Klaus Werner,	examinateur externe

Thèse acceptée le: _____

Sommaire

Les étoiles naines blanches représentent la phase évolutive finale de 97% des étoiles de notre galaxie. Le champ de gravité intense présent à la surface de ces étoiles donne lieu à une stratification chimique importante. Ce processus de tri gravitationnel est responsable, entre autres, de l'extrême pureté chimique des couches externes et du fait que leurs spectres soient habituellement dominés par les raies d'une seule espèce, en général l'hydrogène ou l'hélium. Toutefois, il y a près de 40 ans, la découverte de variations importantes des différents types spectraux en fonction de la température effective de ces étoiles a révélé l'existence de mécanismes physiques pouvant inhiber ce tri gravitationnel.

L'étude décrite dans cette thèse vise à expliquer l'origine des naines blanches riches en hélium plus froides que $T_{\rm eff} = 30,000$ K. Pour ce faire, nous étudierons en détail le processus de dilution convective (pour $T_{\rm eff} > 15,000$ K) lié à l'érosion progressive d'une mince couche radiative d'hydrogène par la zone de convection d'hélium sous-jacente. Nous examinerons également le mécanisme de mélange convectif (pour $T_{\rm eff} < 12,000$ K) décrit par l'homogénéisation complète de l'enveloppe survenant lorsque la zone convective superficielle d'hydrogène rejoint l'enveloppe convective d'hélium plus profonde. Nous porterons une attention particulière au problème de l'origine de l'hydrogène dans certaines naines blanches hybrides riches en hélium.

Dans ce but, nous présentons une analyse de 115 étoiles naines blanches de type DB (raies d'hélium) et de 28 objets froids de type DA (raies d'hydrogène) riches en hélium. Notre approche, basée sur les techniques spectroscopique et photométrique, permet de déterminer avec précision les paramètres atmosphériques tels que la température effective, la gravité de surface et la composition chimique. Grâce à ces méthodes, nous avons identifié des traces d'hydrogène dans 63% de nos DB, révélant ainsi leur nature hybride de type DBA. Nous

avons également constaté la persistance de naines blanches dépourvues d'hydrogène à basse température.

À l'aide de modèles d'enveloppe stellaire détaillés, nous démontrons que les abondances photosphériques prédites par le scénario de dilution convective sont beaucoup plus faibles que celles observées dans les DBA. De plus, nous démontrons que l'hydrogène observé dans le spectre des étoiles DBA et DA froides riches en hélium ne peut provenir de l'accrétion de sources externes, en raison de la création de couches d'hydrogène suffisamment épaisses résistant à l'érosion causée par la convection. Cependant, nos résultats nous permettent de démontrer que les naines blanches DA froides riches en hélium représentent vraisemblablement l'aboutissement du mélange convectif d'une étoile DA possédant une mince couche d'hydrogène en surface.

Afin de résoudre le problème de l'hydrogène dans les naines blanches de type DBA, nous invoquons la possibilité que des quantités importantes d'hydrogène puissent se cacher dans les couches profondes de l'étoile. À partir de cette hypothèse basée sur des modèles réalistes, nous élaborons un mécanisme physique impliquant le dragage convectif de ce réservoir d'hydrogène situé sous la photosphère. Les séquences évolutives obtenues permettent de reproduire les valeurs et le comportement du ratio H/He observés pour la majorité des étoiles DBA. Nous fournissons ainsi pour la première fois une explication satisfaisante pour l'origine de l'hydrogène dans ces objets et, par la même occasion, résolvons potentiellement l'un des problèmes fondamentaux dans l'étude de l'évolution spectrale des étoiles naines blanches.

Mots clés: étoiles: naines blanches - abondances - évolution - paramètres fondamentaux

Abstract

White dwarf stars represent the end point of stellar evolution for 97% of the stars in the Galaxy. The strong gravitational field present at the surface of these stars leads to an important chemical stratification. This gravitational settling process is responsible, namely, for the extreme purity of their outer layers, and leads to optical spectra generally dominated by a single species, most often hydrogen or helium. Nearly 40 years ago, however, the discovery of significant variations of the observed spectral types as a function of effective temperature revealed the existence of several physical mechanisms that could compete with gravitational settling along the cooling sequence.

The main goal of this thesis is to provide an explanation for the origin of helium-atmosphere white dwarfs below $T_{\rm eff} = 30,000$ K. To this end, we study in detail the convective dilution process (for $T_{\rm eff} > 15,000$ K) associated with the gradual erosion of a thin radiative hydrogen layer by the underlying helium convection zone. We also examine the convective mixing mechanism (for $T_{\rm eff} < 12,000$ K) described by the complete homogenization of the outer layers arising when the superficial hydrogen convection zone reaches the deeper convective helium envelope. Particular attention is given to the problem of the origin of hydrogen detected in some helium-atmosphere white dwarfs.

We first present an analysis of 115 DB (helium-line) white dwarfs and 28 cool, helium-rich DA (hydrogen-line) stars. The atmospheric parameters of each star — effective temperature, surface gravity, and chemical composition — are obtained using the so-called spectroscopic and photometric techniques. Our spectroscopic observations reveal the presence of hydrogen in 63% of our DB sample, thus revealing their DBA hybrid nature. We also confirm the persistence of white dwarfs without any detectable traces of hydrogen at low effective temperature.

Using detailed stellar envelope models, we show that the photospheric hydrogen abundances predicted by the convective dilution scenario are much smaller than those measured in DBA white dwarfs. We also demonstrate that the amount of hydrogen observed in DBA stars, as well as in cool, helium-rich DA white dwarfs, cannot be explained by accretion from external sources, since accretion will build a hydrogen layer that is sufficiently thick to resist the erosion caused by convection. Instead, we show that cool, helium-rich DA white dwarfs most likely represent the end product of the convective mixing of DA white dwarfs with sufficiently thin hydrogen layers.

In order to solve the problem of hydrogen in DBA white dwarfs, we invoke the possibility that significant amounts of hydrogen can be hidden within the deep stellar interior. On the basis of this hypothesis, deduced from realistic models, we construct a physical mechanism where some of this hydrogen located deep in the star is being dredged-up to the surface by the growing convective envelope. The resulting simulations reproduce the H/He abundance ratio observed in the majority of DBA white dwarfs. This convective dredge-up scenario provides for the first time a satisfactory explanation for the origin of hydrogen in these objects, thus potentially solving a long-standing problem in white dwarf spectral evolution.

Subject headings: stars: white dwarfs - abundances - evolution - fundamental parameters

Table des matières

Table des figures

Liste des tableaux

Remerciements

Je tiens dans un premier temps à remercier mes directeurs de recherche, Pierre Bergeron et Gilles Fontaine, de m'avoir confié ce projet extraordinaire. Votre encadrement, vos conseils et vos idées m'ont permis de me dépasser, d'explorer des concepts nouveaux et de mener ce doctorat à terme. Merci pour ces cinq années merveilleuses et votre patience.

J'aimerais mentionner quelques contributions indispensables à la réalisation de ce projet. Je remercie John Subasavage de nous avoir gracieusement permis d'utiliser son spectre de WD1919−362 avant sa publication. Je suis également reconnaissant envers Marie-Michèle Limoges, Noemi Giammichele et Loïc Séguin-Charbonneau d'avoir observé plusieurs objets de mon échantillon.

Je souhaite souligner le support de mon épouse, Roxanne, au cours des cinq dernières années. Ton soutien, tes encouragements et ton écoute m'ont aidé à persévérer, à redoubler d'effort et à relever ce défi colossal. Je louange ta patience envers mes interminables querelles impliquant mes simulations, car ces combats nocturnes ont souvent permis de déboucher sur des idées novatrices.

Finalement, je profite de l'occasion pour remercier la générosité de la Faculté des études supérieures et postdoctorales et du Fonds de recherche du Québec − Nature et technologies. Leurs soutiens financiers ont grandement contribué à la poursuite de mes recherches et à la réussite de ce projet.

À la mémoire de Gilles Fontaine

(1948 – 2019)

Chapitre 1

Introduction

1.1 Les étoiles naines blanches

1.1.1 Formation canonique

Phase ultime d'environ 97% des étoiles de notre galaxie, les naines blanches sont les rémanents des objets dont la masse initiale était inférieure à $\sim 8\ M_{\odot}$ sur la séquence principale. Après avoir converti paisiblement de l'hydrogène en hélium dans les régions centrales durant cette phase évolutive, la raréfaction du combustible disponible entraîne une diminution du taux de production d'énergie nucléaire ϵ, en erg cm^{-3} s^{-1}, et la rupture de l'équilibre hydrostatique. Les coeurs de ces étoiles se contractent alors sous l'effet de la gravité causant un réchauffement interne. Cette libération d'énergie gravitationnelle se poursuit jusqu'à ce que la température et la densité du milieu redeviennent favorables à la fusion, et ce, indépendamment de la déplétion partielle de l'hydrogène. À ce stade, le brûlage de l'hydrogène recommence dans une couche mince comprise entre l'enveloppe plus froide et le coeur inerte d'hélium. La chaleur engendrée provoque une expansion significative de l'enveloppe externe et une augmentation de la luminosité ($L \propto R^2$) transformant ainsi l'étoile en géante rouge. Ceci se traduit par un départ de la séquence principale suivi d'une migration rapide vers le haut du diagramme Hertzsprung-Russel tel qu'illustré à la figure 1.1.

Parallèlement, le coeur continue de se contracter jusqu'à l'amorce de la fusion de l'hélium en carbone et en oxygène : c'est le «flash» d'hélium. Ces nouvelles réactions nucléaires réta-

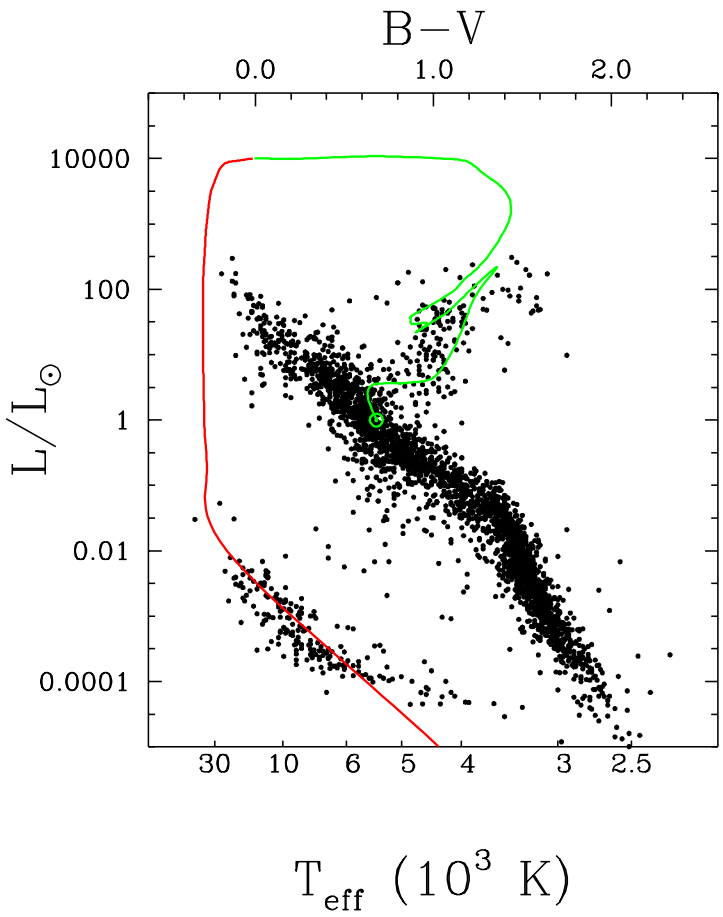

FIGURE 1.1 – Parcours typique d'une étoile de 1 $M_\odot$ dans le diagramme Hertzsprung-Russel. Le trait vert caractérise les étapes évolutives allant de la phase de géante rouge à la formation de la nébuleuse planétaire tandis que le tracé suivi par la naine blanche résultante est indiqué en rouge.

blissent l'équilibre hydrostatique interne et l'étoile débute alors une nouvelle phase, analogue à la séquence principale, appelée branche horizontale. Cette période évolutive, généralement 100 fois plus courte, se poursuit jusqu'à ce que l'hélium vienne également à manquer dans les régions centrales. À ce stade, les étoiles de faible masse sont incapables d'entamer le brûlage des éléments plus massifs en raison de la trop faible température en leur centre. L'astre vieillissant traverse alors un second épisode de fusion en couches distinctes, mais cette fois impliquant l'hydrogène et l'hélium autour d'un coeur de carbone-oxygène inerte. L'étoile quitte la branche horizontale et migre une fois de plus vers le haut du diagramme Hertzsprung-Russel en suivant ce que l'on appelle la branche asymptotique des géantes. Durant cette période, l'ex-

pansion due au chauffage de l'enveloppe externe et les pulses thermiques contribuent à une forte perte de masse vers le milieu interstellaire menant à la formation d'une nébuleuse planétaire. Ultimement privé d'énergie nucléaire, le rémanent de cette évolution, un coeur chaud de carbone-oxygène très pauvre en éléments légers, se contractera considérablement jusqu'à ce que l'équilibre hydrostatique soit de nouveau atteint grâce à la pression de dégénérescence électronique. À ce moment, l'étoile devient une naine blanche.

1.1.2 Propriétés générales

Ancien noyau d'une nébuleuse planétaire, la naine blanche est un objet stellaire compact de petite taille ($\sim$0.01 $R_\odot$) ayant épuisé son potentiel de fusion nucléaire. Soutenu par la pression de dégénérescence électronique, cet astre ne peut que dissiper son énergie via son atmosphère menant à une diminution inexorable de la température interne , incluant la température photosphérique. En effet, tel que mentionné par Fontaine et al. (2001), ces objets sont observés à des températures effectives allant de $T_{\rm eff} \sim 125,000$ K à $\sim$4000 K. Comme cet intervalle représente près de neuf milliards d'années d'évolution pour une naine blanche de masse moyenne (0.6 $M_\odot$), il s'agit donc, à l'instar de la séquence principale, d'une phase évolutive longue et paisible.

En raison de sa petite taille et de sa masse, une naine blanche possède une gravité de surface près de 10,000 fois supérieure à celle de Soleil, soit $\log g \simeq 8.0$ en unité cgs. Cette caractéristique extrême contraint les éléments lourds à sombrer rapidement, en comparaison au temps de refroidissement caractéristique, vers les couches internes de l'atmosphère (Schatzman 1958; Paquette et al. 1986). Ce tri gravitationnel engendre une stratification de l'enveloppe et de l'atmosphère en diverses strates dont la composition chimique est essentiellement pure et dominée par une seule espèce chimique. Dans la vaste majorité des cas ($\sim$80%), ce processus produit une naine blanche composée d'un coeur de carbone-oxygène dégénéré recouvert d'une mince enveloppe d'hélium sur laquelle repose une fine atmosphère d'hydrogène (DA). Dans ce type d'objet, les fractions de masse canoniques respectives de ces deux éléments légers sont de $M_{\rm He}/M_\star \sim 10^{-2}$ et de $M_{\rm H}/M_\star \sim 10^{-4}$. Ces valeurs représentent les quantités maximales pouvant survivre aux derniers épisodes d'éjection et de combustion nucléaire lors des phases

de géante asymptotique et de nébuleuse planétaire (Iben 1984).

Une seconde classe de naines blanches vient toutefois complexifier ce scénario canonique. Ces objets, dits «*Born Again*», sont pratiquement dépourvus d'hydrogène. Cette dichotomie serait causée par des phases supplémentaires, parfois nombreuses, de brûlage nucléaire liées à des passages répétitifs sur la branche des géantes asymptotiques (Werner & Herwig 2006). Ces excursions influenceraient considérablement l'évolution subséquente de l'astre comme le démontre la figure 1.2 pour une étoile de 2 $M_{\odot}$. En effet, ce processus, habituellement causé par un flash d'hélium tardif, contribuerait à la déplétion de l'hydrogène encore présent et serait pressenti pour être à l'origine des naines blanches arborant une atmosphère riche en hélium (non-DA). Il serait aussi lié à l'existence d'une classe exceptionnellement rare d'objets avec une atmosphère composée majoritairement de carbone et d'oxygène (Dufour et al. 2007b).

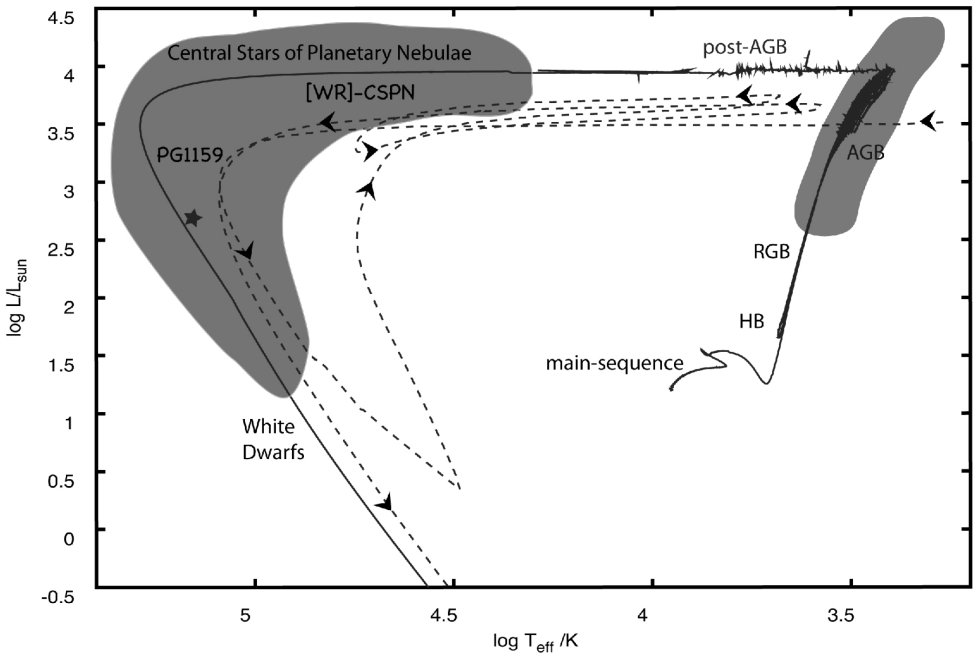

FIGURE 1.2 – Séquence évolutive complète pour une étoile ayant une masse initiale de 2 $M_{\odot}$ et couvrant son départ de la séquence principale jusqu'à sa transformation en naine blanche. Le trait plein représente le tracé attendu pour une étoile évoluée canonique. Le trait hachuré montre une évolution *born-again* pour une étoile de même masse sujette à un flash d'hélium tardif. Cette séquence a été décalée de $\Delta \log T_{\rm eff} = -0.2$ et $\Delta L/L_{\odot} = 0.5$ afin de faciliter la lecture. Le symbole étoilé indique la position de PG 1159−035 (Werner & Herwig 2006).

1.1.3 Classification spectrale

En vertu d'un tri gravitationnel extrêmement efficace et du parcours évolutif de leurs progéniteurs, les naines blanches se déclinent en trois variétés caractérisées par le constituant chimique principal présent à la surface. Devant cette simplicité apparente, il serait logique de présumer que les données spectroscopiques se divisent également en un nombre limité de types spectraux. Toutefois, les spectres observés ont historiquement révélé une surprenante diversité ayant nécessité l'élaboration d'une classification standardisée. Décrites en détail par Wesemael et al. (1993) et utilisées systématiquement depuis la publication du catalogue de McCook & Sion (1999), ces dénominations sont basées sur les raies atomiques, ou moléculaires, dominantes dans le domaine visible [1]. Il est à noter que des symboles supplémentaires peuvent être ajoutés pour dénoter des caractéristiques additionnelles telles que la présence de variabilité (V), d'un champ magnétique (P ou H) et/ou de raies d'émission (E). Ces spécifications dépassent toutefois le cadre de cette thèse et ne sont mentionnées qu'à titre indicatif.

1.1.3.1 Raies d'hydrogène

Le type DA regroupe la vaste majorité des naines blanches connues (∼80%) et est caractérisé par des objets dont le spectre visible est dominé par la présence des raies de la série de Balmer. Associées aux transitions atomiques du niveau $n = 2$, les observations spectroscopiques de ces étoiles peuvent considérablement varier en fonction de la température effective comme le démontre la figure 1.3. Au-dessus de ∼80,000 K, l'atmosphère de ces naines blanches est tellement chaude que les raies d'absorption deviennent très peu profondes en raison de l'ionisation partielle de type $2 \rightarrow \infty$. À l'opposé, un maximum d'intensité, coïncidant avec l'occupation maximale de ce niveau atomique, survient aux alentours de 13,000 K. À des températures effectives plus petites, cette occupation commence progressivement à chuter. Sous $T_{\rm eff} \sim 5000$ K, cette dernière est si faible que l'hydrogène disparait spectroscopiquement. À ce stade, le spectre dépourvu de raies est dominé par le continu et se classe comme un objet de type DC [2].

1. Pour le carbone, tout le spectre électromagnétique est considéré.
2. En refroidissant, les non-DA termineront également leur évolution sous forme de DC

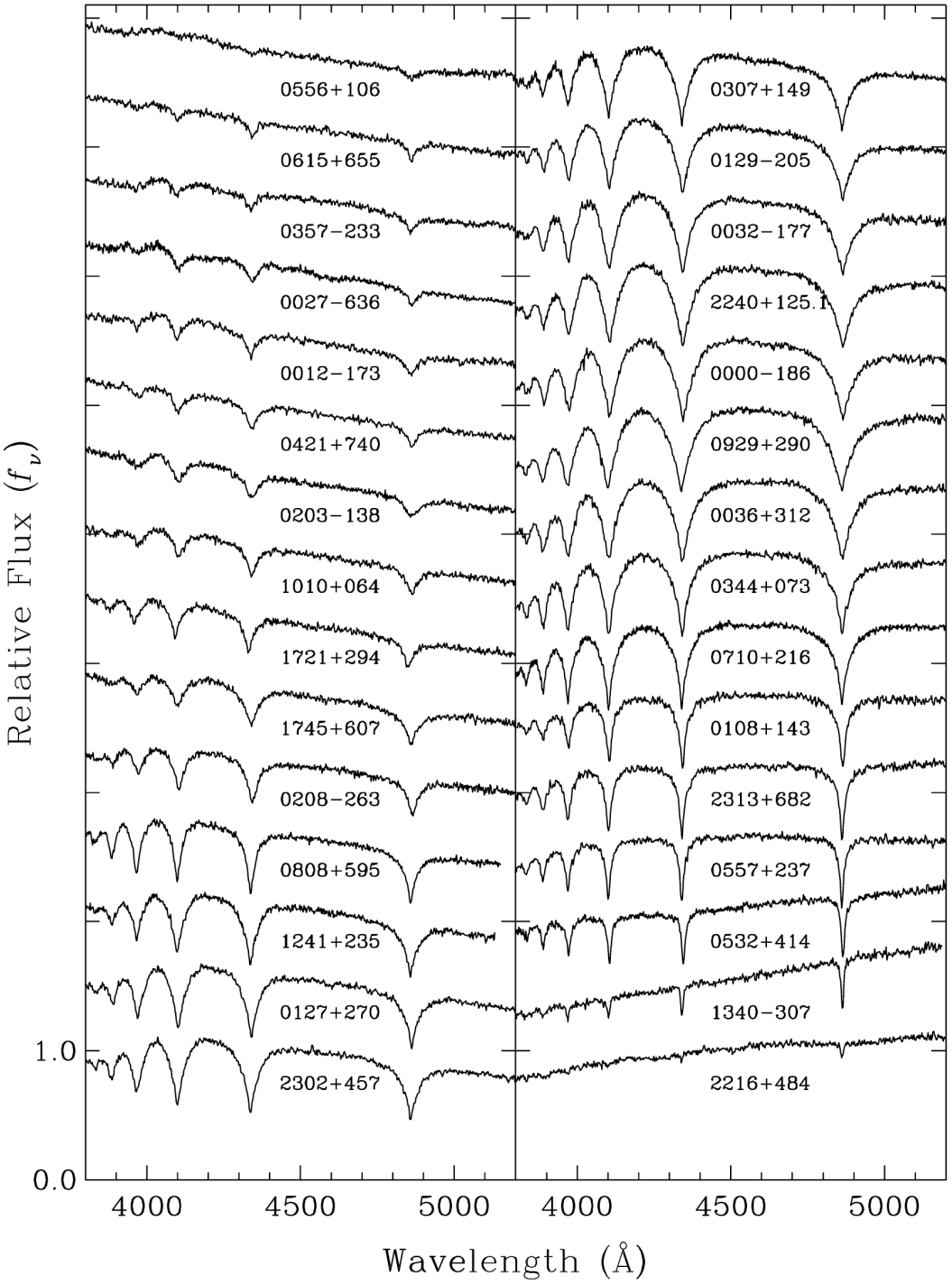

FIGURE 1.3 – Spectres visibles d'un échantillon de naines blanches de type DA. Les spectres ont été normalisés par rapport à leur valeur à 4500 Å. La température effective décroît du coin supérieur gauche au coin inférieur droit (Gianninas et al. 2011).

Il est important de noter qu'un type spectral ne garantit pas la composition chimique au niveau de la photosphère. Un exemple de ce phénomène concerne les étoiles de type DQ (raies de carbone) pour lesquelles l'atmosphère est pratiquement pure en hélium en vertu d'une abondance relative de $\log \mathrm{C/He} \sim -4$ (voir Dufour et al. 2005). Cette propriété est reliée au fait que, pour $T_{\rm eff} < 12,000$ K, l'hélium devient spectroscopiquement invisible et peut donc potentiellement être présent en proportion arbitraire sans exhiber de signature spectroscopique. Plusieurs sous-groupes de naines blanches répondent à cette description, incluant notamment des objets froids de type DA observés par Bergeron et al. (2001). Malgré la présence de Hα, les données photométriques de la figure 1.4 montrent clairement que ces objets ne peuvent contenir que des traces d'hydrogène ($\log \mathrm{H/He} \sim -3$). En effet, la raie d'absorption s'avère moins profonde et plus évasée en raison de l'élargissement van der Waals induit par l'hélium. La photométrie est également exempte du saut de Balmer causant des couleurs $u-g$, ou $B-V$, beaucoup moins rouges. La compréhension et la caractérisation de cette population d'étoiles DA froides riches en hélium constituent un des enjeux principaux de cette thèse.

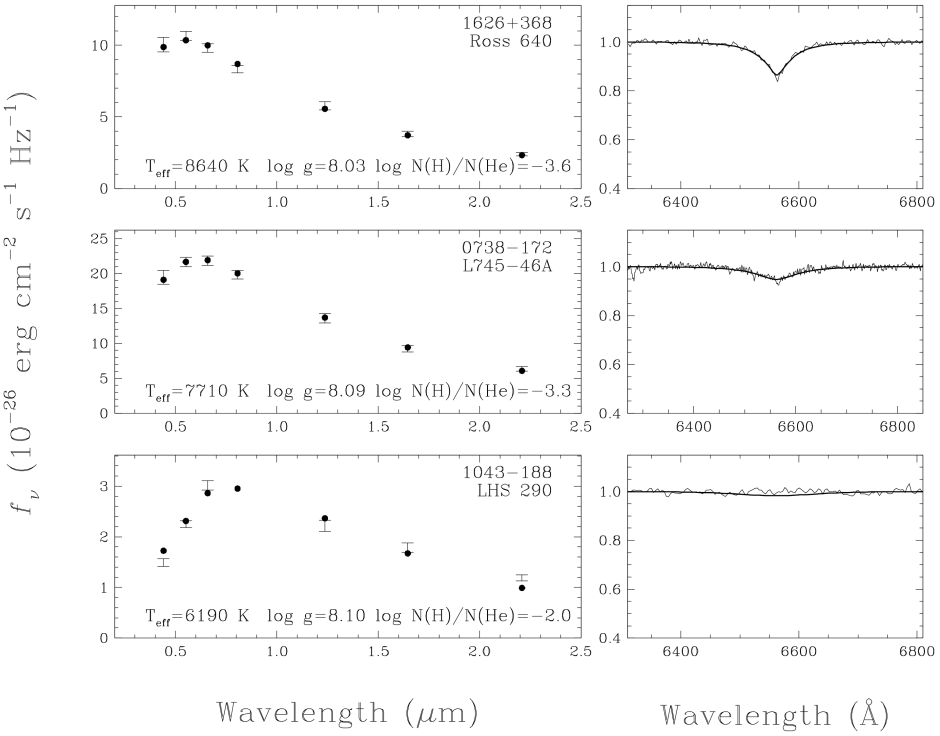

FIGURE 1.4 – Meilleure solution photométrique pour des naines blanches avec une composition mixte d'hydrogène et d'hélium. L'abondance relative H/He est déterminée (ou contrainte)par l'ajustement de la raie Hα (Bergeron et al. 2001).

1.1.3.2 Raies d'hélium

Les non-DA englobent toutes les naines blanches dont le spectre n'est pas dominé par l'hydrogène. En dépit de leur rareté relative (∼20%), cette deuxième famille hérite d'une grande diversité, incluant notamment les types spectraux PG 1159, *hot-wind* DO [3], DO, DB, DQ et DZ (métaux). Néanmoins, dans le cadre de cette thèse, seuls les objets ayant une signature spectroscopique propre à l'hélium seront abordés en détail. L'une de ces classes regroupe les étoiles de type DO et est caractérisée par la présence de raies d'hélium partiellement ionisé (He II). Comme le montre les données observationnelles de la figure 1.5, ces objets couvrent un très large éventail de températures effectives. Aux alentours de 125,000 K, les raies sont peu profondes en raison de l'ionisation presque complète de l'atmosphère. Avec le refroidissement, l'absorption s'intensifie et le spectre affiche éventuellement une combinaison de He II et de d'hélium neutre (He I) annonçant un changement de l'état d'ionisation. Cette transition devrait théoriquement se poursuivre jusqu'à ce que le milieu soit trop froid pour créer du He II.

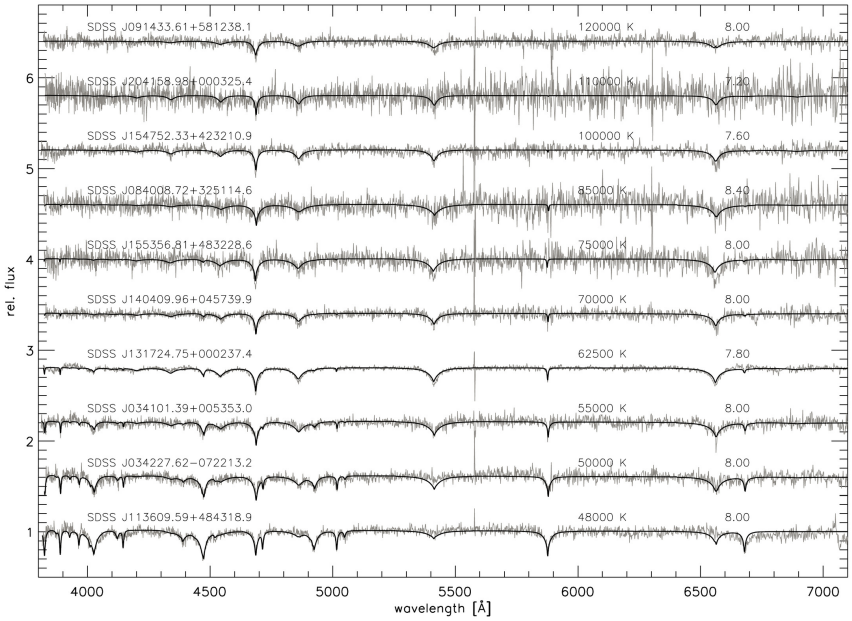

FIGURE 1.5 – Spectres visibles normalisés (gris) pour des naines blanches de type DO ainsi que le modèle d'atmosphère correspondant (noir). Les données sont présentées en ordre décroissant de température effective (du haut vers le bas) et décalées verticalement pour faciliter la lecture (Hügelmeyer et al. 2005).

3. Ce sous-type chaud d'étoiles DO est caractérisé par la présence de raies d'absorption métalliques liées à de très hauts niveaux d'excitation (voir Reindl et al. 2014).

Pour des températures effectives inférieures à ∼40,000 K, l'abondance photosphérique relative de He II est extrêmement faible et le spectre est alors dominé par les raies associées à He I. Ce second et dernier groupe de naines blanches à être caractérisé par une signature propre à l'hélium forme le type spectral DB. À titre d'exemple, la figure 1.6 illustre une partie des données observationnelles de l'échantillon d'objets brillants de Bergeron et al. (2011). Une différence notable, en comparaison au type DA, s'avère être le nombre de raies d'absorption présentes. Ce comportement est relié à la complexité accrue de la configuration électronique de l'hélium neutre. De plus, tout comme les autres classes d'objets mentionnées précédemment, ces étoiles possèdent également un maximum d'opacité, cette fois aux alentours de 24,000 K. Avec le temps, la naine blanche se refroidit et l'énergie disponible diminue causant une disparition progressive des raies d'absorption. Lorsque He I λ4471 se fond finalement dans le continu ($T_{\rm eff} \sim 12,000$ K), l'hélium devient indétectable et toute espèce chimique secondaire peut maintenant s'exprimer spectroscopiquement (ex : DA, DQ, DZ). Sinon, en absence d'élément trace dans l'atmosphère, l'objet devient tout simplement une étoile de type DC.

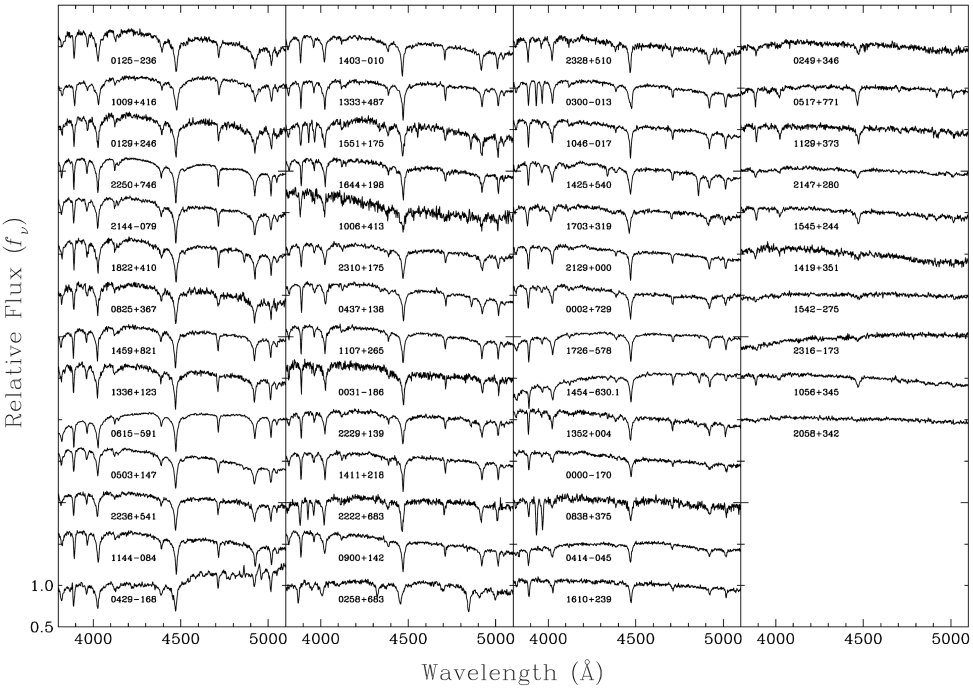

FIGURE 1.6 – Spectres visibles de naines blanches de type DB, affichés en ordre décroissant de température effective (coin supérieur gauche au coin inférieur droit). Tous les spectres ont été normalisés par rapport à leur valeur à 4500 Å et décalés d'un facteur 0.5 pour faciliter la lecture (Bergeron et al. 2011).

1.1.3.3 Types hybrides

Pour de nombreuses naines blanches, les différents types spectraux présentés jusqu'ici peuvent s'avérer insuffisants lorsque les raies d'absorption observées dénotent la présence de plus d'un élément chimique. Afin de classifier la nature particulière de ces objets, il suffit d'utiliser les identifiants appropriés (A, B, O, Q, Z) de manière séquentielle, en ordre décroissant d'intensité. Ces hybrides peuplent sporadiquement l'ensemble de la séquence de refroidissement et chacun des sous-groupes couvre un intervalle de températures effectives qui lui est propre. Comme le montre la figure 1.7, ces naines blanches existent sous diverses formes, incluant notamment les types DAO, DAB, DAZ, DBA, DBZ. L'existence de ces objets apporte les premiers indices concrets que des mécanismes physiques concurrencent le tri gravitationnel en maintenant, ou ajoutant, des éléments au niveau de la photosphère. La nature de ces processus est toujours sujette à débats et représente le coeur de cette thèse. Néanmoins, la découverte de ces hybrides ouvre la porte à une possible évolution spectrale définie par la transition d'un type spectral vers un autre au cours de la vie d'une naine blanche.

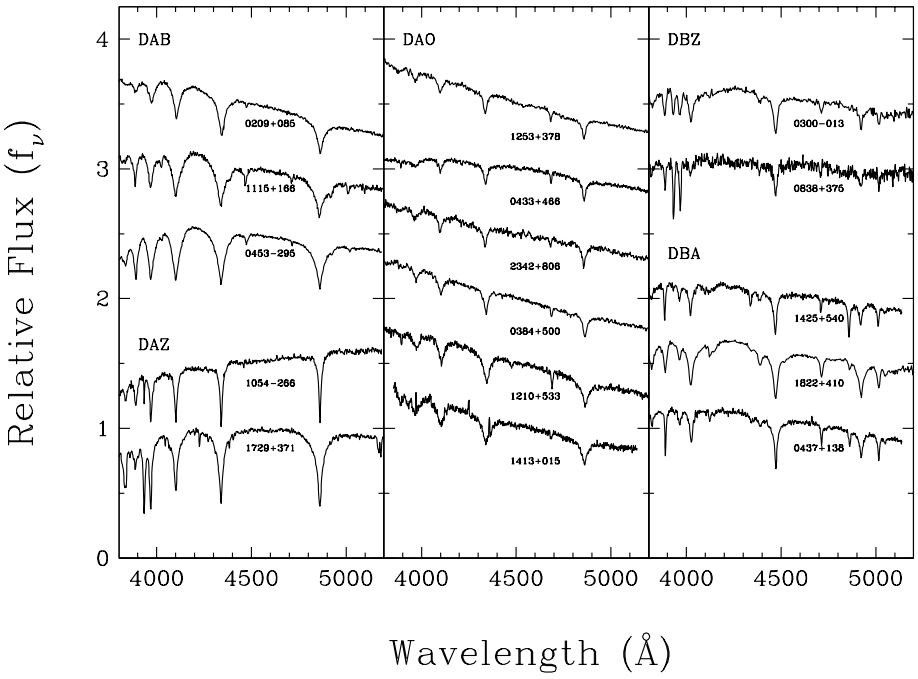

FIGURE 1.7 – Spectres visibles de naines blanches hybrides avec une composition atmosphérique mixte.Tous les spectres ont été normalisés par rapport à leur valeur à 4500 Å et décalés verticalement pour la faciliter la lecture (inspiré de Gianninas et al. 2011, Bergeron et al. 1994, Bergeron et al. 2011).

1.2 Évolution spectrale

Sans compter les nombreux types hybrides, plusieurs anomalies observationnelles ont historiquement suggéré l'éventualité d'une évolution spectrale chez les naines blanches, et ce, depuis plus de trois décennies. Effectivement, en effectuant une analyse du relevé Palomar-Green (PG), Holberg (1987) a noté une absence totale d'étoiles DA très chaudes ($T_{\rm eff} > 80,000$ K). Ce résultat intriguant contrastait alors énormément avec la température effective de 150,000 K estimée par Wesemael et al. (1985) pour PG 1159−035, un objet non-DA. De son côté, l'étude de Liebert et al. (1986) avait permis d'identifier une tendance opposée à plus basse température suggérant l'existence d'un possible désert évolutif exempt de naines blanches non-DA entre ∼45,000 K et ∼30,000 K (brèche des DB ou «DB gap» en anglais). Finalement, Sion (1984) et Greenstein (1986) avaient indépendamment remarqué une diminution d'un facteur quatre du ratio DA/non-DA lorsque $T_{\rm eff} < 10,000$ K, synonyme d'une potentielle seconde inversion de population. Une vue d'ensemble de ces comportements a été abordée en détail par Fontaine & Wesemael (1987) et est reproduite à la figure 1.8.

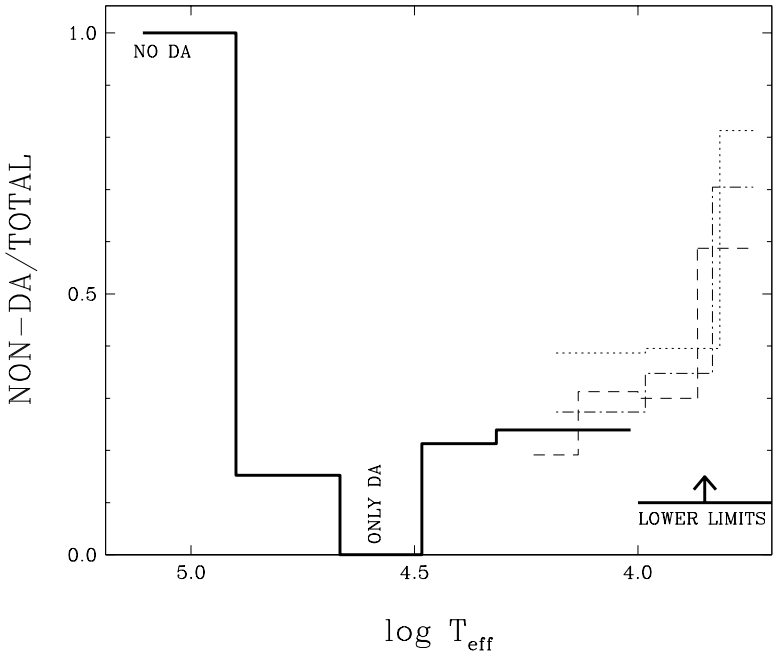

FIGURE 1.8 – Nombre relatif de non-DA en fonction de la température effective. Le trait plein provient de Fleming et al. (1986) et de Liebert et al. (1986), le hachuré de Sion (1984), les autres de Greenstein (1986). Les valeurs sous 10,000 K représentent des limites inférieures liées à la détection de l'hydrogène (Fontaine & Wesemael 1987).

1.2.1 Problème des hautes températures

Devant cette diversité d'irrégularités observationnelles, de nombreuses recherches ont tenté de comprendre, ou de confirmer, l'évolution spectrale des naines blanches, notamment à haute température. Dans une étude systématique visant des noyaux de nébuleuses planétaires, Napiwotzki & Schönberner (1991) ont trouvé un coeur riche en hydrogène, avec potentiellement $T_{\rm eff} > 100,000$ K, au centre de WDHS 1. Toutefois, en raison de la faible luminosité de cet objet, le bruit polluant le spectre rendait impossible toute caractérisation supplémentaire. Grâce à une analyse spectrophotométrique détaillée, Liebert et al. (1994) ont contraint ses paramètres atmosphériques en obtenant des valeurs avoisinant ∼165,000 K et $\log g \sim 7.6$. Arborant uniquement des raies d'hydrogène dans le visible, le coeur de WDHS 1 devenait alors la plus chaude étoile DA connue. Peu de temps après, l'étude de 38 nébuleuses planétaires menée par Napiwotzki & Schoenberner (1995) a révélé que les noyaux riches en hydrogène amorçant la séquence de refroidissement dominaient leur échantillon dans une proportion de 4 : 1. Dans une analyse subséquente, Napiwotzki (1999) a identifié deux objets analogues au noyau de WDHS 1, EGB 1 et WeDe 1, ayant une température effective aux alentours de ∼140,000 K et une gravité de surface de $\log g \sim 7.4$. En combinant tous ces résultats à la figure 1.9, la signature rapportée par Holberg (1987) s'apparente fortement à un biais observationnel. En effet, tous les objets très chauds et riches en hydrogène se retrouvent au centre d'une nébuleuse planétaire. En raison de la faible opacité de l'hydrogène, la détection des raies de Balmer s'avère difficile, car le spectre peut facilement être dominé par des traces de He II, de C IV ou de O IV.

1.2.2 Brèche des DB

Pendant plusieurs années, les naines blanches DB bénéficiant d'une analyse robuste étaient particulièrement rares dans la littérature. Avec à peine plus de 70 objets répertoriés par Voss et al. (2007), l'existence du désert évolutif identifié par Liebert et al. (1986) est longtemps restée statistiquement incertaine. Il a fallu attendre l'arrivée de grands relevés tels que le Sloan Digital Sky Survey (SDSS) afin d'avoir accès à une banque de données suffisante pour traiter la question adéquatement. En effet, Eisenstein et al. (2006) ont rapporté la détection

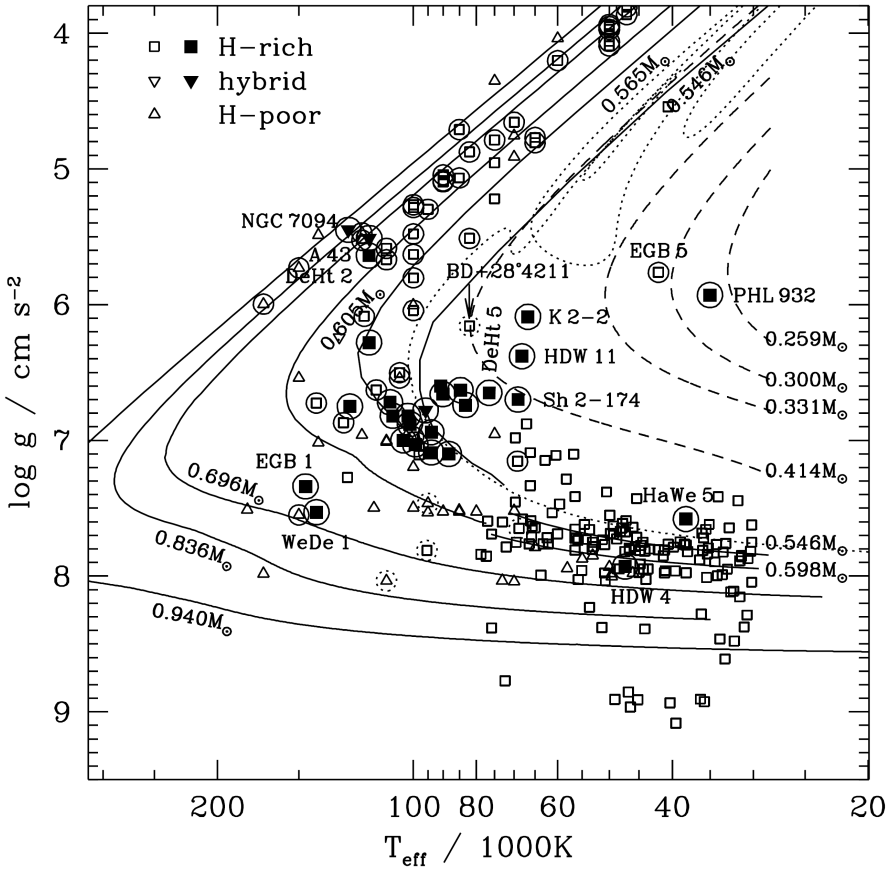

FIGURE 1.9 – Diagramme $T_{\rm eff} - \log g$. Les nouvelles valeurs et les données de la littérature sont représentées par des symboles noirs et blancs, respectivement. Les noyaux de nébuleuses planétaires sont circonscrits par un cercle plein (pointillé si suspectés). Les séquences évolutives post-AGB sont indiquées par des lignes pleines et identifiées en fonction de la masse du rémanent (Napiwotzki 1999).

de six étoiles DB chaudes se trouvant entre 45,000 K et 30,000 K, de même que 22 candidats potentiels. Cette découverte importante ouvrait la porte à l'éventualité que la brèche des DB soit un artéfact pouvant être peuplé graduellement. Avec plus de 30,000 naines blanches identifiées dans le SDSS, dont plus de 2200 étoiles DB, il est maintenant possible d'obtenir un portrait fiable de cette signature emblématique de l'évolution spectrale. Comme le montre la figure 1.10, en dépit des milliers d'objets disponibles, la brèche des DB reste peu peuplée par les objets riches en hélium. Ce résultat indique que, même s'il ne s'agit plus d'un désert complet, le ratio $N_{\rm DA}/N_{\rm DB}$ dans cet intervalle de température est $\sim$2.5 fois supérieur à celui observé aux alentours de 20,000 K (Eisenstein et al. 2006). La brèche reflète donc une phase évolutive statistiquement significative fortement déficitaire en objets de type DB.

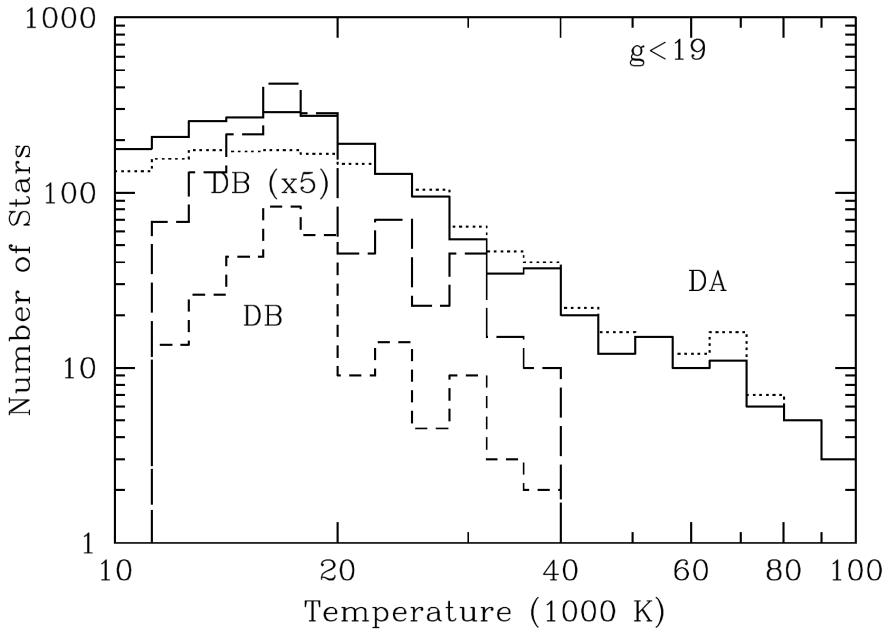

FIGURE 1.10 – Histogramme en température des étoiles DA (trait plein) et DB (tirets) dans le catalogue DR4 du SDSS. Les objets considérés respectent la condition $g > 19$ et incluent les hybrides de type DBA (Eisenstein et al. 2006).

En vertu des récents résultats obtenus grâce au SDSS, une fraction non-négligeable des naines blanches pauvres en hydrogène doit nécessairement subir une transformation de type DO $\rightarrow$ DA. Il existe donc forcément un mécanisme physique réduisant les effets du tri gravitationnel et permettant de modifier la composition chimique de l'atmosphère. Un des modèles les plus populaires pour expliquer ce phénomène a été décrit en détail par Fontaine & Wesemael (1987) et utilise la prémisse d'une infime quantité d'hydrogène initialement diluée dans l'enveloppe d'un progéniteur chaud riche en hélium (ex : PG 1159−035 ou DO). Au cours du refroidissement, l'atmosphère est graduellement enrichie en hydrogène en raison de sa diffusion vers la surface, et ce, jusqu'à la création d'une couche suffisamment importante pour altérer le spectre visible. Comme toutes les naines blanches observées s'avèrent être de type DA à la frontière supérieure de la brèche ($T_{\rm eff} \sim 45,000$ K), la quantité totale d'hydrogène contenue dans le progéniteur ne peut pas être inférieure à $\sim 10^{-16}\ M_{\odot}$ afin de supplanter spectroscopiquement l'hélium. Si la couche s'avère plus mince, ces objets arboreraient alors le type spectral hybride DAO et auraient une atmosphère stratifiée avec l'hydrogène en équilibre diffusif au-dessus de l'enveloppe d'hélium (voir Manseau et al. 2016).

Du côté froid de la brèche, la fonction de luminosité moderne des naines blanches du relevé PG permet de dresser un portrait actuel de la situation. En effet, tel que présenté à la figure 1.11, le nombre relatif d'étoiles DB par unité de volume augmente rapidement lorsque la température effective atteint ∼20,000 K. Signifiant la réapparition des objets non-DA, cette variation se traduit par un changement important de $\log \phi$ quand la magnitude bolométrique ($M_{\rm bol}$) se situe entre neuf et dix. Il est important de noter que ce comportement particulier coïncide avec la croissance d'une zone de convection superficielle due à la recombinaison de l'hélium dans l'enveloppe stellaire. Comme le démontre la figure 1.12, la zone associée à He II amorce une expansion vers l'intérieur de l'étoile et est accompagnée de l'apparition d'une instabilité propre à He I. Suite à la fusion des deux zones aux alentours de 20,000 K, la convection croît significativement pour englober la majorité des couches externes. Cette possible corrélation soutient la très forte probabilité qu'un mécanisme physique cause une transition DA → DB. Le scénario envisagé par Fontaine & Wesemael (1987) implique l'érosion progressive de la couche d'hydrogène en surface par l'enveloppe convective d'hélium sous-jacente. Cette hypothèse nécessite toutefois un faible contenu en hydrogène, de l'ordre de $M_{\rm H} \sim 10^{-15}\ M_{\odot}$, afin de permettre la *dilution convective* de l'atmosphère.

Dans le but de tester cette hypothèse, MacDonald & Vennes (1991) ont effectué plusieurs simulations d'enveloppes stratifiées en équilibre diffusif couvrant un intervalle de températures effectives allant de 80,000 K à 10,000 K. Leurs calculs ont considéré la convection de Schwarschild, de Ledoux et de Kato tout en incluant la lévitation radiative de l'hélium (voir Vennes et al. 1988). Au total, six différentes versions du traitement convectif ont été analysées par cette vaste étude théorique. La figure 1.13 résume sans perdre de généralité les propriétés globales des modèles obtenus par MacDonald & Vennes (1991). Leur résultat le plus encourageant confirmait que l'abondance photosphérique d'hydrogène peut varier considérablement au cours du refroidissement d'une naine blanche et s'arrimait harmonieusement avec le principe d'évolution spectrale. Ils ont également constaté l'existence de dégénérescences, atteignant jusqu'à cinq modèles différents, pour une masse et une température effective données. L'émergence de cette multiplicité reflète la possibilité que la même quantité d'hydrogène soit mélangée à l'intérieur d'une zone de convection variant en taille et en profondeur.

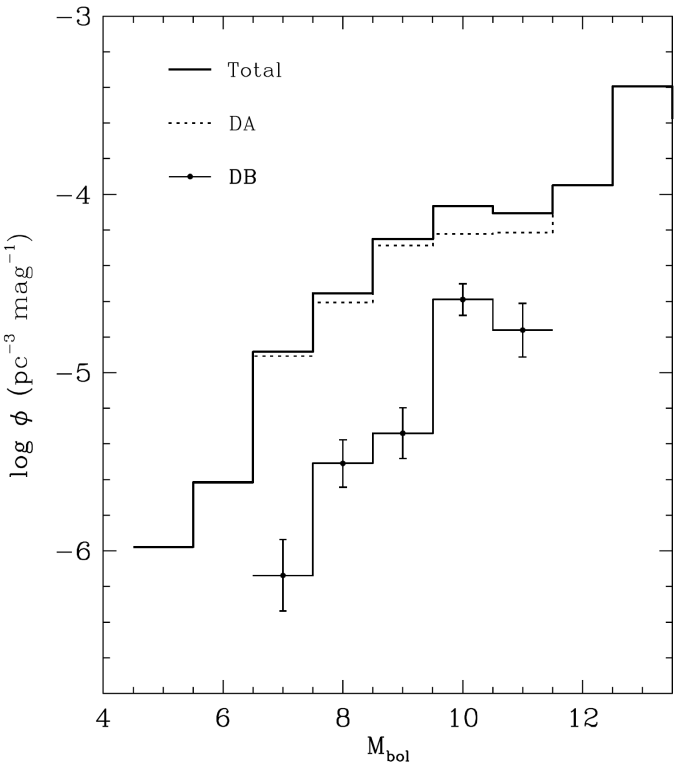

FIGURE 1.11 – Fonction de luminosité obtenue pour l'ensemble des étoiles DB et DA dans le l'échantillon complet du relevé Palomar-Green. La hauteur caractéristique de la galaxie a été fixée à $z_0 = 250$ pc. (Bergeron et al. 2011).

Un point important à noter est que les séquences présentées à la figure 1.13 sont des isogrammes basés sur des modèles statiques. Néanmoins, une analyse qualitative d'une masse en particulier, par exemple $\log M_{\rm H}/M_{\odot} = -14$, permet d'obtenir un aperçu du comportement attendu. Au cours du vieillissement, la lévitation radiative perd en efficacité et l'abondance photosphérique d'hélium diminue (diffusion) jusqu'à ce que $T_{\rm eff}$ atteigne 18,000 K. À ce stade, il n'existe plus, dans ce cadre théorique, de modèle à l'équilibre diffusif pour lequel la quasi-totalité de l'hydrogène est située en surface. Via un saut discontinu, le ratio He/H est alors forcé de rejoindre une nouvelle branche de l'isogramme caractérisée par une atmosphère riche en hélium. Ce changement brusque indique qu'une naine blanche ne peut pas évoluer continuellement à l'équilibre et devra donc subir des transformations dynamiques au fil du temps (i.e. dilution convective). À la lumière de ces constats, les diverses simulations effectuées par de MacDonald & Vennes (1991) soutiennent conceptuellement les deux mécanismes physiques décrits dans cette section, un résultat vital pour l'évolution spectrale.

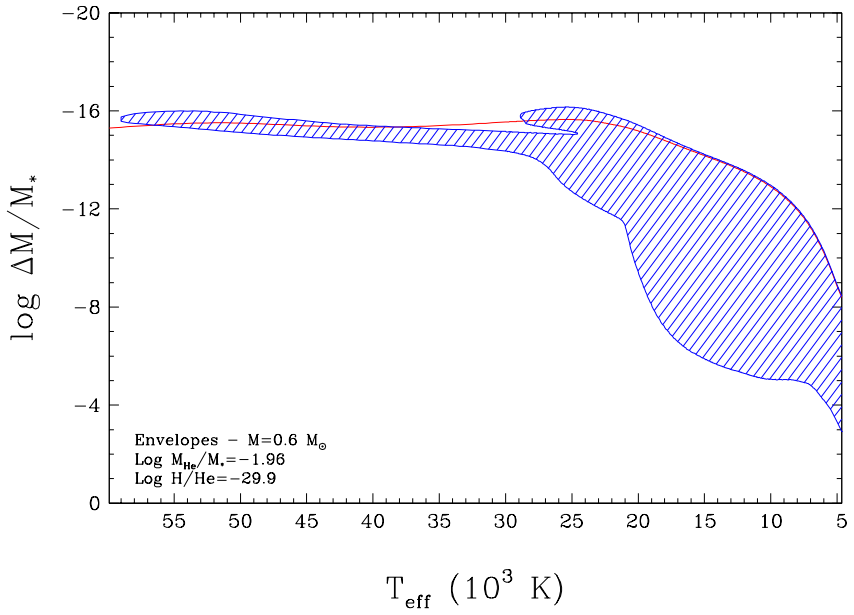

FIGURE 1.12 – Exemple de structures d'enveloppe en fonction de la température effective pour une naine blanche de 0.6 $M_{\odot}$ riche en hélium. La profondeur est exprimée en fonction de la fraction de masse relative au-dessus du point considéré. La convection est dénotée par la section hachurée bleue et la photosphère est indiquée en rouge (inspiré de Rolland et al. 2018).

1.2.3 Variation du ratio DA/non-DA

En vertu des limitations instrumentales de l'époque, la détection de la raie Hα a longtemps représenté un défi technique. L'inversion de population identifiée par Sion (1984) et Greenstein (1986) a donc résisté durant des années à l'usure du temps. L'amélioration des capacités observationnelles a permis à Bergeron et al. (1997) de trouver 20 étoiles DA, anciennement DC, au sein de leur échantillon de 110 naines blanches froides. Grâce à ces reclassifications, le rapport DA/non-DA passait de 4 : 1 à un ratio proche de l'unité pour $T_{\rm eff} < 10,000$ K. Cette valeur allait éventuellement être révisée à la baisse avec l'arrivée de nombreux relevés tels que le Two Micron All Sky Survey (2MASS). En effet, dans leur analyse photométrique de 940 objets, Tremblay & Bergeron (2008) ont déterminé que l'incidence relative de l'hélium augmentait bel et bien à basse température. Cependant, la variation attendue s'est avérée près de deux fois moins importante résultant en un maximum de $N_{\rm H}/N_{\rm He} \sim 0.5$ aux alentours de 8000 K. Comme le démontre la figure 1.14, un comportement similaire a été de nouveau observé avec les données de 492 naines blanches à l'intérieur de 40 pc (Limoges et al. 2015).

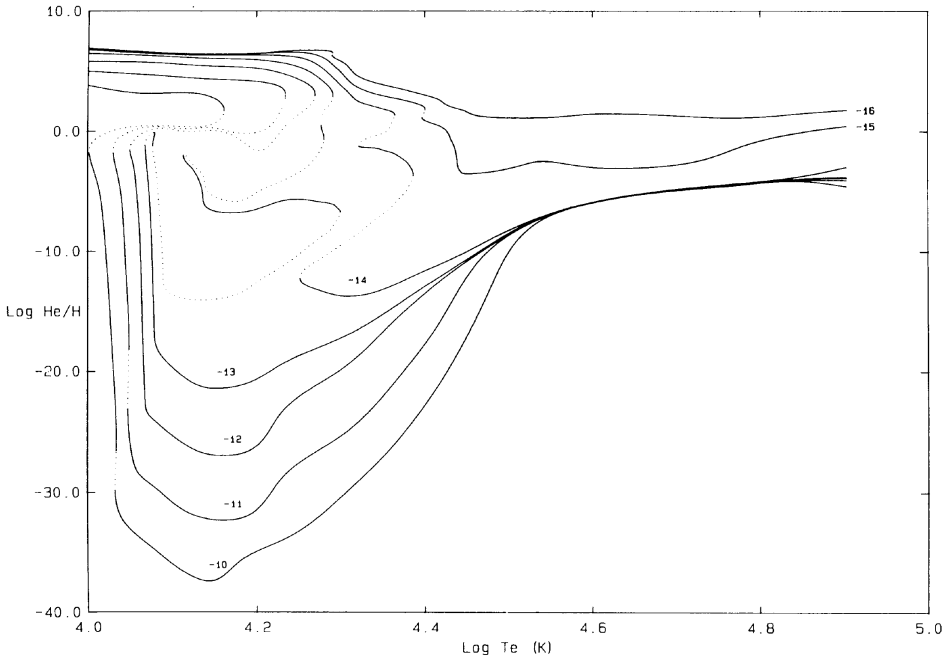

FIGURE 1.13 – Isogrammes de la masse totale d'hydrogène $M_{\rm H}$ en fonction de la température effective et du ratio He/H (en masse) à une profondeur optique de $\tau_R = 2/3$. La convection utilise le critère de Schwarschild et une paramétrisation de la longueur de mélange de $\alpha = 1$. Les contours sont indexés avec la valeur de $\log M_{\rm H}$ en masse solaire. Les modèles soupçonnés instables sont identifiés à l'aide de traits pointillés (MacDonald & Vennes 1991).

Malgré une ampleur rectifiée par de récents relevés, l'augmentation du nombre de naines blanches riches en hélium à basse température demeure une signature réelle de l'évolution spectrale. De plus, ce comportement coïncide avec une phase de croissance convective dans l'enveloppe stellaire comme le montre la figure 1.15. En présence d'une couche suffisamment épaisse ($M_{\rm H} > 10^{-13}\ M_\odot$), la formation des instabilités thermodynamiques liées à He II et He I est essentiellement supprimée rendant impossible toute dilution. Toutefois, lorsque la température chute sous 12,000 K, la zone de convection superficielle d'hydrogène en surface plonge vers l'intérieur de l'étoile, et ce, jusqu'à rejoindre l'enveloppe sous-jacente d'hélium. À ce stade, plusieurs interprètent le résultat de cette rencontre par la dispersion complète et uniforme de l'hydrogène dans de la zone convective commune créant un objet spectroscopiquement riche en hélium (Koester 1976; Vauclair & Reisse 1977; Dantona & Mazzitelli 1979). Ce processus physique, nommé *mélange convectif*, ne doit pas être confondu avec la dilution convective pour laquelle la couche superficielle d'hydrogène est purement radiative au moment de la transition.

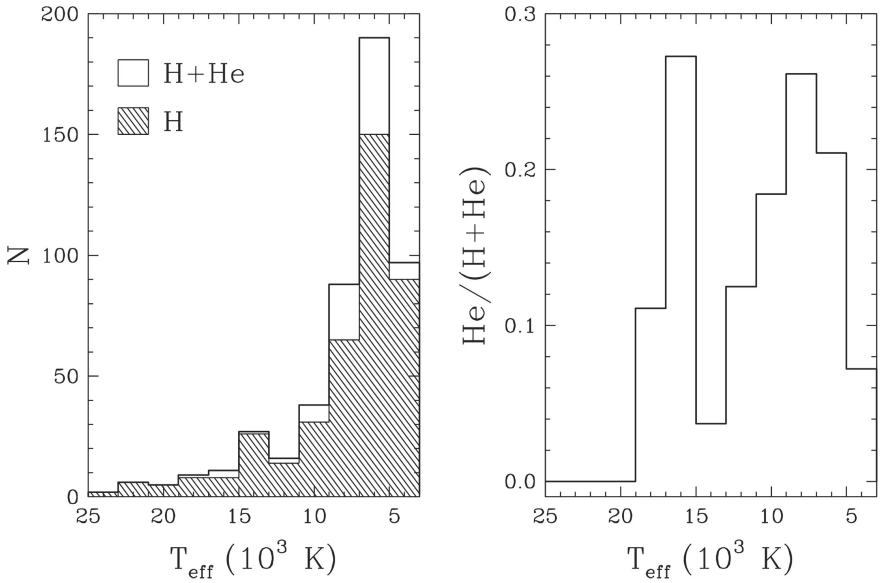

FIGURE 1.14 – Gauche: nombre total de naines blanches (blanc) de même que la population riche en hydrogène (hachuré) en fonction de la température effective. Droite: nombre relatif d'objets riches en hélium en fonction de la température effective (Limoges et al. 2015).

1.3 Importance des éléments traces

Sans compter les deux phénomènes identifiés précédemment, une dernière classe de signatures observationnelles peut potentiellement être reliée à l'évolution spectrale. En effet, les objets hybrides sont généralement caractérisés par un spectre composite reflétant la présence d'éléments traces dans l'enveloppe et l'atmosphère stellaires. Cette propriété permet d'étudier le refroidissement des naines blanches sous un autre angle et d'imposer des contraintes supplémentaires sur les mécanismes physiques pressentis pour expliquer la répartition globale des différents types spectraux. Les étoiles DBZ, DAZ, DZA et DZ représentent des exemples parfaits pour lesquels le contenu en métaux est habituellement bien compris. Comme ces objets sont détectés à plus basse température ($T_{\rm eff} < 16,000$ K), le tri gravitationnel aurait amplement eu le temps de faire disparaître ces éléments lourds de la surface. Conséquemment, ils doivent nécessairement provenir d'une source extérieure incluant vraisemblablement les disques de débris constitués de planétoïdes, d'astéroïdes ou de comètes détruits par les forces de marée colossales en jeu (Jura 2003; Jura et al. 2009; Zuckerman et al. 2011; Xu et al. 2018). À l'opposé, il est important de mentionner qu'aucun consensus concernant l'occurrence de

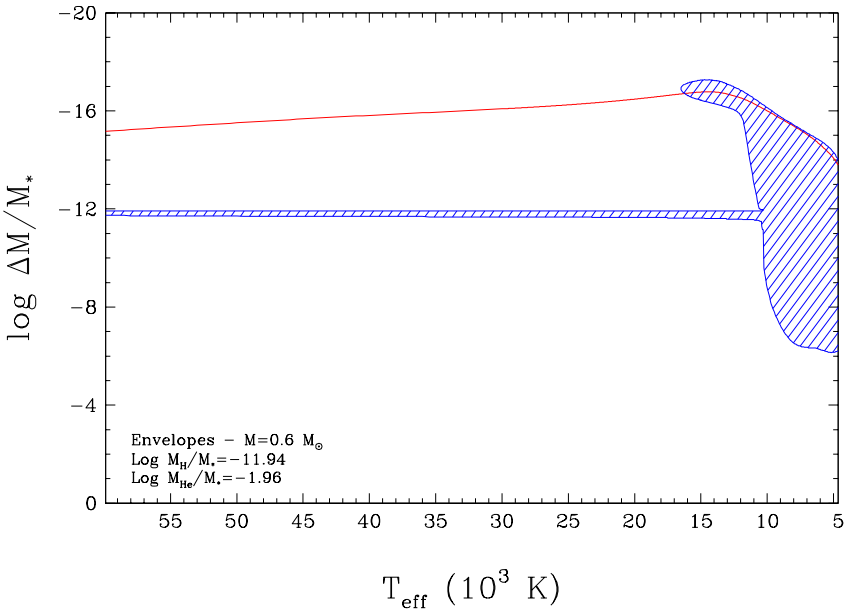

FIGURE 1.15 – Exemple de structures d'enveloppes en fonction de la température effective pour une naine blanche stratifiée de 0.6 $M_{\odot}$. La profondeur est exprimée en fonction de la fraction de masse relative au-dessus du point considéré. La convection est dénotée par la section hachurée bleue et la photosphère est indiquée en rouge. La convection à haute température est reliée au choix d'une interface s'apparentant à la fonction de Heaviside et est présumée ne pas être physique. (inspiré de Rolland et al. 2018).

trace d'hydrogène au niveau de la photosphère des naines blanches riches en hélium n'existe actuellement. La caractérisation des propriétés physiques et l'étude des étoiles DBA et DA froides riches en hélium représentent donc un enjeu incontournable pour l'évolution spectrale et motive la grande majorité des travaux présentés dans cette thèse.

1.3.1 Naines blanches de type DBA

Découvertes en grand nombre à partir de 20,000 K, les naines blanches de type DBA possèdent un spectre exhibant une combinaison de raies d'hélium et de la série de Balmer. Avec des abondances photosphériques allant de $\log \mathrm{H/He} = -2$ à $\log \mathrm{H/He} = -6$, ces hybrides peuvent potentiellement imposer des contraintes cruciales à la compréhension de l'évolution spectrale comme le démontre la figure 1.16. Malgré plus de 375 objets connus, leur détection demeure toutefois limitée par les capacités instrumentales. Cette réalité expose l'importance de l'enjeu lié à l'obtention d'observations à haut rapport signal-sur-bruit et, idéalement, de la

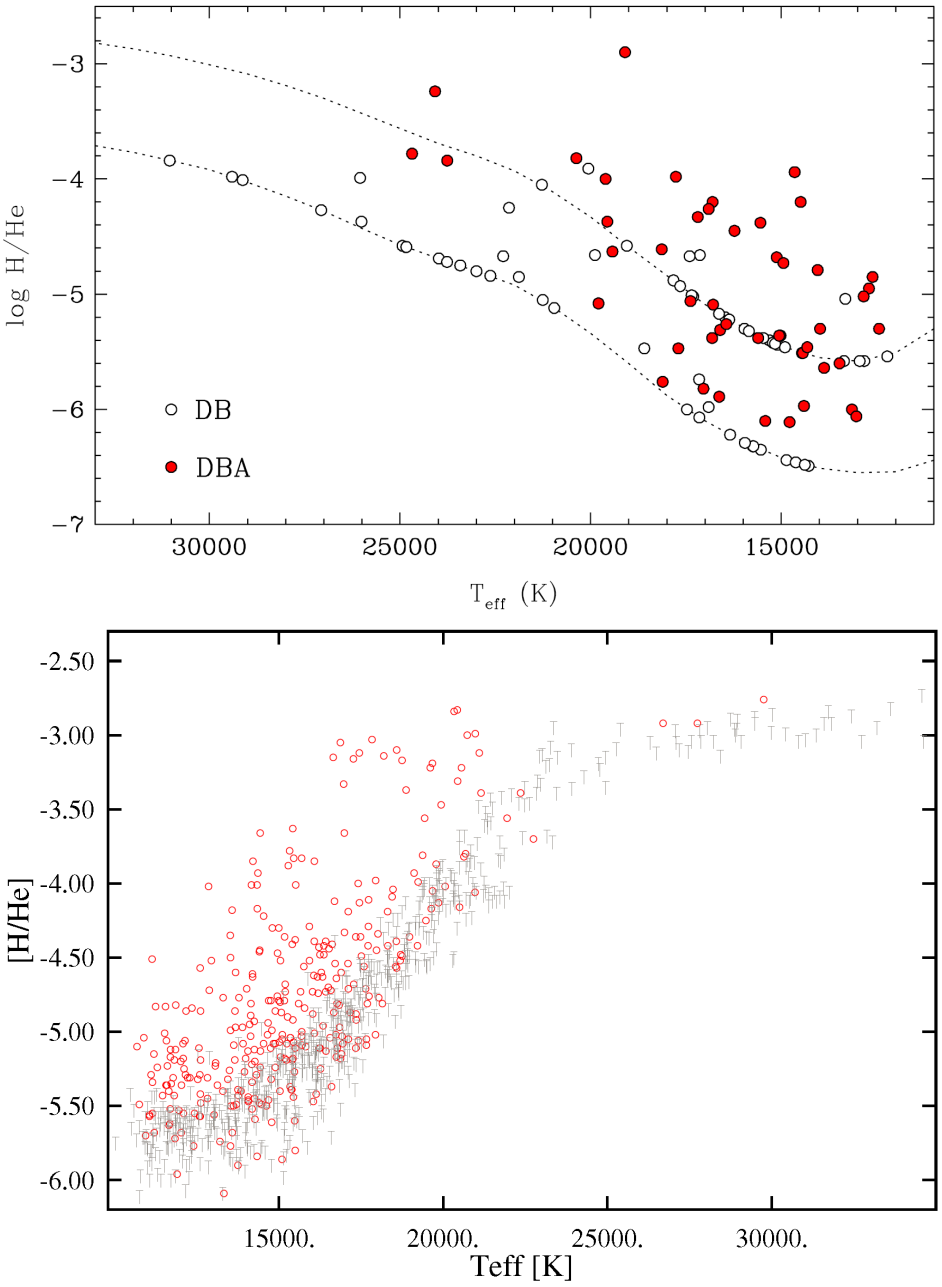

FIGURE 1.16 – Haut : abondance d'hydrogène en fonction de la température effective pour des étoiles de type DB (blanc) et DBA (rouge). Les limites de détection imposées par Hα (courbe inférieure) et Hβ (courbe supérieure) sont indiquées à l'aide de lignes pointillées. Les abondances déterminées pour les objets DB représentent des limites supérieures (Bergeron et al. 2011). Bas: abondance d'hydrogène en fonction de la température effective. Les cercles rouges indiquent une détection et les symboles gris sont des limites supérieures. (Koester & Kepler 2015). Notez l'inversion des échelles en température propre à chaque panneau.

raie Hα afin de caractériser adéquatement les étoiles DBA.

Présentes majoritairement en-deçà de ∼20,000 K, leur existence coïncide avec les phases de croissance convective identifiées précédemment à la figure 1.12. De plus, le comportement du ratio H/He semble, à première vue, correspondre avec une disparition progressive de l'hydrogène au niveau de la photosphère. Ces propriétés intrigantes ont historiquement mené à la conclusion que ces hybrides sont probablement le résidu du processus de dilution convective visant à expliquer la brèche des DB (Voss et al. 2007; Bergeron et al. 2011; Koester & Kepler 2015). En dépit de l'élégance de ce scénario, la masse totale inférée pour reproduire les données doit se situer entre $M_{\rm H} = 10^{-13}\ M_{\odot}$ et $10^{-10}\ M_{\odot}$. Cette quantité d'hydrogène devrait techniquement inhiber la formation des instabilités hydrodynamiques associées à l'hélium, limitant la possibilité d'éroder les couches de surface (voir figure 1.15). Un tel progéniteur apparaitrait indéniablement sous la forme d'une étoile DA et aurait évolué avec une enveloppe stratifiée jusqu'à des températures effectives beaucoup plus basses ($T_{\rm eff} \sim 12,000$ K). Une seconde approche envisage plutôt que la dilution convective engendre des abondances beaucoup trop faibles pour expliquer les naines blanches DBA et nécessiterait donc l'existence de sources externes d'hydrogène. MacDonald & Vennes (1991) ont aussi convergé vers ce paradoxe à l'aide de leur simulations d'enveloppes comme en témoigne la figure 1.17.

En raison des incohérences reliées à la dilution convective, une alternative aux mécanismes physiques misant sur l'origine fossile s'est avérée nécessaire. Favorisant plutôt les sources externes, l'accrétion est la solution plus couramment utilisée pour tenter de résoudre le problème. Selon ce scénario, un progéniteur riche en hélium serait progressivement enrichi, notamment en hydrogène, grâce à une pollution provenant du milieu interstellaire, de planétoïdes, d'astéroïdes ou de comètes (Voss et al. 2007; MacDonald & Vennes 1991; Bergeron et al. 2011; Koester & Kepler 2015). Comme la convection dans l'enveloppe s'intensifie avec le temps (voir figure 1.12), l'abondance photosphérique pourrait alors diminuer lorsque que la température effective chute sous 20,000 K. Malgré la simplicité de cette hypothèse, les taux nécessaires, allant de $\dot{M}_{\rm H} = 10^{-21}\ M_{\odot}$/an à $\dot{M}_{\rm H} = 10^{-19}\ M_{\odot}$/an, posent problème. En effet, ils excèdent d'au moins 100 fois les valeurs obtenues par Dufour et al. (2007a) pour les étoiles DZA. Les données disponibles semblent donc indiquer que l'efficacité de l'accrétion d'hydrogène ne se-

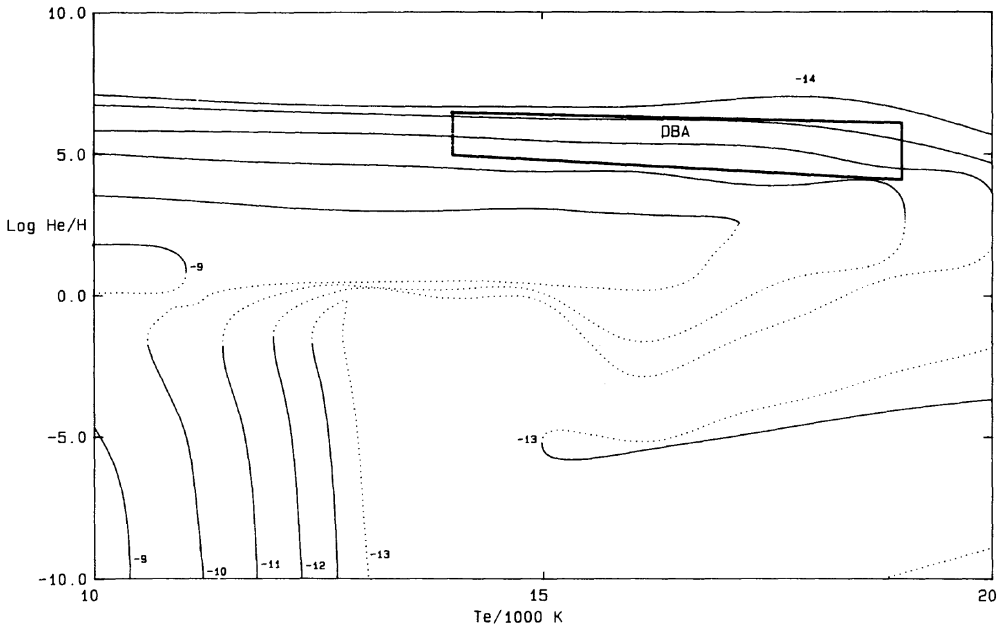

FIGURE 1.17 – Emplacement des naines blanches de type DBA à l'intérieur du diagramme H/He – $T_{\rm eff}$. (MacDonald & Vennes 1991).

rait pas uniforme d'une population à l'autre. De plus, ces taux dépassent également la limite supérieure de 5×10^{-21} $M_{\odot}$/an calculée par MacDonald & Vennes (1991) et imposée par l'existence des objets de type DB à 15,000 K. En dépit de ses faiblesses, le scénario d'accrétion pourrait potentiellement s'arrimer avec la prédiction de Koester & Kepler (2015) envisageant une éventuelle omniprésence des hybrides DBA grâce à des observations de qualité.

Malgré ces lacunes, certains cas particuliers semblent soutenir l'hypothèse de l'accrétion en raison de la présence commune de métaux et de raies de la série de Balmer dans leur spectre. Des candidats tels que GD 40, GD 61 et G241-6 possèdent également une surabondance relative en oxygène souvent associée à la réception de matériel riche en eau à la surface de ces naines blanches (Jura & Xu 2010; Farihi et al. 2013; Raddi et al. 2015; Gentile Fusillo et al. 2017). Comme le montre la figure 1.18, une autre caractéristique en leur faveur concerne la similitude entre les abondances photosphériques calculées pour ces objets et les résultats connus pour les étoiles DZA et DBA. De plus, les taux d'accrétion nécessaires pour représenter ces astres suroxygénés correspondent aux valeurs envisagées pour les autres groupes d'hybrides contenant des traces d'hydrogène. Indépendamment du petit nombre de prototypes connus, ces différents facteurs ont mené à l'émergence d'une théorie stipulant que l'accrétion de débris riches en eau

pourrait expliquer toutes les traces d'hydrogène observées dans les enveloppes riches en hélium.

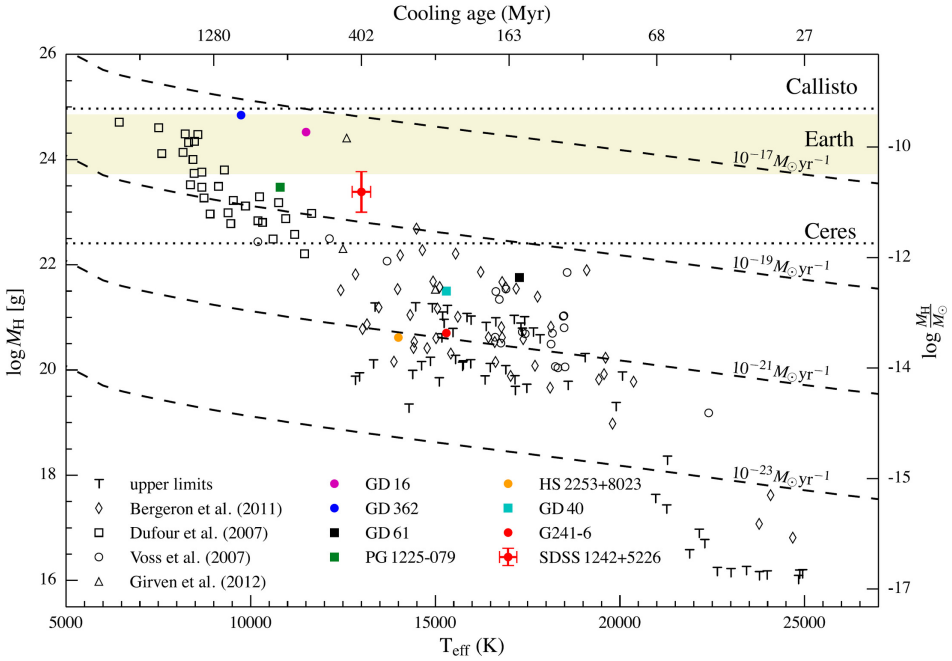

FIGURE 1.18 – Masse totale d'hydrogène en gramme (axe gauche), ou en masse solaire (axe droit), dans la zone de convection de naines blanches riches en hélium en fonction de $T_{\rm eff}$. Les temps de refroidissement pour une DB typique de Bergeron et al. (2011) sont indiqués par l'axe supérieur. Les objets du champ (voir légende) ont été ajoutés à des fins de complétude. Les lignes pointillées et la région ombragée représentent la masse d'hydrogène en eau pour Ceres, Callisto et la Terre. Les tracés hachurés suivent l'accrétion cumulative au fil du temps (Raddi et al. 2015).

1.3.2 Naines blanches de type DA riches en hélium

Avec la disparition des raies d'hélium sous 12,000 K, la composition chimique des naines blanches froides s'avère bien souvent plus complexe que le type spectral ne le laisse entrevoir. Identifiés à la figure 1.4, L745-46A et Ross 640 représentent deux exemples concrets de cette situation en vertu de données photométriques pauvres en hydrogène combinées à un spectre arborant une raie Hα peu profonde et évasée. Cette signature observationnelle particulière trahit la présence d'une enveloppe et d'une atmosphère riches en hélium causant de l'élargissement van der Waals et l'absence du saut de Balmer. Actuellement, plus d'une quarantaine d'objets similaires à ces deux DZA prototypes ont été trouvés grâce à divers relevés, incluant notamment Dufour et al. (2007a), Giammichele et al. (2012) et Limoges et al. (2015). En rai-

son de la diffusion des métaux vers les couches internes, leur présence est couramment associée à des processus d'accrétion. Toutefois, les abondances photosphériques d'hydrogène inférées, allant de $\log \mathrm{H/He} = -5$ à $\log \mathrm{H/He} = -3$, semblent relativement élevées pour être expliquées uniquement par des sources externes (Dufour et al. 2007a). Comme les températures effectives auxquelles ces naines blanches sont observées coïncident avec la convection illustrée à la figure 1.15, ces auteurs spéculent que l'hydrogène serait d'origine primordial (DA). Un tel objet posséderait une couche de surface avec $M_{\mathrm{H}} \sim 10^{-10}\ M_{\odot}$ et serait possiblement sujet au mélange convectif. Par extension, il pourrait donc potentiellement exister un sous-groupe d'étoiles de type DA froids riches en hélium et exempts de métaux. La caractérisation d'une telle population permettrait de confirmer, ou d'infirmer, ce mécanisme physique tout en éclaircissant le portrait de l'évolution spectrale à basse température.

1.4 Format de cette thèse

Ce constat de l'état des connaissances sur l'évolution spectrale des naines blanches a permis de réaliser que ce processus est loin d'être entièrement compris. Plus spécifiquement, plusieurs phénomènes complexes impliquant les objets riches en hélium, notamment la brèche des DB et l'existence des DBA, figurent à l'avant plan du débat opposant l'origine primordiale (dilution convective) et l'accrétion provenant de sources externes. Un des buts premiers de cette thèse est d'identifier, ou à défaut de contraindre, les mécanismes inhibant les effets de la gravité afin de mieux comprendre qualitativement, mais surtout quantitativement, le comportement du ratio H/He pour $T_{\mathrm{eff}} < 30,000$ K. Dans cette optique, une étude consacrée à l'analyse et à l'origine des naines blanches de type DBA et DA riches en hélium a été entreprise et documentée dans deux articles publiés (ou soumis) dans *The Astrophysical Journal*.

Au chapitre 2, nous examinerons le comportement observationnel du ratio H/He sous 30,000 K en effectuant une analyse détaillée d'un échantillon constitué de naines blanches DB et DBA brillantes de même que des DA froides riches en hélium provenant du SDSS. Grâce à de nouveaux spectres de la région Hα, nous tenterons d'imposer des contraintes plus strictes aux paramètres atmosphériques de ces objets, notamment l'abondance d'hydrogène photosphérique. Nous revisiterons ensuite les scénarios de dilution convective, de mélange

convectif et d'accrétion afin de vérifier si l'un d'entre eux pourrait être à l'origine des DB, DBA, DZA et DA froides riches en hélium.

Au chapitre 3, nous explorerons les effets de la température effective, du ratio H/He dans la zone de convection d'hélium et du profil de composition global sur la structure thermodynamique de l'enveloppe stellaire. Avec cette caractérisation de l'espace des paramètres, nous tenterons de développer un modèle numérique cohérent de la dilution convective pouvant reproduire les abondances observées. Nous testerons également un scénario évolutif habituellement réservé aux DQ, le dragage convectif, afin d'expliquer la disparité entre les masses d'hydrogène inférées et l'abondance photosphérique. Une conclusion terminera cette thèse au chapitre 4.

1.5 Déclaration de l'étudiant

Les articles constituant cette thèse, de même que le contenu des annexes, représentent l'aboutissement de mes travaux réalisés dans le cadre du programme de doctorat. Tout au long de ce projet, j'ai pu bénéficier de l'aide et de l'apport complémentaires de mes deux directeurs de recherche. En effet, la première partie de cette étude a fait appel à l'expertise théorique de Pierre Bergeron pour l'analyse et la détermination des paramètres atmosphériques des naines blanches de notre échantillon. De son côté, Gilles Fontaine a partagé ses connaissances des modèles d'enveloppes stellaires et des scénarios d'évolution spectrale afin de me permettre d'approfondir la question et de comparer les prédictions avec les observations.

Pour l'article présenté au chapitre 2, j'ai d'abord déterminé les paramètres atmosphériques de 115 naines blanches DB et DBA à partir des données disponibles et des modèles de Pierre Bergeron. Sous sa supervision, j'ai également procédé au calcul des propriétés globales de cet échantillon. Avec l'optique d'étendre notre couverture en température effective, j'ai développé une méthode d'analyse hybride, combinant à la fois photométrie et spectroscopie, afin de me pencher sur 28 étoiles DA froides riches en hélium identifiées dans le SDSS. Une fois la caractérisation complète de l'échantillon terminée, je me suis attaqué au problème de l'évolution spectrale à l'aide du code de Gilles Fontaine. En variant le type d'enveloppe (homogène ou stratifiée), la température effective (plus de 500 points), le contenu en hydrogène (20 à 30 abondances) ainsi que l'efficacité convective, j'ai généré quatre grilles de modèles synthétiques

me permettant d'étudier l'effet de ces différents paramètres sur la structure thermodynamique résultante. Grâce à ces simulations, j'ai produit six cartes théoriques reflétant le ratio H/He photosphérique prédit pour la dilution convection, le mélange convectif et l'accrétion, respectivement. En les combinant aux données observationnelles, j'ai finalement testé ces trois mécanismes physiques en collaboration avec mes deux directeurs de recherche. Une fois les différents calculs achevés, j'ai rédigé la première ébauche du texte et produit toutes les figures nécessaires à l'article. Les révisions et versions subséquentes ont été réalisées conjointement avec mes directeurs de recherche.

En ce qui concerne le chapitre 3, nous désirions améliorer notre approche et nos modèles afin d'en augmenter le réalisme. Grâce à de petites modifications apportées par Gilles Fontaine, il nous est maintenant possible de produire des enveloppes avec une répartition arbitraire de l'hydrogène. En utilisant une représentation conceptuelle simple du processus de dilution convective, j'ai développé un algorithme d'optimisation permettant de trouver itérativement une solution auto-cohérente tout en conservant la forme générale du profil d'abondance souhaité. Par la suite, j'ai caractérisé les propriétés de ces nouveaux modèles dans le but de les comparer à notre méthodologie initiale. À l'aide de ces simulations, j'ai revisité mes deux cartes de dilution convective pour vérifier si nos améliorations donnaient un résultat plus satisfaisant. J'ai également remis le scénario d'accrétion à l'épreuve afin de le confirmer ou de l'abandonner définitivement. J'ai ensuite imaginé un nouveau mécanisme physique basé sur le dragage de l'hydrogène et visant à expliquer l'existence des étoiles de type DBA. Pour approfondir cette hypothèse, j'ai recalculé deux grilles d'enveloppes synthétiques et généré les cartes évolutives pour les confronter aux observations disponibles. À l'instar du premier article, j'ai rédigé la vaste majorité du texte initial et générer les figures nécessaires. Les révisions et versions subséquentes ont été réalisées conjointement avec Pierre Bergeron.

Chapitre 2

On the Spectral Evolution of Helium-atmosphere White Dwarfs Showing Traces of Hydrogen

B., Rolland [1], P., Bergeron [1], and G., Fontaine [1]

Published April 13th 2018 in

The Astrophysical Journal

Volume 857, Number 1

1. Département de Physique, Université de Montréal, C.P. 6128, Succ. Centre-Ville, Montréal, Québec, H3C 3J7

2.1 Abstract

We present a detailed spectroscopic analysis of 115 helium-line (DB) and 28 cool, He-rich hydrogen-line (DA) white dwarfs based on atmosphere fits to optical spectroscopy and photometry. We find that 63% of our DB population show hydrogen lines, making them DBA stars. We also demonstrate the persistence of pure DB white dwarfs with no detectable hydrogen feature at low effective temperatures. Using state-of-the art envelope models, we next compute the total quantity of hydrogen, $M_{\rm H}$, that is contained in the outer convection zone as a function of effective temperature and atmospheric H/He ratio. We find that some $(T_{\rm eff}, M_{\rm H})$ pairs cannot physically exist as a homogeneously mixed structure; such combination can only occur as stratified objects of the DA spectral type. On that basis, we show that the values of $M_{\rm H}$ inferred for the bulk of the DBA stars are too large and incompatible with the convective dilution scenario. We also present evidence that the hydrogen abundances measured in DBA and cool, helium-rich white dwarfs cannot be globally accounted for by any kind of accretion mechanism onto a pure DB star. We suggest that cool, He-rich DA white dwarfs are most likely created by the convective mixing of a DA star with a thin hydrogen envelope; they are not cooled down DBA's. We finally explore several scenarios that could account for the presence of hydrogen in DBA stars.

2.2 Introduction

The extreme chemical purity of white dwarf atmospheres can be attributed to the intense gravitational field present at the surface of these stars, causing all the heavy elements to sink rapidly out of sight (Schatzman 1945). This gravitational settling process should thus produce white dwarf atmospheres that are completely dominated by hydrogen — or DA stars. However, it is well known that a significant fraction of the white dwarf population is hydrogen-deficient — e.g., PG 1159, DO, DB, DQ, DZ, and some DC stars (Wesemael et al. 1993) — and a very small fraction even have carbon-dominated atmospheres (Dufour et al. 2007b). More importantly, the relative number of white dwarfs of a given spectral type varies considerably as a function of effective temperature, indicating that there exist several physical mechanisms

that compete with gravitational settling to alter the chemical composition of the outer layers of white dwarfs as they evolve along the cooling sequence. Such physical mechanisms include convective mixing, convective dredge-up from the core, accretion from the interstellar medium or circumstellar material, radiative levitation, and stellar winds. Understanding the so-called *spectral evolution of white dwarf stars* has always remained a fundamental topic of research in the white dwarf field, in particular with the large number of new discoveries in the Sloan Digital Sky Survey (SDSS; see, e.g., Kleinman et al. 2013).

Probably the most significant evidence for the spectral evolution of white dwarfs, discussed at length in Fontaine & Wesemael (1987), is the existence of a "DB-gap", a range in effective temperature between $T_{\rm eff} \sim 30,000$ K and 45,000 K where only DA stars are found, while helium-atmosphere white dwarfs exist both above (the DO stars) and below (the DB stars) the gap. One model proposed by Fontaine & Wesemael to account for this gap starts with hot white dwarf progenitors with hydrogen-deficient atmospheres (PG 1159 or DO stars) containing only minute amounts of hydrogen thoroughly diluted within the stellar envelope. As these stars cool off, hydrogen would gradually float up to the surface, thus building an atmosphere enriched with hydrogen. The fact that all white dwarfs turn into DA stars by the time they reach $T_{\rm eff} \sim 45,000$ K imposes a lower limit on the total amount of hydrogen present in the hot progenitors, of the order of $M_{\rm H} \sim 10^{-16}\ M_{\odot}$. Hybrid white dwarfs with thinner hydrogen layers floating in diffusive equilibrium on top of the helium envelope would appear as DAO stars, bearing the signature of chemically stratified atmospheres (see Manseau et al. 2016 and references therein).

Below the red edge of the gap ($T_{\rm eff} \lesssim 30,000$ K), the reappearance in large numbers of helium-atmosphere white dwarfs — DB stars in this case — has been interpreted in terms of the dilution of a thin, superficial hydrogen *radiative* layer ($M_{\rm H} \sim 10^{-15}\ M_{\odot}$) by the underlying and more massive convective helium envelope (Fontaine & Wesemael 1987). In this paper, we refer to this mechanism as the *convective dilution scenario* (see also MacDonald & Vennes 1991). Even though the large number of white dwarfs discovered in the SDSS has unveiled the existence of many hot DB stars in the gap, the fraction of DB white dwarfs within the gap remains significantly lower than that found at lower temperatures, and we are thus dealing

with a DB deficiency rather than a true gap. Nevertheless, the float-up model and convective dilution scenario discussed above must occur for a significant fraction of white dwarfs, perhaps of the order of ∼20% (Bergeron et al. 2011).

Another important signature of the spectral evolution of white dwarfs, also discussed in Fontaine & Wesemael (1987), is the spectacular increase in the ratio of non-DA to DA stars below $T_{\rm eff} \sim 10,000$ K, which jumps from a value around 25% above this temperature to a value near unity below it. This sudden increase in the number of non-DA stars (i.e., DQ, DZ, DC) in this temperature range has been interpreted as the result of the mixing of the superficial *convective* hydrogen layer with the deeper and much more massive convective helium envelope (Koester 1976; Vauclair & Reisse 1977; Dantona & Mazzitelli 1979). We will refer to this mechanism as the *convective mixing scenario*, as opposed to the *convective dilution scenario* discussed above, in which the hydrogen superficial layer is purely radiative.

One way to further our understanding of the spectral evolution of helium-atmosphere white dwarfs below $T_{\rm eff} \sim 30,000$ K is to determine the hydrogen abundance in these stars, often present as a trace element, and to study the hydrogen abundance pattern as a function of effective temperature. Indeed, a large fraction of DB white dwarfs shows traces of hydrogen — the DBA stars — if observed at sufficiently high signal-to-noise ratio (S/N). Koester & Kepler (2015) even suggested, based on their analysis of the DB stars in the DR10 and DR12 of the SDSS, that perhaps *all* DB white dwarfs would show hydrogen if the resolution and S/N were high enough. The origin of hydrogen in DBA stars has remained a mystery, and the subject of controversy as well. While it seems reasonable to assume that the presence of hydrogen in these stars has a residual origin — the leftovers from the convective dilution scenario discussed above — the total mass of hydrogen inferred in those stars, which is homogeneously mixed in the convective stellar envelope, lies in the range $M_{\rm H} = 10^{-13}$ to 10^{-10} $M_{\odot}$ (Voss et al. 2007; Bergeron et al. 2011; Koester & Kepler 2015). The problem with these estimates is that DA progenitors with such thick hydrogen layers would easily survive the convective dilution process, and thus never turn into DB stars in the first place (MacDonald & Vennes 1991). The most common way around this problem is to assume that the DA progenitors have hydrogen layers thin enough (of the order of $M_{\rm H} \sim 10^{-15}$ $M_{\odot}$) to allow the DA-to-DB transition below

$T_{\rm eff} \sim 30,000$ K, and that significant amounts of hydrogen are then accreted onto the DB star from external sources such as the interstellar medium, disrupted asteroids, small planets, and even comets (MacDonald & Vennes 1991; Bergeron et al. 2011; Koester & Kepler 2015; Gentile Fusillo et al. 2017). These accretion scenarios can easily account for the observed hydrogen abundances in DBA stars, assuming reasonable accretion rates.

Also of key interest is the presence of hydrogen in much cooler ($T_{\rm eff} \lesssim 10,000$ K) helium-atmosphere white dwarfs, the prototypes of which are the DZA stars L745-46A and Ross 640 (see, e.g., Figure 14 of Giammichele et al. 2012), which show broad and shallow Hα absorption features resulting from van der Waals broadening in a helium-dominated atmosphere. Traces of hydrogen have now been detected in many DZ stars from the SDSS (Dufour et al. 2007a). The origin of hydrogen in these objects, whether it has a residual origin — cooled off DBA stars or convectively mixed DA stars — or has been accreted from external bodies, remains an open question.

In this paper, we revisit the problem of the spectral evolution of helium-atmosphere white dwarfs below $T_{\rm eff} \sim 30,000$ K, by studying the hydrogen abundance pattern in these stars as a function of effective temperature. We first present in Section 2.3 a detailed model atmosphere analysis of relatively bright DB and DBA white dwarfs, as well as cool He-rich DA stars drawn from the SDSS. In Section 2.4, we describe our stellar envelope models with stratified and homogeneous chemical compositions appropriate for these stars, which are then used in Section 2.5 to explore and test various scenarios that could account for the observed hydrogen abundance pattern, and discuss possible evolutionary channels that could produce DB, DBA, and cool He-rich DA and DZA stars. Our conclusions follow in Section 2.6.

2.3 Hydrogen Abundance Pattern in He-Atmosphere White Dwarfs

2.3.1 Hydrogen in DBA stars

2.3.1.1 Spectroscopic Observations

Our sample of bright, helium-line DB and DBA stars is based on an extension of the 108 DB white dwarfs analyzed in detail in Bergeron et al. (2011). In particular, high S/N

spectra of 6 additional DB stars, selected from the electronic version of the Catalogue of Spectroscopically Identified White Dwarfs [2] (McCook & Sion 1999, hereafter WD Catalog), have been secured with the Steward Observatory 2.3 m Bok Telescope equipped with the Boller & Chivens spectrograph. The $4\farcs5$ slit together with the 600 line mm^{-1} grating blazed at 3568 Å in first order provides a spectral coverage from about 3500 to 5250 Å at a resolution of ∼6 Å FWHM (see also Bergeron et al. 2015). Also included are 1919−362 [3] from Subasavage et al. (2017), as well as the 4 new DB stars discovered by Limoges et al. (2015, see their Figure 15) in the course of their spectroscopic survey of the SUPERBLINK proper motion catalog. We also secured a new optical spectrum for PG 1654+160 using the same setup. These additional optical spectra are displayed in Figure 2.1 in order of decreasing effective temperature; the other blue spectra in our sample have already been displayed in Figure 5 of Bergeron et al. (2011). Note the particular strength of the hydrogen lines in PB 8252 (0025−032).

Because we are mostly interested here in studying the hydrogen abundance pattern in helium-atmosphere white dwarfs, we also improved the sample of DB stars from Bergeron et al. (2011) by acquiring 54 high signal-to-noise Hα spectra missing from our original data set (see also Bergeron et al. 2015). These spectra have been obtained with the NOAO Mayall 4-m telescope; the adopted configuration allows a spectral coverage of $\lambda\lambda$3800–6700, at an intermediate resolution of ∼6 Å FWHM. These spectra are displayed in Figure 2.2. Note how the strength of Hα varies considerably from object to object, and how it is particularly strong for PB 8252 (0025−032) and Lan 143 (0258+683). Hydrogen is now detected in 63% of the DB stars in our sample, a value somewhat lower than the estimated 75% fraction of DBA white dwarfs obtained by Koester & Kepler (2015) using their best spectra. Four objects in our sample still lack Hα spectroscopic data — L715−34 (0308−565), BPM 17731 (0418−539), L151-81A (1454−630.1), and GD 27 (0220+480) — and these are excluded from our analysis for homogeneity purposes. Our final sample thus includes 115 DB white dwarfs, among which 73 are DBA stars.

A significant advantage of our extended sample is its homogeneity, both in terms of wavelength coverage and S/N. Even though its size is modest in comparison to the SDSS sample

2. http://www.astronomy.villanova.edu/WDCatalog/index.html
3. We omit in the remainder of this paper the WD prefix for conciseness.

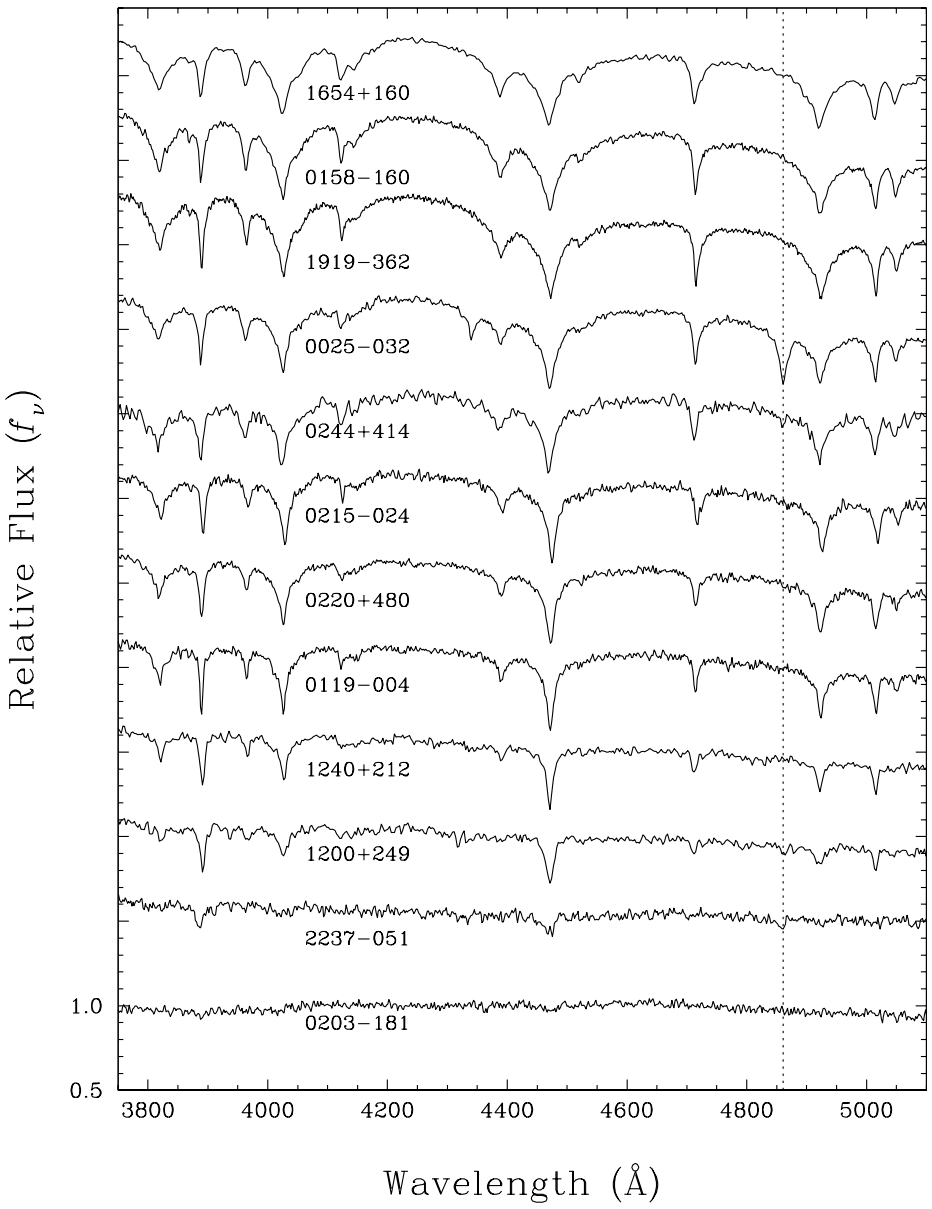

FIGURE 2.1 – Optical (blue) spectra for the 11 new DB stars included in our extended sample, as well as a new spectrum for PG 1654+160; the remaining spectra used in our analysis are displayed in Figure 5 of Bergeron et al. (2011). The spectra are normalized at 4500 Å and shifted vertically from each other by a factor of 0.5 for clarity. The effective temperature decreases from top to bottom. The location of Hβ is shown by a dotted line.

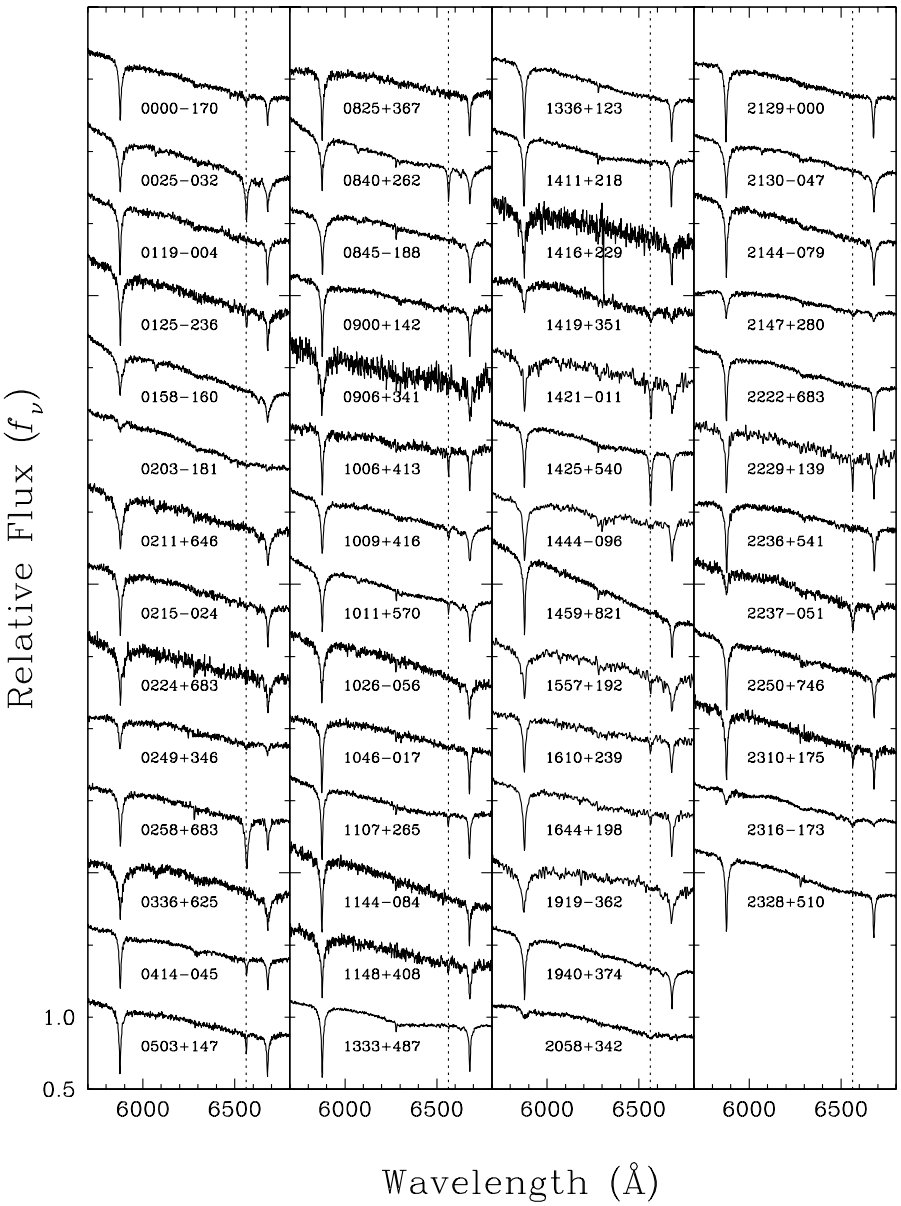

FIGURE 2.2 – New spectra near the Hα region for 54 DB and DBA stars in our extended sample, together with the DB star from Subasavage et al. (2017, 1919−362). The spectra are shown in order of right ascension, normalized at 6200 Å, and shifted vertically from each other by a factor of 0.5 for clarity. The location of Hα is shown by a dotted line.

(Koester & Kepler 2015), the quality of our spectra is superior in terms of S/N. Indeed, because the exposure time of a given SDSS spectrum is constant for all targets on a given plate, the corresponding S/N is necessarily a function of the magnitude of the star, resulting in typical sensitivity between S/N $\sim$ 5 and 20. In comparison, the majority of our spectra have S/N well above 50, with an average around 80.

2.3.1.2 Model Atmosphere Analysis

Our model atmospheres and synthetic spectra are identical to those described at length in Bergeron et al. (2011) and references therein. These models are built from the LTE model atmosphere code described in Tremblay & Bergeron (2009) and references therein, in which the improved Stark profiles of neutral helium of Beauchamp et al. (1997) have been incorporated. These detailed profiles of more than 20 neutral helium lines take into account the transition from the impact to the quasistatic regime for electrons, the transition from quadratic to linear Stark broadening, as well as forbidden components. We also include in the cooler models van der Waals broadening following the treatment of Deridder & van Renspergen (1976). For the treatment of the hydrogen lines, we rely on the improved calculations for Stark broadening of Tremblay & Bergeron (2009), as well as resonance broadening and nonresonant broadening for the Balmer lines in the cooler models, as also described in Tremblay & Bergeron. Convective energy transport is treated within the ML2 version of the mixing-length theory with a value of $\alpha = \ell/H$ — the ratio of the mixing length to the pressure scale height — set to 1.25, following the prescription of Bergeron et al. (2011). All hydrogen and helium level populations are computed using the occupation probability formalism of Hummer & Mihalas (1988), which is also included in the calculations of the corresponding bound-bound, bound-free, and pseudo-continuum opacities. Our model grid has been extended to the regime of cool, He-rich DA stars, and now covers a range of effective temperature between $T_{\rm eff} = 40,000$ K and 6000 K by steps of 1000 K, while $\log g$ ranges from 7.0 to 9.0 by steps of 0.5 dex. In addition to pure helium models, we also calculated models with $\log {\rm H/He} = -7.0$ to -1.5 by steps of 0.5. Illustrative spectra are displayed in Figure 1 of Bergeron et al. (2011) for various values of effective temperatures, surface gravities, and convective efficiencies, while we show in Figure

2.3 synthetic spectra at $\log g = 8$ for various effective temperatures — including our extension to low temperatures — and hydrogen-to-helium abundance ratios. Note that for the largest hydrogen abundance shown in this plot (H/He = 10^{-2}), the star would appear as a normal DB white dwarf at high effective temperatures, but as a pure DA star below $T_{\rm eff} \sim 12,000$ K, when the helium lines vanish.

Because of the complexity and degeneracy of the atmospheric parameter space for DB stars, the values derived from various studies for $T_{\rm eff}$, $\log g$, and H/He can differ significantly, as illustrated, for instance, by Voss et al. (2007, see their Figures 3 and 4) who compare the results of the SPY survey with those of independent studies (Beauchamp et al. 1999; Friedrich et al. 2000; Castanheira et al. 2006). One major reason for these discrepancies is the lack of sensitivity of the neutral helium lines to effective temperature in hotter DB stars. Indeed, for a given set of H/He, $\log g$, and α, the equivalent width of He I λ4471 reaches a plateau between 20,000 K and 30,000 K (see Figure 2 of Bergeron et al. 2011); a similar behavior can be observed in our model spectra displayed in Figure 2.3. As a result, two solutions exist for a given DB star, one on each side of the maximum strength of He I λ4471. As discussed by Bergeron et al. (2011), this degeneracy can be lifted with the use of spectroscopic observations at Hα, which add an additional constraint to the solution.

Our fitting procedure is similar to that described at length in Bergeron et al. (2011). Since in most cases our Hα spectra are independent of our blue data, we first fit the blue spectrum with pure helium models to obtain an estimate of $T_{\rm eff}$ and $\log g$. The Hα spectrum is then used to determine the hydrogen abundance — or upper limits on H/He — at these particular values of $T_{\rm eff}$ and $\log g$. The procedure is then repeated iteratively until an internal consistency is reached. An example of our solution for PB 8252 (0025−032, HE 0025−0317) — a new object added to the sample of Bergeron et al. (2011) — is displayed in Figure 2.4. The Hα absorption feature shown in the inset serves as an important constraint on the hydrogen abundance. This fitting procedure is reliable when the Hα absorption line is present in the optical spectrum. When no feature is visible, only upper limits on the hydrogen abundance can be determined. We adopt a detection limit of 200 mÅ for the equivalent widths of Hα based on the S/N of our DB spectra. For high S/N spectra with no detectable hydrogen feature, the value of H/He

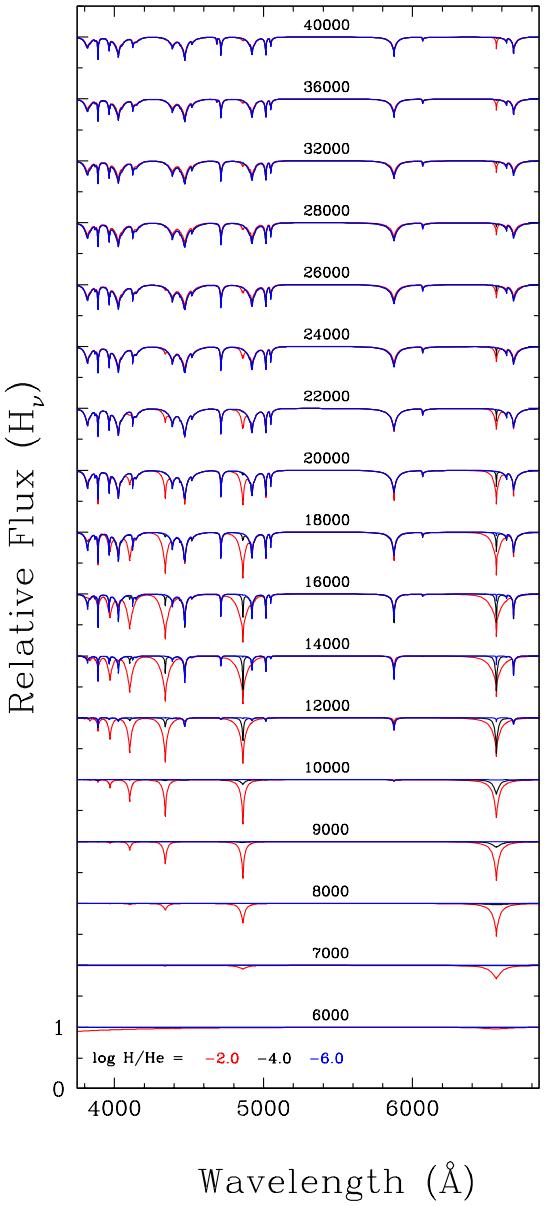

FIGURE 2.3 – Synthetic spectra of homogeneous H/He models at $\log g = 8$ for various effective temperatures and hydrogen abundances of H/He $= 10^{-6}$ (blue), 10^{-4} (black), and 10^{-2} (red). All spectra are normalized to a continuum set to unity and offset from each other by a factor of 1.0 for clarity.

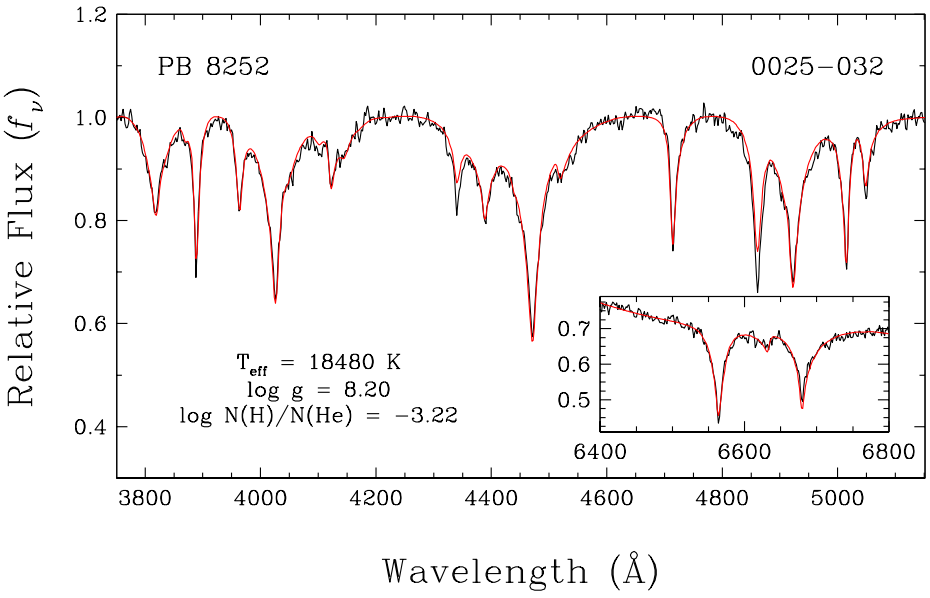

FIGURE 2.4 – Example of a full spectroscopic fit where the Hα line profile (inset) is used to measure, or constrain, the hydrogen abundance of the overall solution.

is set to the appropriate upper limit for the corresponding temperature. In cases where the spectrum is noisier, however, our fitting procedure may find an upper limit to the hydrogen abundance that is larger than that inferred from this upper limit.

2.3.1.3 Selected Results

Because of the inclusion of additional objects and new Hα spectroscopic data to our sample of bright DB stars, we present here an update of the relevant results from Bergeron et al. (2011). The atmospheric parameters for all 115 DB and DBA white dwarfs in our enlarged sample are provided in Table 2.1; pure DB stars in this table correspond to the objects where only an upper limit on the hydrogen abundance is given. For completeness, we also include the four objects listed in Section 2.3.1.1 that still lack Hα data (these are noted in the table). For each star we give the stellar mass (M) and white dwarf cooling age ($\log \tau$) obtained from evolutionary models similar to those described in Fontaine et al. (2001) but with C/O cores, $q(\mathrm{He}) \equiv M_{\mathrm{He}}/M_{\star} = 10^{-2}$ and $q(\mathrm{H}) = 10^{-10}$, which are representative of helium-atmosphere

white dwarfs[4]. The absolute visual magnitude (M_V) and luminosity (L) are determined using the improved calibration of Holberg & Bergeron (2006), while the distance D is obtained by combining M_V with the magnitude V, also given in the table. Since the presence or not of hydrogen features is crucial to our understanding of the origin of DB stars, we provide as online material our spectroscopic fits for all white dwarfs in our sample, where the left panels show the blue portion of our spectroscopic fits, while the right panels show the corresponding region near Hα.

The hydrogen abundances as a function of effective temperature for all DB stars in our sample, but with Hα spectra available to us, are displayed in Figure 2.5. Also shown are the upper limits on the hydrogen abundance for DB stars, as determined from the absence of Hα. In general, the pure DB stars are aligned on these observational limits but as discussed above, some objects have noisier data and these limits are simply not reached. The ratio of DBA stars to the total number of white dwarfs in our sample now reaches 63%, significantly higher than the value of 44% reported by Bergeron et al. (2011), thanks to our improved high S/N spectroscopic data at Hα, which revealed the presence of hydrogen in objects where Hβ was spectroscopically invisible. This higher ratio now compares favorably well with the value of 75% reported by Koester & Kepler (2015) for the highest S/N DB spectra in the SDSS, although this ratio drops to a value of 32% in their overall sample. The results of Koester & Kepler for the DBA white dwarfs from the SDSS — i.e., with hydrogen features detected — are also reproduced in Figure 2.5. Although both sets of hydrogen abundance determinations overlap very nicely, the upper limits for the DB stars in our sample are about 1 dex smaller due to the much higher S/N of our observations compared to the SDSS spectra, as discussed above, thus putting more severe constraints on the amount of hydrogen present in the DB stars with no detectable Hα feature.

The mass distribution as a function of effective temperature is shown in Figure 2.6 for the same white dwarfs as in Figure 2.5. These results are comparable to those displayed in Figure 21 of Bergeron et al. (2011), although all cool white dwarfs that appeared massive in their analysis now *all show hydrogen features*, while DB stars in our sample without detectable Hα

4. See http://www.astro.umontreal.ca/∼bergeron/CoolingModels.

TABLE 2.1 – Atmospheric Parameters of DB and DBA White Dwarfs

WD	Name	$T_{\rm eff}$ (K)	log g	log H/He	$M/M_\odot$	M_V	log $L/L_\odot$	V	D(pc)	log τ	Notes
0000−170	G266-32	13,880 (361)	8.63 (0.12)	−5.67 (0.52)	0.98 (0.07)	12.51	−2.67	14.69	27	8.86	
0002+729	GD 408	14,410 (351)	8.27 (0.09)	−5.95 (0.79)	0.76 (0.06)	11.79	−2.36	14.33	32	8.52	
0017+136	Feige 4	18,130 (438)	8.08 (0.05)	−4.63 (0.21)	0.65 (0.03)	10.98	−1.85	15.37	75	8.07	
0025−032	PB 8252	18,480 (437)	8.20 (0.04)	−3.22 (0.04)	0.72 (0.02)	11.12	−1.89	15.69	82	8.14	
0031−186	KUV 00312−1837	15,020 (396)	8.43 (0.11)	−5.35 (0.34)	0.86 (0.07)	11.96	−2.39	16.66	87	8.60	
0100−068	G270-124	19,820 (531)	8.06 (0.04)	−5.14 (1.06)	0.64 (0.03)	10.78	−1.68	13.95	43	7.91	
0112+104	EGGR 409	31,040 (1056)	7.83 (0.03)	$<$ −3.84 (0.84)	0.53 (0.02)	9.89	−0.75	15.36	123	7.20	1
0119−004	G271-47A	16,060 (404)	8.07 (0.06)	−6.27 (1.70)	0.63 (0.04)	11.23	−2.05	16.00	89	8.24	
0125−236	G274-39	16,550 (436)	8.24 (0.07)	−5.21 (0.32)	0.74 (0.05)	11.43	−2.11	15.38	61	8.33	
0129+246	PG 0129+247	16,450 (461)	8.27 (0.09)	−5.26 (0.40)	0.76 (0.06)	11.49	−2.13	16.09	83	8.35	
0158−160	G272-B2A	24,130 (1369)	7.94 (0.03)	$<$ −4.67 (1.39)	0.57 (0.02)	10.40	−1.26	14.38	62	7.38	
0203−181	HE 0203−180	12,180 (652)	8.90 (0.42)	−5.70 (2.43)	1.14 (0.24)	13.35	−3.12	16.00	33	9.16	
0211+646	Lan 150	20,700 (719)	8.00 (0.04)	$<$ −5.18 (2.18)	0.60 (0.03)	10.62	−1.57	17.43	230	7.77	
0214+699	Lan 158	29,130 (1329)	7.88 (0.05)	$<$ −4.01 (0.97)	0.55 (0.02)	10.07	−0.89	16.60	202	6.96	
0215−024	PB 6822	16,870 (402)	8.12 (0.09)	−5.96 (1.35)	0.66 (0.06)	11.19	−2.00	16.13	97	8.20	
0220+480	GD 27	16,570 (403)	8.33 (0.05)	$<$ −5.12 (0.21)	0.80 (0.03)	11.57	−2.16	15.11	51	8.39	2
0224+683	Lan 142	18,270 (471)	8.23 (0.10)	$<$ −5.69 (2.42)	0.74 (0.07)	11.18	−1.92	17.78	208	8.18	
0244+414	PM J02478+4138	17,170 (439)	8.28 (0.10)	−4.73 (0.27)	0.77 (0.06)	11.41	−2.07	17.40	157	8.31	
0249+346	KUV 02499+3442	13,360 (436)	9.02 (0.21)	−5.54 (1.16)	1.20 (0.11)	13.36	−3.05	16.40	40	9.15	
0249−052	KUV 02498−0515	17,630 (549)	8.15 (0.08)	−5.37 (0.43)	0.68 (0.05)	11.13	−1.94	16.60	123	8.16	
0258+683	Lan 143	14,390 (364)	8.14 (0.10)	−4.08 (0.05)	0.68 (0.07)	11.60	−2.29	16.80	109	8.44	
0300−013	GD 40	14,620 (399)	7.99 (0.12)	−6.14 (1.58)	0.58 (0.07)	11.34	−2.17	15.56	69	8.32	
0308−565	L175-34	22,840 (2016)	8.07 (0.05)	$<$ −4.82 (3.04)	0.64 (0.03)	10.60	−1.43	14.07	49	7.63	2
0336+625	Lan 174	23,960 (2532)	8.09 (0.05)	−4.25 (1.40)	0.66 (0.03)	10.60	−1.36	17.15	203	7.57	
0349+015	KUV 03493+0131	24,860 (1936)	7.95 (0.05)	$<$ −4.59 (1.79)	0.58 (0.03)	10.39	−1.22	17.20	230	7.32	
0414−045	HE 0414−043	13,470 (334)	8.14 (0.10)	−5.61 (0.32)	0.68 (0.07)	11.76	−2.40	15.70	61	8.53	
0418−539	BPM 17731	19,090 (464)	8.10 (0.03)	$<$ −4.57 (0.20)	0.66 (0.02)	10.90	−1.77	15.32	76	8.00	2
0423−145	HE 0423−143	16,900 (401)	8.08 (0.07)	$<$ −5.98 (1.23)	0.64 (0.04)	11.12	−1.97	16.21	104	8.17	
0429−168	HE 0429−165	15,540 (415)	7.99 (0.15)	$<$ −6.35 (3.11)	0.59 (0.09)	11.20	−2.07	15.82	83	8.24	
0435+410	GD 61	16,790 (408)	8.18 (0.08)	−4.21 (0.07)	0.70 (0.05)	11.30	−2.04	14.86	51	8.26	
0437+138	LP 475-242	15,120 (361)	8.25 (0.07)	−4.68 (0.06)	0.75 (0.04)	11.65	−2.27	14.92	45	8.45	
0503+147	KUV 05034+1445	15,640 (382)	8.09 (0.06)	−5.46 (0.28)	0.65 (0.04)	11.33	−2.11	13.80	31	8.29	
0513+260	KUV 05134+2605	24,740 (1334)	8.21 (0.03)	−3.77 (0.34)	0.74 (0.02)	10.76	−1.38	16.70	154	7.67	1
0517+771	GD 435	13,150 (337)	8.13 (0.12)	−5.97 (0.76)	0.67 (0.08)	11.80	−2.44	16.01	69	8.55	
0615−591	L182-61	15,770 (373)	8.04 (0.04)	$<$ −6.32 (1.08)	0.61 (0.03)	11.23	−2.07	13.92	34	8.25	
0716+404	GD 85	17,150 (408)	8.08 (0.06)	$<$ −5.99 (1.28)	0.64 (0.04)	11.09	−1.95	14.94	58	8.16	
0825+367	CBS 73	16,100 (443)	8.10 (0.09)	$<$ −6.26 (2.47)	0.65 (0.06)	11.27	−2.07	17.00	139	8.26	
0835+340	CSO 197	22,230 (1348)	8.25 (0.05)	$<$ −4.63 (1.83)	0.76 (0.03)	10.89	−1.59	16.00	105	7.90	
0838+375	CBS 78	13,520 (553)	8.20 (0.49)	$<$ −6.54 (5.89)	0.71 (0.31)	11.83	−2.43	17.71	149	8.56	
0840+262	TON 10	17,700 (420)	8.28 (0.04)	−4.18 (0.06)	0.77 (0.03)	11.33	−2.01	14.78	49	8.26	
0840+364	CBS 82	21,260 (863)	8.15 (0.05)	$<$ −5.05 (2.60)	0.69 (0.03)	10.80	−1.61	17.03	176	7.86	
0845−188	L748-70	17,470 (418)	8.15 (0.06)	−6.00 (1.55)	0.69 (0.04)	11.16	−1.95	15.55	75	8.18	
0900+142	PG 0900+142	14,860 (351)	8.07 (0.09)	$<$ −6.43 (1.30)	0.63 (0.06)	11.43	−2.19	16.48	102	8.35	

TABLE 2.1 – Continued

WD	Name	$T_{\rm eff}$ (K)	log g	log H/He	$M/M_{\odot}$	M_V	log $L/L_{\odot}$	V	D(pc)	log τ	Notes
0902+293	CBS 3	18,610 (502)	8.02 (0.07)	< −5.60 (2.22)	0.60 (0.04)	10.82	−1.76	17.00	171	7.98	
0906+341	CBS 94	17,750 (480)	8.12 (0.13)	< −5.71 (2.35)	0.67 (0.09)	11.08	−1.91	17.00	152	8.14	
0921+091	PG 0921+092	19,470 (522)	8.01 (0.04)	−4.72 (0.43)	0.60 (0.03)	10.73	−1.68	16.19	123	7.90	
0948+013	PG 0948+013	16,810 (430)	8.09 (0.05)	−5.38 (0.29)	0.65 (0.03)	11.16	−1.99	15.59	76	8.19	
0954+342	CBS 114	26,060 (1797)	7.98 (0.06)	< −4.03 (0.49)	0.60 (0.03)	10.38	−1.15	17.20	231	7.25	1
1006+413	KUV 10064+4120	15,030 (465)	8.80 (0.19)	−5.18 (0.49)	1.08 (0.11)	12.66	−2.67	17.83	108	8.91	
1009+416	KUV 10098+4138	16,600 (456)	8.67 (0.07)	−5.43 (0.47)	1.01 (0.04)	12.17	−2.40	16.33	67	8.70	
1011+570	GD 303	17,610 (475)	8.16 (0.05)	−5.34 (0.28)	0.69 (0.03)	11.16	−1.95	14.57	48	8.18	
1026−056	PG 1026−057	18,080 (425)	8.11 (0.07)	< −5.86 (1.32)	0.66 (0.04)	11.03	−1.87	16.94	152	8.10	
1038+290	Ton 40	16,630 (390)	8.10 (0.07)	−5.86 (0.82)	0.66 (0.05)	11.20	−2.01	16.94	140	8.22	
1046−017	GD 124	14,620 (352)	8.15 (0.12)	< −6.46 (1.62)	0.68 (0.08)	11.57	−2.26	15.81	70	8.42	
1056+345	G119-47	12,440 (336)	8.23 (0.14)	−5.33 (0.23)	0.73 (0.10)	12.09	−2.60	15.58	49	8.69	
1107+265	GD 128	15,130 (357)	8.11 (0.06)	−5.77 (0.46)	0.65 (0.04)	11.43	−2.18	15.89	78	8.35	
1115+158	PG 1115+158	23,890 (1726)	7.91 (0.05)	−3.89 (0.46)	0.56 (0.03)	10.36	−1.26	16.12	142	7.37	1
1129+373	PG 1129+373	13,040 (358)	8.16 (0.16)	−6.08 (1.25)	0.69 (0.10)	11.87	−2.47	16.23	74	8.58	
1144−085	PG 1144−085	15,730 (377)	8.06 (0.06)	< −6.32 (1.37)	0.63 (0.04)	11.28	−2.09	15.95	86	8.27	
1148+408	KUV 11489+4052	17,530 (615)	8.34 (0.10)	−5.51 (0.88)	0.81 (0.06)	11.45	−2.06	17.33	150	8.33	
1149−133	PG 1149−133	20,370 (574)	8.30 (0.03)	−3.77 (0.13)	0.78 (0.02)	11.08	−1.78	16.29	109	8.08	
1200+249	PM J12033+2439	13,820 (363)	8.22 (0.13)	−5.20 (0.20)	0.73 (0.09)	11.82	−2.41	18.00	171	8.55	
1240+212	PM J12430+2057	14,390 (364)	8.06 (0.11)	< −6.37 (1.68)	0.62 (0.07)	11.48	−2.24	17.37	150	8.39	
1252−289	EC 12522-2855	21,880 (756)	8.03 (0.03)	< −4.82 (1.17)	0.62 (0.02)	10.59	−1.49	15.85	112	7.69	
1311+129	LP 497-114	22,440 (584)	7.90 (0.04)	−1.94 (0.11)	0.55 (0.02)	10.39	−1.37	16.26	149	7.51	
1326−037	PG 1326−037	19,950 (533)	8.03 (0.04)	< −4.81 (0.53)	0.61 (0.02)	10.71	−1.65	15.60	94	7.87	
1332+162	PB 3990	16,780 (419)	8.17 (0.06)	−5.08 (0.26)	0.70 (0.04)	11.28	−2.04	15.98	86	8.25	
1333+487	GD 325	15,420 (370)	8.01 (0.09)	−6.37 (1.66)	0.60 (0.05)	11.24	−2.09	14.02	35	8.27	
1336+123	LP 498-26	15,950 (405)	8.01 (0.07)	−6.29 (1.90)	0.60 (0.04)	11.17	−2.03	14.72	51	8.22	
1351+489	PG 1351+489	26,070 (1522)	7.91 (0.04)	< −4.42 (0.90)	0.56 (0.02)	10.28	−1.11	16.38	166	7.18	1
1352+004	PG 1352+004	13,980 (340)	8.05 (0.09)	−5.31 (0.17)	0.62 (0.06)	11.54	−2.29	15.72	68	8.42	
1403−010	G64-43	15,420 (372)	8.10 (0.06)	−6.08 (0.91)	0.65 (0.04)	11.37	−2.14	15.90	80	8.32	
1411+218	PG 1411+219	14,970 (369)	8.02 (0.07)	−6.26 (1.19)	0.60 (0.04)	11.32	−2.15	14.30	39	8.31	
1415+234	PG 1415+234	17,390 (478)	8.19 (0.06)	−5.08 (0.35)	0.71 (0.04)	11.23	−1.99	16.80	129	8.22	
1416+229	KUV 14161+2255	17,890 (444)	8.25 (0.12)	< −5.91 (2.21)	0.75 (0.08)	11.26	−1.97	16.60	117	8.22	
1419+351	GD 335	12,730 (620)	8.77 (0.40)	−5.19 (0.62)	1.06 (0.24)	12.98	−2.94	16.89	60	9.05	
1421−011	PG 1421−011	16,900 (411)	8.19 (0.07)	−4.28 (0.07)	0.71 (0.05)	11.30	−2.04	15.97	85	8.26	
1425+540	G200-39	14,410 (341)	7.89 (0.06)	−4.26 (0.03)	0.53 (0.04)	11.24	−2.14	15.04	57	8.29	
1444−096	PG 1444−096	17,030 (429)	8.26 (0.07)	−5.66 (0.91)	0.76 (0.04)	11.40	−2.07	14.98	52	8.30	
1445+152	PG 1445+153	20,420 (780)	8.05 (0.06)	< −5.24 (2.74)	0.63 (0.03)	10.71	−1.62	15.55	92	7.84	
1454−630	L151-81A	14,030 (334)	7.95 (0.07)	−4.83 (0.06)	0.56 (0.04)	11.39	−2.22	16.60	110	8.36	2
1456+103	PG 1456+103	24,050 (1206)	7.91 (0.06)	−3.27 (0.14)	0.55 (0.03)	10.35	−1.25	15.89	128	7.35	1
1459+821	G256-18	16,020 (397)	8.08 (0.06)	< −6.28 (1.59)	0.64 (0.04)	11.25	−2.06	14.78	50	8.25	
1540+680	PG 1540+681	22,240 (1304)	7.96 (0.04)	< −4.43 (0.89)	0.58 (0.02)	10.47	−1.42	16.19	139	7.58	
1542+182	GD 190	22,620 (978)	8.04 (0.02)	< −4.84 (1.41)	0.63 (0.01)	10.57	−1.44	14.72	67	7.62	
1542−275	LP 916-27	12,700 (384)	9.13 (0.14)	−4.99 (0.64)	1.26 (0.08)	13.70	−3.23	15.49	22	9.25	

TABLE 2.1 – Continued

WD	Name	$T_{\rm eff}$ (K)	log g	log H/He	$M/M_\odot$	M_V	log $L/L_\odot$	V	D(pc)	log τ	Notes
1545+244	Ton 249	12,850 (331)	8.19 (0.12)	−5.00 (0.11)	0.70 (0.08)	11.94	−2.51	15.78	58	8.61	
1551+175	KUV 15519+1730	15,280 (380)	7.80 (0.12)	−4.41 (0.08)	0.48 (0.06)	10.97	−1.99	17.50	202	8.15	
1557+192	KUV 15571+1913	19,510 (546)	8.15 (0.05)	−4.30 (0.26)	0.69 (0.03)	10.93	−1.76	15.40	78	8.01	
1610+239	PG 1610+239	13,280 (332)	8.13 (0.11)	−5.74 (0.42)	0.67 (0.07)	11.77	−2.42	15.34	51	8.53	
1612−111	GD 198	23,430 (1782)	7.96 (0.04)	$<$ −4.75 (2.10)	0.58 (0.02)	10.44	−1.33	15.53	104	7.46	
1644+198	PG 1644+199	15,210 (360)	8.14 (0.06)	−5.68 (0.39)	0.68 (0.04)	11.47	−2.19	15.20	55	8.37	
1645+325	GD 358	24,940 (1114)	7.92 (0.03)	$<$ −4.58 (0.88)	0.56 (0.01)	10.34	−1.19	13.65	45	7.28	1
1654+160	PG 1654+160	26,140 (1211)	7.91 (0.03)	$<$ −4.40 (0.64)	0.56 (0.02)	10.27	−1.10	16.55	180	7.17	1
1703+319	PG 1703+319	14,440 (360)	8.46 (0.10)	−5.54 (0.37)	0.88 (0.06)	12.10	−2.48	16.25	67	8.67	
1708−871	L7-44	23,980 (1686)	8.05 (0.03)	$<$ −4.69 (1.93)	0.63 (0.02)	10.55	−1.34	14.38	58	7.51	
1709+230	GD 205	19,590 (504)	8.08 (0.03)	−4.07 (0.14)	0.65 (0.02)	10.83	−1.71	14.90	65	7.95	
1726−578	L204-118	14,320 (340)	8.20 (0.06)	−5.46 (0.19)	0.71 (0.04)	11.70	−2.33	15.27	51	8.49	
1822+410	GD 378	16,230 (383)	8.00 (0.06)	−4.45 (0.06)	0.59 (0.04)	11.11	−2.00	14.39	45	8.19	
1919−362		23,610 (988)	8.10 (0.02)	−4.22 (0.44)	0.66 (0.01)	10.62	−1.40	13.60	39	7.61	
1940+374	L1573-31	16,850 (406)	8.07 (0.09)	−5.97 (1.50)	0.64 (0.06)	11.13	−1.97	14.51	47	8.18	
2034−532	L279-25	17,160 (403)	8.47 (0.05)	−5.78 (0.59)	0.89 (0.03)	11.73	−2.19	14.46	35	8.48	
2058+342	GD 392A	12,210 (447)	9.05 (0.21)	−5.18 (1.09)	1.22 (0.11)	13.64	−3.23	15.68	25	9.24	
2129+000	G26-10	14,350 (349)	8.25 (0.12)	$<$ −6.49 (1.65)	0.74 (0.08)	11.77	−2.36	15.27	50	8.52	
2130−047	GD 233	18,110 (426)	8.11 (0.07)	−5.79 (1.36)	0.66 (0.04)	11.02	−1.87	14.52	50	8.09	
2144−079	G26-31	16,340 (408)	8.18 (0.05)	$<$ −6.22 (1.45)	0.70 (0.03)	11.36	−2.09	14.82	49	8.30	
2147+280	G188-27	12,940 (399)	8.86 (0.19)	−5.74 (0.96)	1.11 (0.10)	13.10	−2.97	14.68	20	9.08	
2222+683	G241-6	14,920 (383)	8.00 (0.19)	$<$ −6.43 (2.84)	0.59 (0.12)	11.31	−2.15	15.65	73	8.31	
2229+139	PG 2229+139	14,870 (352)	8.15 (0.06)	−4.91 (0.08)	0.69 (0.04)	11.55	−2.24	15.99	77	8.41	
2234+064	PG 2234+064	23,770 (1770)	8.07 (0.03)	$<$ −4.72 (2.10)	0.65 (0.02)	10.58	−1.37	16.03	122	7.56	
2236+541	KPD 2236+5410	15,590 (379)	8.28 (0.07)	$<$ −6.34 (1.67)	0.77 (0.05)	11.63	−2.23	16.19	81	8.43	
2237−051	PHL 363	13,100 (460)	8.73 (0.24)	−4.87 (0.21)	1.04 (0.14)	12.83	−2.85	14.00	17	8.99	
2246+120	PG 2246+121	26,840 (1433)	7.92 (0.04)	$<$ −4.30 (0.65)	0.56 (0.02)	10.25	−1.06	16.73	197	7.13	1
2250+746	GD 554	16,560 (390)	8.15 (0.03)	$<$ −6.18 (0.68)	0.69 (0.02)	11.28	−2.05	16.69	120	8.26	
2253−062	GD 243	17,190 (436)	8.07 (0.09)	−4.35 (0.13)	0.64 (0.06)	11.07	−1.93	15.06	62	8.14	
2310+175	KUV 23103+1736	15,150 (370)	8.37 (0.07)	−5.38 (0.23)	0.82 (0.04)	11.84	−2.34	15.88	64	8.54	
2316−173	G273-13	12,640 (421)	9.11 (0.18)	−5.08 (0.87)	1.25 (0.10)	13.67	−3.22	14.08	12	9.24	
2328+510	GD 406	14,500 (362)	8.03 (0.16)	−6.47 (2.09)	0.61 (0.10)	11.43	−2.21	15.09	54	8.36	
2354+159	PG 2354+159	24,830 (1670)	8.15 (0.03)	$<$ −4.59 (1.78)	0.70 (0.02)	10.67	−1.34	15.78	105	7.58	

Notes. – (1) Variable white dwarf of the V777 Her class. (2) Hydrogen abundance based on Hβ.

have normal masses. As discussed by Bergeron et al., the high masses inferred for these cool DBA stars can probably be attributed to some inaccurate treatment of van der Waals broadening in our models (Beauchamp et al. 1996). We can also see a definite trend for the bulk of white dwarfs in our sample to show higher masses ($\sim$0.7 $M_{\odot}$) at low effective temperatures than at the hot end of the sample ($\lesssim$ 0.6 $M_{\odot}$).

2.3.2 Hydrogen in cool, He-rich DA stars

2.3.2.1 Spectroscopic and Photometric Observations

Because we are interested in studying the hydrogen abundance pattern in all helium-atmosphere white dwarfs below $T_{\rm eff} \sim 30,000$ K, we also need to extend our search to the cool end of the white dwarf sequence by including cool, helium-atmosphere DA and DZA stars such as L745-46A and Ross 640 discussed in the Introduction, which are usually found in the $\sim$8000–12,000 K temperature range. In general, the only hydrogen line visible in their spectra is Hα, which appears very broad and shallow as a result of van der Waals broadening. These He-rich DA white dwarfs can be easily distinguished from the much cooler ($T_{\rm eff} \lesssim 6000$ K), hydrogen-atmosphere DA stars in which the Hα absorption feature is much sharper (see, e.g., Figure 23 of Bergeron et al. 1997). The latter are also much redder photometrically.

With this idea in mind, we searched the Data Release 7 from the SDSS catalog of Kleinman et al. (2013) with $(g-r) < 0.5$, $(u-g) < 0.8$, and a magnitude cut-off of $g < 19.5$, and retained 28 He-rich DA white dwarf candidates, previously identified by P. Dufour (private communication). This sample is not complete in any sense, but it is considered representative of the hydrogen abundance pattern in cool, helium-rich atmospheres. These cool, He-rich DA stars can be analyzed using a hybrid photometric and spectroscopic technique, described in the next section, which requires *ugriz* photometry as well as optical spectra in the region around Hα. The *ugriz* photometry for our 28 SDSS white dwarfs was taken from Kleinman et al. (2013) while the corresponding spectra were retrieved from the SDSS database; these cover the 4000–9200 Å wavelength range, with an average signal-to-noise ratio of S/N $\sim$ 15.

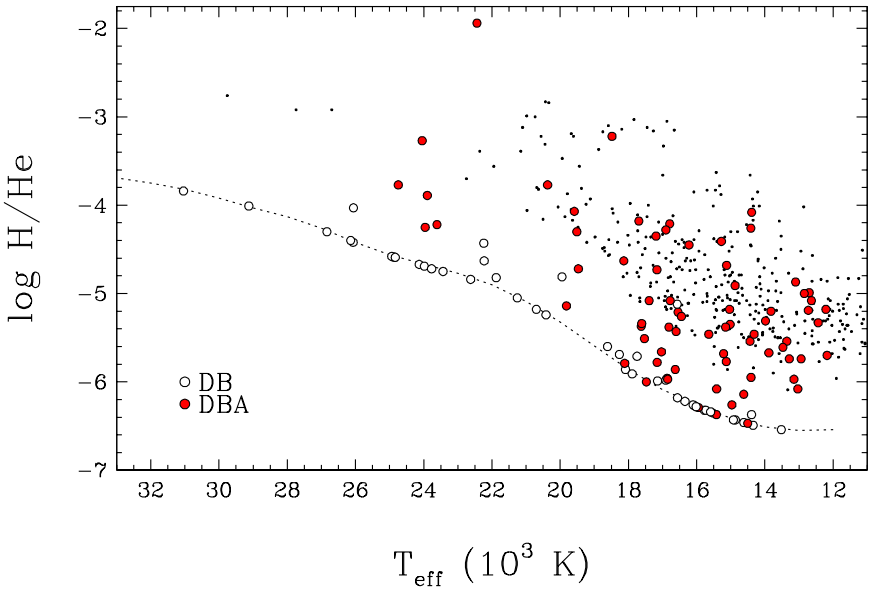

FIGURE 2.5 – Hydrogen-to-helium abundance ratio as a function of effective temperature for all DB (white symbols) and DBA (red symbols) white dwarfs in our sample. Limits on the hydrogen abundance set by our spectroscopic observations at Hα (200 mÅ equivalent width) are shown by the dotted line; the hydrogen abundances for DB stars thus represent only upper limits. Also shown as small dots are the results from Koester & Kepler (2015) for DBA white dwarfs (hydrogen detected) in the SDSS.

2.3.2.2 Model Atmosphere Analysis

An examination of the theoretical spectra displayed in Figure 2.3 reveals that the number of hydrogen and helium absorption lines that can be detected in the optical spectra of cool ($T_{\rm eff} \lesssim 12,000$ K), helium-dominated atmospheres becomes increasingly small. As a result, the spectroscopic technique alone fails to yield reliable measurements of the atmospheric parameters for such white dwarfs. In order to overcome this problem, we developed a hybrid approach that relies on both photometry and spectroscopy near the Hα region (see also Giammichele et al. 2012). The first step is based on the photometric technique developed by Bergeron et al. (1997, 2001), where the observed magnitudes are converted into average fluxes and compared to the predictions of model atmosphere calculations. Briefly, every magnitude m_λ is transformed into an average flux f_λ^m using the relation

$$m_\lambda = -2.5 \log f_\lambda^m + c_m \tag{2.1}$$

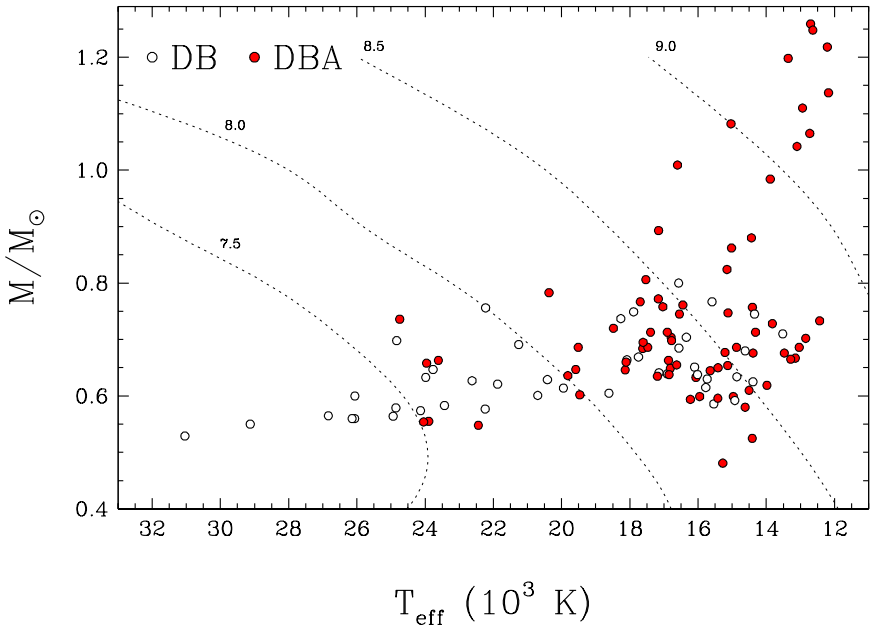

FIGURE 2.6 – Distribution of mass as a function of effective temperature for the 42 DB (white symbols) and 73 DBA (red symbols) white dwarfs in our sample. Also shown as dotted lines are the theoretical isochrones from our evolutionary models, labeled as $\log \tau$ where τ is the white dwarf cooling age in years.

where

$$f_\lambda^m = \frac{\int_0^\infty f_\lambda S_m(\lambda)\,\lambda\,d\lambda}{\int_0^\infty S_m(\lambda)\,\lambda\,d\lambda}\ , \tag{2.2}$$

f_λ is the monochromatic flux received at Earth from the star, c_m is a zero point calibration constant, and $S_m(\lambda)$ is the transmission function of the corresponding bandpass. The zero points and transmission functions are taken from Holberg & Bergeron (2006), where an expression similar to that above is also provided for the SDSS *ugriz* photometric system (AB_{95}). These average observed fluxes can then be compared with the model predictions using the relation

$$f_\lambda^m = 4\pi\,(R/D)^2\,H_\lambda^m \tag{2.3}$$

where R/D is the ratio of the radius of the star to its distance from Earth, and H_λ^m is the average model flux obtained by substituting f_λ in Equation 2.2 for the monochromatic

Eddington fluxes H_λ, which depend on the atmospheric parameters $T_{\rm eff}$, $\log g$, and H/He.

The fitting procedure relies on the Levenberg-Marquardt nonlinear least-square method where the χ^2 value is taken as the sum over all bandpasses of the difference between both sides of Equation 2.3, properly weighted by the corresponding observational uncertainties. Only $T_{\rm eff}$ and the solid angle $\pi\,(R/D)^2$ are considered free parameters at a fixed value of the hydrogen abundance. In principle, trigonometric parallax measurements can be used to constrain the $\log g$ value, but since no such data is available for our sample of cool, He-rich DA white dwarfs from the SDSS, we simply assume $\log g = 8$ throughout. When a satisfactory fit to the energy distribution is reached at some initial value of the hydrogen abundance, the resulting values of $T_{\rm eff}$ and $\log g$ are then used to measure the hydrogen-to-helium abundance ratio (H/He) by fitting the Hα spectroscopic data using the same fitting procedure as that described above for the DBA white dwarfs. The entire procedure is then repeated iteratively until a consistent set of $T_{\rm eff}$, $\log g$, and H/He values is reached. Because the limits on the hydrogen abundance depend on the S/N of the observations at Hα, and that the average S/N of our cool white dwarf sample from the SDSS is $\sim$5.4 times lower than the average of our hotter DB sample, we adopt a detection limit of 1100 mÅ for the equivalent width of Hα.

2.3.2.3 Selected Results

Our fits to the 28 cool, He-rich DA white dwarfs in the SDSS sample are displayed in Figure 2.7. The main panels show the photometric fits to the observed *ugriz* energy distributions, while the insets show the corresponding spectroscopic fits in the region covering Hα and He I λ5876. Since it also possible that some of these objects could be unresolved DA+DC white dwarf binaries, we also made sure that our solutions are consistent with the observed spectra in the blue portion of the spectrum (Hβ and blueward), within the signal-to-noise of the observations. The atmospheric parameters for all objects, assuming a value of $\log g = 8$, are provided in Table 2.2, together with the same information as in Table 2.1, with the exception that the absolute magnitude is given here for the g filter (M_g). We also added a note for possible DA+DC systems.

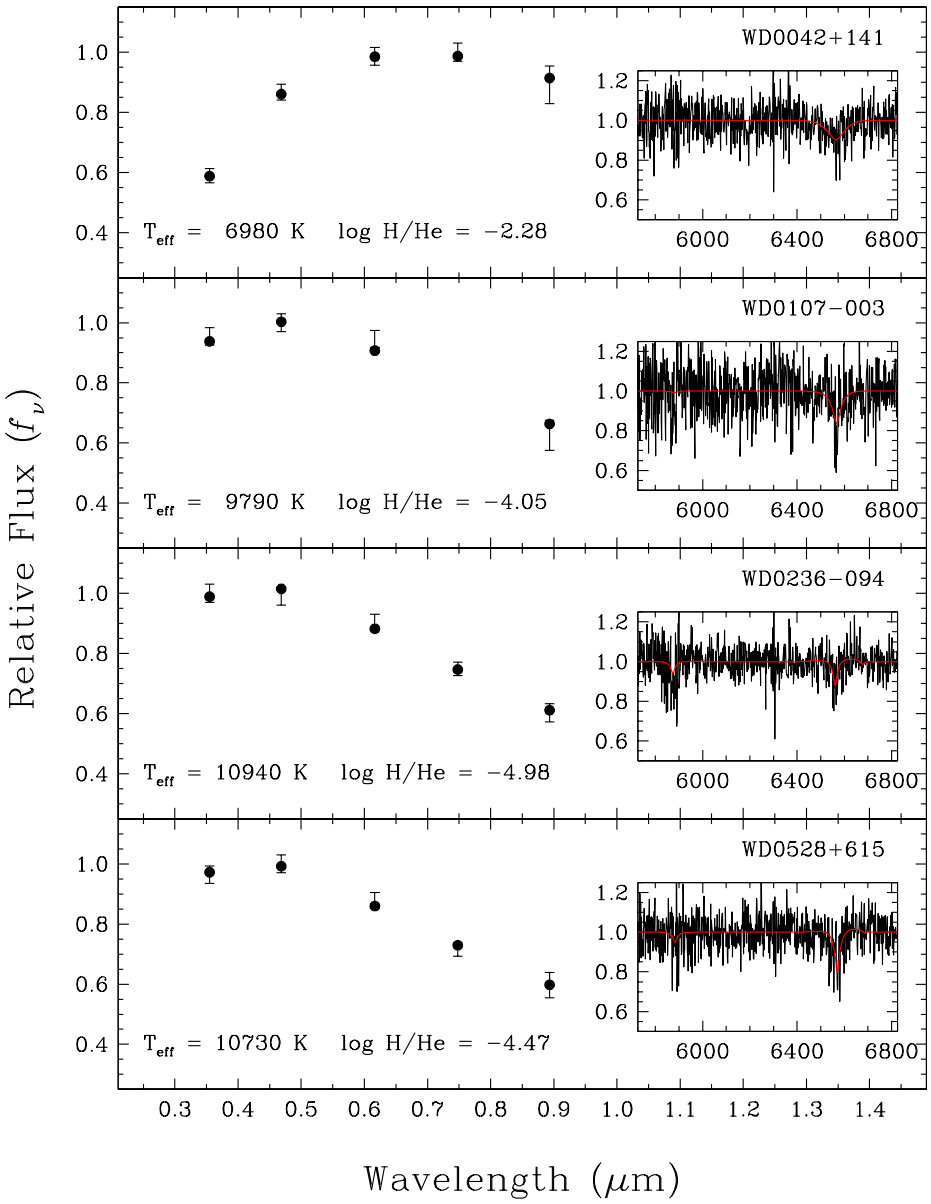

FIGURE 2.7 – Fits obtained from the hybrid fitting method for cool, He-rich DA stars with homogeneous models at $\log g = 8$. The *ugriz* photometric observations are represented by error bars, while the model fluxes are shown by filled circles. The inset shows our fit to the spectrum near the Hα region, normalized to a continuum set to unity, which is used to measure the hydrogen abundance.

TABLE 2.2 – Atmospheric Parameters of Cool, He-rich DA White Dwarfs

WD	Name	$T_{\rm eff}$ (K)	log g	log H/He	$M/M_{\odot}$	M_g	log $L/L_{\odot}$	g	D(pc)	log τ	Notes
0042+141	SDSS J004513.88+142248.1	6980 (197)	8.00	−2.28 (0.13)	0.57	13.68	−3.48	19.20	126	9.19	
0107−003	SDSS J011012.48−000313.5	9790 (434)	8.00	−4.05 (0.23)	0.58	12.34	−2.88	19.38	255	8.82	
0236−094	SDSS J023856.77−092653.6	10,940 (463)	8.00	−4.98 (0.26)	0.58	12.00	−2.69	18.43	193	8.69	
0528+615	SDSS J074250.80+222444.7	10,730 (462)	8.00	−4.47 (0.20)	0.58	12.05	−2.72	19.27	277	8.71	
0739+225	SDSS J074250.80+222444.7	8330 (236)	8.00	−3.44 (0.30)	0.58	12.93	−3.17	19.13	173	9.01	
0748+314	SDSS J075113.24+313249.4	11,490 (550)	8.00	−4.72 (0.09)	0.58	11.85	−2.60	19.19	293	8.63	
0829+532	SDSS J083317.40+531335.5	11,350 (534)	8.00	−4.76 (0.16)	0.58	11.89	−2.62	18.82	243	8.65	
0838+204	SDSS J084113.94+203018.7	8980 (277)	8.00	−3.39 (0.17)	0.58	12.65	−3.04	18.66	159	8.92	
0844+364	SDSS J084757.57+362649.1	9400 (303)	8.00	−3.60 (0.24)	0.58	12.48	−2.96	19.46	248	8.86	
0859+094	SDSS J090150.74+091211.3	8320 (218)	8.00	−2.71 (0.20)	0.58	12.94	−3.17	18.60	135	9.01	
1023+142	SDSS J102626.01+135745.0	8780 (255)	8.00	−3.44 (0.22)	0.58	12.73	−3.07	18.92	172	8.94	
1157+072	SDSS J115948.51+070708.7	9940 (328)	8.00	−4.61 (0.18)	0.58	12.30	−2.86	17.55	112	8.80	
1203+343	SDSS J120555.16+341813.4	11,330 (445)	8.00	−5.31 (0.15)	0.58	11.89	−2.63	18.29	190	8.65	
1246+021	SDSS J124909.03+015559.3	7350 (176)	8.00	−2.38 (0.14)	0.57	13.45	−3.38	18.84	119	9.13	
1307+454	SDSS J130916.90+452342.6	9750 (325)	8.00	−3.82 (0.17)	0.58	12.36	−2.89	18.82	195	8.82	
1345+513	SDSS J134710.47+511640.8	9280 (263)	8.00	−3.46 (0.16)	0.58	12.53	−2.98	18.49	155	8.88	
1409+114	SDSS J141209.94+112902.6	7280 (162)	8.00	−2.12 (0.15)	0.57	13.49	−3.40	18.65	107	9.14	
1412−009	SDSS J141516.10−010912.1	8520 (225)	8.00	−3.25 (0.17)	0.58	12.85	−3.13	18.26	120	8.98	1
1506+017	SDSS J150856.93+013557.0	8060 (186)	8.00	−3.30 (0.15)	0.58	13.07	−3.22	17.98	96	9.04	
1519+397	SDSS J152145.91+393128.1	7980 (182)	8.00	−2.95 (0.17)	0.58	13.11	−3.24	18.54	122	9.05	
1556+110	SDSS J155903.81+105614.8	8530 (213)	8.00	−2.87 (0.15)	0.58	12.84	−3.12	18.52	136	8.98	1
1558+077	SDSS J160053.84+074803.4	6870 (155)	8.00	−2.14 (0.14)	0.57	13.76	−3.50	19.39	133	9.22	1
1617−003	SDSS J161948.91+003445.3	10,440 (359)	8.00	−4.23 (0.18)	0.58	12.14	−2.77	17.88	140	8.75	
1623+222	SDSS J162535.21+221516.4	8620 (242)	8.00	−3.52 (0.18)	0.58	12.80	−3.11	18.75	154	8.97	2
1625+305	SDSS J162721.62+304320.2	8460 (224)	8.00	−3.60 (0.23)	0.58	12.87	−3.14	18.74	149	8.99	
1644+202	SDSS J164645.22+200701.5	9370 (311)	8.00	−3.91 (0.20)	0.58	12.49	−2.96	19.37	237	8.87	
2116+110	SDSS J211852.10+111756.5	11,080 (412)	8.00	−5.37 (0.19)	0.58	11.96	−2.67	16.66	87	8.68	
2134+112	SDSS J213621.56+113726.8	11,390 (521)	8.00	−4.61 (0.16)	0.58	11.88	−2.62	18.29	191	8.64	

(1) Possible unresolved DA+DC degenerate binary. (2) g band omitted during atmospheric parameter determination.

The hydrogen abundances as a function of effective temperature for all cool, He-rich DA white dwarfs in our sample are displayed in Figure 2.8, together with our spectroscopic results for the DB and DBA stars; also shown are the limits on the hydrogen abundance for both subsamples. For completeness, we reproduce in this figure the results of Dufour et al. (2007a) for the DZA white dwarfs from the SDSS, for which the hydrogen abundances have been determined spectroscopically, as well as the three bright DZA stars from Giammichele et al. (2012). The location of our cool, He-rich DA stars and DZA white dwarfs in this plot indicates that these two populations are very alike. They cover essentially the same range of hydrogen abundances, with a similar dispersion, and most importantly, they display the same behavior with respect to effective temperature. Note that cool, He-rich DA/DZA white dwarfs most certainly exist below the detection threshold at Hα displayed in Figure 2.8, although objects with very large hydrogen abundances have not been found in our analysis. Since hydrogen has been detected — or inferred — in 27% of the DZ stars analyzed by Dufour et al. (2007a), our results suggest, as a conservative estimate, that the cool, He-rich DA white dwarfs represent around 25% of the total DC population below ∼12,000 K, at least in the range of temperature where Hα can be detected in helium-rich atmospheres ($T_{\rm eff} \gtrsim 6000$ K).

The results displayed in Figure 2.8 represent the best picture we have so far of the hydrogen abundance pattern in helium-atmosphere white dwarfs below $T_{\rm eff} \sim 30,000$ K, both in terms of the quality of the photometric and spectroscopic data currently available to us, but also in terms of model atmospheres and fitting techniques. Any viable model of the spectral evolution of white dwarfs involving the convective dilution — or mixing — of the thin hydrogen layer with the deeper helium envelope, or accretion from the interstellar medium or other external bodies, must be able to account self-consistently for the observed hydrogen abundance pattern depicted in Figure 2.8.

2.4 Model Envelope Structures

In the absence of competing mechanisms, gravitational settling would gradually make the hydrogen present in DBA white dwarfs and cool, He-rich DA/DZA stars float up to the surface, resulting in the creation of a hydrogen-dominated atmosphere in a time frame much smaller

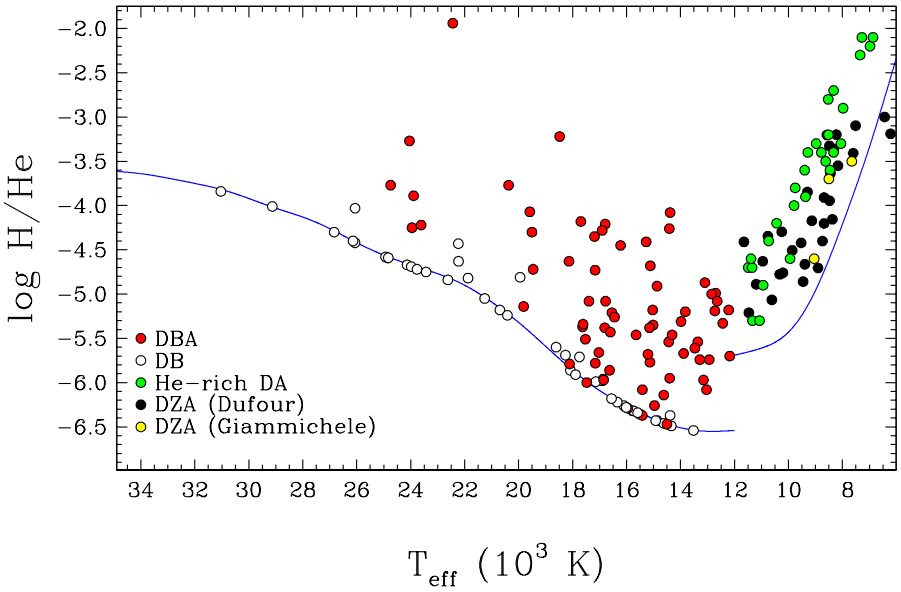

FIGURE 2.8 – Hydrogen-to-helium abundance ratio as a function of effective temperature for all DB, DBA, and cool, He-rich DA white dwarfs in our SDSS sample; the DZA stars from Dufour et al. (2007a) and Giammichele et al. (2012) are also displayed. The hydrogen detection limits at Hα are indicated by blue lines for the subsamples above and below $T_{\rm eff} = 12,000$ K.

than the typical white dwarf cooling time. In the temperature range considered here ($T_{\rm eff} \lesssim 30,000$ K), however, convective energy transport within the thick helium envelope is the main mechanism competing with element diffusion, and hydrogen is thus expected to be thoroughly mixed within the helium convection zone, resulting in a helium-dominated atmosphere with a homogeneous H/He abundance profile. As discussed in the Introduction, the progenitors of some of the DB white dwarfs are probably DA stars with sufficiently thin radiative hydrogen layers, of the order of $M_{\rm H} \sim 10^{-15}\ M_{\odot}$, which are transformed into helium-atmosphere white dwarfs as a result of the *convective dilution* of this thin hydrogen layer with the deeper and more massive convective helium envelope. Cool ($T_{\rm eff} \lesssim 12,000$ K), helium-atmosphere white dwarfs that show only traces of hydrogen (and sometimes metals), on the other hand, could be interpreted as DBA stars that have simply cooled off, or alternatively, they could also be interpreted as the result of convectively mixed DA stars, when the bottom of the hydrogen convection zone in a DA white dwarf eventually reaches the underlying and more massive

convective helium envelope, resulting in the *convective mixing* of the hydrogen and helium layers, a process believed to occur when the hydrogen layer mass is in the range $M_{\rm H} \sim 10^{-14} - 10^{-6}\ M_{\odot}$.

The structure of both types of DA progenitors described above is thus a thin hydrogen layer — convective or not — sitting on top of a massive helium envelope. To describe these structures, as well as the homogeneously mixed hydrogen and helium structures, we make use of the latest version of the Montréal white dwarf model-building code in its envelope mode (see Brassard & Fontaine 1994 for a first description). This code uses the same input physics as the full evolutionary models described at length in Fontaine et al. (2001), but with updates discussed briefly in Giammichele et al. (2016). Models with both homogeneously mixed and chemically stratified compositions have been computed for a large set of effective temperatures, stellar masses, and assumed convective efficiencies. These are described in turn.

2.4.1 Homogeneously Mixed Composition Models

Our static, homogeneously mixed models are characterized by $q(\mathrm{env}) \equiv M_{\rm env}/M_{\star} = 10^{-2}$ — which are representative of helium-rich white dwarfs — with a homogeneous hydrogen and helium abundance profile from the surface to the bottom of the stellar envelope. Note that the presence of hydrogen uniformly distributed below the mixed H/He convection zone may not be very realistic, but, importantly, it does not affect in any way the location of the bottom of this convection zone in our structures. We use these models below to compute the mass of hydrogen contained in the convection zone only. Our homogeneous grid covers a range of effective temperature between $T_{\rm eff} = 60,000$ K and 30,000 K by steps of 500 K, and between $T_{\rm eff} = 30,000$ K and 4000 K by steps of 50 K. The hydrogen mass fraction in the envelope ranges from $\log X = -8.5$ to -2.5 by steps of 0.5 dex, and from $\log X = -2.50$ to 0.35 with a varying mesh between 0.20 or 0.25 dex. We also explore the so-called ML2/$\alpha = 0.6$ and $\alpha = 2$ parameterizations of the mixing-length theory to treat convective energy transport. These two values bracket the convective efficiencies mostly used in the context of white dwarf atmospheres and envelopes (see, e.g., Tassoul et al. 1990; Tremblay et al. 2015).

Envelope structures for various hydrogen-to-helium abundance ratios (H/He), stellar masses,

and convective efficiencies, are displayed in Figures 2.9 and 2.10 for ML2/$\alpha = 0.6$ and $\alpha = 2$ models, respectively. The extent of the convection zones (color coded with the fraction of the total flux carried out by convection) as well as the location of the photosphere are indicated in each panel. The smallest and largest hydrogen abundances illustrated here correspond to almost pure helium and pure hydrogen compositions, respectively, in terms of their structures. In the most helium-rich models with ML2/$\alpha = 0.6$, a small convection zone is present at high temperatures, due to the partial ionization of He II, but with only ∼1% of the flux transported by convection; the depth of this convection zone is significantly larger with $\alpha = 2$, with a much larger fraction of the total flux being transported by convection. Below $T_{\rm eff} \sim 28,000$ K, a second, more superficial, convection zone appears, due this time to the partial ionization of He I. Eventually, both convection zones merge below ∼25,000 K. As the hydrogen content is increased, the temperature at which these two convection zones merge decreases, and another convection zone develops due to the partial ionization of hydrogen (mixed with the superficial helium convection zone), which appears as a bump at the top of the convection zone near 16,000 K in the models with $\log {\rm H/He} \gtrsim +0.26$ shown in Figures 2.9 and 2.10. In addition, we note that the increase in hydrogen content gradually delays the development of the deep, mixed H/He convection zone. At the largest hydrogen abundances illustrated here, the convection zone due to the partial ionization of He II at high temperatures is also totally suppressed. Finally, in the range of effective temperatures and hydrogen abundances where DBA white dwarfs are found in our sample ($T_{\rm eff} \sim 12,000 - 30,000$ K, $\log {\rm H/He} < -4$), the structure of the helium convection zone remains unaffected by the presence of hydrogen. In this particular temperature range, hydrogen starts to affect the structure of the convection zone only above $\log {\rm H/He} \sim -3.4$.

For the cooler envelope models ($T_{\rm eff} \lesssim 10,000$ K) displayed in Figures 2.9 and 2.10 — more representative of the cool, He-rich DA stars analyzed above — the situation is somewhat different. First, we note that the top of the convection zone, which coincides with the location of the photosphere, becomes increasingly deeper in cooler models as a result of the decrease in total opacity. Since neutral helium is particularly transparent with respect to hydrogen at low temperatures ($T_{\rm eff} \lesssim 6000$ K), the location of the photosphere and the top of the convection

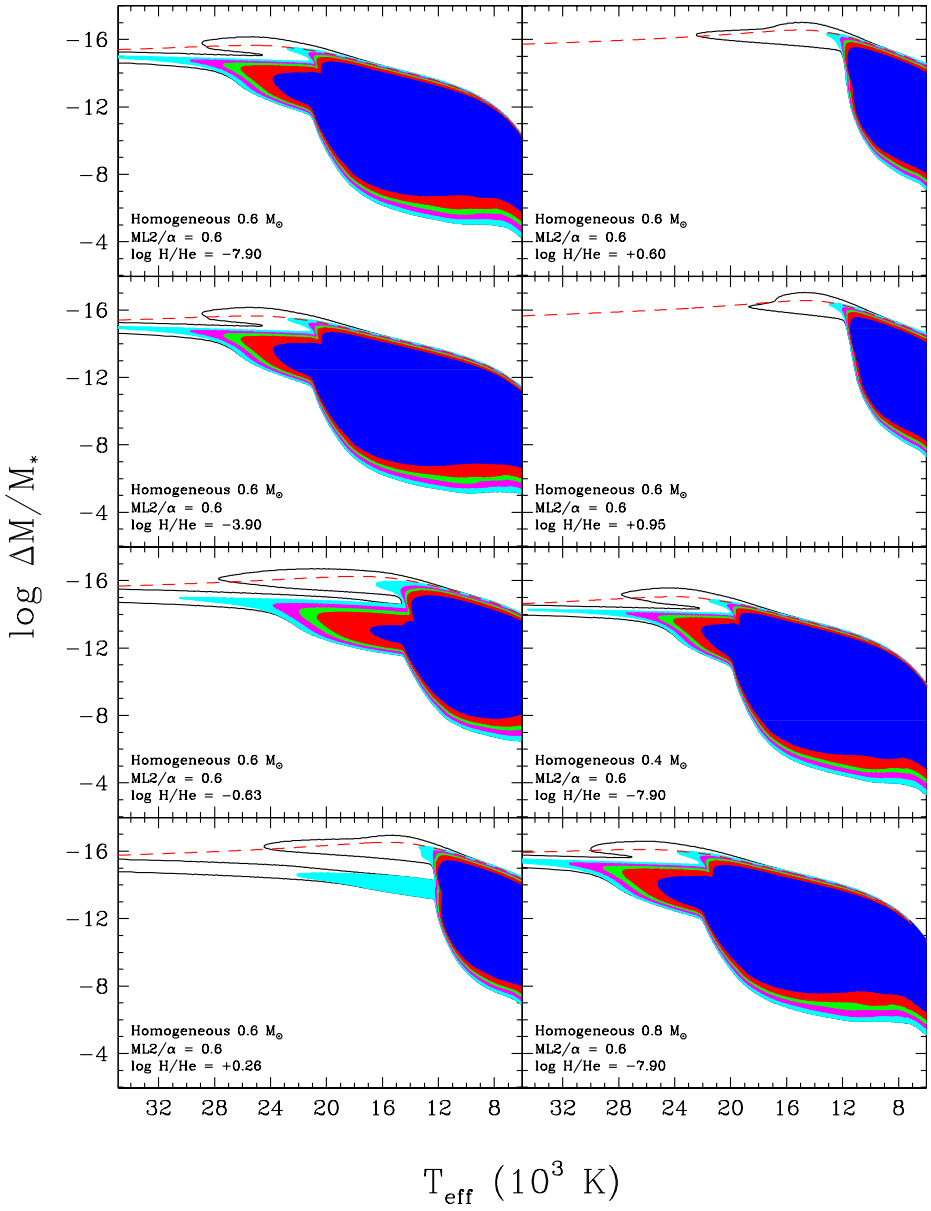

FIGURE 2.9 – Examples of envelope structures for white dwarf models with homogeneously mixed compositions as a function of effective temperature. The depth is expressed as the fractional mass above the point of interest with respect to the total mass of the star. The models illustrated here are (from upper left to bottom right) for 0.6 $M_{\odot}$ with increasing hydrogen abundances, with the exception of the last two panels that show the results at 0.4 and 0.8 $M_{\odot}$ for an almost pure helium composition, and they all assume a ML2/$\alpha = 0.6$ parameterization of the convective efficiency. The red dashed line corresponds to the location of the photosphere, while the contours with various colors represent the convection zones with 0.1, 1, 50, 75, 85, and 95% of the total flux being transported by convection.

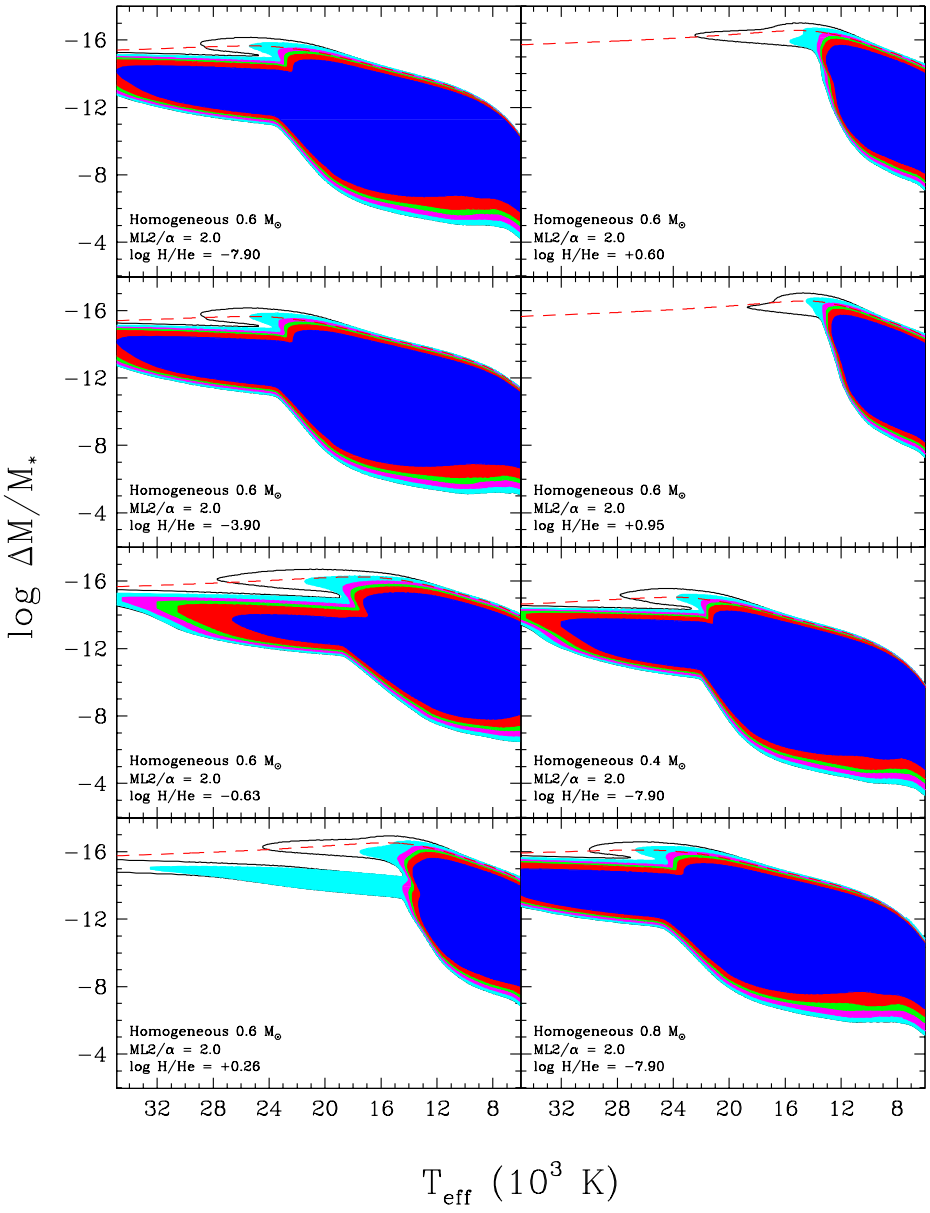

FIGURE 2.10 – Same as Figure 2.9 but for models assuming a ML2/$\alpha = 2$ parameterization of the convective efficiency.

zone are orders of magnitude deeper (when expressed in fractional mass) in the cool, hydrogen-poor models than in the hydrogen-rich models. The effect on the location of the bottom of the mixed H/He convection zone is also significant.

As discussed above, the behavior of the ML2/$\alpha = 2$ models displayed in Figure 2.10 are qualitatively similar to the ML2/$\alpha = 0.6$ models, with the notable exception that at a given effective temperature, the mixed H/He convection zone extends significantly deeper in the star. This implies that for a given hydrogen-to-helium abundance ratio observed at the photosphere, a larger hydrogen mass will be inferred using models with more efficient convection. Below roughly 10,000 K, however, convection becomes adiabatic and both sets of envelope structures are identical at the bottom of the convection zone. We also note that the assumed convective efficiency has a negligible effect at the surface. Finally, an examination of our almost pure helium models at 0.4 and 0.8 $M_{\odot}$ reveals that the He II convection zone starts to plunge into the star at higher temperatures in more massive white dwarfs — $T_{\rm eff} \sim 30,000$ K at 0.8 $M_{\odot}$ compared to ∼25,000 K at 0.4 $M_{\odot}$ — but the convection zone in the more massive models does not extend as deep below ∼20,000 K. Since these differences remain small, we find it reasonable to assume only 0.6 $M_{\odot}$ models in our discussion of the various evolutionary scenarios described below.

2.4.2 Stratified Composition Models

Our static, stratified composition models are characterized again by thick stellar envelopes of $q(\mathrm{env}) = 10^{-2}$, but composed this time of a pure hydrogen envelope in diffusive equilibrium on top of a deeper helium mantle. This stratified model grid covers the same range of effective temperature as before, and the hydrogen layer mass varies between $\log q(\mathrm{H}) = \log M_{\mathrm{H}}/M_{\star} = -17.4$ and -4.0 by steps of 0.5 dex. Examples of these stratified models are displayed in Figures 2.11 and 2.12 for various values of $q(\mathrm{H})$, stellar masses, and convective efficiencies. Note that in these models, the hydrogen layer is forced to remain in diffusive equilibrium on top of the helium layer, and is thus never allowed to mix with the underlying helium envelope, which of course may not be physically realistic in some cases.

In the thinnest hydrogen layer sequence displayed here, $\log q(\mathrm{H}) = -16.43$, the structure of

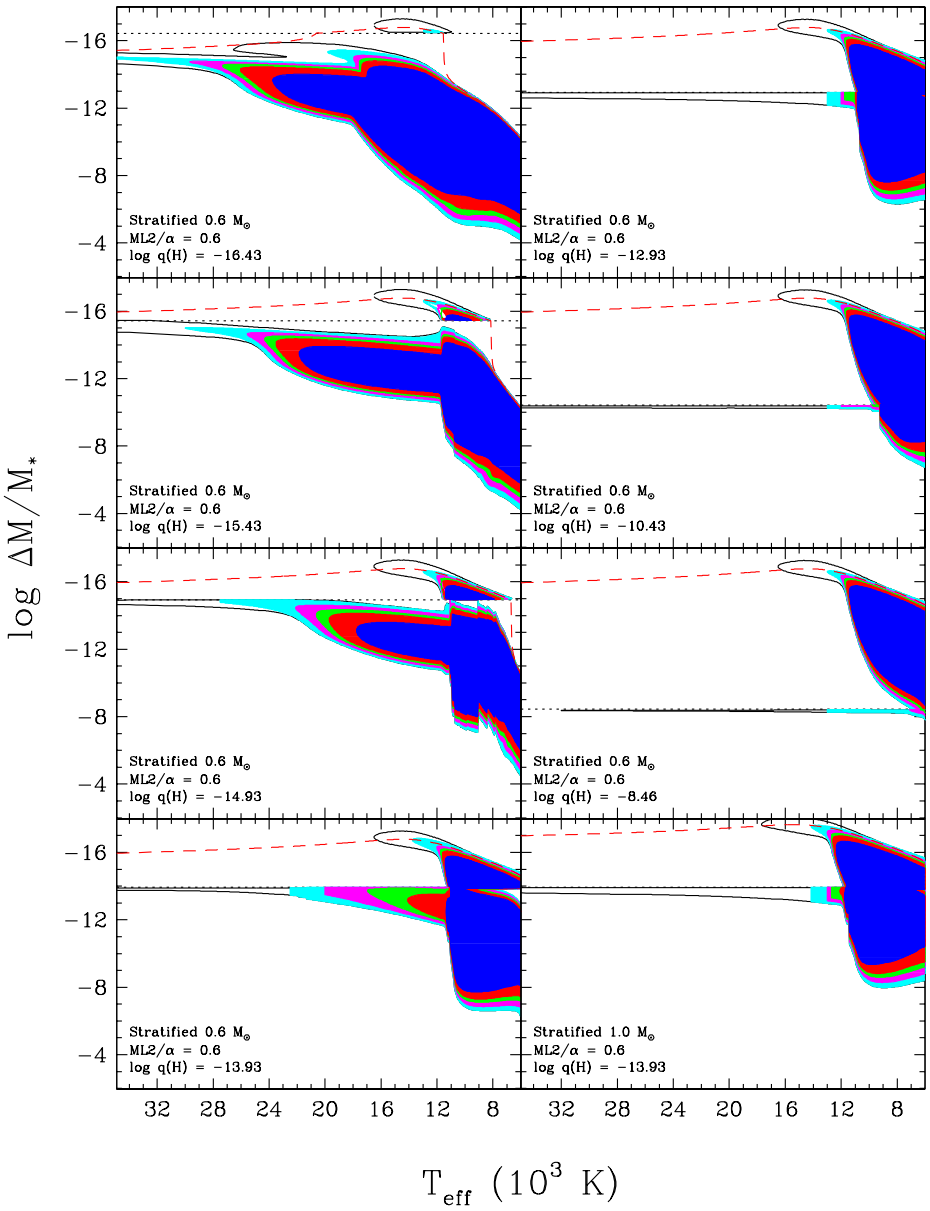

FIGURE 2.11 – Same as Figure 2.9 but for stratified models. The models illustrated here are for 0.6 $M_\odot$ with increasing thickness of the hydrogen layer (from upper left to bottom right) expressed as $\log q(\mathrm{H}) = \log M_\mathrm{H}/M_\star$, with the exception of the bottom right panel that shows the results at 1.0 $M_\odot$ and $\log q(\mathrm{H}) = -13.93$ — i.e., the same value of $\log q(\mathrm{H})$ as the panel to the left. The value of $\log q(\mathrm{H})$ is indicated by a black dotted line in each panel. The results shown here assume a ML2/$\alpha = 0.6$ parameterization of the convective efficiency.

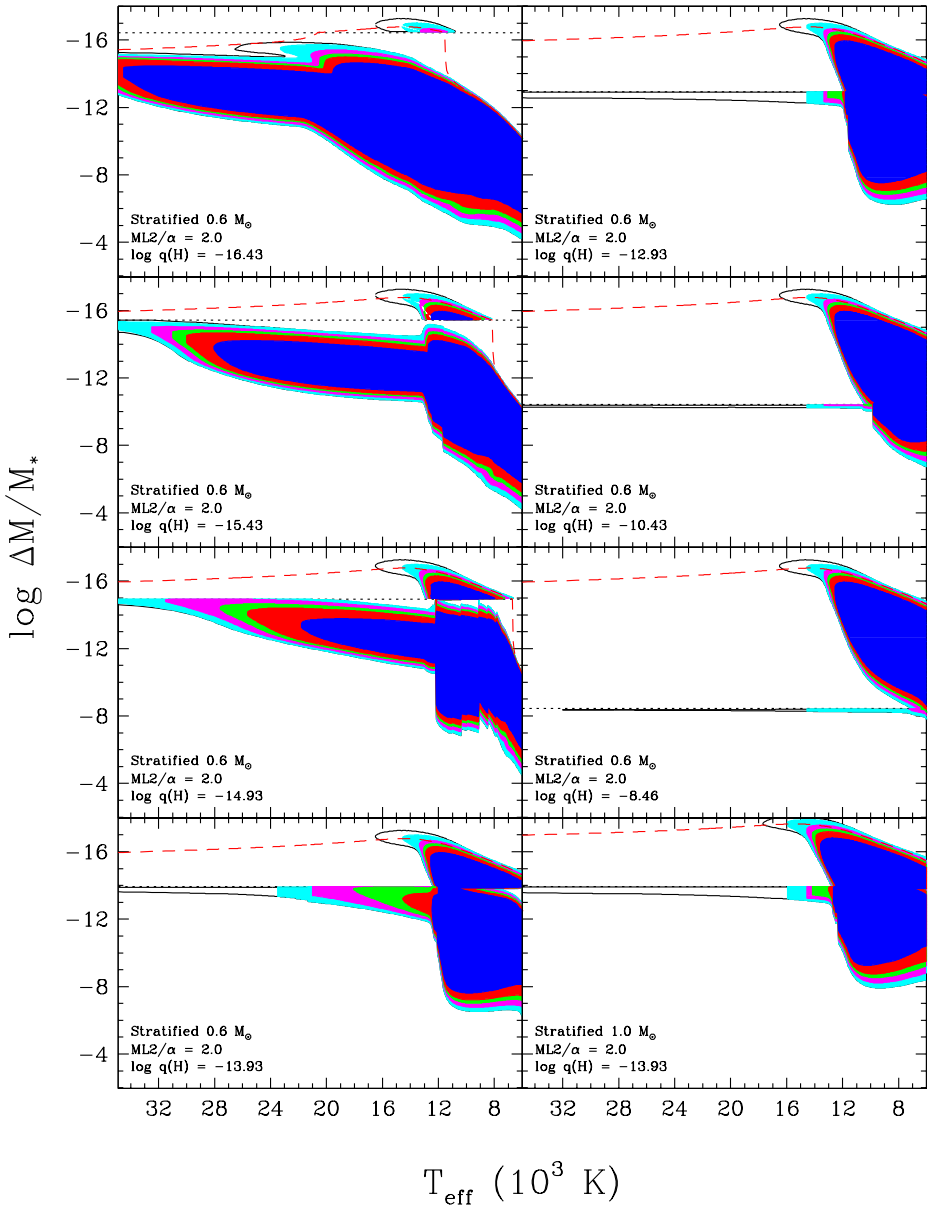

FIGURE 2.12 – Same as Figure 2.11 but for models assuming a ML2/$\alpha = 2$ parameterization of the convective efficiency.

the helium convection zone above $T_{\rm eff} \sim 20,000$ K is nearly identical to the almost pure helium sequences shown in Figures 2.9 and 2.10. In cooler models, however, even the presence of a small amount of hydrogen at the surface of the star affects the location of the bottom of the helium convection zone, although such thin hydrogen layers would have certainly been convectively diluted by the helium convection zone at higher effective temperatures. As the thickness of the hydrogen layer is increased, the extent of the helium convection zone is significantly reduced at high temperatures ($T_{\rm eff} \gtrsim 15,000$ K), to the point that it is conceivable that the hydrogen layer in these models always remains in diffusive equilibrium on top of the helium envelope — when $\log q({\rm H}) = -13.93$ for instance — at least until the star cools down to $T_{\rm eff} \sim 12,000$ K or so, where *convective mixing* might occur.

Indeed, below $T_{\rm eff} \sim 16,000$ K, a small hydrogen convection zone starts to develop at the surface of these models. At lower effective temperatures, the bottom of the hydrogen convection zone becomes deeper, eventually reaching the underlying helium convection zone. At this point, it is believed that the hydrogen layer will be thoroughly mixed with the deeper and more massive helium convection zone, resulting in homogeneous H/He convective envelope structures, such as those illustrated in Figures 2.9 and 2.10. Furthermore, the temperature at which this mixing process occurs, and the resulting hydrogen-to-helium abundance ratio at the photosphere, will be a strongly dependent function of the thickness of the hydrogen layer of the DA progenitor — the thicker the hydrogen envelope, the lower the mixing temperature. Note that according to the models shown here, a DA star is never expected to mix if $\log q({\rm H}) \gtrsim -6$, which corresponds to the maximum depth of the hydrogen convective zone.

As for the homogeneous models, both the hydrogen and the helium convection zones extend much deeper at a given effective temperature in the models assuming the ML2/$\alpha = 2$ convective efficiency, shown in Figure 2.12. The most important consequence in the present context is that the convective mixing process will occur at higher effective temperatures in more efficient models. Finally, the effect of mass is illustrated in the bottom right panel of Figures 2.11 and 2.12 where we show the results at 1.0 $M_{\odot}$ and $\log q({\rm H}) = -13.93$, which can be directly compared with the left panel at 0.6 $M_{\odot}$ with the same value of $\log q({\rm H})$. For a fixed value of $\log q({\rm H})$, all convection zones are shifted upward in the more massive models;

remember that $\log q(\mathrm{H}) \equiv \log M_{\mathrm{H}}/M_{\star}$ is scaled with respect to the mass of the star, so a given value of $\log q(\mathrm{H})$ implies a more massive hydrogen layer in a more massive star. Consequently, the extent of the helium convection zone at high temperatures is much smaller, but more importantly in the present context, the effective temperature at which the hydrogen convection zone connects with the helium convective envelope is about $\sim$500 K higher.

2.4.3 Total Hydrogen Mass

We now attempt to estimate the total mass of hydrogen present in a given helium-atmosphere white dwarf, after the superficial hydrogen layer has been thoroughly diluted — or convectively mixed — with the underlying helium envelope. Our working assumption is that *all* available hydrogen is found in a region covering the superficial convection zone extended below by a diffusion tail that must be created as the result of ordinary diffusion. As discussed in Section 2.4.1, our homogeneously mixed models are perfectly suitable to estimate the mass of hydrogen contained in the convection zone. We recall in this context that the presence of hydrogen below the mixed H/He convection zone — and in particular the way it is distributed in these regions — does not affect in any way the location of the bottom of this convection zone in our structures.

Next, the ratio R of the mass of hydrogen contained in the diffusive tail over that contained in the convection zone can be estimated analytically following the approach of Vennes et al. (1988). Under the assumptions that 1) diffusive equilibrium has been reached, and 2) hydrogen is a trace species (H $\ll$ He) in the convection zone, one can show that,

$$R = \frac{A_1}{A_1 Z_2 - A_2(Z_1 + 1)}, \tag{2.4}$$

where A_1 (Z_1) is the atomic weight (average charge) of the dominant element (helium here), and A_2 (Z_2) is the atomic weight (average charge) of hydrogen at the bottom of the convection zone. Under conditions of most interest here, hydrogen is completely ionized at the bottom of the convection zone ($Z_2 = 1$) while helium is nearly so ($Z_1 \simeq 2$). Taking $A_1 = 4$ and $A_2 = 1$, one finds $R \simeq 4$, i.e., there is four times more hydrogen "hidden" in the diffusion tail than present in the convection zone.

This value of R is necessarily an upper limit because of the following circumstances. First, if helium is not completely ionized, the diffusion tail is steeper and contains less hydrogen. For instance, assuming that $Z_1 = 1$ (He II), one finds $R = 2$. Second, the neglect of thermal diffusion in our derivation leads also to an overestimate of R as the diffusion tail would again be steeper otherwise. Third, the assumption of complete diffusive equilibrium may not be fully justified in the deeper regions of the diffusion tail as the diffusion timescale there may not be negligible anymore in front of the cooling timescale. And fourth, residual nuclear burning around $\log q \sim -4$ also limits the extension of the diffusion tail and its hydrogen content. In practice, we assume somewhat arbitrarily in the remainder of our analysis that $R = 2$. Hence, the total amount of hydrogen, $M_{\rm H}$, is equal to that measured in the convection zone with our uniformly mixed models multiplied by $(1 + R)$.

Under these assumptions, it is now possible to calculate the total mass of hydrogen contained in our grid of homogeneous models at various effective temperatures as a function of the observed photospheric hydrogen abundance H/He. The results are summarized in Figure 2.13 where we show, for the two convective efficiencies explored in our analysis, the total hydrogen mass contained in the model as a function of H/He at various effective temperatures ranging from $T_{\rm eff} = 6000$ K to 40,000 K. An illustrative example for a total hydrogen mass of $M_{\rm H} = 10^{-13}\ M_{\odot}$ is also indicated by a red dashed line. For this particular mass value (but other values as well), we can see that at certain effective temperatures ($T_{\rm eff} = 18,000$ K for instance), there are multiple values of H/He possible [5], generally separated by orders of magnitude, for the same total hydrogen mass. This degeneracy reflects the possibility of mixing the same total amount of hydrogen in a deep, or in a shallow, helium convection zone (see also MacDonald & Vennes 1991).

A careful analysis of the results shown in Figure 2.13 also provides valuable information on the evolution of white dwarfs with homogeneously mixed H/He compositions. For instance, there is no homogeneously mixed envelope structure above $T_{\rm eff} \sim 20,000$ K with a hydrogen mass of $\log M_{\rm H}/M_{\odot} = -13$ for ML2/$\alpha = 0.6$ models (or above $T_{\rm eff} \sim 25,000$ K with $\alpha = 2$).

5. Note that MacDonald & Vennes (1991) find more solutions than we find here for some $T_{\rm eff}$ values because their grid includes models where helium is considered a trace element in diffusive equilibrium within the superficial hydrogen-rich layer (see their Figure 6).

Envelope structures with such large hydrogen masses can only be stratified (see Figure 2.11), corresponding to DA star configurations. These considerations will thus define an area in the $T_{\rm eff}$ – H/He parameter space inaccessible via normal white dwarf evolution with a constant hydrogen mass, as discussed further below.

2.5 Evolutionary Scenarios

2.5.1 Results from MacDonald & Vennes (1991)

Before discussing our own results, it is worth here summarizing some of the calculations from MacDonald & Vennes (1991) most relevant to our study. MacDonald & Vennes investigated stratified hydrogen/helium envelope models that are in full diffusive equilibrium for effective temperatures between 10,000 and 80,000 K, and including convective mixing using both Schwarschild and Ledoux criteria with different convective efficiencies. Their results can be best summarized by examining their Figure 1 (Schwarzschild convection with $\alpha = 1$) where contours of constant total hydrogen mass are shown for $\log M_{\rm H}/M_{\odot} = -16$ to -10 (by steps of 1.0 dex) in a diagram of He/H ratios (measured at a Rosseland optical depth of 2/3) as a function of effective temperature. To avoid further confusion, it is important to mention that MacDonald & Vennes refer to helium-to-hydrogen ratios (He/H) measured in *mass*, while we use throughout our analysis the inverse ratio (H/He) measured in *number*. Note also that since these are models in full equilibrium, all the hydrogen present in the envelope has already reached the surface in the hottest models ($T_{\rm eff} = 80,000$ K). By examining this figure, one can see that at a given effective temperature, there can be multiple envelope structures (up to five in some cases) that have the same total mass of hydrogen. This is further illustrated in their Figure 6 where the He/H ratio is shown as a function of mass depth for five envelope models with $\log M_{\rm H}/M_{\odot} = -13$ at $T_{\rm eff} = 15,000$ K. As discussed above, such multiple solutions reflect the possibility of mixing hydrogen and helium in convection zones of various thicknesses and depths (shown by the flat He/H profiles in their Figure 6). In the same figure, model A (a typical DA structure with almost all the hydrogen floating at the surface) and model E (a typical DB structure with hydrogen being diluted in the deep helium convective envelope) correspond

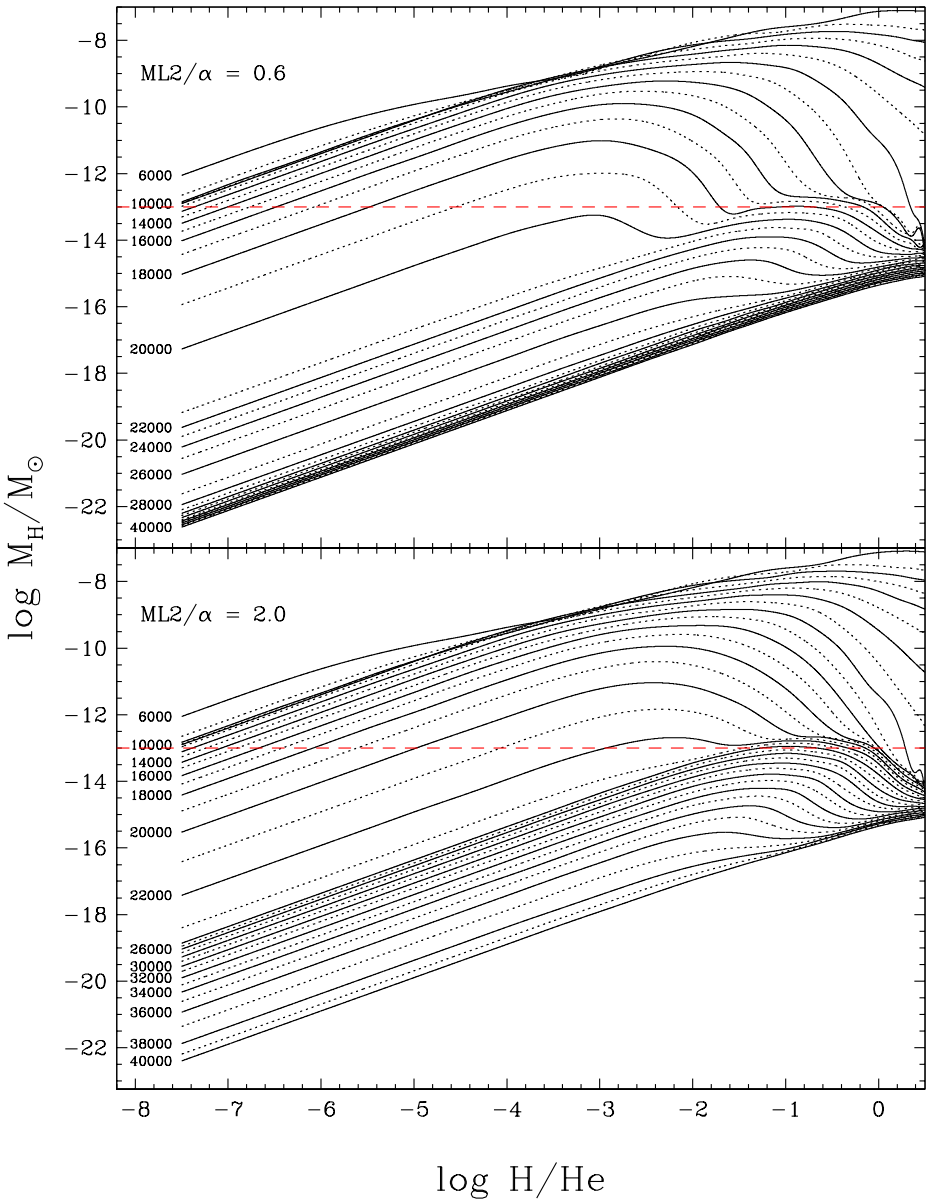

FIGURE 2.13 – Total hydrogen mass contained in homogeneously mixed H/He envelope models at 0.6 $M_\odot$ for various effective temperatures (labeled on each curve) as a function of the observed photospheric hydrogen abundance (H/He). The results are shown for two different convective efficiencies. An illustrative example for a total hydrogen mass of $\log M_{\rm H}/M_\odot = -13$ is indicated by a red dashed line in each panel.

approximately to our own stratified and homogeneous envelope models, respectively. But there are also intermediate solutions (see also our Figure 2.13), which as discussed by MacDonald & Vennes, are either unstable (dotted lines in their Figure 1) or unlikely to occur in nature.

As discussed by the authors, the contours in their Figure 1 are not to be interpreted as evolutionary tracks, but the evolution of white dwarfs with fixed hydrogen mass can still be determined by studying the appropriate contour in the following way. For instance, MacDonald & Vennes (see their Section 3) discuss a particular example at $\log M_{\rm H}/M_{\odot} = -13$. As the star cools from $T_{\rm eff} = 80,000$ K down to ∼35,000 K, the photospheric helium abundance — always a trace element — remains nearly constant, and then starts to decrease (following the lower branch in their Figure 1) since radiative acceleration no longer supports helium below 35,000 K. The He/H ratio reaches a minimum value near $T_{\rm eff} = 14,000$ K, and then starts to increase steadily again due to the onset of the hydrogen convection zone, until a minimum in effective temperature is reached at $T_{\rm eff} = 11,700$ K, which corresponds to the point where both helium and hydrogen convection zones connect. At this point, the He/H ratio discontinuously jumps to the upper branch of the contour. In our own terminology, this corresponds to the *convective mixing scenario* (see Figures 2.11 and 2.12).

Another example worth considering is the case with $\log M_{\rm H}/M_{\odot} = -14$. Again, as the star cools, the photospheric helium abundance decreases steadily, eventually reaches a minimum value, and starts to rise slowly. However, for this particular total hydrogen mass value, the coolest model on the lower branch is at $T_{\rm eff} = 17,900$ K, that is, cooler stratified hydrogen/helium envelope models in diffusive equilibrium where almost all the hydrogen floats on top of the star do not exist within their theoretical framework. So again here, the He/H ratio discontinuously jumps to the upper branch of the contour, reaching the DB star configurations. This corresponds to what we referred to as the *convective dilution scenario*. Note that MacDonald & Vennes refer to both convective mixing and convection dilution scenarios as *convective dredge-up*. In particular, their Table 1 provides effective temperatures at which the so-called convective dredge-up occurs ($T_{\rm ed}$) for different total hydrogen masses and assumed convection models, but it is important to realize that these $T_{\rm ed}$ values include both convective dilution (above $T_{\rm eff} \sim 13,000$ K) and convective mixing (below $T_{\rm eff} \sim 13,000$ K) processes.

More importantly, we want to emphasize here that the effective temperatures at which the convection dilution process occurs in the study of MacDonald & Vennes are based on static equilibrium models. In other words, the convective dilution process itself is not modeled in any way. Following the example above with $\log M_{\rm H}/M_{\odot} = -14$, no particular event occurs below $T_{\rm eff} \sim 17,900$ K. This is just the temperature below which no envelope models can be found within the framework assumed by the authors. For instance, for the same value of $M_{\rm H}$, our stratified envelope models extend to much lower temperatures (see bottom left panel of Figure 2.11) because we simply forced hydrogen to remain in equilibrium on top of the helium convection zone. Hence the real question is whether the underlying helium convection zone becomes efficient enough to dilute the superficial hydrogen layer, and if so, at which temperature. This is a *dynamical process*, which, to our knowledge, has never been modeled properly. With these considerations in mind, we now present the results of our own simulations.

2.5.2 Convective Dilution Scenario

We attempt in this section to interpret the hydrogen abundance pattern observed in DB/DBA white dwarfs and cool, He-rich DA/DZA stars, as depicted in Figure 2.8. We first begin by exploring the scenario where a thin, superficial hydrogen layer of a given mass has been convectively diluted within the helium envelope, resulting in a homogeneously mixed H/He convection zone, with some of this hydrogen lying below the convection zone, as discussed in Section 2.4.3. More specifically, we *assume* the hydrogen layer has been convectively diluted, and we do not pay attention to the dilution process, for the moment. The results of our simulations for homogeneously mixed models at 0.6 $M_{\odot}$ are presented in Figure 2.14 for both the ML2/$\alpha = 0.6$ and $\alpha = 2$ versions of the mixing-length theory, together with the observed hydrogen abundance pattern reproduced from Figure 2.8. Each curve in this plot represents the location of white dwarf stars with a constant value of $\log M_{\rm H}/M_{\odot}$, labeled in the figure. These results are similar to those presented in Figures 1 and 2 of MacDonald & Vennes (1991), although our calculations are restricted to H/He < 1 (i.e. the upper portions of their figures). For the models with $\log M_{\rm H}/M_{\odot} \lesssim -14$, the sudden change of slope near 20,000 K for the ML2/$\alpha = 0.6$ models ($\sim$23,000 K for the $\alpha = 2$ models) corresponds to the

temperature where the bottom of the helium convection zone sinks deep into the star (see the top left panel of Figures 2.9 and 2.10, where hydrogen is considered a trace element).

The hottest DBA stars in our sample near $T_{\rm eff} \sim 24,000$ K have inferred total hydrogen masses around $\log M_{\rm H}/M_{\odot} \sim -16.5$ with ML2/α = 0.6 models, and around -15 with α = 2 models. Larger hydrogen masses are required with α = 2 models to produce the same photospheric hydrogen abundance since the convection zone is much deeper in these models (see Figures 2.9 and 2.10). Notice that these hot DBA white dwarfs will rapidly evolve as DB stars at lower effective temperatures — below our Hα detection threshold — when the hydrogen content becomes increasingly more diluted within the growing helium convection zone, a conclusion also reached by Koester & Kepler (2015, see their Section 5.1). The bulk of the DBA stars in our sample, however, is found at lower temperatures ($T_{\rm eff} \lesssim 20,000$ K). Bergeron et al. (2011) showed that this corresponds to the temperature range where the DB/DA ratio reaches a value of 25%, based on the luminosity function obtained from the subset of white dwarfs identified in the Palomar-Green survey, while this fraction drops to only half this value above $T_{\rm eff} \sim 20,000$ K. As mentioned above, this corresponds also to the temperature at which the bottom of the helium convection zone sinks rapidly into the stellar envelope, strongly suggesting that the convective dilution model is the most likely scenario responsible for the transformation of some DA white dwarfs into DBA stars.

The results of Figure 2.14 indicate that the bulk of the DBA stars in our sample can be explained in terms of homogeneous models with total hydrogen masses between $\log M_{\rm H}/M_{\odot} = -13$ and -10 according to our ML2/α = 2 models. Note how the DBA abundance determinations are well contained within these two boundaries. In particular, a DBA star in this temperature range ($T_{\rm eff} \lesssim 20,000$ K) is expected to show Hα almost all the way down to ∼12,000 K when the helium lines vanish. This is not necessarily the case with the ML2/α = 0.6 models, which require thinner hydrogen layers of the order of $\log M_{\rm H}/M_{\odot} \sim -15$ to account for the DBA stars around 20,000 K; hydrogen features in these stars would rapidly become undetectable as they cool off by only ∼2000 K or so.

The cool, He-rich DA/DZA white dwarfs in Figure 2.14 require much larger hydrogen masses, ranging from $\log M_{\rm H}/M_{\odot} = -11$ to -8, regardless of the assumed convective efficiency.

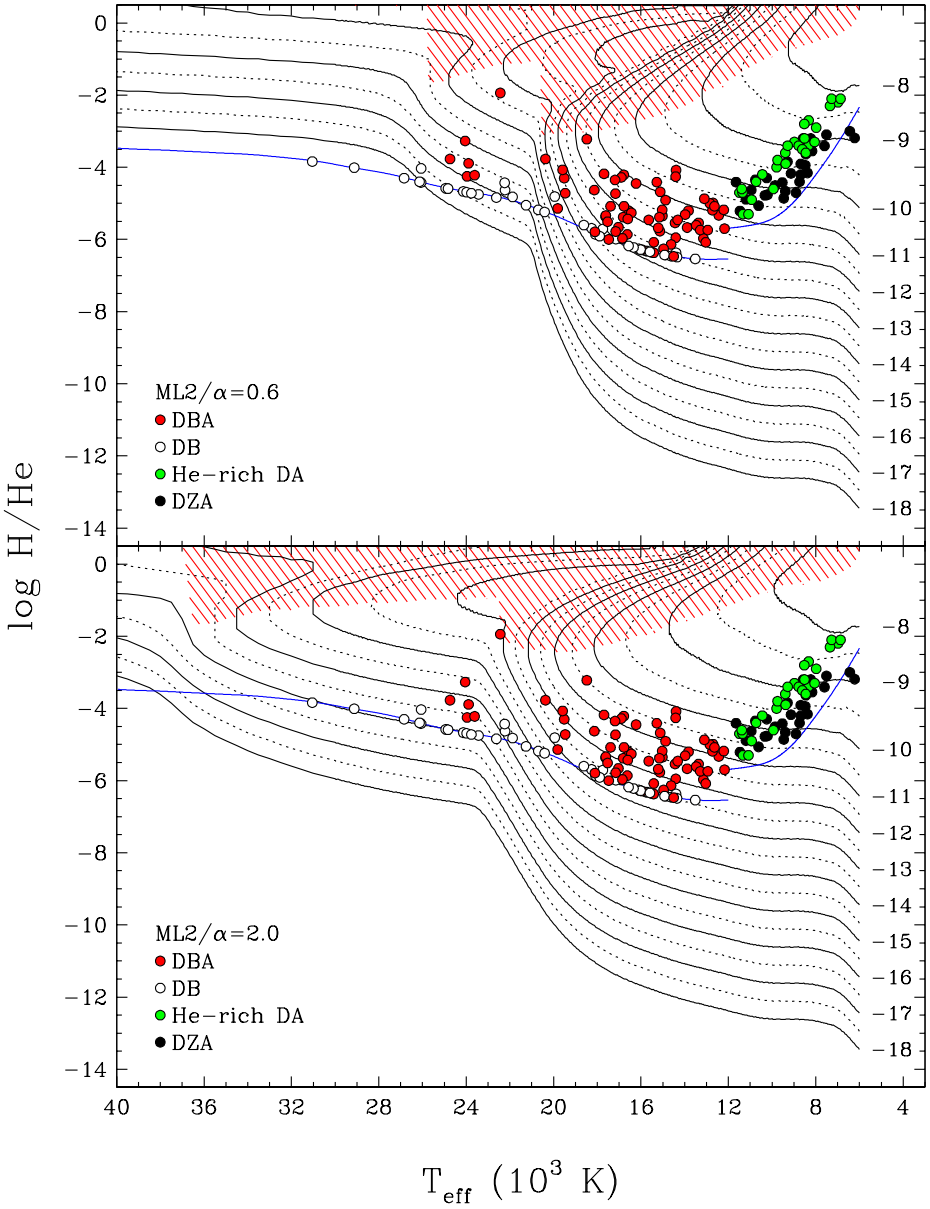

FIGURE 2.14 – Results of our simulations for homogeneously mixed models at 0.6 $M_{\odot}$ for both the ML2/α = 0.6 (upper panel) and α = 2 (lower panel) versions of the mixing-length theory. Each curve is labeled with the corresponding value of $\log M_{\rm H}/M_{\odot}$. Results from Figure 2.8 are also reproduced; limits on the hydrogen abundance set by our spectroscopic observations are shown by the solid blue lines. The red hatched regions represent the forbidden region through which white dwarfs cannot evolve continuously with a constant total hydrogen mass (see text).

Clearly, the progenitors of these objects are not DBA white dwarfs, which have much lower hydrogen content; DBA stars are likely to evolve instead into DC stars below $T_{\rm eff} \sim 12,000$ K since their expected hydrogen abundances will be below our Hα detection threshold in this temperature range. Note, however, that the distinction between these two populations cannot be easily made at the boundary near 12,000 K, and some of the He-rich DA/DZA white dwarfs with the lowest hydrogen abundances can probably be interpreted as cooled off DBA stars. We can also see that under the assumption of a constant total hydrogen mass, a given He-rich DA/DZA star will evolve at an almost constant photospheric hydrogen abundance, and will eventually (and rather quickly) turn into a DC star, that is, below our Hα detection threshold. Because of the large differences in total hydrogen mass between the DBA white dwarfs and the cool, He-rich DA/DZA stars, we must conclude that the latter have a different origin, most likely resulting from the mixing of the convective hydrogen layer with the deeper helium convection zone, a scenario we explore further in Section 2.5.4.

We now turn our attention to the convective dilution process more specifically. In order for a DBA star to cool off with a constant total mass of hydrogen already homogeneously mixed within the convective layer, it must be able to evolve *continuously* from the left to the right in Figure 2.14 along a single sequence with a given value of $\log M_{\rm H}/M_{\odot}$. In other words, the sequence cannot turn back towards higher temperatures at any point (see also MacDonald & Vennes 1991). These considerations thus allow us to define a region in the $T_{\rm eff}$ – H/He parameter space — represented by the red hatched regions in Figure 2.14 — through which white dwarfs cannot evolve continuously with a constant hydrogen mass. For instance, we already presented an example in Figure 2.13 where we showed that homogeneously mixed stellar envelopes with a total hydrogen mass of $\log M_{\rm H}/M_{\odot} = -13$ could not exist above $T_{\rm eff} \sim 20,000$ K with ML2/$\alpha = 0.6$ (or above $T_{\rm eff} \sim 25,000$ K with $\alpha = 2$), in agreement with the results of Figure 2.14. White dwarfs containing such large amounts of hydrogen can only exist as chemically stratified white dwarfs above these temperatures, with hydrogen floating in diffusive equilibrium on top of the helium envelope, corresponding to a DA star configuration. Similar conclusions can be reached from an examination of the results displayed in Figures 1 and 2 of MacDonald & Vennes (1991).

The results presented in Figure 2.14 indicate that some white dwarfs can indeed evolve with a constant hydrogen mass diluted within the convection zone, but only if the total hydrogen mass is very small, i.e. $\log M_{\rm H}/M_{\odot} \lesssim -15.5$ for ML2/$\alpha = 0.6$ models, and $\log M_{\rm H}/M_{\odot} \lesssim -16$ for $\alpha = 2$ models. Incidentally, the hottest DBA stars in our sample near $T_{\rm eff} \sim 24,000$ K can be explained by this scenario, but only if the convective efficiency is low. All the cooler DBA stars in our sample can only be explained by some kind of *dynamical transformation*, such as the convective dilution scenario, where the superficial hydrogen layer of a chemically stratified DA white dwarf is convectively diluted by the underlying helium convective envelope. In other words, this convective dilution process will allow a given DA star to cross the red-hatched region in Figure 2.14, directly into the region where DBA stars are found. The question is, under which physical circumstances?

As discussed in Section 2.5.1, MacDonald & Vennes (1991) concluded that DA stars could be transformed into DB white dwarfs near $T_{\rm eff} \sim 18,000$ K if the hydrogen layer mass was of the order of $\log M_{\rm H}/M_{\odot} \sim -14$. We emphasize that this so-called convective dredge-up temperature ($T_{\rm ed}$) given in their Table 1 corresponds simply to the coolest stratified DA model in their grid for this particular hydrogen layer mass (i.e., the coolest point on the lower branch in their Figure 1). If we now take these results at face value, this implies — according to our results displayed in Figures 2.11 and 2.12 — that the convective dilution of a hydrogen layer with $\log M_{\rm H}/M_{\odot} \sim -14$ will occur near $T_{\rm eff} \sim 20,000$ K if at least ∼50% of the total energy flux (the magenta contours) is transported by convection [6]. If we adopt arbitrarily this fraction of the total flux for the convective dilution process to occur, we find that the DA-to-DB transition will take place at $T_{\rm eff} \sim 32,000$ K for $\alpha = 2$ models with $\log M_{\rm H}/M_{\odot} \sim -15$, a temperature that is entirely consistent with the results of MacDonald & Vennes (see the S2 results in their Table 1). More importantly, however, for hydrogen layers between $\log M_{\rm H}/M_{\odot} = -13$ and -10, where the bulk of the DBA stars in our sample are found, the underlying helium convection zone is almost completely inhibited, and the thin convection zone still present in our models is most certainly too inefficient (less than 1% of the total flux) to dilute the superficial hydrogen layer.

6. Note that the hydrogen layer masses in Figures 2.11 and 2.12 are given in terms of $\log q({\rm H}) \equiv \log M_{\rm H}/M_{\star} = \log M_{\rm H}/M_{\odot} - 0.22$ for a 0.6 $M_{\odot}$ white dwarf.

We must therefore conclude that most — but not all — helium-atmosphere white dwarfs below $T_{\rm eff} \sim 30,000$ K that contain traces of hydrogen cannot be explained in terms of a convective dilution scenario. The total amount of hydrogen present in these white dwarfs implies that their DA progenitors had hydrogen layers that were far too thick to allow the convective dilution process to occur. A similar conclusion has also been reached by MacDonald & Vennes (1991). The most common solution proposed to solve this problem is to assume that a significant fraction of DB stars are indeed the result of a convective dilution scenario, with DA progenitors having very thin hydrogen layers ($\log M_{\rm H}/M_{\odot} \lesssim -15$). After the DA-to-DB transition, accretion of hydrogen from the interstellar medium or other external bodies (comets, disrupted asteroids, etc.) increases the hydrogen content in the stellar envelope, up to the level observed in DBA stars (see, e.g., MacDonald & Vennes 1991). We explore this scenario more quantitatively in the next section.

2.5.3 Accretion of Hydrogen from External Sources

Our results from the previous section strongly suggest that a simple convective dilution model with a constant hydrogen mass is an unlikely evolutionary scenario for the origin of DBA and cool, He-rich DA/DZA white dwarfs. We explore here the possibility of accretion from external sources, either from the interstellar medium, or from other bodies such as comets, disrupted asteroids, or small planets. To model this process, the various episodes of accretion occurring during the white dwarf evolution are averaged with a constant accretion rate. We first compute the total accreted mass of hydrogen for various rates ranging from $\log M_{\rm H}/M_{\odot} = -27.5$ to -17.0 per year by steps of 0.5 dex using the cooling times of a typical DB star at 0.6 $M_{\odot}$ (see Section 2.3.1.3). For a given effective temperature, these hydrogen masses are then converted into hydrogen-to-helium abundance ratios using our $T_{\rm eff}$ – H/He parameter space map (Figure 2.13). We assume here for simplicity that the material has been accreted on top of a pure helium atmosphere; results obtained with a small initial hydrogen mass of $\log M_{\rm H}/M_{\odot} \sim -15$ are almost identical to those presented here since such a small amount of hydrogen yields photospheric abundances of only H/He $\sim 10^{-10} - 10^{-8}$ in the temperature range where most of the DBA stars are found (see Figure 2.14).

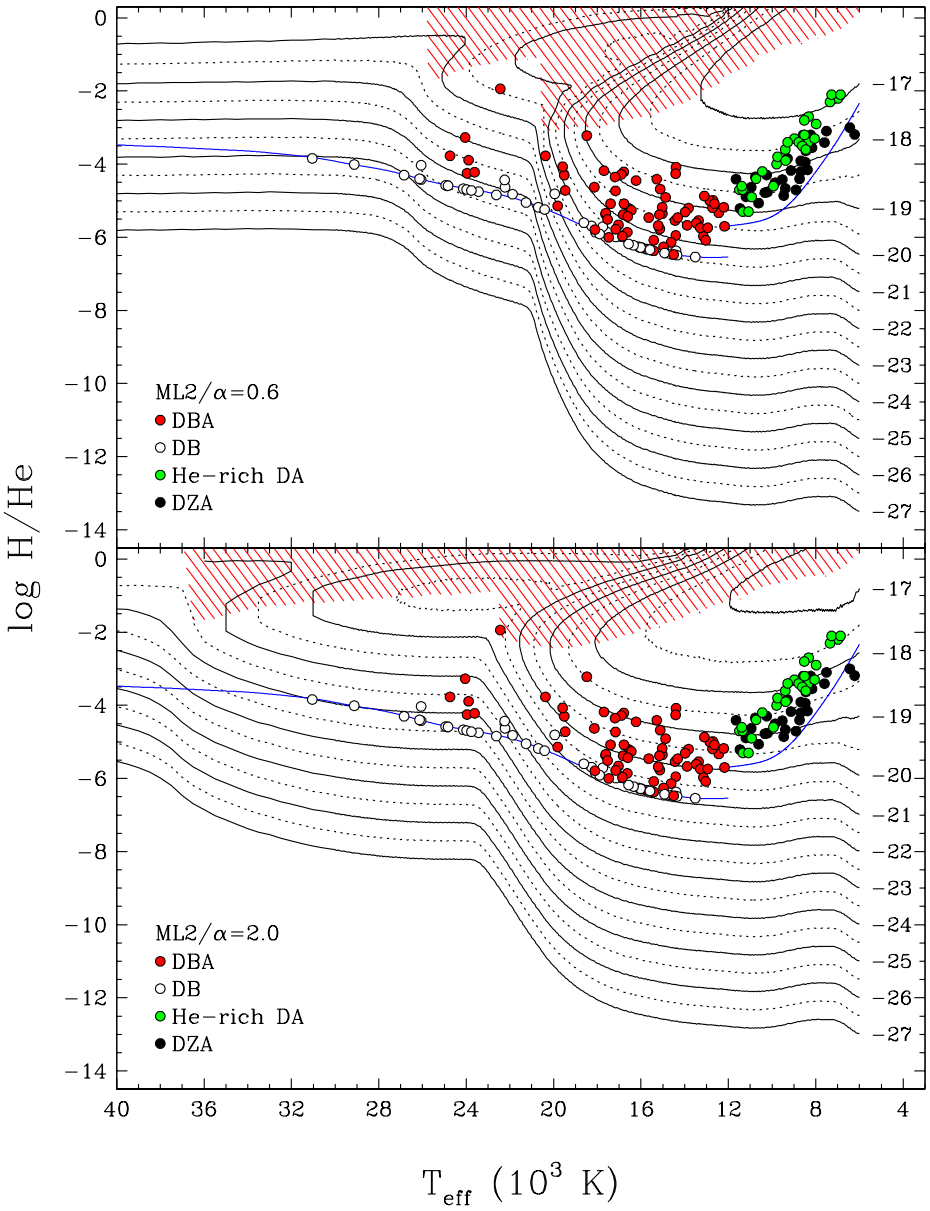

FIGURE 2.15 – Results of our accretion simulations for models at 0.6 $M_\odot$ subject to constant accretion rates of hydrogen. Each curve is labeled with the corresponding total mass of hydrogen accreted in $M_\odot$ per year on a logarithmic scale. Calculations are shown for both the ML2/$\alpha = 0.6$ (upper panel) and $\alpha = 2$ (lower panel) versions of the mixing-length theory. Results from Figure 2.8 are also reproduced. The red hatched regions represent the forbidden region through which white dwarfs cannot evolve continuously (see text).

Results of these simulations are displayed in Figure 2.15 for both prescriptions of the mixing-length theory considered in this study. Our results indicate that the amount of hydrogen observed in the bulk of DBA white dwarfs in our sample can be accounted for with average accretion rates ranging from 10^{-22} to 10^{-19} $M_{\odot}$ yr^{-1}, and from 10^{-20} to 10^{-17} $M_{\odot}$ yr^{-1} for the cool, He-rich DA/DZA stars. These rates are totally compatible with those estimated in previous studies (MacDonald & Vennes 1991; Dufour et al. 2007a; Voss et al. 2007; Bergeron et al. 2011; Koester & Kepler 2015). The fundamental problem with this accretion scenario, however, is that for such a range of accretion rates, our simulations at higher effective temperatures predict hydrogen abundances in the $T_{\rm eff}$ – He/H plane where homogeneously mixed models cannot evolve in a continuous fashion. In other words, for the accretion model to be valid, the evolutionary tracks would have to cross the "forbidden" red hatched regions in Figure 2.15, as was the case for the convective dilution scenario.

As a simple example, a pure DB star will take roughly $\sim$10^7 years to cool down to $T_{\rm eff}$ = 30,000 K (see Figure 2.6), and even for an accretion rate as low as 10^{-20} $M_{\odot}$ yr^{-1}, will have accumulated $\sim$10^{-13} $M_{\odot}$ of hydrogen during this period. By referring to the results shown in Figure 2.13, one can see that this configuration is impossible as a homogeneously mixed white dwarf, with either version of the mixing-length theory. Such an object can only exist as a DA star, with all the hydrogen floating in diffusive equilibrium on top of the helium envelope, which according to Figures 2.9 and 2.10 (right panels), will not mix until it reaches $T_{\rm eff} \sim 11,000$ K. We are thus forced to conclude that the hydrogen abundances measured in DBA white dwarfs, and cool He-rich DA/DZA stars as well, cannot be accounted for by any kind of accretion mechanism onto a pure helium DB star. Our conclusion remains the same even if we allow for an initial hydrogen mass of $\log M_{\rm H}/M_{\odot} \sim -15$ instead of a DB white dwarf with a pure helium atmosphere.

Note that it is always possible to invoke the accretion of large bodies such as comets, disrupted asteroids, or small planets as the source of hydrogen in DBA stars if the accretion process begins only *after* the white dwarf has evolved through the forbidden red hatched region in Figure 2.15 — either as a pure helium-atmosphere DB star or as a DA star with a very thin hydrogen layer — but this would require extraordinary circumstances for such a process

to occur precisely below 20,000 K for a significant fraction of DB stars.

2.5.4 Convective Mixing Scenario

At lower effective temperatures ($T_{\rm eff} \lesssim 13,000$ K), DA white dwarfs with thin enough hydrogen layers may get a second opportunity to turn into helium-dominated atmospheres as a result of *convective mixing*, which occurs when the bottom of the superficial hydrogen convective envelope sinks into the star, and eventually connects with the underlying and more massive helium convection zone (see Figures 2.11 and 2.12). At this point, it is generally assumed that both hydrogen and helium convection zones merge, with the total hydrogen content homogeneously mixed within this H/He convective layer. As discussed in the Introduction, convective mixing is the most likely explanation to account for the significant increase in the ratio of non-DA to DA stars below $T_{\rm eff} \sim 10,000$ K. After convective mixing occurs, the star will continue its evolution with a homogeneously mixed envelope with constant total hydrogen mass, a scenario already described in Section 2.5.2. Our stratified model structures, displayed in Figures 2.11 and 2.12, indicate that this mixing process can occur if the mass of the hydrogen layer is in the range $\log M_{\rm H} \sim 10^{-15}$ to 10^{-6} $M_\star$, where the upper limit is set by the maximum depth reached by the bottom of the hydrogen convection zone near $T_{\rm eff} \sim 5000$ K (see also Figure 40 of Bergeron et al. 1997). However, for hydrogen layers thinner than $M_{\rm H} \sim 10^{-14}$ $M_\star$, the convective dilution process discussed in Section 2.5.2 is most likely to occur at much higher temperatures ($T_{\rm eff} \gtrsim 20,000$ K), hence a more realistic lower limit for the occurrence of convective mixing is set here at $M_{\rm H} = 10^{-14}$ $M_\star$. To model the convective mixing scenario, we thus calculated the effective temperature at which the hydrogen and helium convection zones connect in a 0.6 $M_\odot$ stratified envelope model, for a given value of the total hydrogen mass $M_{\rm H}$. From that point on, we assume complete mixing, and follow the evolution at lower effective temperatures using the homogeneous sequences with the corresponding value of $M_{\rm H}$, as described in Section 2.5.2.

Results of our convective mixing simulations are displayed in Figure 2.16 for both prescriptions of the mixing-length theory considered is this study. The blue solid line in this figure indicates the effective temperature at which mixing occurs, and the predicted H/He abun-

dance ratio upon mixing. After mixing, the white dwarf evolves at a constant value of $M_{\rm H}$ in the region represented by the cyan area in Figure 2.16. The particular behavior of the mixing temperature as a function of H/He can be explained qualitatively in the following way. Since the bottom of the hydrogen convection zone gets deeper as the white dwarf cools off (see right panels of Figures 2.11 and 2.12), the effective temperature at which convective mixing occurs will depend strongly on the thickness of the hydrogen layer — the thicker the hydrogen envelope, the lower the mixing temperature. Furthermore, since the depth of the mixed H/He convection zone remains almost constant in this temperature range (see Figures 2.9 and 2.10), the predicted H/He abundance ratio upon mixing increases with decreasing mixing temperature, as shown by our simulations in Figure 2.16. This mixing temperature can also be made significantly hotter in our calculations if we allow for even a modest convective overshooting. For instance, we show in Figure 2.17 the extent of the convection zones in a typical sequence of stratified models from our grid, by allowing both hydrogen and helium convection zones to overshoot over a distance of one pressure scale height, a completely reasonable assumption (see, for instance, Tremblay et al. 2015). In the example displayed in Figure 2.17, this simple prescription increases the mixing temperature by ~ 500 K. The results of convective overshooting applied to all our models are indicated by the dashed blue line in Figure 2.16.

Also reproduced in Figure 2.16 are the hydrogen abundances measured in cool, He-rich DA/DZA stars, which are the objects of interest in the present context. As discussed in Section 2.5.2, under the assumption of a constant total hydrogen mass, He-rich DA/DZA stars will evolve at an almost constant photospheric hydrogen abundance, and will eventually turn into DC (or DZ) stars, that is, below our Hα detection threshold (see Figure 2.8). Due to these observational limitations, the observed sequence in Figure 2.16 defines in fact only the blue edge of a region in $T_{\rm eff}$ and H/He where these objects could be found; higher signal-to-noise observations should allow the detection of hydrogen in helium-rich atmospheres at even lower temperatures.

Interestingly enough, the overall trend of the H/He abundance ratio predicted by the convective mixing scenario, as a function of the mixing temperature, represents an excellent match to the blue edge defined by the measured hydrogen abundances in cool, He-rich DA

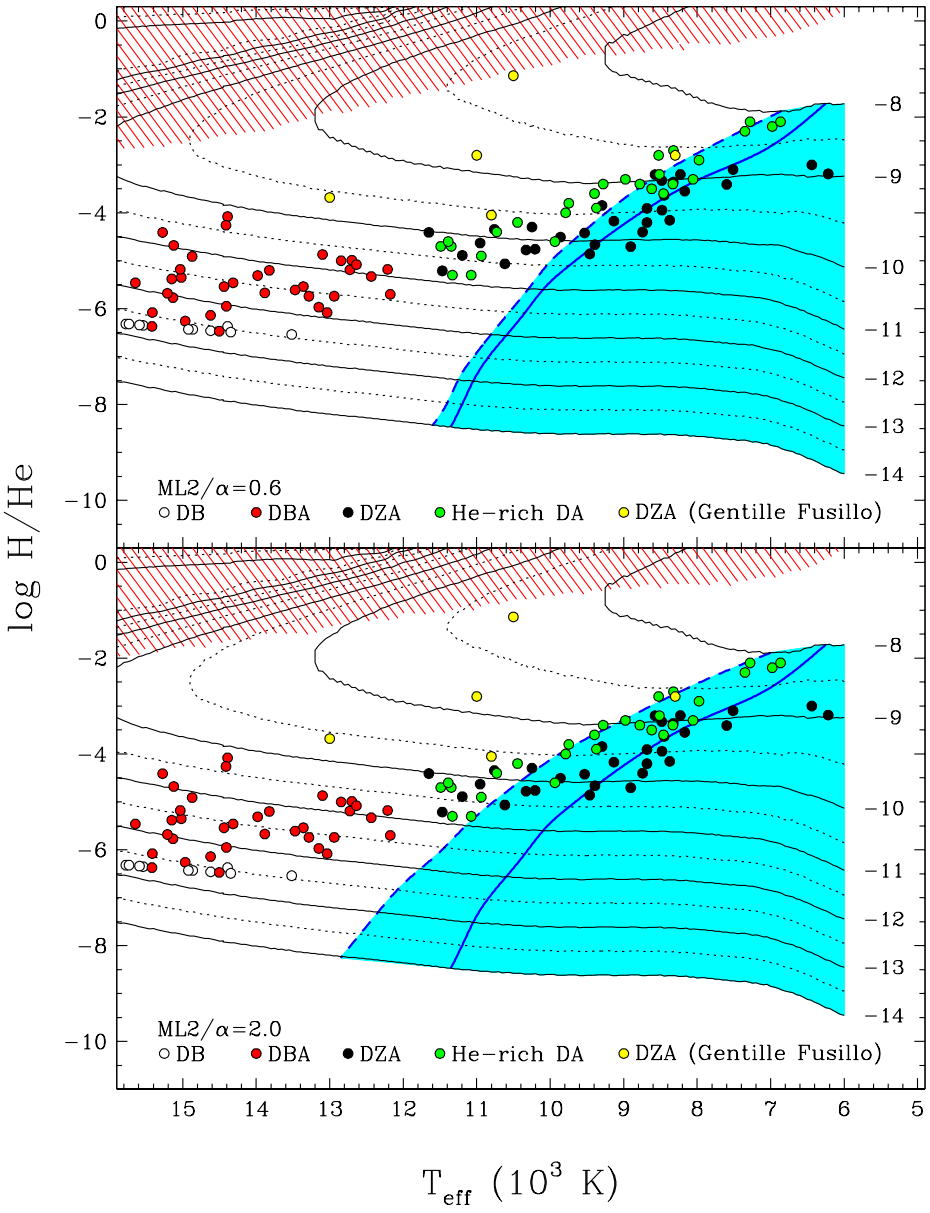

FIGURE 2.16 – Results of our convective mixing simulations for models at 0.6 $M_{\odot}$, assuming that after mixing occurs, the total hydrogen mass is distributed in the way described in Section 2.4.3. Each curve is labeled with the corresponding value of $\log M_{\rm H}/M_{\odot}$. The solid blue line shows the predicted hydrogen-to-helium abundance ratio as a function of the temperature at which mixing occurs, while the dashed blue line allows for convective overshooting over one pressure scale height; the filled cyan area represents the region where white dwarfs will evolve after mixing has occurred. Calculations are shown for both the ML2/α = 0.6 (upper panel) and $\alpha = 2$ (lower panel) versions of the mixing-length theory. Results from Figure 2.8 are also reproduced, together with the objects discussed in Gentile Fusillo et al. (2017, see text).

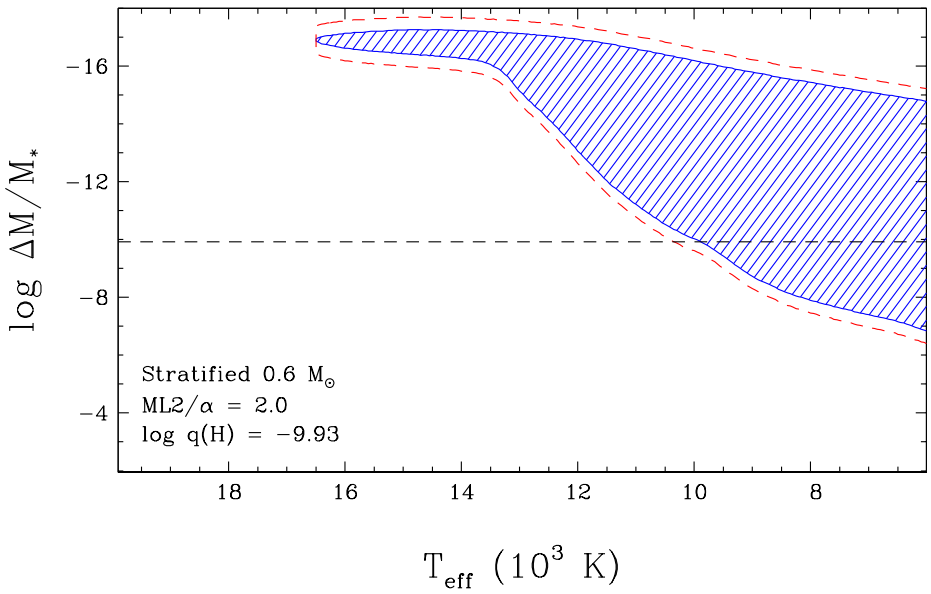

FIGURE 2.17 – Example of envelope structures, as a function of effective temperature, for chemically stratified white dwarf models, with parameters given in the figure. The convection zones are shown by the hatched region, while the red dashed line shows the extent of the hydrogen and helium convection zones allowing for convective overshooting over a distance of one pressure scale height.

and DZA stars, particularly if we allow for a more convective efficiency (ML2/α = 2) and a modest convective overshooting (cyan region defined by the dashed blue line in the bottom panel of Figure 2.16). More specifically, the convective mixing scenario predicts higher hydrogen abundances in cooler white dwarfs, as observed here. Also, note the absence of white dwarfs at $T_{\rm eff} \sim 10,000$ K in our sample with large hydrogen abundances, as predicted by the models. The overall agreement between the location of the cool, He-rich DA/DZA stars and the region predicted by our simulations (shown in cyan) clearly demonstrates that the convective mixing scenario is the most plausible interpretation for the presence of traces of hydrogen in cool, helium-atmosphere white dwarfs.

In the same context, we also show in Figure 2.16 the five helium-atmosphere white dwarfs with exceptionally high hydrogen abundances discussed in Gentile Fusillo et al. (2017) and references therein; these are, from hottest to coolest, SDSS J124231.07+522626.6, GD 16, PG 1225−079, GD 362, and GD 17. While the amount of hydrogen in these objects has

been considered exceptional, thus requiring large external sources of hydrogen — from the accretion of water-bearing planetesimals for instance — our results indicate that even though this is probably true for SDSS J124231.07+522626.6, GD 16, and GD 362, *convective mixing alone* can provide sufficient amounts of hydrogen without invoking additional sources in the case of PG 1225−079 and GD 17.

We end this section by summarizing in Table 2.3 the effective temperatures at which the transition from a hydrogen-atmosphere to a helium-atmosphere white dwarf occurs as a function of the thickness of the hydrogen layer ($\log M_{\rm H}/M_{\odot}$), for both the convective dilution and convective mixing scenarios, and for both prescriptions of the mixing-length theories assumed in our study. We also provide the predicted hydrogen-to-helium abundance ratios when the transition occurs. As discussed in Section 2.5.2, we simply assume here that the convection dilution process occurs when ∼50% of the total energy flux is transported by convection, and for the convective mixing process, we allow both hydrogen and helium convection zones to overshoot over a distance of one pressure scale height, as discussed above. When comparing our results with those presented in Table 1 of MacDonald & Vennes (1991), we find that our transition temperatures compare remarkably well with their convective dredge-up temperatures, both qualitatively and quantitatively, especially given the many different assumptions made in both studies. And once again here, we want to emphasize that neither of these two analyses have properly modeled the convective dilution process, which is a time-dependent *dynamical process*.

TABLE 2.3 – Hydrogen- to Helium-Atmosphere Transition Temperatures

	ML2/$\alpha = 0.6$		ML2/$\alpha = 2.0$	
$\log M_{\rm H}/M_{\odot}$	$T_{\rm eff}$ (K)	$\log$ H/He	$T_{\rm eff}$ (K)	$\log$ H/He
−15.0	22,100	−2.8	31,500	−0.3
−14.5	21,000	−2.6	27,950	−2.7
−14.0	19,350	−5.1	22,250	−3.8
−13.5	16,850	−6.6	18,000	−6.6
−13.0	11,250	−7.5	12,350	−7.3
−12.5	11,050	−7.0	12,100	−6.9
−12.0	10,850	−6.7	11,800	−6.4
−11.5	10,550	−6.1	11,450	−6.0
−11.0	10,300	−5.6	11,150	−5.5
−10.5	10,050	−5.1	10,800	−5.0
−10.0	9700	−4.6	10,400	−4.6
−9.5	9250	−4.0	9900	−4.0
−9.0	8650	−3.3	9100	−3.4
−8.5	7850	−2.6	8150	−2.6
−8.0	6850	−1.9	7000	−1.9

2.6 Discussion

2.6.1 The origin of hydrogen in DBA stars

The existence of a DB-gap — or DB-deficiency — in the 30,000 to 45,000 K temperature range clearly demonstrates that the DA-to-DB transition must necessarily occur in nature below 30,000 K or so. The only viable physical mechanism for this transition to occur in this temperature regime is the convective dilution of a thin radiative hydrogen layer at the surface of a DA star with the deeper and more massive convective helium zone. Bergeron et al. (2011) showed, however, that the significant increase in the number of DB stars in this temperature range occurs only below $T_{\rm eff} \sim 20,000$ K, rather than the canonical 30,000 K, where the hottest DB white dwarfs have been identified in the PG survey. This makes perfect sense when looking at our Figures 2.11 and 2.12, since the helium convection zone becomes efficient only at much lower temperatures in stratified H/He atmospheres. Since most, but not all, DB white dwarfs below ∼20,000 K in our sample now show traces of hydrogen, with respect to our previous analysis (Bergeron et al. 2011), it is reasonable to conclude that hydrogen must have a primordial origin.

Actually, 63% of all DB white dwarfs in our enlarged sample are DBA stars, but this fraction increases to 75% if we consider only the objects below 20,000 K. We note that pure DB stars — at least in the optical — still exist in this temperature range, with limits as low as H/He $\lesssim 10^{-6}$. Because of the higher S/N of our sample, these limits are much more stringent than those reported by Koester & Kepler (2015) based on SDSS spectra. We can identify at least two, or perhaps three, channels that could account for the existence of these hydrogen-deficient DB stars. The first one corresponds to the hot DB white dwarfs in the gap. These, apparently, did not have enough hydrogen left in their envelope to build a hydrogen atmosphere and to become DA stars over time, and they will most likely evolve as helium-rich atmospheres throughout their lifetime. The hottest DB stars in our sample above $T_{\rm eff} \sim 25,000$ K probably belong to this category. A second channel corresponds to DA stars with very thin hydrogen layers — of the order of $M_{\rm H} \sim 10^{-15}\ M_{\odot}$ — that would turn into DBA stars at $T_{\rm eff} \sim 24,000$ K according to our results displayed in Figure 2.14. But as shown in the same figure, such objects

would rapidly turn into pure DB stars as the small amount of hydrogen present in these stars is further diluted in the growing helium convection zone at lower effective temperatures. Finally, there is probably a third, but numerically less important channel producing hydrogen-deficient DB stars at low temperatures, the so-called Hot DQ stars (Dufour et al. 2007b). As discussed in Bergeron et al. (2011, see also Dufour et al. 2008), because the coolest Hot DQ star currently known has a temperature near 18,000 K, these must somehow turn into DB white dwarfs at lower effective temperatures, through a process currently unknown. But the number of known Hot DQ stars is so small, that this particular channel is certainly negligible from an ensemble point of view.

The convective dilution scenario alone can probably account for the amount of hydrogen in the few hottest DBA stars in our sample near $T_{\rm eff} \sim 24,000$ K. It is worth mentioning in this context that the hot ($T_{\rm eff} \sim 30,000$ K) DBA star SDSS 1509−0108, which Manseau et al. (2016, see their Figure 14) interpreted as a chemically stratified white dwarf with $\log M_{\rm H}/M_{\odot} \sim -16.7$, represents an obvious progenitor of these hottest DBA stars in our sample. For the bulk of the DBA white dwarfs, however, the total amount of hydrogen inferred from the photospheric hydrogen abundance is simply too large. DA progenitors with such large hydrogen masses — of the order of $M_{\rm H} \sim 10^{-13}\ M_{\odot}$— would have stratified atmospheres with hydrogen layers so thick that they would not stand a chance to turn into helium-atmosphere DB stars in the appropriate temperature range. We thus conclude that the total mass of hydrogen estimated in DBA stars, assuming complete mixing within the stellar envelope, is too large, and incompatible with a scenario involving the transformation of a DA star progenitor into a DB white dwarf through the convective dilution of a thin hydrogen atmosphere with the deeper and more massive helium convection zone. DA stars with such massive hydrogen layers would not mix until they reach temperatures that are significantly cooler than the entire DBA population.

Accretion of hydrogen from external sources has thus been invoked repeatedly to explain the total mass of hydrogen determined in DBA stars. One of the most recent studies by Veras et al. (2014) suggested, for instance, the gradual accretion of hydrogen from exo-Oort cloud comets. However, we found in our study that the required amount of accreted material, with even a moderate accretion rate, would build a superficial hydrogen layer thick enough by the

time the white dwarf reaches a temperature of $T_{\rm eff} \sim 30,000$ K, that this object — presumably a DA star — would never turn into a helium-atmosphere DB star. Another obvious problem with the accretion scenario is that even modest amounts of hydrogen accreted at the surface of hot helium-atmosphere white dwarfs in the ∼30,000 K temperature range would easily show up spectroscopically since the extent of the helium convection zone at these temperatures is too small to allow any significant dilution of the accreted material into the deeper envelope (see Figures 2.9 and 2.10). We thus conclude that the hydrogen abundances measured in DBA stars cannot be accounted for by any kind of accretion mechanism onto a pure helium DB star progenitor.

Hence we are left with no satisfactory explanation for the presence of hydrogen in the bulk of DBA white dwarfs at the observed abundance level. One explanation proposed by Genest-Beaulieu & Bergeron (2017) is that perhaps hydrogen tends to float in the radiative zone on top of the photosphere rather than being completely mixed within the helium convection zone. They explored this possibility by calculating spectra with an abundance profile given by the diffusive equilibrium approximation in the radiative layers above the convection zone, as illustrated, for instance, in Figure 6 of MacDonald & Vennes (1991). Based on their preliminary calculations, Genest-Beaulieu & Bergeron suggested that the hydrogen-to-helium abundance ratios measured in DBA white dwarfs could be overestimated by perhaps 2 orders of magnitude due to the inhomogeneous H and He abundance profiles in the upper radiative atmosphere. The inhomogeneous profile was only used in their calculation of the synthetic spectrum, however, and the next step, currently underway, is to implement this inhomogeneous hydrogen abundance profile in the calculation of the atmospheric structure itself to get a self-consistent solution.

Yet another possibility, not envisaged explicitly in our analysis, is that primordial hydrogen, highly diluted in a post-born-again PG1159 progenitor, may not have had the time to diffuse upward completely during the cooling process, contrary to what is generally assumed. In that case, not all of the hydrogen would find itself distributed in the convection zone of a DBA star (including a diffusion tail), so that the *observable* hydrogen content could be much less than the actual amount of that element in a given star. With passing time, more hydrogen would

enrich the convection zone of a DBA star from below (as opposed to from above as in the case of accretion). Such a process could potentially explain why a DBA star at $T_{\rm eff} \sim 18,000$ K, say, with a relatively large quantity of hydrogen in its outer convection zone, could still be the descendant of a $T_{\rm eff} \sim 25,000$ K star rather characterized by a much smaller amount of hydrogen pollution in its convective atmosphere-envelope. To go further in that direction, however, requires demanding and detailed time-dependent calculations combining evolution, convective mixing, and diffusion. This is beyond the scope of the present paper but deserves consideration for the future.

2.6.2 The origin of hydrogen in cool, He-rich DA/DZA stars

We have shown that the presence of hydrogen in cool ($T_{\rm eff} \lesssim 12,000$ K), helium-rich atmosphere white dwarfs discovered in the SDSS is a common phenomenon, although the exact fraction showing Hα remains undetermined. The hydrogen abundances determined in these objects define a sequence in the H/He – $T_{\rm eff}$ diagram — with cooler objects showing larger hydrogen abundances — which overlaps with the abundances measured in DZA white dwarfs, suggesting that the only difference between these two populations is the presence or not of a source of accreted material such as comets, disrupted asteroids, small planets, etc. The cool edge of the sequence is probably just a selection effect due to the increasing difficulty of detecting Hα at low temperatures (see the detection threshold in Figure 2.8). The blue edge of the sequence is well defined, however, and objects to the left of this sequence could easily be detected; they are thus obviously rare, with a few exceptions discussed in Gentile Fusillo et al. (2017) and in Section 2.5.4 (see Figure 2.16). The blue edge of the sequence must therefore have an astrophysical origin.

Our envelope models with constant total hydrogen mass (see Figure 2.14) clearly show that DBA white dwarfs will not turn into cool, He-rich DA stars, but will instead become DC stars when the hydrogen abundances fall below the detection threshold at low temperatures ($T_{\rm eff} \lesssim 12,000$ K). Instead our simulations indicate that convective mixing of the thin hydrogen layer with the deeper helium convection zone is the most likely explanation for the presence of hydrogen in cool, He-rich DA/DZA white dwarfs. After mixing, these stars will evolve at an

almost constant hydrogen abundance (see Figure 2.16), eventually turning into DC or DZ stars when Hα falls below the detection threshold. With these considerations in mind, if we assume that the non-DA to DA ratio below ∼10,000 K is near unity (see, e.g., Fontaine & Wesemael 1987) and that ∼20% of white dwarfs are DB/DBA stars in the appropriate temperature range (Bergeron et al. 2011), we can estimate that convective mixing eventually occurs for 40% of cool DA stars.

It is also interesting in this context to speculate about the origin of cool DQ stars. Since practically none of them show traces of hydrogen (with a few notable exceptions where a CH feature is present), perhaps the progenitors of these stars are the pure DB stars that show no traces of hydrogen either. Then the reason why some cool non-DA white dwarfs show carbon features while others do not could be related to the same reason why some DB stars appear to have very little, or no hydrogen at all. In the latter case, hydrogen has probably been completely depleted during the earlier born-again post-AGB evolutionary phases. Perhaps then, the overall stellar structure of the progenitor has been affected in such a way to facilitate the carbon dredge-up from the core at low effective temperatures. This could even explain the absence of DQZ stars if these earlier post-AGB phases have somehow managed to wipe out any material surrounding the white dwarf progenitor, preventing any further accretion of heavy elements during the course of its evolution.

We also note that the highest mixing temperature in Figure 2.16 is $T_{\rm eff} \sim 13,000$ K, which occurs for $M_{\rm H} = 10^{-14}\ M_{\odot}$ in ML2/$\alpha = 2$ models, that is *above* the blue edge of the ZZ Ceti instability strip (see for instance Figure 33 of Gianninas et al. 2011), while the red edge of the strip at $T_{\rm eff} \sim 11,000$ K corresponds to a mixing temperature of models with $M_{\rm H} \sim 10^{-11}$. Hence it is possible that DA stars mix above, or even within, the ZZ Ceti instability strip, implying that asteroseismological analyses of ZZ Ceti stars may not be sampling the entire range of hydrogen layer masses in DA stars.

Many of the ideas and speculations presented in this paper can be studied further by performing statistical analyses of large white dwarf samples such as the SDSS sample. Unfortunately, there are many selection effects in the SDSS, and it is therefore difficult to define a statistically meaningful sample to study the spectral evolution of white dwarf stars. To do

things properly, one would require accurate distances for these white dwarfs, a situation that will greatly be improved with the trigonometric parallax measurements from the *Gaia* mission that will be released in the very near future.

2.7 Acknowledgements

We would like to thank the director and staff of Steward Observatory and Kitt Peak National Observatory for providing observing time for this project. We are also grateful ro M.-M. Limoges, N. Giammichele, L. Séguin-Charbonneau, and E. M. Green for acquiring some of the spectra used in our analysis. This work was supported in part by the NSERC Canada and by the Fund FRQ-NT (Québec).

Chapitre 3

A Convective Dredge-Up Model as the Origin of Hydrogen in DBA White Dwarfs

B., Rolland [1], P., Bergeron [1], and G., Fontaine [1]

To be submitted to

The Astrophysical Journal

1. Département de Physique, Université de Montréal, C.P. 6128, Succ. Centre-Ville, Montréal, Québec, H3C 3J7

3.1 Abstract

We revisit the problem of the formation of DB white dwarfs, as well as the origin of hydrogen in DBA stars, using a new set of envelope model calculations with stratified and mixed hydrogen/helium compositions. We first describe an approximate model to simulate the so-called convective dilution process, where a thin, superficial hydrogen radiative layer is gradually eroded by the underlying and more massive convective helium envelope, thus transforming a DA white dwarf into a DB star. We show that this convective dilution process is able to account for the large increase in the number of DB white dwarfs below $T_{\rm eff} \sim 20,000$ K, but that the residual hydrogen abundances expected from this process are still orders of magnitude lower than those observed in DBA white dwarfs. Scenarios involving the accretion of hydrogen from the interstellar medium or other external bodies have often been invoked to explain these overabundances of hydrogen. In this paper, we describe a new paradigm where hydrogen, initially diluted within the thick stellar envelope, is still present and slowly diffusing upward in the deeper layers of a $T_{\rm eff} \sim 20,000$ K white dwarf. When the convective dilution process occurs, the bottom of the mixed H/He convection zone sinks deep into the star, resulting in large amounts of hydrogen being dredged-up to the stellar surface, a phenomenon similar to that invoked in the context of DQ white dwarfs.

3.2 Introduction

White dwarf stars represent the endpoint of stellar evolution of more than 97% of the stars in the Galaxy, and the determination of their properties thus provides a variety of useful information on the star formation history in our galaxy, and on stellar evolution in general. Having exhausted the nuclear fuel at their center, white dwarfs enter the cooling sequence at effective temperatures around 150,000 K, and gradually cool off at an almost constant radius over several billion years. Because of their high surface gravity of the order of $\log g = 8$, chemical separation induced by gravitational settling is quite efficient, and the leftover from previous evolutionary phases rapidly float to the surface, while heavier elements sink out of sight, thus producing mostly hydrogen- or helium-dominated atmospheres (Schatzman 1958;

Paquette et al. 1986). White dwarfs are found in a variety of flavors: The DA stars, whose spectra are dominated by hydrogen lines, comprise about 80% of the white dwarf population, and their atmospheres are presumably hydrogen-rich. The remaining 20% are generally referred to as non-DA stars. These include the DB (DO) stars, whose spectra are dominated by neutral (ionized) helium lines, the DQ stars that show molecular carbon Swan bands, the DZ stars with metallic absorption features, and the DC stars, which are completely featureless (Wesemael et al. 1993). Moreover, traces of chemical elements are also found at the surface of many white dwarfs, producing a large variety of spectral subtypes (e.g., DAB, DAZ, DBA, DBQ, DBZ, DZA, etc.) depending on the dominant chemical atmospheric constituent. However, these various spectral types are found only in some specific range of temperatures, indicating that there exist several physical mechanisms that compete with gravitational settling to alter the chemical composition of the outer layers of white dwarfs as they evolve along the cooling sequence. Such physical mechanisms include convective mixing, convective dredge-up from the core, accretion from the interstellar medium or circumstellar material, radiative acceleration, and stellar winds (Fontaine & Wesemael 1987).

Perhaps the most significant signature of this spectral evolution of white dwarf stars is the transformation of DA stars into DB stars below $T_{\rm eff} \sim 30,000$ K or so. More than 30 years ago, the ultraviolet-excess Palomar-Green (PG) survey (Green et al. 1986) revealed an almost complete absence of helium-atmosphere white dwarfs between $T_{\rm eff} \sim 45,000$ K, where the coolest DO stars were found, and ∼30,000 K, where the hottest DB white dwarfs appeared in large number (see also Liebert et al. 1986). This so-called DB gap suggested that a fraction of DA stars, about 20%, must turn into DB white dwarfs at some point along the cooling sequence. Even though this gap has now been partially filled by the discovery of very hot DB stars in the Sloan Digital Sky Survey (SDSS, Eisenstein et al. 2006), the number of DB stars in the gap still remains a factor of 2.5 lower than what is expected from the luminosity function. The physical mechanism proposed to explain this DB deficiency as well as the sudden increase in the number of DB stars is the float-up model (Fontaine & Wesemael 1987), where small amounts of hydrogen thoroughly diluted in the envelope of hot white dwarf progenitors, slowly diffuse to the surface, thus gradually transforming a helium-dominated atmosphere into

a hydrogen-rich atmosphere by the time the white dwarf reaches the blue edge of the DB gap near $T_{\rm eff} \sim 45,000$ K. At lower effective temperatures, $T_{\rm eff} \lesssim 30,000$ K, the onset of the helium convection zone would eventually dilute the superficial *radiative* hydrogen layer — a process referred to as convective dilution — thus transforming a DA star into a DB white dwarf, provided that the hydrogen layer is thin enough ($M_{\rm H} \sim 10^{-15}\ M_{\odot}$).

A second significant signature of the spectral evolution of white dwarf stars occurs below $T_{\rm eff} \sim 12,000$ K or so, where the fraction of non-DA to DA white dwarfs increases drastically (Greenstein 1986; Tremblay & Bergeron 2008; Limoges et al. 2015). The most likely explanation for this phenomenon is a process referred to as convective mixing, where the bottom of the superficial *convective* hydrogen layer plunges into the star as it cools off, eventually reaching the deeper and much more massive convective helium layer if the hydrogen layer is thinner than $M_{\rm H}/M_{\star} \lesssim 10^{-6}$ (Koester 1976; Vauclair & Reisse 1977; Dantona & Mazzitelli 1979). At this particular point, hydrogen and helium are convectively mixed into a single mixed H/He convection zone. Because the mixing temperature is a function of the mass of the hydrogen layer (for thicker hydrogen layers, the mixing occurs at lower effective temperatures), the resulting hydrogen-to-helium abundance ratio upon mixing is also a function of the thickness of the hydrogen layer.

Both the convective dilution and the convective mixing processes have been explored quantitatively by MacDonald & Vennes (1991), and more recently by Rolland et al. (2018, hereafter RBF18). In particular, RBF18 showed (see their Figure 16) that the convective mixing scenario predicts H/He abundance ratios upon mixing that agree extremely well with those determined in cool ($T_{\rm eff} < 12,000$ K), He-rich DA white dwarfs where hydrogen (mostly Hα) is detected. Also shown is that these He-rich DA stars will rapidly turn into DC white dwarfs once hydrogen falls below the limit of detectability. RBF18 also explored quantitatively the outcome of the convective dilution process, by predicting the H/He abundance ratios as a function of effective temperature for various thicknesses of the hydrogen layer (see their Figure 14), *assuming the dilution process has already occurred*. The results indicate that hydrogen layer masses between $\log M_{\rm H}/M_{\odot} = -13$ and -10 (according to ML2/$\alpha = 2$ models) are required to account for the presence of hydrogen in the bulk of DBA stars in the range $20,000$ K $\lesssim T_{\rm eff} \lesssim 12,000$ K, ana-

lyzed by RBF18. However, white dwarfs with such large hydrogen layer mass would not mix until they reach temperatures below $T_{\rm eff} \sim 12,000$ K or so. For the convective dilution process to occur, the hydrogen layer mass must be much smaller, of the order of $\log M_{\rm H}/M_{\odot} \lesssim -15$. For such thin hydrogen layers, the H/He ratios predicted in the temperature range where most DBA stars are found are at least three orders of magnitude *smaller* that the observed ratios. In other words, there is much more hydrogen in the outer layers of DBA stars than expected from a simple convective dilution process. This problem has been known for a long time (see MacDonald & Vennes 1991 and references therein).

Even though there is little doubt that the convective dilution process is responsible for transforming a significant fraction (∼20%) of DA stars into DB white dwarfs, the origin of hydrogen in DBA stars is still a subject of debate. Since the hydrogen abundances measured in DBA stars appear too high to have a residual origin, external sources of hydrogen have often been invoked to account for the observed abundances, either from the interstellar medium or from other bodies such as comets, disrupted asteroids, small planets, etc. (MacDonald & Vennes 1991, Jura 2003, Raddi et al. 2015, Gentile Fusillo et al. 2017, Veras et al. 2014). On the other hand, Bergeron et al. (2011) noticed that a lot of the DB white dwarfs in their sample showed no traces of hydrogen, particularly at low effective temperatures, with very stringent upper limits. Such cool hydrogen-deficient DB stars could only have evolved from hotter white dwarf progenitors that contain negligible amounts of hydrogen in their outer stellar envelopes. Based on this observation, Bergeron et al. (2011) found it difficult to reconcile the existence of these "pure" DB white dwarfs with a scenario involving any form of accretion of hydrogen to explain its presence in the photosphere of DBA stars. The authors thus concluded that the presence of hydrogen in DBA stars must be residual, a conclusion also reached by Koester & Kepler (2015). Bergeron et al. (2011) also suggested that perhaps the convective dilution process is not complete, and that hydrogen somehow floats on top of the photosphere rather than being forcefully mixed by the helium convection zone, although Koester & Kepler (2015) considered this scenario unlikely since the convection velocities in the mixed H/He convection zone are many orders of magnitude larger than the diffusion velocities of hydrogen in helium.

At the same time, some white dwarfs with helium-dominated atmospheres have such excep-

tionally large hydrogen abundances — which are also correlated with the presence of metals in large quantities — that there is absolutely no doubt that in these cases hydrogen must have been accreted, most likely from water-rich asteroid debris (Farihi et al. 2013; Raddi et al. 2015, Gentile Fusillo et al. 2017 and references therein). Such objects include SDSS J124231.07+522626.6, GD 16, PG 1225−079, GD 362, and GD 17, also reproduced in Figure 16 of RBF18, which shows the exceptionally large hydrogen abundances measured in these stars with respect to other DBA stars and cool, helium-rich DA white dwarfs. More importantly in the present context, Gentile Fusillo et al. (2017) looked at the population of He-atmosphere white dwarfs from Koester & Kepler (2015), and found that the incidence of hydrogen was strongly correlated with the presence of metals, suggesting that perhaps the majority of helium-rich atmosphere white dwarfs containing hydrogen and metals are likely to have accreted at least some fraction of their hydrogen content in the form of water or hydrated minerals in rocky planetesimal. Since hydrogen will always remain in the mixed H/He convection zone, while the metals will eventually diffuse away from the photospheric regions, perhaps this accretion mechanism can explain the presence of hydrogen *in all DBA stars*.

The question of the accretion of hydrogen, either from the interstellar medium or from other external bodies, has been investigated by RBF18 — see their Section 4.4 and Figure 15. By assuming an average accretion rate over the years, RBF18 found that the required amount of accreted material, with even a moderate accretion rate, would build a superficial hydrogen layer thick enough by the time the white dwarf reaches a temperature of $T_{\rm eff} \sim 30,000$ K, that this object — presumably a DA star — would never turn into a helium-atmosphere DB white dwarf. Based on these arguments, it was concluded that the hydrogen abundances measured in DBA stars could not be accounted for by any kind of accretion mechanism onto a pure helium DB star progenitor. Of course, one obvious solution around this problem is to invoke a scenario where accretion of hydrogen-rich asteroid debris begins only *after* the DA-to-DB transition has occurred, in which case accretion would proceed on a white dwarf with an atmosphere already convectively mixed. Note that so far, this is the only viable scenario to account for the large hydrogen abundances measured in the bulk of DBA white dwarfs. But the question remains: even though there is probably no doubt that hydrogen is accreted in large amounts in some

helium-rich white dwarfs, is accretion responsible for the presence of hydrogen in the bulk of DBA stars?

Given the importance of this question, and given the fact that RBF18 used a rather crude envelope models in their exploratory calculations, we first revisit the questions of convective dilution and of accretion onto DB white dwarfs in the light of more realistic models, as described in Sections 3.3 and 3.4, respectively. We find similar conclusions as RBF18 at the qualitative level. We next present in Section 3.5 an alternative scenario where hydrogen might be dredged up from the deep envelope interior. This is based on the general observation that large amounts of hydrogen (compared to what is needed to form a DA atmosphere, $\sim 10^{-15}\ M_{\odot}$) might still be diluted in the deep envelope, especially if a typical DBA white dwarf descend from PG1159 objects as discussed, for instance, in Quirion et al. (2012). We further discuss our results and conclude in Section 3.6.

3.3 The Convective Dilution Process

Without the presence of any competing mechanism, gravitational settling would progressively force lighter elements — hydrogen in the particular case of DBA white dwarfs — to float to the stellar surface. Due to the relatively high $\log g$ values present in white dwarfs, this migration process should eventually produce a hydrogen-rich atmosphere in a time frame much smaller than the typical evolutionary cooling time [2]. However, for effective temperatures below $T_{\rm eff} \sim 30,000$ K, the deep helium envelope of DB stars becomes convective, thus inhibiting element diffusion. In the case of DA white dwarfs, convection will not set in until the star reaches a temperature of 16,000 K or so. However, if the hydrogen layer is thin enough, of the order of $M_{\rm H} \lesssim 10^{-15}\ M_{\odot}$, DA stars are expected to turn into helium-atmosphere white dwarfs as a result of the erosion of this outer radiative hydrogen layer by the deeper and more massive convective helium envelope — a *convective dilution* process. Within this framework, hydrogen is thus expected to be thoroughly mixed within the convection zone, resulting in a helium-dominated atmosphere with a homogeneous H/He abundance profile.

2. The formation timescale for a DA atmosphere should indeed be relatively short, but this does not mean that all the hydrogen initially present in the star has separated completely from the helium in the deeper regions.

RBF18 explored the convective dilution scenario by using two sets of envelope model calculations: models with homogeneous H/He abundance profiles, and chemically stratified models. In the case of stratified models, the hydrogen layer of a given mass was forced to sit on top of the helium layer, in a very approximate way, and was thus never allowed to mix with the underlying helium envelope. This is obviously not a physically realistic situation, in most cases. A more suitable and physical approach is thus required to model properly the kind of stellar envelopes associated with the convective dilution scenario. We describe a new approach in this section.

3.3.1 Model Envelope Structures

To explore further the convective dilution process, we use the latest version of the Montréal white dwarf model-building code, which includes the same input physics as the full evolutionary models described at length in Fontaine et al. (2001), but with updates discussed briefly in Giammichele et al. (2016). Here we take advantage of a customized version of the code in its envelope configuration (see Brassard & Fontaine 1994 for a first description) where an arbitrary abundance profile can be provided as an input to the model in the form of the mass fractions of hydrogen, helium, carbon, and oxygen as a function of depth. If possible, the program will then try to compute a self-consistent numerical solution with these fixed prerequisites. We use this particular feature of our code to revise the stratified and homogeneous models of RBF18, which we describe in turn.

In RBF18, our stratified models were built using a very rough approximation, where the hydrogen layer was basically sitting on top of the helium envelope, leading to spurious convection zones extending over a few layers near the H/He transition region of our hottest models (see Figure 11 of RBF18). These where due to too sharp a transition in composition at the H/He interface. These approximate thermodynamic structures will be referred to as *seed* models for our improved calculations. Here, we thus go one step further and first solve the diffusion equation to compute the equilibrium H/He abundance profile (see, e.g., Vennes et al. 1988) using these approximate seed models. The resulting abundance profile is then fed back into our code to recompute a new thermodynamic structure that is consistent with this profile; the

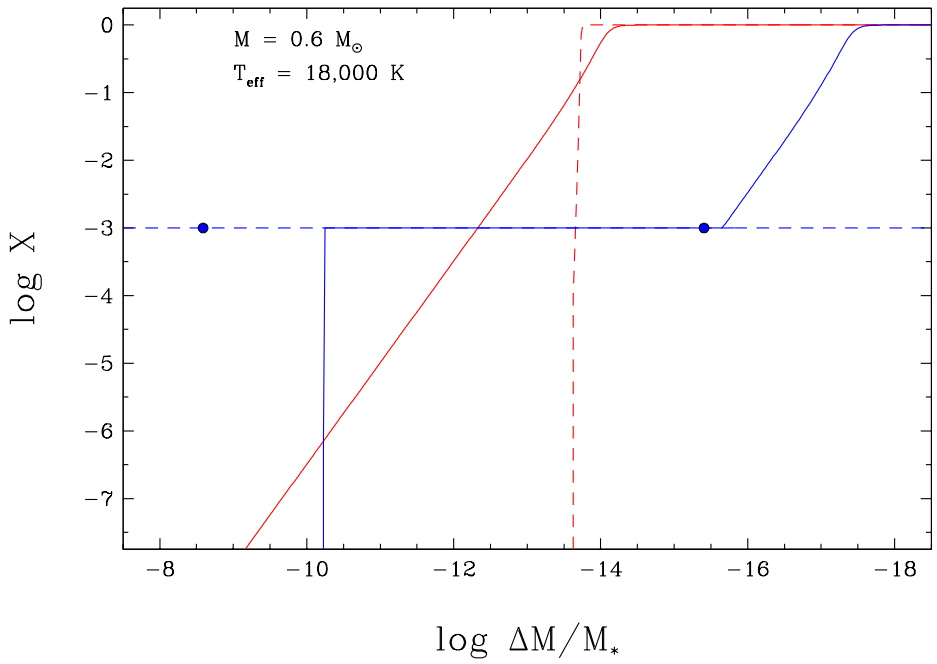

FIGURE 3.1 – Hydrogen mass fraction as a function of depth, expressed as the fractional mass above the point of interest with respect to the total mass of the star, for various types of envelope structures at $T_{\rm eff} = 18,000$ K. Chemically stratified ($\log M_{\rm H}/M_\star = -13.77$) and mixed H/He models ($\log X = -3$) are shown in red and blue, respectively. Our approximate seed models (see text) are represented by dashed lines, while our improved structures are shown as solid lines. The extent of the convection zone in the seed mixed model is indicated with blue dots. All models have been calculated with the ML2/$\alpha = 0.6$ parameterization of the mixing-length theory.

entire procedure is repeated until convergence. The hydrogen mass fraction as a function of depth resulting from this improved model structure is compared in Figure 3.1 (red solid line) with our previous calculations taken from RBF18 (red dashed line) for a typical 0.6 $M_\odot$ model at $T_{\rm eff} = 18,000$ K with $\log M_{\rm H}/M_\star = -13.77$ ($M_\star$ is the mass of the star). As can be seen, the H/He abundance profile in diffusive equilibrium from our improved calculations provides a much smoother transition between the hydrogen and helium layers than our previous models where the transition region is fairly abrupt.

The effect of these improved calculations on the extent of the convection zones, as a function of $T_{\rm eff}$, is illustrated in Figure 3.2 for models at 0.6 $M_\odot$ with $\log M_{\rm H}/M_\star = -13.77$, where our new results are compared with our earlier calculations presented in RBF18 (see their Figure

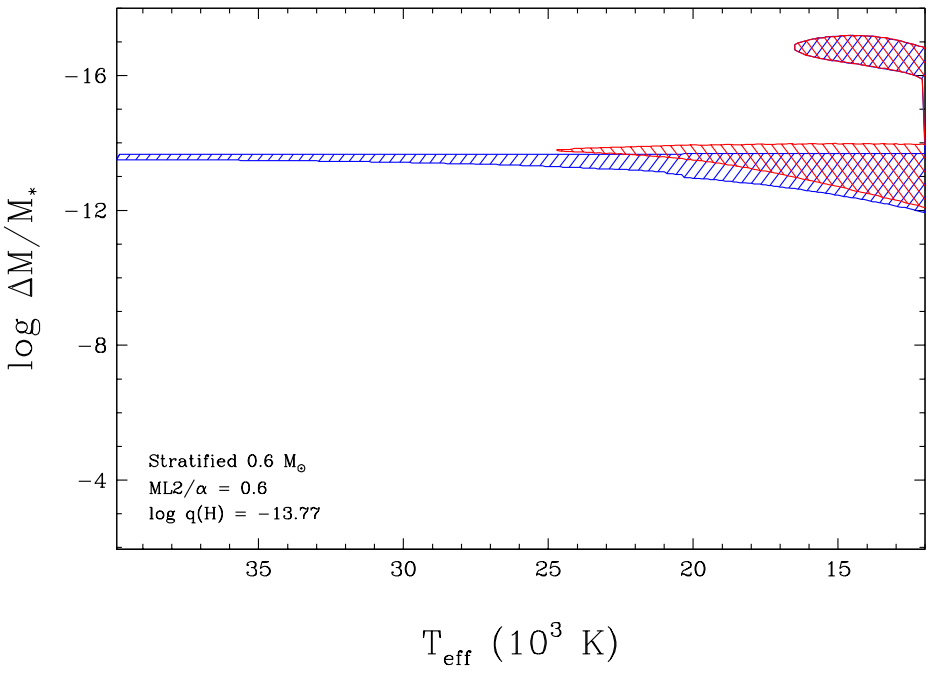

FIGURE 3.2 – Examples of envelope structures for a 0.6 $M_{\odot}$ white dwarf with chemically stratified compositions. The extent of the convection zones are shown by the hatched regions. The models shown in blue correspond to the original calculations presented in RBF18, while those in red are obtained by solving the diffusion equation to compute the equilibrium H/He abundance profile (see also Figure 3.1).

11). The spurious convection zones near the H/He transition region that were present in our earlier calculations (see the discussion above) have all but vanished in our improved models. Also, we can see that at lower effective temperatures, the extent of the helium convective zone has slightly shifted upwards. Note that in our calculations, we neglect the fact that the abundance profile should be constant throughout the convection zone (as opposed to what is displayed by the red solid line in Figure 3.1), because in all cases explored here, either the extent of the convection zone is extremely small — as in Figure 3.2 — or hydrogen remains a trace element, and is thus not affecting the extent of the convection zone. For completeness, we would like to point out that the models displayed in Figure 3.2 are comparable to the solution A shown in Figure 6 of MacDonald & Vennes (1991), where some small amounts of hydrogen is mixed within a shallow helium convection zone, but where most of the hydrogen floats at the surface of the star.

We also revisited our chemically homogeneous models from RBF18 (see their Figures 9 and 10), in which a constant and homogeneous H/He composition was assumed from the surface to the bottom of the stellar envelope, characterized by $M_{\rm env}/M_\star = 10^{-2}$. These earlier models will now serve as seed models for our improved calculations. Here the constant H/He abundance ratio (or equivalently, the hydrogen mass fraction) throughout the stellar envelope is replaced by a piece-wise function that follows these simple criteria: (1) the H/He abundance profile above the convection zone is assumed to be in diffusive equilibrium [3]; (2) the abundance profile must be continuous from the bottom of the convection zone to the surface; (3) the abundance profile is assumed to be constant throughout the convection zone, and set to the H/He abundance ratio of the corresponding seed model; (4) the hydrogen abundance below the convection zone is set to zero. As discussed in RBF18, the presence of hydrogen below the convective layer has no effect on the extent of the convection zone.

An example of this construct is displayed in Figure 3.1 for a 0.6 $M_\odot$ model at $T_{\rm eff} = 18,000$ K (blue solid line); the constant hydrogen mass fraction of the corresponding seed model is also indicated (blue dashed line). Contrary to our previous calculations, the hydrogen abundance above the convection zone (the convection zone is represented by the flat region at $\log X = -3$) increases steadily towards the surface, as expected from a diffusive equilibrium profile (see also Figure 6 of MacDonald & Vennes 1991). More importantly in the present context, the presence of hydrogen at the surface has the effect of modifying the extent of the mixed H/He convection zone underneath, as indicated by the two blue dots in Figure 3.1, which show the extent of the convection zone in our homogeneous seed model. In particular, the bottom of the convection zone has moved significantly higher in the envelope of our new models. Eventually, if there is too much hydrogen at the surface, convection in the deeper envelope will become completely inhibited. When this situation occurs, we should recover the stratified models described above. Again, we would like to point out that our improved model displayed in Figure 3.1 is comparable, in this case, to the solution E shown in Figure 6 of MacDonald & Vennes (1991), where a large amount of hydrogen is mixed within a deep helium convection zone, with very little hydrogen floating at the surface of the star.

3. This approximation is identical to that described in MacDonald & Vennes (1991).

Following this procedure, we calculated a full grid of these envelope models assuming, for the time being, the ML2/α = 0.6 parameterization of the mixing-length theory to treat convective energy transport [4]. Our grid covers a range of effective temperature between $T_{\rm eff}$ = 12,000 K and 60,000 K by steps of 100 K, and hydrogen mass fraction in the convection zone [5], $X_{\rm cz}$, ranging from $\log X_{\rm cz} = -7.75$ to -0.25 by steps of 0.25 dex, thus covering essentially the entire range between pure helium and nearly pure hydrogen compositions.

The hydrogen mass fraction as a function of depth is displayed in Figure 3.3 for 0.6 $M_{\odot}$ models at $T_{\rm eff}$ = 20,000 K, and with various values of the hydrogen mass fraction in the mixed H/He convection zone ($X_{\rm cz}$). In each model, the extent of the convection zone can be identified by the flat part of the abundance profile. Similar envelope structures are displayed in Figure 3.4, but this time as a function of effective temperature. Here the extent of the convection zone is shown by the hatched region, while the location of the photosphere is indicated by the red line. Note that, because of the way these models are constructed, the total hydrogen mass present in the stellar envelope varies as a function of effective temperature for a given value of $X_{\rm cz}$. Therefore, these must not be interpreted as evolutionary sequences in any way.

Also reproduced by the dashed lines in Figure 3.4 is the extent of the convection zone in our previous homogeneous models. These can be used to evaluate the effects of the additional superficial hydrogen layer on the model structure, a single example of which was displayed in Figure 3.1. In the most helium-rich models, the new envelope structures are essentially identical to their homogeneous counterparts, where convection zones due to the partial ionization of He II and He I are both present, and merge below ∼25,000 K. As the hydrogen content in the convection zone is increased, differences between the homogeneous models and our new calculations become more apparent. Although the extent of the convection zone is significantly reduced in both sets of models when the hydrogen content is increased, the effect is much more pronounced in our new calculations, in particular at low effective temperature, where the entire convection zone moves higher in the envelope by an amount ranging from 0.5 dex (top of the convection zone) to sometimes more than two orders of magnitude (bottom). We also note a

4. The ML2/α = 2.0 parameterization was also considered for all our calculations. The figures related to these results are available in the online journal.

5. If more than one convection zone is present, the hydrogen mass fraction of the deepest and most massive convection zone — usually associated with He II — is adopted.

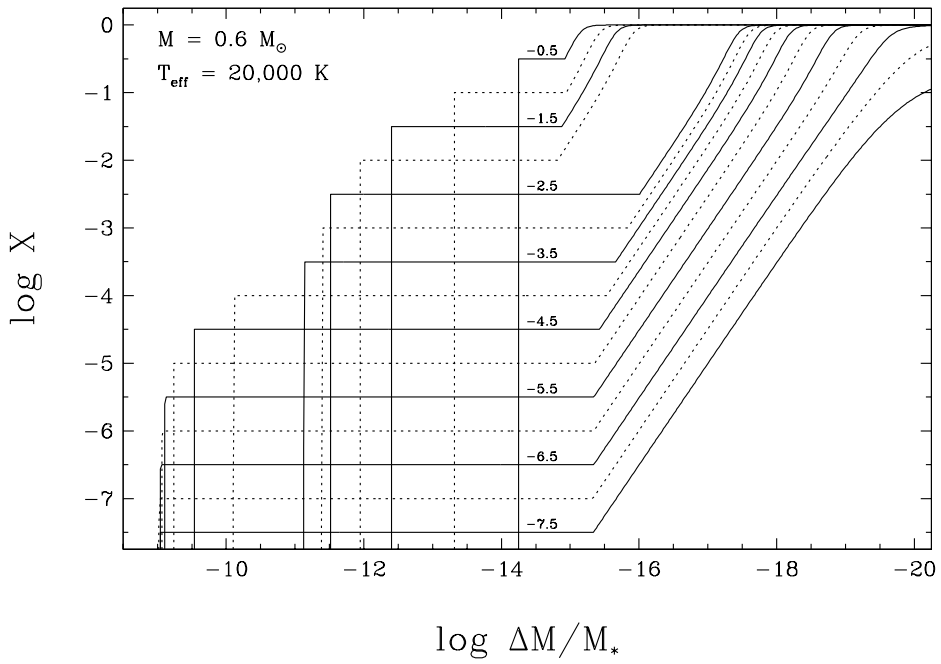

FIGURE 3.3 – Hydrogen mass fraction as a function of depth for our new envelope models at 0.6 $M_{\odot}$, $T_{\rm eff} = 20,000$ K, and with various values of the hydrogen mass fraction in the mixed H/He convection zone ($\log X_{\rm cz}$), labeled in the figure.

migration of the photosphere towards the surface, resulting from the increased opacity due to hydrogen in the upper layers, in particular below $T_{\rm eff} \sim 20,000$ K.

For $\log X_{\rm cz} > -3.5$, the superficial convection zone caused by the partial ionization of He I starts to form at lower effective temperatures — due to the increased abundance of hydrogen at the surface — until it is completely suppressed when $\log X_{\rm cz} \gtrsim -1.75$, a phenomenon that is not observed in our homogeneous models. In the most hydrogen-rich models displayed here, the convection zone is also unable to reach the deeper layers of the envelope below ∼15,000 K, and it is confined to $\log \Delta M/M_{\star} < -11$. In contrast, our previous homogeneous models go much deeper.

3.3.2 Total Hydrogen Mass

The new calculations described in the previous section allow us to explore the convective dilution process in greater detail. We remind the reader that this process describes the outcome of a DA white dwarf for which the superficial hydrogen layer has been thoroughly diluted

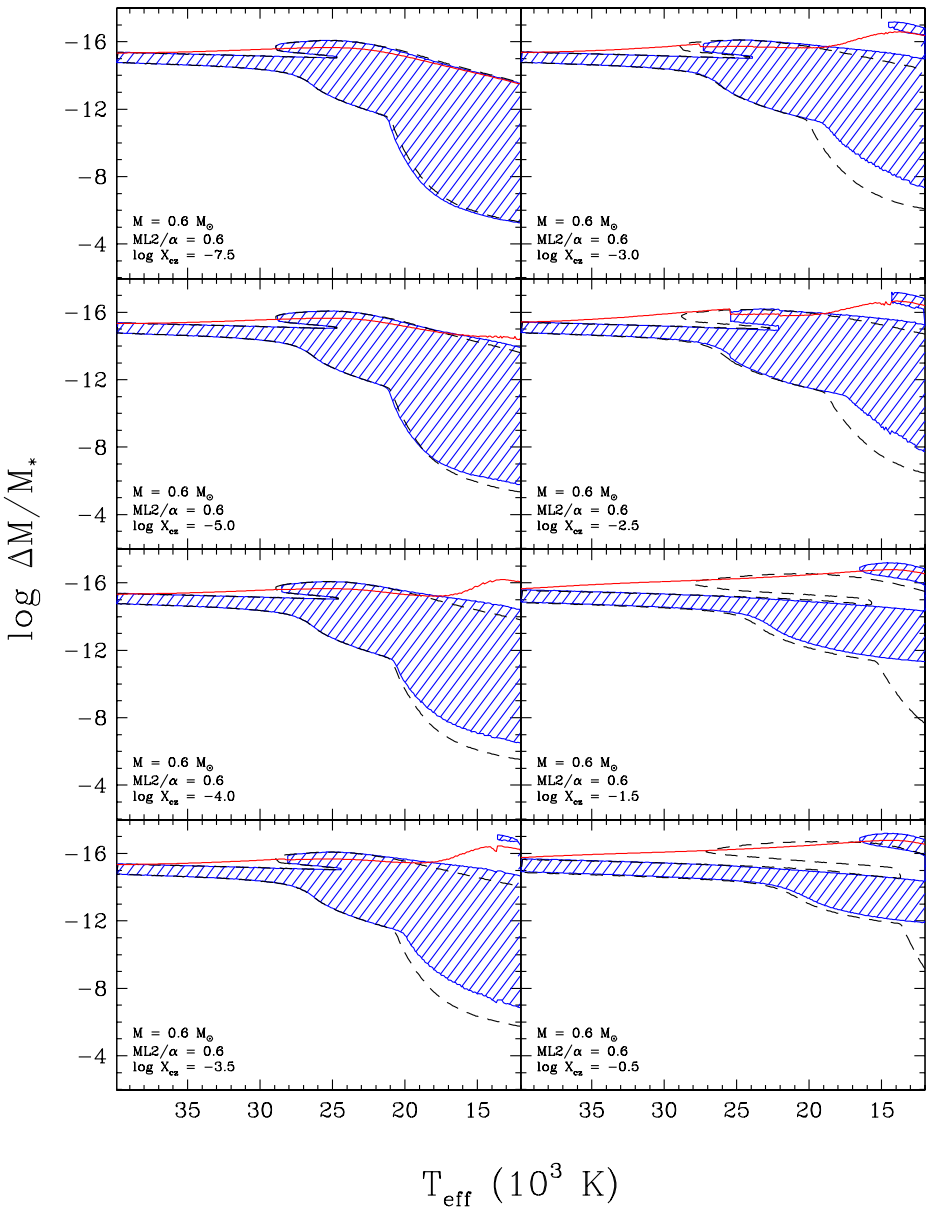

FIGURE 3.4 – Examples of our new envelope models for white dwarf models at 0.6 $M_{\odot}$, and with increasing hydrogen mass fraction in the convection zone, $X_{\rm cz}$, from upper left to bottom right. The convection zones are shown by the hatched region, while the red solid line indicates the location of the photosphere. For comparison, the dashed lines indicate the extent of the convection zone for models with a homogeneous abundance profile throughout the stellar envelope.

within the underlying helium convection zone. To predict the behavior of this physical process as a function of time (i.e., with decreasing effective temperature), we must perform a detailed analysis of the $T_{\rm eff} - M_{\rm H}$ parameter space in order to identify the contours of constant total hydrogen mass. To do so, we first compute the total amount of hydrogen present in each stellar envelope of our model grid. The results of these calculations are presented in Figure 3.5 where we show the total hydrogen mass content, $M_{\rm H}$, as a function effective temperature for various values of the hydrogen mass fraction in the convection zone, $X_{\rm cz}$. To make things clear, each curve in this plot corresponds to a series of envelope models similar to those shown in Figure 3.4 (each panel corresponds to a given value of $X_{\rm cz}$), where the total hydrogen mass has been integrated at each temperature.

The first feature that arises naturally from our calculations is the existence of an upper limit to the total hydrogen mass that a white dwarf can contain given our assumed envelope structures. For instance, there is no envelope structure above $T_{\rm eff} \sim 22,000$ K with a total hydrogen mass of $\log M_{\rm H}/M_{\odot} = -14.5$ (for ML2/$\alpha = 0.6$ models). Stellar envelopes having such a large, or even larger, hydrogen mass would require $\log X_{\rm cz} \rightarrow 0$ (i.e. $X_{\rm cz} \rightarrow 1$), and can only exist if their structure is chemically stratified, corresponding to the DA star configurations described earlier. Since similar constraints can be obtained at all effective temperatures, this defines a region in the $T_{\rm eff} - M_{\rm H}$ parameter space, represented by the red hatched area in Figure 3.5, where white dwarfs can only exist as chemically stratified DA stars.

By using the results displayed in Figure 3.5, it is now possible to follow the evolution of $X_{\rm cz}$ as a function of decreasing effective temperature for a given value of $M_{\rm H}$ by drawing a straight horizontal line across the diagram at the appropriate value. One can see that there is a unique solution for $X_{\rm cz}$ at all temperatures for all values of $\log M_{\rm H}/M_{\odot} < -16$. For larger values of $M_{\rm H}$, there is also a unique solution as long as the temperature remains high ($T_{\rm eff} \gtrsim 25,000$ K); this can be explained by the fact that at these temperatures, the extent of the convection zone is relatively independent of the amount of hydrogen diluted within the convective envelope, as observed in Figure 3.4. At lower temperatures and higher total hydrogen content, however, there are multiple solutions for the same value of $M_{\rm H}$, generally separated by orders of magnitude, resulting from the feedback effect of hydrogen at the surface.

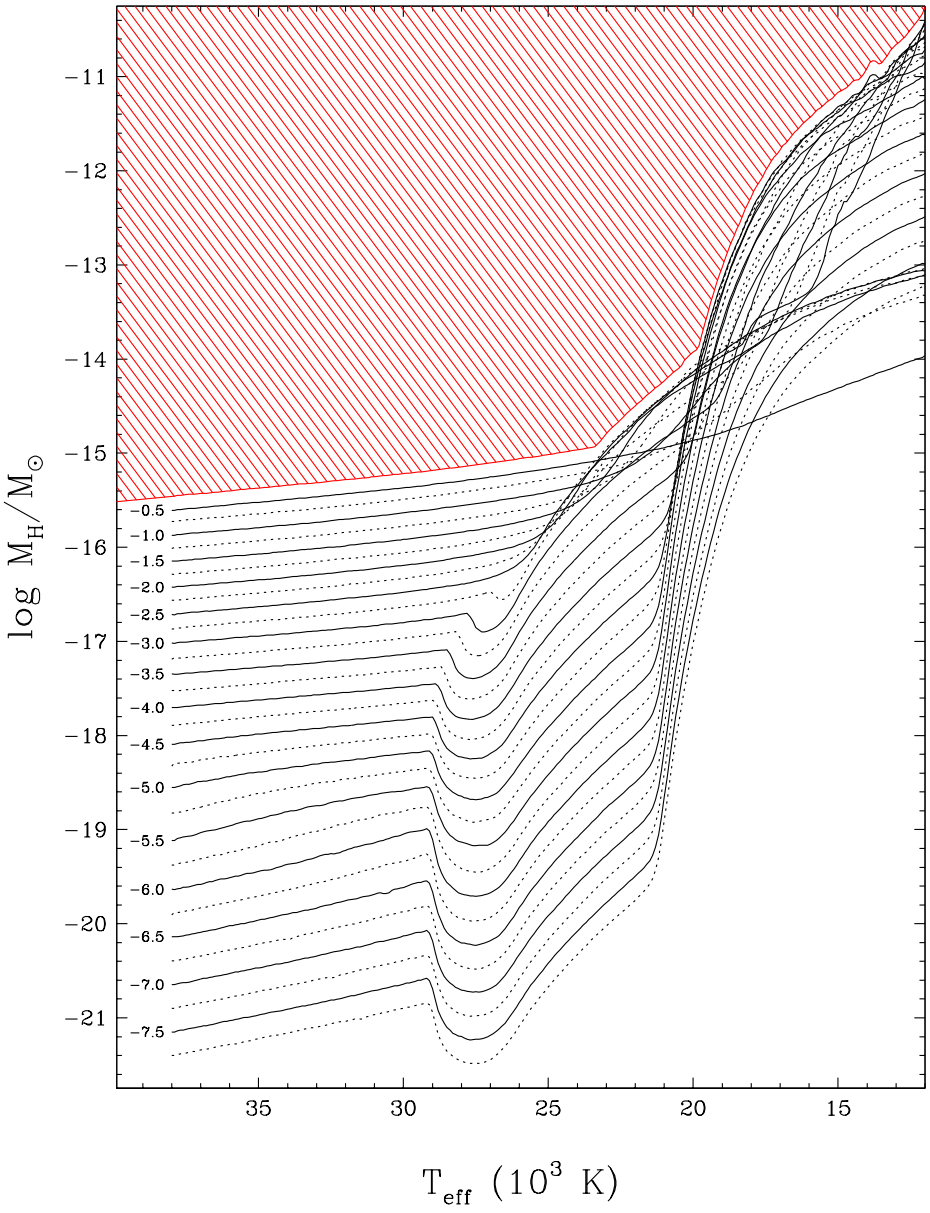

FIGURE 3.5 – Total hydrogen mass, $M_{\rm H}$, in our improved envelope models at 0.6 $M_{\odot}$ as a function of effective temperature, and for various values of the hydrogen mass fraction in the convection zone, $X_{\rm cz}$, labeled on each curve. The region where white dwarfs should appear as DA stars is indicated by the red hatched area.

Indeed, a careful examination of the results shown in Figure 3.4 reveals that for large values of $X_{\rm cz}$ ($\log X_{\rm cz} \gtrsim -2.5$), the convection zone below 25,000 K shrinks faster than the increasing hydrogen abundance, resulting in a gradual decrease of the total hydrogen mass contained in the stellar envelope. These degeneracies thus simply reflect the possibility of mixing the same total amount of hydrogen in a deep, or in a shallow, convection zone.

Note that MacDonald & Vennes (1991) also found such multiple solutions for some $T_{\rm eff}$ values — see in particular their Figures 1 and 6 — some of which were unstable. In general, there is one solution corresponding to a DA star configuration (the chemically stratified model), and one corresponding to a DBA star configuration (hydrogen appears as a trace in the mixed convection zone), but in some cases there is another solution where helium is considered a trace element in diffusive equilibrium within the superficial hydrogen-rich layer (the solution C in their Figure 6). As discussed by MacDonald & Vennes, these last solutions probably do not exist in nature.

We can use similar considerations to decide which solution to adopt in our analysis. In Figure 3.6, we show the photospheric hydrogen-to-helium abundance ratio, measured in our models at an optical depth of $\tau_R = 2/3$, as a function of effective temperature, and for various values of the hydrogen mass fraction in the convection zone, $X_{\rm cz}$. Since we are interested in DBA star configurations where hydrogen is always a trace element, we can use these results to lift the degeneracies by adopting in Figure 3.5 the appropriate solution for $X_{\rm cz}$ that is representative of DBA white dwarfs. For instance, below $T_{\rm eff} \sim 20,000$ K, the H/He ratio is always larger than 10^4 when $\log X_{\rm cz} > -2$. Such high photospheric abundances are more representative of hydrogen-rich atmospheres (i.e., DA stars) and thus cannot be used to explain the bulk of DBA white dwarfs. At higher effective temperatures, however, they might in some cases represent the transition models between a stratified and a fully diluted envelope.

3.3.3 Convective Dilution Simulations

In order to follow the spectral evolution of white dwarfs with a constant total hydrogen mass, we start with a chemically stratified model at high effective temperature ($T_{\rm eff} \sim 60,000$ K) and a given value of $M_{\rm H}$. We then search a model (with our new envelope structures)

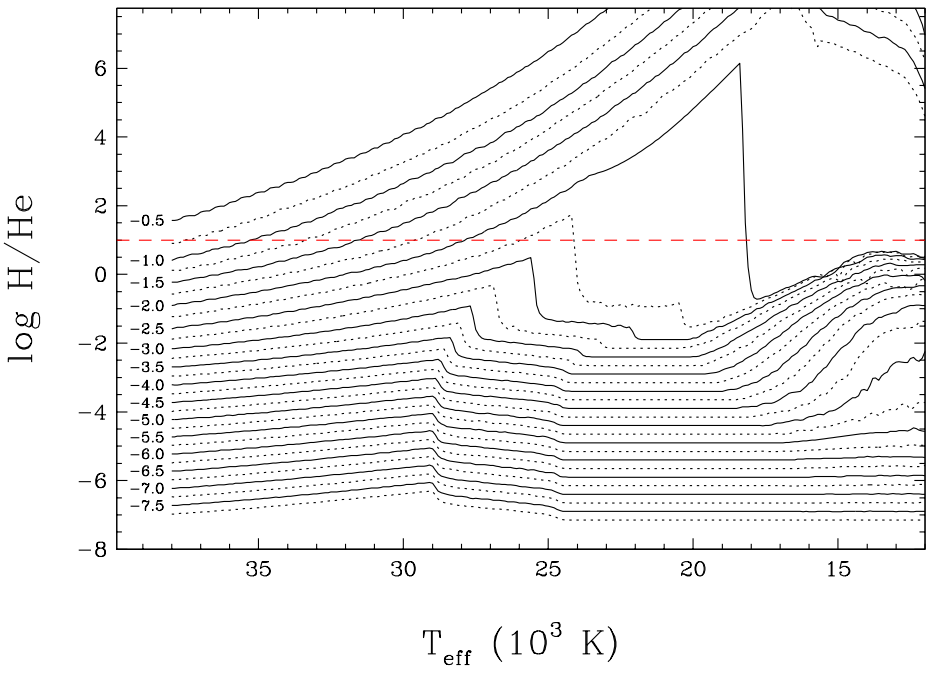

FIGURE 3.6 – Hydrogen-to-helium abundance ratio measured at the photosphere ($\tau_R = 2/3$) of our 0.6 $M_\odot$ envelope models as a function of effective temperature. Each curve is labeled by the value of the hydrogen mass fraction in the convection zone, $\log X_{\rm cz}$. The limit above which an object is assumed to appear as a DA white dwarf is indicated by the red dashed line.

in the $T_{\rm eff} - M_{\rm H}$ parameter space (see Figure 3.5) for which the convection zone corresponds to its stratified counterpart. If no such convective envelope exists, we repeat the procedure with a slightly cooler stratified model until an appropriate match is found. At that point, we only rely on our new envelope structures and always select, for a given value of $M_{\rm H}$, the slightly cooler model with the closest value of $X_{\rm cz}$. This approach offers a simple and efficient way to discriminate between the different $T_{\rm eff} - M_{\rm H}$ degeneracies at a given effective temperature, and thus ensures a near-continuity in the evolution of the thermodynamic structures.

Examples of our envelope structures with constant values of the total hydrogen mass present in the stellar envelope, $M_{\rm H}$, are displayed in Figure 3.7. The location of the photosphere as well as the extent of the convection zones are indicated in each panel. Even though these sequences represent static envelope models, we believe they provide a good representation of the convective dilution scenario, which, in reality, is a much more complex dynamical

process. We first note that, within our framework, white dwarfs with a total hydrogen mass of $\log M_{\rm H}/M_{\odot} \geq -13.75$ will never undergo dilution. Such objects should remain DA stars until the superficial hydrogen convection zone reaches the deeper convective helium layers (when $T_{\rm eff} < 12,000$ K), at which point convective mixing occurs if the hydrogen layer is not too thick (see Figure 16 of RBF18). At the other end of the mass spectrum, our models are almost identical to pure helium-envelope white dwarfs if $\log M_{\rm H} \lesssim -16.0\ M_{\odot}$. For such thin hydrogen layers, there is not enough hydrogen accumulated at the surface of the star to appear as a DA white dwarf (see Figures 3 and 4 of Manseau et al. 2016). Instead, these objects would appear as stratified DAB stars, with a thin hydrogen layer floating in diffusive equilibrium at the stellar surface.

Our version of the convective dilution mechanism should thus be effective for white dwarf envelopes containing an amount of hydrogen ranging from $10^{-16}\ M_{\odot}$ to $10^{-14}\ M_{\odot}$. The *transition temperatures* at which this physical process is expected to occur are summarized in Table 3.1. We can see that depending on the thickness of the hydrogen layer, the DA-to-DB transition takes place over a narrow range of mixing temperatures, namely between $T_{\rm eff} \sim 25,000$ K and ∼15,000 K. The sudden transition in surface abundance can be observed in Figure 3.7 when the photosphere, indicated by the red line, moves from the radiative hydrogen layer into the mixed H/He convection zone. As noted by many authors, including MacDonald & Vennes (1991) and RBF18, there is a direct correlation between the mixing temperature and $M_{\rm H}$, the latter delaying the growth of the underlying helium convection zone. Even if our approach is not based on time-dependent calculations, we can expect the duration of this dynamical transformation to be much shorter than the typical cooling time, spanning at most 500 K or $\sim 10^7$ years. Since the depletion of the superficial hydrogen layer leads to a rapid growth of the helium convection zone, convective dilution can be viewed as a cascade-like process, which becomes increasingly efficient as hydrogen gradually disappears from the surface.

We now compare the predictions of our convective dilution model with the photospheric H/He abundance pattern observed in DB and DBA white dwarfs. The results of our simulations are presented in Figure 3.8, together with the determination of the hydrogen-to-helium

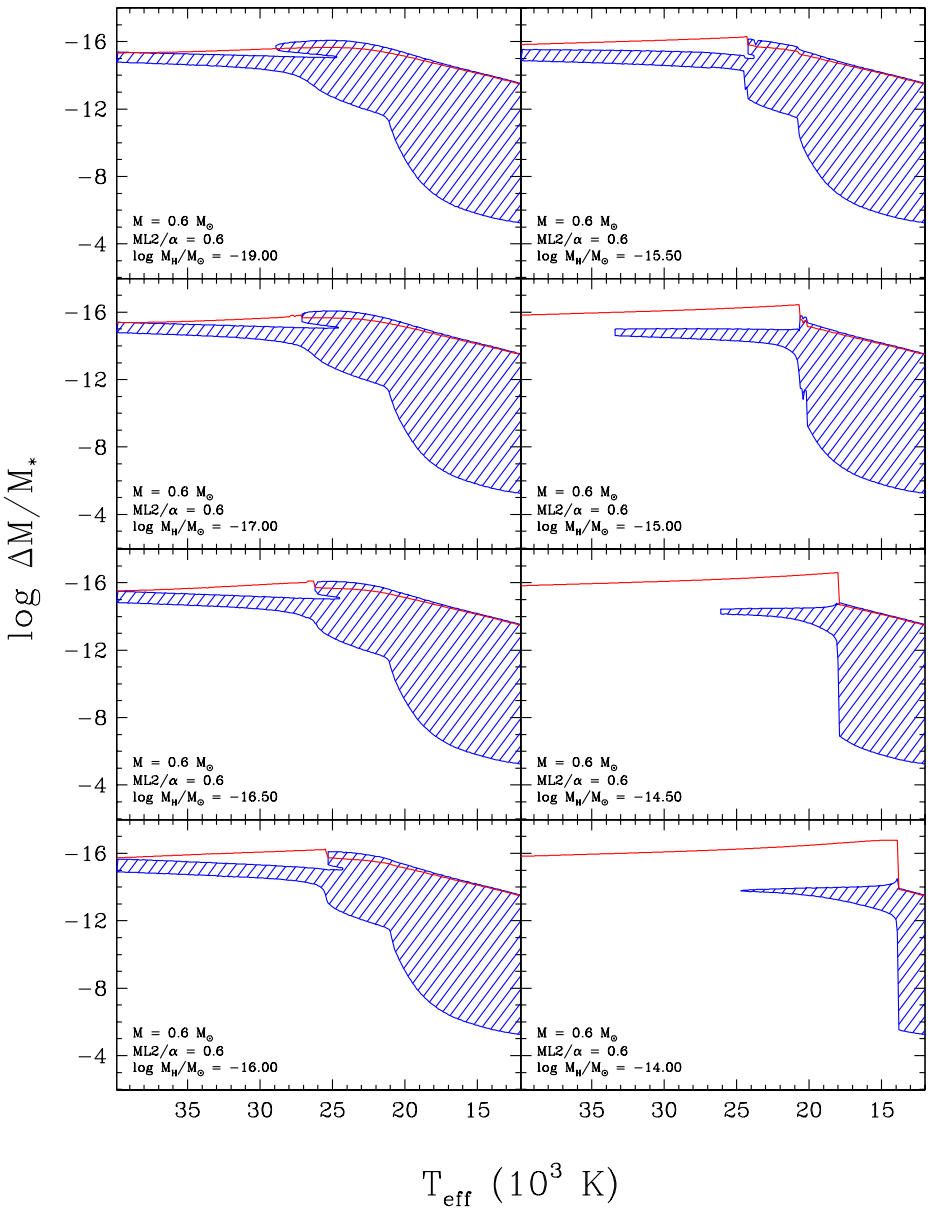

FIGURE 3.7 – Examples of envelope structures for white dwarf models subject to a convective dilution process as a function of effective temperature. The depth is expressed as the fractional mass above the point of interest with respect to the total mass of the star. The red solid line corresponds to the location of the photosphere, and the convection zones are shown by the hatched region. The models illustrated here are (from upper left to bottom right) for 0.6 $M_{\odot}$ with increasing total hydrogen mass in the stellar envelope. The results shown here assume a ML2/α = 0.6 parameterization of the convective efficiency.

TABLE 3.1 – Hydrogen- to Helium-Atmosphere Transition Temperatures

$\log M_{\rm H}/M_{\odot}$	$T_{\rm eff}$ (K)
−16.00	25,400
−15.75	24,800
−15.50	24,200
−15.25	23,500
−15.00	20,600
−14.75	19,300
−14.50	17,900
−14.25	16,100
−14.00	13,800

abundance ratio, as a function of effective temperature, for all DB and DBA white dwarfs in the sample of RBF18 (see their Figure 5) and in the SDSS sample of Koester & Kepler (2015). Our results indicate that white dwarfs above $T_{\rm eff} \sim 22,000$ K can easily be explained if the total hydrogen mass is lower than $\log M_{\rm H}/M_{\odot} \sim -16.5$. As mentioned above, these objects have never been genuine DA stars at higher temperatures, and their most likely progenitors are the hot DB stars identified in the DB-gap by Eisenstein et al. (2006). Note that the few DBA white dwarfs in this temperature range will rapidly evolve into DB stars, with no detectable traces of hydrogen, as a result of the growth of the helium convective zone with decreasing effective temperature, which should efficiently dilute any residual amount of hydrogen present in the outer layers (see also Koester & Kepler 2015). Interestingly enough, the DBA star LP 497-114 (WD 1311+129) — the most hydrogen-rich object in Figure 3.8 near $T_{\rm eff} \sim 22,000$ K — lies close to the $10^{-15.25}$ $M_{\odot}$ transformation branch, suggesting that this white dwarf might be in the process of being convectively mixed, as suggested by Bergeron et al. (2011, see their Section 5.4), who also reported spectroscopic variations in this object (see their Figure 28).

The bulk of DB and DBA white dwarfs in Figure 3.8 is found below 20,000 K, however, where the bottom of the helium convection zone sinks rapidly into the stellar envelope. The significant increase in the number of DB white dwarfs in this temperature range can be most easily explained by the convective dilution process, with a total hydrogen mass in the range $-16 < \log M_{\rm H}/M_{\odot} < -14$ according to our calculations. However, if the mixing temperatures predicted by our simulations agree well with the increased number of DB white dwarfs, the amount of residual hydrogen expected after mixing has occurred is several orders of magnitude

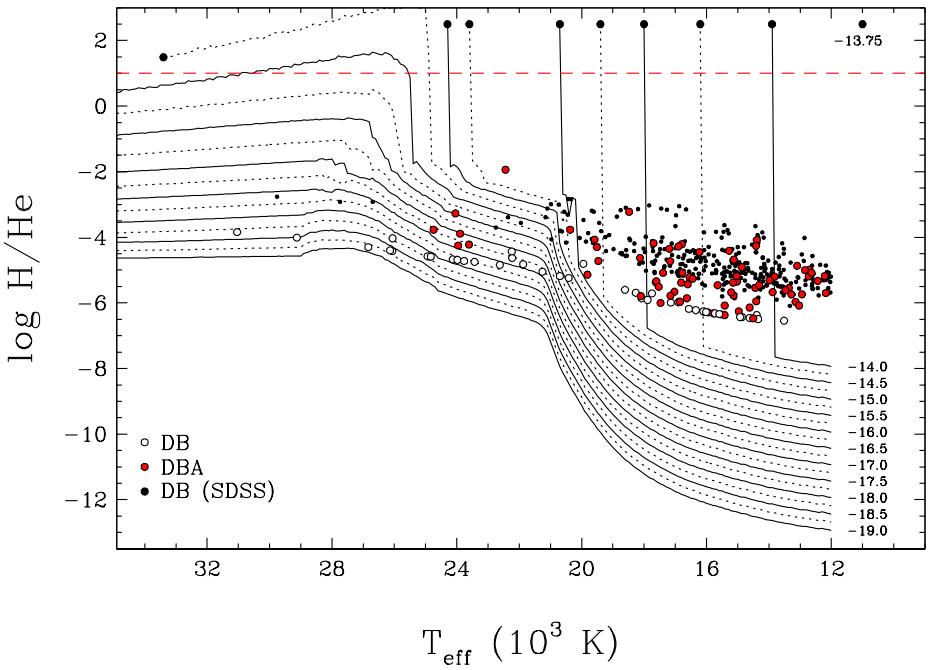

FIGURE 3.8 – Results of our convective dilution simulations for models at 0.6 $M_{\odot}$ for the ML2/α = 0.6 version of the mixing-length theory. Each curve is labeled with the corresponding value of $\log M_{\rm H}/M_{\odot}$. The red dashed line indicates our empirical limit above which a white dwarf should appear as a DA star. Observed hydrogen abundances, or limits, for DB and DBA white dwarfs from RBF18 and Koester & Kepler (2015) are also reproduced.

below the observed abundances in DBA stars, a conclusion also reached in all previous investigations (see RBF18, MacDonald & Vennes 1991, and references therein). As discussed by RBF18, in order to match the observed hydrogen abundances in DBA white dwarfs, hydrogen layer masses larger than $\log M_{\rm H}/M_{\odot} \sim -13$ are required, in which case the convective dilution process becomes impossible.

We must therefore conclude that most, but not all, helium-atmosphere white dwarfs cooler than $T_{\rm eff} \sim 30,000$ K containing traces of hydrogen cannot be explained in terms of our version of the convective dilution scenario. The most common solution proposed to solve this problem is to assume that a significant fraction of DB stars are indeed the result of a convective dilution scenario, with DA progenitors having very thin hydrogen layers ($\log M_{\rm H}/M_{\odot} \leq -15$), but that after the DA-to-DB transition has occurred, accretion of hydrogen from the interstellar medium or other external bodies (comets, disrupted asteroids, etc.) increases the hydrogen content in

the stellar envelope, up to the level observed in DBA white dwarfs. But as discussed in RBF18 (see their Figure 15), the amount of accreted material required to account for the observed abundances in DBA stars will most likely build a thick enough hydrogen layer in the earlier evolutionary phases, such that the convective dilution process will again become impossible. In the next section, we explore the effect of accretion more quantitatively.

3.4 Accretion from External Sources

To study the effect of the accretion of hydrogen from external sources, we repeat our previous calculations by considering a constant accretion process onto a pure helium-envelope white dwarf at 0.6 $M_{\odot}$. We consider various accretion rates ranging from $\dot{M} = 10^{-27}$ $M_{\odot}$ yr^{-1} to $10^{-16.5}$ $M_{\odot}$ yr^{-1} by steps of 0.25 dex, and calculate the total accreted mass of hydrogen as a function of the white dwarf cooling time, or equivalently, as a function of effective temperature. The total accreted mass of hydrogen as a function of $T_{\rm eff}$ is displayed in Figure 3.9 for various values of the accretion rate. As in Figure 3.5, the red hatched area represents the region in the $T_{\rm eff} - M_{\rm H}$ parameter space where white dwarfs can only appear as chemically stratified DA stars. The hydrogen- to helium-atmosphere transition temperatures from Table 3.1 is also reproduced. As can already be seen from this figure, if the average accretion rate is too large, $\dot{M} \gtrsim 10^{-22}$ $M_{\odot}$ yr^{-1}, the star will have accumulated so much hydrogen that it will necessarily appear as a DA white dwarf in the entire temperature range displayed here.

We show in Figure 3.10 how our envelope structures, subject to the convective dilution process, are affected by the presence of accretion from external sources of hydrogen. The main noticeable behavior is the cumulative effect of hydrogen on the development of a massive convection zone, which gradually disappears with increasing accretion rate. As previously anticipated, the growth of the convection zone is almost completely inhibited if the average accretion rate exceeds $\sim 10^{-22.25}$ $M_{\odot}$ yr^{-1}. Such white dwarfs should be able to build a sufficiently thick hydrogen-rich envelope to still appear as a DA star below 20,000 K, thus avoiding the transformation into a DBA hybrid.

The photospheric hydrogen abundances as a function of $T_{\rm eff}$ predicted by our convective dilution model in the presence of accretion are displayed in Figure 3.11. These results confirm

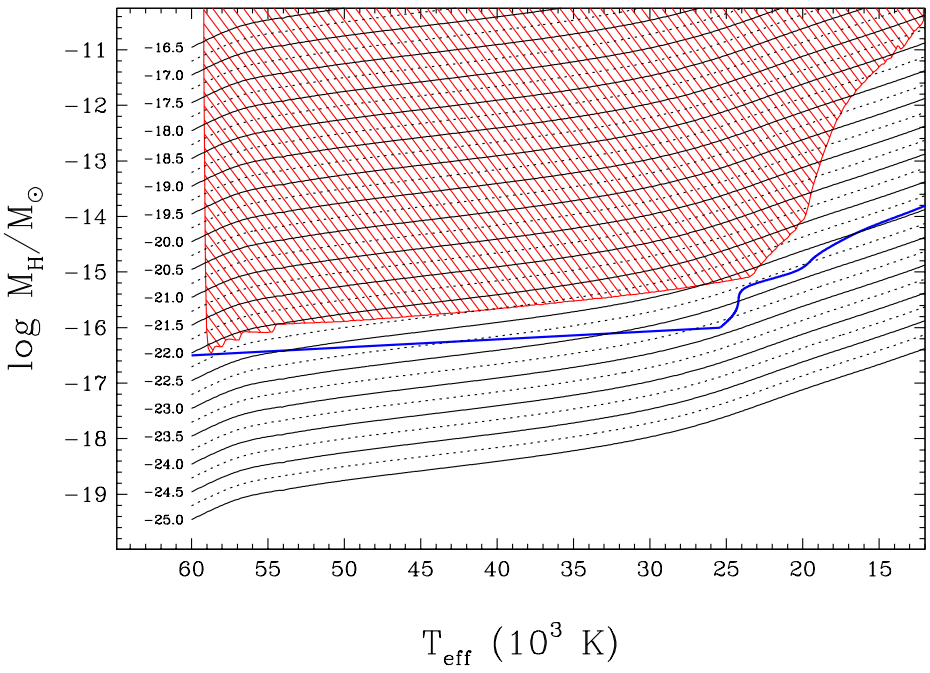

FIGURE 3.9 – Total accreted mass of hydrogen onto a 0.6 $M_{\odot}$ pure helium-envelope white dwarf as a function of effective temperature and for various accretion rates. Each curve is labeled with the corresponding accretion rate in solar mass per year (on a logarithmic scale). The red hatched area represents the region where white dwarfs can only appear as chemically stratified DA stars. The hydrogen- to helium-atmosphere transition temperatures (see Table 3.1) is indicated by the blue line.

our previous expectations, that the convective dilution process will occur in the presence of accretion, but only for extremely low accretion rates of $\dot{M} \lesssim 10^{-23}$ $M_{\odot}$ yr^{-1}. This upper limit is 2 to 5 orders of magnitude smaller than the accretion rate required to account for the observed hydrogen abundances in DBA white dwarfs (see Figure 15 of RBF18 in particular). But according to our calculations, such high accretions rates will produce DA star progenitors with hydrogen layers that are thick enough to prevent any form of DA-to-DB transformation in the appropriate range of temperature. Note that we exclude here the scenario where large bodies such as small planets, comets, or disrupted asteroids have been accreted *after mixing has occurred*, as often invoked in objects such as GD 16, GD 17, GD 40, GD 61, G241-6, PG 1225+079, and HS 2253+8023, which all show evidence of accretion of water-rich material (Raddi et al. 2015, Gentile Fusillo et al. 2017). However, we do not believe that this particular scenario applies to the bulk of DBA white dwarfs, although it cannot be completely ruled out.

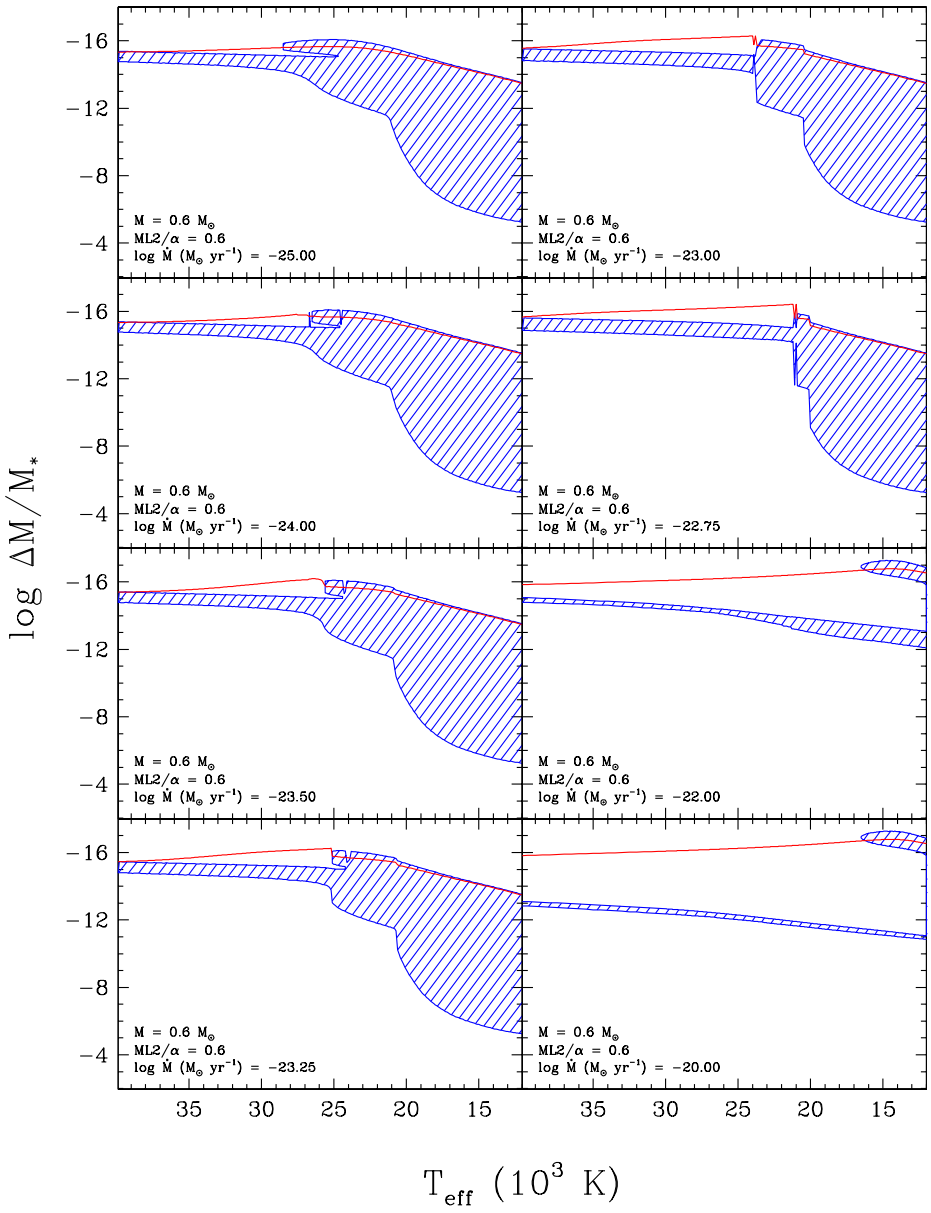

FIGURE 3.10 – Examples of envelope structures for white dwarf models subject to a convective dilution process, similar to those shown in Figure 3.8, but by also taking into account accretion from external sources of hydrogen. The models illustrated here are (from upper left to bottom right) for 0.6 $M_{\odot}$ with increasing hydrogen accretion rates expressed in solar masses per year.

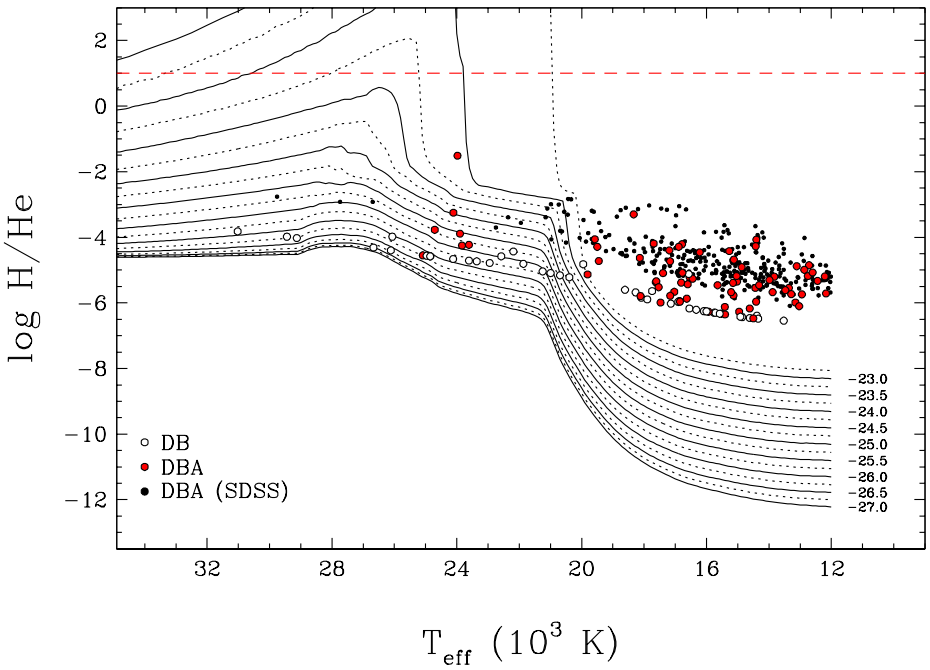

FIGURE 3.11 – Same as Figure 3.8, but for a 0.6 $M_{\odot}$ pure helium envelope white dwarf subject to accretion. Each curve is labeled with the corresponding accretion rate in solar mass per year (on a logarithmic scale).

Hence, we conclude that the amount of hydrogen observed in DBA stars cannot be explained as having a residual origin — the leftovers from the convective dilution scenario — nor can it be accounted for by accretion, at least in terms of an average accretion rate. In the next section, we present an alternative possibility as a solution to the problem of hydrogen in DBA white dwarfs.

3.5 A Convective Dredge-up Model

3.5.1 The Hydrogen Diffusion Tail

As part of an independent investigation aimed at studying the spectral evolution of hot white dwarfs (A. Bédard et al. 2019, in preparation), we performed time-dependent diffusion calculations, with a particular interest in following the diffusion of hydrogen towards the surface — the so-called float-up model — the mechanism believed to be responsible for turning most hot, helium-atmosphere white dwarfs into DA stars by the time they reach the red edge of the

DB gap (Fontaine & Wesemael 1987). As an illustrative example, we discuss here a particular white dwarf evolutionary track at 0.6 $M_{\odot}$, the details of which will be presented elsewhere. We begin with a typical PG1159 progenitor that has evolved through late thermal flash episodes, where the content of both hydrogen and helium has been significantly depleted (Werner & Herwig 2006). Our initial stellar envelope is thus composed of a homogeneous mixture of H/He/C/O all the way from the surface to a depth of $\log M_{\rm env}/M_{\star} = -1.87$, surrounding an inner C/O core. The chemical composition of the atmosphere and envelope of our initial model is characterized by mass fractions of $X({\rm H}) = 10^{-6}$, $X({\rm He}) = 0.42$, $X({\rm C}) = 0.43$, and $X({\rm O}) = 0.15$, corresponding to a total amount of hydrogen of $\log M_{\rm H}/M_{\star} = -7.62$ (or $\log M_{\rm H}/M_{\odot} = -7.84$), thoroughly diluted within the deep stellar envelope. Possible residual nuclear burning of hydrogen is neglected.

As time proceeds, helium rapidly rises to the surface, transforming the PG1159 progenitor into a DO white dwarf, and eventually into a DB star at lower effective temperatures. Hydrogen also diffuses upward, but much more slowly, eventually reaching the outer surface, at which point the object becomes a DA white dwarf. We show in Figure 3.12 a snapshot at $T_{\rm eff} = 20,247$ K of the hydrogen and helium mass fractions as a function of depth. Note that in this particular sequence, the amount of hydrogen accumulated in the outer envelope, $\log M_{\rm H}/M_{\star} \sim -11$, is way too large for any convective dilution process to occur, and this star will turn into a DC white dwarf — or a helium-rich DA star — way below $T_{\rm eff} = 10,000$ K. Nevertheless, what these calculations reveal, is that even if hydrogen is a trace element in the envelope, its abundance profile is always far from equilibrium because of the extremely large diffusion timescales in the deeper layers. In particular, near $T_{\rm eff} \sim 20,000$ K, only $M_{\rm H} \sim 10^{-11}\ M_{\star}$ of hydrogen has accumulated in the outer layers of the white dwarf, which represents an extremely small fraction — about 0.04% — of the total hydrogen content present in the entire star ($\log M_{\rm H}/M_{\star} = -7.62$). As a comparison, we show the hydrogen profile (in red) in full diffusive equilibrium that has a similar thickness of the outer hydrogen layer.

These results thus reveal the possibility that substantial amounts of hydrogen can still be located in the deeper layers of a white dwarf, regardless of the amount already accumulated at the surface. Furthermore, since the photosphere is usually close to the surface at these effective

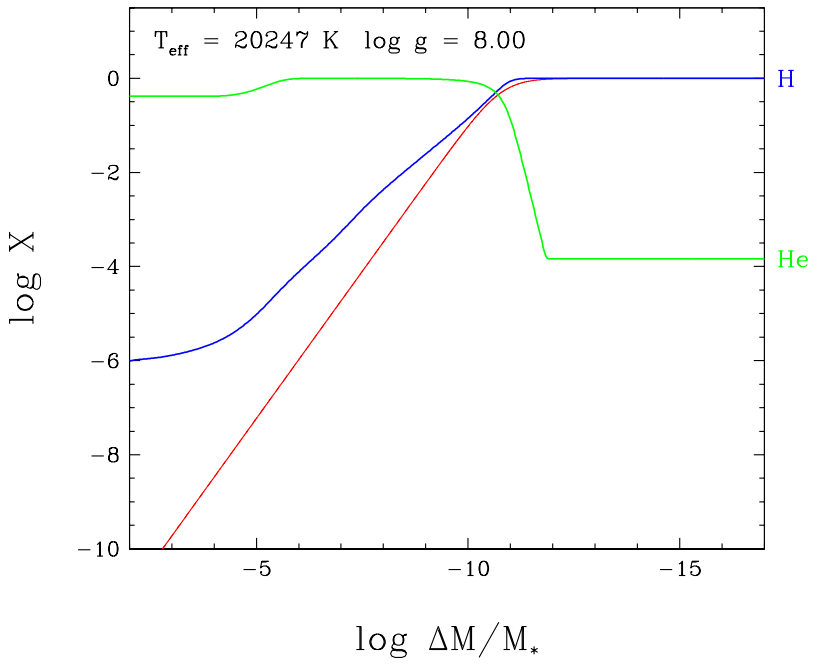

FIGURE 3.12 – Hydrogen (blue) and helium (green) mass fractions as a function of depth, taken from time-dependent calculations of a 0.6 $M_{\odot}$ white dwarf with a total hydrogen mass fraction of $X(\mathrm{H}) = 10^{-6}$ in the envelope. Also displayed is a diffusive equilibrium profile containing $\sim 10^{-11}$ $M_{\star}$ of hydrogen (red line).

temperatures ($\log \Delta M/M_{\star} \sim -15.5$), the majority of the hydrogen in the envelope would thus sit in a deep reservoir, inaccessible to spectroscopic observations.

3.5.2 Approximate Abundance Profiles

We now attempt to take into account the conclusions of the previous subsection — summarized in Figure 3.12 — into our convective dilution simulations described in Section 3.3. To this end, we thus consider that the overall hydrogen abundance profile can be represented by the combination of a deep reservoir and a surface contribution. Because of this massive reservoir, the superficial hydrogen layer keeps building up as a function of time (or decreasing effective temperature). For the sake of simplicity, we assume here that this profile is time-independent, and that the only relevant abundance profile is that when convective dilution occurs.

Due to the extremely large diffusion timescales found in the deeper layers, the hydrogen reservoir remains virtually unaffected in the earlier white dwarf phases, and only a small fraction

of the total hydrogen mass has reached the surface at the temperature where the convective dilution process takes place (0.04% in the example above). We therefore assume that the hydrogen mass fraction is nearly constant for $\log \Delta M/M_\star \lesssim -4$. In the outer layers, however, the abundance profile will, by comparison, reach its equilibrium value more quickly than in the deeper regions. For the surface contribution, we thus rely on full diffusive equilibrium profiles similar to those already described in Section 3.3.1 (see also MacDonald & Vennes 1991 and Manseau et al. 2016). Below this superficial hydrogen layer of mass $M_{\rm H}$, we use two simple power laws (with exponents $-9/10$ and $-3/4$) to describe the hydrogen tail displayed in Figure 3.12. In the deeper regions, we then connect this tail to the massive reservoir at $\log \Delta M/M_\star \sim -4$. This connection defines the hydrogen mass fraction in the deeper envelope, and by definition the total initial mass fraction of the star. Note that the exact value is not important in the present context since the bottom of the H/He convection zone never reaches these deeper regions.

Examples of these approximate hydrogen abundance profiles are displayed in Figure 3.13 for various values of the hydrogen surface layer mass, $M_{\rm H}$. For comparison, we also reproduced the detailed profile from Figure 3.12, which is perfectly represented by our approximate profile with $\log M_{\rm H}/M_\odot = -10.35$. We can also see that with decreasing value of $M_{\rm H}$, the hydrogen mass fraction in the deeper layers decreases as well, as expected. We acknowledge that these profiles represent only an approximation of the true profiles, but we are confident that our approach represents a good characterization of the fully time-dependent, evolutionary calculations, and that we can capture the essential information required to revise the spectral evolution of DBA white dwarfs.

3.5.3 Convective Dredge-up Simulations

In order to follow the spectral evolution of white dwarfs subject to convective dredge-up, we first assume that all of the hydrogen belonging to the surface contribution (as described above) has reached the surface and obeys our new stratified envelope structures. With this approximation, we only need to take into account the contribution from the deep hydrogen reservoir. We then follow the same procedure outlined in Section 3.3, but the target value of

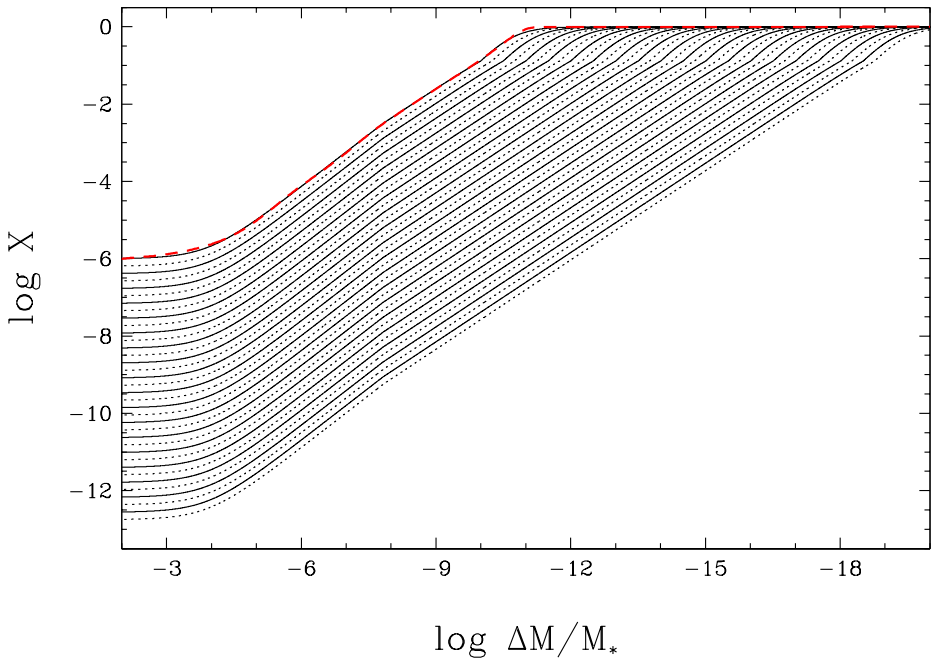

FIGURE 3.13 – Hydrogen mass fraction as function of depth for our approximate abundance profiles in a 0.6 $M_{\odot}$ white dwarf. The thickness of the hydrogen surface layer ranges from $\log M_{\rm H}/M_{\odot} = -19.0$ to -10.5 by steps of 0.25 dex (from right to left). The detailed hydrogen profile, reproduced from Figure 3.12, is represented by the red dashed line together with our profile for $\log M_{\rm H}/M_{\odot} = -10.35$.

$M_{\rm H}$ is updated at every temperature step by adding the mass of hydrogen dredged-up by the growing H/He convection zone. Since the reservoir contains only trace amounts of hydrogen, the extent of the convection zone will not be affected (see RBF18), and the transition temperatures that take into account the convective dredge-up process are virtually identical to those given in Table 3.1. However, the resulting hydrogen abundances at the photosphere, after mixing has occurred, should be significantly different. We now test this new paradigm by comparing the predictions of our convective dredge-up simulations with the photospheric H/He abundances measured in DB and DBA white dwarfs.

The results of our simulations are presented in Figure 3.14, which can be compared directly with Figure 3.8, where the dredge-up process has been ignored. Our results clearly demonstrate that *the addition of the deep hydrogen reservoir represents the key element to reproduce the observed hydrogen abundances in the bulk of DBA white dwarfs*. The H/He abundance ratio

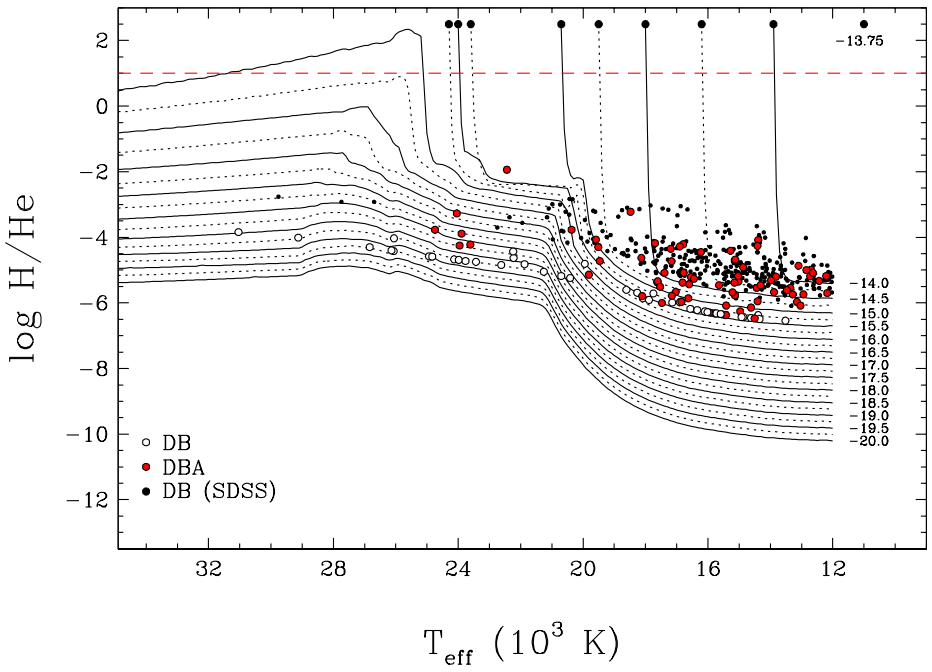

FIGURE 3.14 – Same as Figure 3.8, but for a 0.6 $M_{\odot}$ white dwarf undergoing convective dredge-up. Each curve is labeled with the corresponding initial hydrogen mass at the surface in solar mass (on a logarithmic scale).

at $T_{\rm eff} = 15,000$ K is predicted ∼2.3 dex larger by including the dredge-up process. With this scenario, a significant fraction of all DBA white dwarfs can be explained with an initial superficial hydrogen layer mass lower than $\log M_{\rm H}/M_{\odot} \sim -14$, combined with a progressive enrichment from the deeper envelope layers. At the same time, the hottest DBA stars can still be explained by surface layers thinner than $\log M_{\rm H}/M_{\odot} \sim -16.5$, but the predicted hydrogen abundances at lower temperatures would probably be undetectable, even within the context of the dredge-up scenario. We note that some of the DBA white dwarfs in Figure 3.14 would require even larger hydrogen abundances, but we believe that such large abundances could probably be produced by using more accurate hydrogen abundance profiles than those displayed in Figure 3.13, or even by including some convective overshooting at the bottom of the mixed H/He convection zone, or both. The point remains that convective dredge-up of hydrogen is the most plausible scenario to account for the presence of hydrogen in the bulk of DBA white dwarfs.

3.6 Discussion

We presented a series of improved envelope models, both with stratified and mixed chemical compositions, with the aim of simulating the convective dilution process, where a thin radiative superficial hydrogen layer is gradually eroded by the deeper helium convection zone. This process is believed to be responsible for the DA-to-DB transformation below the red edge of the DB gap near $T_{\rm eff} \sim 30,000$ K, although our calculations reveal that the convective dilution mechanism becomes efficient only below $T_{\rm eff} \sim 20,000$ K, when the bottom of the helium convective envelope plunges deep into the stellar interior. If the mass of the outer hydrogen layer is too large ($\log M_{\rm H}/M_{\odot} \gtrsim -14$), however, convective energy transport in the underlying helium envelope is suppressed, thus preventing this convection dilution process to occur. Even though the actual mixing process is obviously a complicated, time-dependent dynamical process, we believe that our static envelope models provide a fairly accurate description of the DA-to-DB transformation, in particular in terms of the effective temperatures at which this process occurs as a function of the hydrogen layer mass, as given in Table 3.1.

We note that our transition temperatures differ slightly from those provided in Table 1 of MacDonald & Vennes (1991), probably because of significant differences between their approach and ours, the most important of which is the distribution of the total hydrogen mass within the stellar envelope. In our calculations, hydrogen is distributed entirely within the mixed H/He convection zone as well as at the stellar surface where it is assumed to be in diffusive equilibrium. More importantly, there is no hydrogen below the convection zone (note that we refer here to our calculations of the convective dilution process described in Section3.3.3, where there is no deep hydrogen reservoir). In MacDonald & Vennes, there is also a deep hydrogen diffusion tail underneath the mixed H/He convection zone (see their Figure 6), which sometimes may involve most of the total hydrogen content. In their calculations, the authors indeed assume that a full equilibrium has been reached at every $T_{\rm eff}$ value, allowing any amount of hydrogen present in the star to achieve a diffusive equilibrium, even below the convection zone. Hence at a given effective temperature and hydrogen mass fraction in the convection zone, $X_{\rm cz}$, the total integrated hydrogen mass in our model is much smaller than in their model, thus explaining the differences between the results in our Table 3.1 and their

Table 1.

This being said, we believe our approach is probably more realistic in the context of the convective dilution process. Let us assume for instance that a hot DA white dwarf with a fully radiative hydrogen layer of $M_{\rm H} = 10^{-15}\ M_{\odot}$ sits in diffusive equilibrium on top of a helium envelope. When helium becomes convective, some of the hydrogen layer will be mixed within the convection zone, and some of it might leak at the bottom of the convective envelope, but certainly not to the point of achieving a full diffusive equilibrium profile. This must be particularly true when the bottom of the mixed H/He convection zone plunges rapidly into the stellar interior near $T_{\rm eff} \sim 20,000$ K. Hence it is probably better in the present context to assume that there is no hydrogen below the convection zone, at least when determining the DA-to-DB transition temperatures.

Although the exact amount of hydrogen present in the outer layers of the DA progenitor determines the temperature at which the convective dilution process will occur, the resulting hydrogen-to-helium abundance ratio measured at the photosphere of DBA white dwarfs may have little to do with this residual mass of hydrogen, in particular if there is a massive reservoir of hydrogen present in the deep stellar interior, which can be dredged-up to the surface by the mixed H/He convective envelope. This is the new paradigm we explored quantitatively in Section 3.5.

The overall spectral evolution picture that emerges from these calculations is the following. As discussed above, we begin with a typical PG1159 progenitor that has evolved through late thermal flash episodes (Werner & Herwig 2006). In such a star, the content of both hydrogen and helium has been significantly depleted, and the stellar envelope has an extremely uniform chemical composition through intense convective mixing within the deep stellar envelope. The exact amount of hydrogen and helium thoroughly diluted within the deep stellar envelope is unknown, but might be extremely small if we are to explain the existence of the so-called "Hot DQ" stars (Dufour et al. 2007b), whose atmospheres are dominated by carbon. During the earlier phases, this homogeneous chemical profile is maintained by a strong stellar wind, which eventually dies out at the end of the PG1159-phase (Quirion et al. 2012). As the star cools off, helium begins to diffuse upward, thus transforming the PG1159 progenitor into a DO white

dwarf. Eventually, hydrogen will also reach the surface, producing DAO white dwarfs, which will in time turn into chemically stratified DAO or DAB white dwarfs, and eventually into DA stars depending on the amount of hydrogen that has accumulated at the surface (see, e.g., Manseau et al. 2016). The important point in this scenario is that the amount of hydrogen that has reached the surface at a given point in time — i.e., at a given effective temperature — may represent only a small fraction of the total mass present in the stellar envelope. Most importantly, the hydrogen abundance profile remains always far from equilibrium because of the extremely large diffusion timescales of hydrogen in the deeper layers.

If the amount of hydrogen accumulated at the surface of the white dwarf is small enough — $\log M_{\rm H}/M_{\odot} \lesssim -14$ according to our results given in Table 3.1 — the convective dilution of this thin hydrogen layer by the more massive underlying convective helium envelope will occur, at a mixing temperature that depends on the hydrogen layer mass. At this point, the bottom of the mixed H/He convective reaches deep into the stellar interior, where large amounts of hydrogen may still reside. The convective dredge-up process that follows may potentially carry large amounts of hydrogen to the stellar photosphere, depending on the exact quantity of hydrogen present in the deeper interior. In this scenario, the amount of hydrogen originally present at the surface, prior to the convective dilution process, represents only a negligible fraction of the total mass of hydrogen present in the mixed H/He convective envelope after the dredge-up process has occurred.

On the other hand, if the amount of hydrogen accumulated at the surface of the white dwarf progenitor is too small — $\log M_{\rm H}/M_{\odot} \lesssim -16$ according to Manseau et al. (2016) — the star will never become a genuine DA white dwarf, and will only appear as a stratified DAB star, as discussed in Section 3.3.3. In this context, we interpreted the hot DBA white dwarfs near $T_{\rm eff} \sim 24,000$ K in Figure 3.8 as descendants of such hydrogen-poor progenitors. We also mentioned that with time, these DBA white dwarfs would eventually turn into DB stars, with no detectable traces of hydrogen, when the growth of the mixed H/He convective zone below $T_{\rm eff} \sim 20,000$ K completely dilutes any amount of hydrogen present in the outer layers. However, within the context of the convective dilution scenario, it is also possible that the growth of the convection zone is accompanied by a hydrogen enrichment from the deeper

layers into the photospheric regions, in which case the star could remain a DBA white dwarf.

If the convective dilution scenario is the correct explanation for the observed abundances of hydrogen in the bulk of DBA white dwarfs, we are forced to conclude that the pure DB stars below $T_{\rm eff} = 20,000$ K — those that show no Hα absorption feature whatsoever — must have very little hydrogen left in their stellar envelope, even in the deeper regions, most likely because of very intense and repeated late thermal flash episodes in their earlier evolutionary phases. If this is indeed the case, these hydrogen-free DB stars could represent the progenitors of the cool DQ white dwarfs, in which hydrogen is rarely detected spectroscopically, as opposed to other cool, non-DA degenerates (the DZA stars in particular).

Finally, it is clear that accretion of hydrogen from external sources — mostly from comets, disrupted asteroids, and small planets — play an important role in the spectral evolution of helium-atmosphere white dwarfs. In fact, the extreme hydrogen and metal abundances measured in some of these objects can only be explained by such accretion mechanisms. However, as discussed in Section 3.4, accretion needs to proceed *after* the convective dilution process has occurred, otherwise, even modest average accretion rates would build over time a hydrogen layer so thick that the DA-to-DB transition becomes impossible. For these reasons, we believe that the convective dredge-up model, proposed in this paper to explain the origin of hydrogen in the *bulk of DBA white dwarfs*, represents a more plausible scenario. One could even argue that, if the overall picture described above is correct, hydrogen enrichment due to convective dredge-up is an unavoidable outcome. Additional time-dependent calculations such as those illustrated in Figure 3.12 should eventually shed some light on this issue.

3.7 Acknowledgments

We are grateful to C. Genest-Beaulieu and A. Bédard for useful discussions. This work was supported in part by the NSERC Canada and by the Fund FRQ-NT (Québec). G.F. also acknowledges the contribution of the Canada Research Chair Program.

Chapitre 4

Conclusion

4.1 Résumé

Cette thèse rapporte les résultats de notre étude portant sur l'évolution spectrale des étoiles naines blanches riches en hélium et l'origine de l'hydrogène dans les hybrides de type DBA. Ce projet a été rendu possible grâce à la bonification de l'échantillon de Bergeron et al. (2011) et à l'amélioration des données spectroscopiques disponibles. Pour ce faire, nous avons incorporé les données disponibles de 10 étoiles DB provenant du relevé SUPERBLINK (Limoges et al. 2015) et du *Catalogue of Spectroscopically Identified White Dwarfs* (McCook & Sion 1999). Nous avons également bénéficié de 61 nouveaux spectres, dont 54 de la région Hα, obtenus avant cette étude aux télescopes de 4 m du NOAO et au Bok de 2.3 m du Steward Observatory (Bergeron et al. 2015). En y incluant 28 étoiles DA froides riches en hélium du SDSS, notre nouvel échantillon contient maintenant 143 objets couvrant l'ensemble de la plage en température pour laquelle des traces d'hydrogène ont été observées dans des naines blanches riches en hélium.

Afin d'en caractériser les propriétés, nous avons déterminé la température effective, la gravité de surface et la composition chimique de tous les objets à notre disposition à l'aide des techniques spectroscopique et photométrique. L'utilisation de la raie Hα permet de détecter des abondances 10 fois plus faibles que les seuils limites inférés par Hβ. Grâce à cette analyse, nous avons identifié des traces d'hydrogène dans 63% de nos étoiles DB, dépassant ainsi la valeur

de 44% obtenue par Bergeron et al. (2011). Ce résultat reste toutefois légèrement inférieur à l'estimation de 75% faite par Koester & Kepler (2015) en considérant les meilleurs spectres du SDSS. Nous avons également remarqué la persistance de naines blanches dépourvues de toutes traces d'hydrogène. Ce sous-groupe laisse présager l'existence d'une population d'objets riches en hélium distincte des DBA et suivant potentiellement le schéma évolutif DO $\rightarrow$ DB $\rightarrow$ DC. En ce qui concerne les étoiles DA froides riches en hélium, nos déterminations des abondances photosphériques concordent avec les valeurs mesurées par Dufour et al. (2007a) pour les hybrides de type DZA. De plus, la corrélation entre H/He et $T_{\rm eff}$ suggère fortement que ces 28 objets ne sont pas le résultat du refroidissement des DBA, mais bien un troisième sous-groupe à l'intérieur de notre échantillon.

Par la suite, nous nous sommes attaqués à l'épineuse question de l'évolution spectrale. Pour ce faire, nous avons calculé de nombreuses séries de modèles d'enveloppe homogènes et stratifiés afin de quantifier les effets de l'hydrogène et de l'efficacité convective sur la structure thermodynamique d'une naine blanche. Tout comme l'avait précédemment noté MacDonald & Vennes (1991), nos simulations ont permis de constater l'existence de dégénérescences pour certaines paires ($M_{\rm H}$, H/He). Cette réalité reflète la possibilité de diluer la même quantité d'hydrogène dans une zone de convection plus ou moins étendue. Grâce à cette caractérisation de l'espace des paramètres, nous avons généré des cartes d'isogrammes de masse dans le but de suivre le comportement du ratio H/He en fonction de la température effective.

Cette première tentative a fortement suggéré que les étoiles DB et les DBA chaudes sont le résultat du processus de dilution convective combiné à une très mince couche d'hydrogène de surface ($\log M_{\rm H}/M_{\odot} \sim -16$). Cependant, cet exercice nous a permis de constater que la majorité des étoiles DBA sont incompatibles avec ce mécanisme physique, car les valeurs de $M_{\rm H}$ nécessaires pour les expliquer mèneraient à la formation d'objets pouvant résister à l'érosion convective. Par un raisonnement similaire, nous avons également dû exclure l'accrétion de sources externes, car l'accumulation progressive de matière mène inévitablement à la formation d'une couche d'hydrogène relativement épaisse. Malgré ces revers, nos calculs semblent indiquer que les naines blanches DA froides riches en hélium sont fort probablement le produit du mélange convectif d'une étoile DA possédant une mince couche d'hydrogène en surface, soit

entre 10^{-11} $M_{\odot}$ et 10^{-8} $M_{\odot}$.

Afin de résoudre ces divers problèmes, nous avons amélioré le réalisme de nos modèles d'enveloppe dans l'espoir de caractériser plus adéquatement l'évolution spectrale. Nos nouvelles structures thermodynamiques montrent clairement que l'ajout d'hydrogène en surface cause la migration de la zone de convection et de la photosphère vers la surface à basse température effective. Grâce à ces changements, nous avons pu confirmer nos observations préliminaires selon lesquelles les étoiles DB et DBA chaudes résultent de la dilution convective d'une très mince couche d'hydrogène ($\log M_{\rm H}/M_{\odot} \sim -16.5$). Nous avons également pu contraindre à $-16 < \log M_{\rm H} < -14$ les masses pouvant expliquer l'augmentation significative du nombre de DB sous 20,000 K. Nous avons aussi démontré que l'accrétion transformerait de façon permanente une DB en DA, et ce, avant qu'elle n'atteigne 30,000 K. Malgré ces constats encourageants, ces nouveaux calculs ont réitéré l'incompatibilité de la majorité des naines blanches DBA avec le scénario de dilution convective en raison des abondances d'hydrogène trop faibles prédites dans l'intervalle de $M_{\rm H}$ mentionné ci-dessus. Les abondances d'hydrogène observées ne semblent donc pas pouvoir être expliquées par des origines fossiles ou externes les plus souvent envisagées.

Finalement, devant cette impasse, une simulation temporelle de la diffusion nous a permis de constater que des quantités importantes d'hydrogène peuvent se trouver profondément dans la naine blanche. Selon ces calculs, seulement $\sim$0.04% de la masse totale d'hydrogène aurait atteint la surface après un refroidissement jusqu'à 20,000 K résultant en un profil d'abondance chimique très loin de l'équilibre diffusif. Afin d'incorporer ce résultat à nos modèles d'enveloppe, nous avons élaboré un nouveau mécanisme physique basé sur le dragage convectif d'un réservoir massif d'hydrogène situé sous la photosphère. Grâce à cette approche alternative, l'enrichissement des couches externes causé par la croissance de la zone de convection vient palier au problème des faibles abondances d'hydrogène en augmentant les prédictions du ratio H/He de $\sim$2.3 dex. Nous pouvons maintenant reproduire fidèlement la majorité des abondances d'hydrogène mesurées dans les naines blanches de type DBA en combinant le dragage à une couche d'hydrogène ayant initialement $\log M_{\rm H} \leq -14$. Nous nous permettons donc de conclure que le dragage convectif est à l'origine de la présence de l'hydrogène dans les étoiles

DBA de notre échantillon.

4.2 Importance des résultats

Comme nous l'avons indiqué dans la section précédente, l'acquisition de spectres dans la région de Hα permet de détecter des abondances beaucoup plus faibles en comparaison de l'utilisation de Hβ. Avec des valeurs observées pouvant atteindre $\log \mathrm{H/He} \sim -6.5$, les contraintes imposées par notre étude s'avèrent près de 10 fois plus strictes que les limites découlant du SDSS (Koester & Kepler 2015). Avec l'inclusion des étoiles DA froides riches en hélium, notre échantillon offre, à ce jour, le portrait le plus représentatif du comportement du ratio H/He en-deçà de $T_{\mathrm{eff}} = 30,000$ K. Il s'agit d'un avantage indéniable pour toute tentative de tester les hypothèses de l'évolution spectrale.

Nous tenons à souligner que le passage à des modèles incluant la diffusion de l'hydrogène vers la surface est crucial en termes de notre capacité à reproduire fidèlement la physique gouvernant les enveloppes stellaires des naines blanches. Malgré cette amélioration, l'accrétion échoue toujours à reproduire les résultats observationnels en raison de l'importante accumulation d'hydrogène. Combiné à l'échec obtenu avec des modèles homogènes, l'hypothèse d'une origine externe doit définitivement être abandonnée pour la quasi-totalité des étoiles DBA. Néanmoins, le recours à l'accrétion pourrait potentiellement être justifié pour quelques objets arborant des abondances anormalement élevées (voir Raddi et al. 2015, Gentile Fusillo et al. 2017).

L'évolution spectrale des naines blanches constitue une question ouverte ayant plus de 35 ans. Cette thèse fournit donc plusieurs résultats cruciaux à notre compréhension de ce phénomène. Tout d'abord, avec le rejet des sources externes, la persistance jusqu'à 12,000 K d'observations dépourvues de toutes traces d'hydrogène suggère que ces objets sont les analogues des étoiles DB chaudes observées entre 45,000 K et 30,000 K (Eisenstein et al. 2006). Leur spectre se transformera donc vraisemblablement selon le schéma DO $\rightarrow$ DB $\rightarrow$ DC.

En ce qui concerne les naines blanches DA froides riches en hélium, le mélange convectif semble le mécanisme responsable de l'existence de ces objets. De plus, la similitude avec les hybrides de type DZA (Dufour et al. 2007a) laisse présager que ces objets résultent de la combi-

naison de l'accrétion de métaux et du mélange convectif. Nous sommes donc vraisemblablement en présence de chemins évolutifs de type DA(H) → DA(He) → DC et DA → DZA → DZ (ou DC).

L'origine de l'hydrogène dans les étoiles DBA constitue la conclusion la plus importante de cette étude dans le cadre de l'évolution spectrale des naines blanches riches en hélium. En effet, l'utilisation du dragage convectif, un mécanisme habituellement invoqué dans les naines blanches de type DQ (raies de carbone), représente un changement de paradigme majeur. Bien que ce processus utilise certaines des prémisses de la dilution convective, il est exempt des problèmes précédemment identifiés pour ce type d'hybrides (voir MacDonald & Vennes 1991, Bergeron et al. 2011, Koester & Kepler 2015). Cette thèse apporte donc une solution élégante à une question qui perdure depuis des décennies.

4.3 Perspectives d'avenir

Dans le futur, plusieurs avenues s'offrent à la communauté scientifique afin d'approfondir nos connaissances sur l'évolution spectrale des étoiles naines blanches riches en hélium.

La sonde *Gaia*, un projet du *European Space Agency* (ESA), a été lancée en 2013 avec la mission de créer la carte la plus vaste et la plus précise de notre galaxie en fournissant des mesures astrométriques pour près d'un milliard d'étoiles. L'accès à des mesures de parallaxes extrêmement précises permettra de mesurer, et donc imposer, la valeur de $\log g$ dans les méthodes d'analyses spectroscopiques et photométriques. Cette contrainte améliorera potentiellement la détermination des autres paramètres atmosphériques en jeu ($T_{\rm eff}$, H/He). Le calcul de spectres synthétiques correspondant à nos structures thermodynamiques, surtout en termes de la stratification chimique, serait une autre avenue d'investigation pertinente. Une analyse spectroscopique à partir de tels modèles nous permettrait de comparer les résultats obtenus avec les abondances mesurées habituellement avec des modèles homogènes.

D'autre part, une révision de nos calculs d'enveloppes avec différentes efficacités convectives apporterait une meilleure compréhension des conditions nécessaires pour que le dragage convectif soit viable. L'ajout du dépassement convectif (*convective overshooting*) pourrait également raffiner les conclusions de notre étude. Finalement, une des prochaines étapes de ce

projet serait de confirmer nos résultats à l'aide de simulations évolutives complètes, dépendantes du temps.

Bibliographie

Beauchamp, A., Wesemael, F., & Bergeron, P. 1997, ApJS, 108, 559

Beauchamp, A., Wesemael, F., Bergeron, P., Fontaine, G., Saffer, R. A., Liebert, J., & Brassard, P. 1999, ApJ, 516, 887

Beauchamp, A., Wesemael, F., Bergeron, P., Liebert, J., & Saffer, R. A. 1996, in Astronomical Society of the Pacific Conference Series, Vol. 96, Hydrogen Deficient Stars, ed. C. S. Jeffery & U. Heber, 295

Bergeron, P., Leggett, S. K., & Ruiz, M. T. 2001, ApJS, 133, 413

Bergeron, P., Rolland, B., Limoges, M.-M., Giammichele, N., Séguin-Charbonneau, L., & Green, E. M. 2015, in Astronomical Society of the Pacific Conference Series, Vol. 493, 19th European Workshop on White Dwarfs, ed. P. Dufour, P. Bergeron, & G. Fontaine, 33

Bergeron, P., Ruiz, M. T., & Leggett, S. K. 1997, ApJS, 108, 339

Bergeron, P., Wesemael, F., Beauchamp, A., Wood, M. A., Lamontagne, R., Fontaine, G., & Liebert, J. 1994, ApJ, 432, 305

Bergeron, P., Wesemael, F., Dufour, P., Beauchamp, A., Hunter, C., Saffer, R. A., Gianninas, A., Ruiz, M. T., Limoges, M.-M., Dufour, P., Fontaine, G., & Liebert, J. 2011, ApJ, 737, 28

Brassard, P. & Fontaine, G. 1994, in IAU Colloq. 147: The Equation of State in Astrophysics, ed. G. Chabrier & E. Schatzman, Vol. 147, 560

Castanheira, B. G., Kepler, S. O., Handler, G., & Koester, D. 2006, A&A, 450, 331

Dantona, F. & Mazzitelli, I. 1979, A&A, 74, 161

Deridder, G. & van Renspergen, W. 1976, A&AS, 23, 147

Dufour, P., Bergeron, P., & Fontaine, G. 2005, ApJ, 627, 404

Dufour, P., Bergeron, P., Liebert, J., Harris, H. C., Knapp, G. R., Anderson, S. F., Hall, P. B., Strauss, M. A., Collinge, M. J., & Edwards, M. C. 2007a, ApJ, 663, 1291

Dufour, P., Fontaine, G., Liebert, J., Schmidt, G. D., & Behara, N. 2008, ApJ, 683, 978

Dufour, P., Liebert, J., Fontaine, G., & Behara, N. 2007b, Nature, 450, 522

Eisenstein, D. J., Liebert, J., Koester, D., Kleinmann, S. J., Nitta, A., Smith, P. S., Barentine, J. C., Brewington, H. J., Brinkmann, J., Harvanek, M., Krzesiński, J., Neilsen, Jr., E. H., Long, D., Schneider, D. P., & Snedden, S. A. 2006, AJ, 132, 676

Farihi, J., Gänsicke, B. T., & Koester, D. 2013, Science, 342, 218

Fleming, T. A., Liebert, J., & Green, R. F. 1986, ApJ, 308, 176

Fontaine, G., Brassard, P., & Bergeron, P. 2001, PASP, 113, 409

Fontaine, G. & Wesemael, F. 1987, in IAU Colloq. 95: Second Conference on Faint Blue Stars, ed. A. G. D. Philip, D. S. Hayes, & J. W. Liebert, 319–326

Friedrich, S., Koester, D., Christlieb, N., Reimers, D., & Wisotzki, L. 2000, A&A, 363, 1040

Genest-Beaulieu, C. & Bergeron, P. 2017, in Astronomical Society of the Pacific Conference Series, Vol. 509, 20th European White Dwarf Workshop, ed. P.-E. Tremblay, B. Gaensicke, & T. Marsh, 201

Gentile Fusillo, N. P., Gänsicke, B. T., Farihi, J., Koester, D., Schreiber, M. R., & Pala, A. F. 2017, MNRAS, 468, 971

Giammichele, N., Bergeron, P., & Dufour, P. 2012, ApJS, 199, 29

Giammichele, N., Fontaine, G., Brassard, P., & Charpinet, S. 2016, ApJS, 223, 10

Gianninas, A., Bergeron, P., & Ruiz, M. T. 2011, ApJ, 743, 138

Green, R. F., Schmidt, M., & Liebert, J. 1986, ApJS, 61, 305

Greenstein, J. L. 1986, ApJ, 304, 334

Holberg, J. B. 1987, in IAU Colloq. 95: Second Conference on Faint Blue Stars, ed. A. G. D. Philip, D. S. Hayes, & J. W. Liebert, 285–295

Holberg, J. B. & Bergeron, P. 2006, AJ, 132, 1221

Hügelmeyer, S. D., Dreizler, S., Werner, K., Krzesiński, J., Nitta, A., & Kleinman, S. J. 2005, A&A, 442, 309

Hummer, D. G. & Mihalas, D. 1988, ApJ, 331, 794

Iben, Jr., I. 1984, ApJ, 277, 333

Jura, M. 2003, ApJ, 584, L91

Jura, M., Muno, M. P., Farihi, J., & Zuckerman, B. 2009, ApJ, 699, 1473

Jura, M. & Xu, S. 2010, AJ, 140, 1129

Kleinman, S. J., Kepler, S. O., Koester, D., Pelisoli, I., Peçanha, V., Nitta, A., Costa, J. E. S., Krzesinski, J., Dufour, P., Lachapelle, F.-R., Bergeron, P., Yip, C.-W., Harris, H. C., Eisenstein, D. J., Althaus, L., & Córsico, A. 2013, ApJS, 204, 5

Koester, D. 1976, A&A, 52, 415

Koester, D. & Kepler, S. O. 2015, A&A, 583, A86

Liebert, J., Bergeron, P., & Tweedy, R. W. 1994, ApJ, 424, 817

Liebert, J., Wesemael, F., Hansen, C. J., Fontaine, G., Shipman, H. L., Sion, E. M., Winget, D. E., & Green, R. F. 1986, ApJ, 309, 241

Limoges, M.-M., Bergeron, P., & Lépine, S. 2015, ApJS, 219, 19

MacDonald, J. & Vennes, S. 1991, ApJ, 371, 719

Manseau, P. M., Bergeron, P., & Green, E. M. 2016, ApJ, 833, 127

McCook, G. P. & Sion, E. M. 1999, ApJS, 121, 1

Napiwotzki, R. 1999, A&A, 350, 101

Napiwotzki, R. & Schoenberner, D. 1995, A&A, 301, 545

Napiwotzki, R. & Schönberner, D. 1991, in NATO Advanced Science Institutes (ASI) Series C, Vol. 336, NATO Advanced Science Institutes (ASI) Series C, ed. G. Vauclair & E. Sion, 39

Paquette, C., Pelletier, C., Fontaine, G., & Michaud, G. 1986, ApJS, 61, 197

Quirion, P.-O., Fontaine, G., & Brassard, P. 2012, ApJ, 755, 128

Raddi, R., Gänsicke, B. T., Koester, D., Farihi, J., Hermes, J. J., Scaringi, S., Breedt, E., & Girven, J. 2015, MNRAS, 450, 2083

Reindl, N., Rauch, T., Werner, K., Kepler, S. O., Gänsicke, B. T., & Gentile Fusillo, N. P. 2014, A&A, 572, A117

Rolland, B., Bergeron, P., & Fontaine, G. 2018, ApJ, 857, 56

Schatzman, E. 1945, Annales d'Astrophysique, 8, 143

Schatzman, E. L. 1958, White dwarfs

Sion, E. M. 1984, ApJ, 282, 612

Subasavage, J. P., Jao, W.-C., Henry, T. J., Harris, H. C., Dahn, C. C., Bergeron, P., Dufour, P., Dunlap, B. H., Barlow, B. N., Ianna, P. A., Lépine, S., & Margheim, S. J. 2017, AJ, 154, 32

Tassoul, M., Fontaine, G., & Winget, D. E. 1990, ApJS, 72, 335

Tremblay, P.-E. & Bergeron, P. 2008, ApJ, 672, 1144

—. 2009, ApJ, 696, 1755

Tremblay, P.-E., Ludwig, H.-G., Freytag, B., Fontaine, G., Steffen, M., & Brassard, P. 2015, ApJ, 799, 142

Vauclair, G. & Reisse, C. 1977, A&A, 61, 415

Vennes, S., Pelletier, C., Fontaine, G., & Wesemael, F. 1988, ApJ, 331, 876

Veras, D., Shannon, A., & Gänsicke, B. T. 2014, MNRAS, 445, 4175

Voss, B., Koester, D., Napiwotzki, R., Christlieb, N., & Reimers, D. 2007, A&A, 470, 1079

Werner, K. & Herwig, F. 2006, PASP, 118, 183

Wesemael, F., Green, R. F., & Liebert, J. 1985, ApJS, 58, 379

Wesemael, F., Greenstein, J. L., Liebert, J., Lamontagne, R., Fontaine, G., Bergeron, P., & Glaspey, J. W. 1993, PASP, 105, 761

Xu, S., Rappaport, S., van Lieshout, R., Vanderburg, A., Gary, B., Hallakoun, N., Ivanov, V. D., Wyatt, M. C., DeVore, J., Bayliss, D., Bento, J., Bieryla, A., Cameron, A., Cann, J. M., Croll, B., Collins, K. A., Dalba, P. A., Debes, J., Doyle, D., Dufour, P., Ely, J., Espinoza, N., Joner, M. D., Jura, M., Kaye, T., McClain, J. L., Muirhead, P., Palle, E., Panka, P. A., Provencal, J., Randall, S., Rodriguez, J. E., Scarborough, J., Sefako, R., Shporer, A., Strickland, W., Zhou, G., & Zuckerman, B. 2018, MNRAS, 474, 4795

Zuckerman, B., Koester, D., Dufour, P., Melis, C., Klein, B., & Jura, M. 2011, ApJ, 739, 101

Annexe A

Solutions Supplémentaires

En raison des contraintes d'espace imposées sur les publications dans *The Astrophysical Journal*, certaines figures de l'article présenté au Chapitre 2 sont absentes du corps du texte. Ces dernières ont déplacées vers le contenu électronique au choix de l'éditeur. À des fins de complétude, nous ajoutons cette annexe afin d'inclure l'ensemble des éléments laissés de côté précédemment.

Une version actualisée de la Figure 18 de Bergeron et al. (2011) répertoriant les meilleures solutions obtenues lors de l'ajustement des spectres avec nos modèles d'atmosphère est tout d'abord présentée à la Figure A.1. L'ensemble couvre 12 panneaux et inclue les 115 naines blanches DB et DBA de notre échantillon de même que les quatre objets sans données Hα.

Par la suite, nous ajoutons les parties manquantes de la Figure 2.7. Ce graphique répertoriait les solutions obtenues lors de l'ajustement hybrides des spectres et de la distribution spectrale d'énergie (photométrie) disponibles pour les étoiles DA froides riches en hélium. Le touts comprend 6 panneaux totalisant 24 objets.

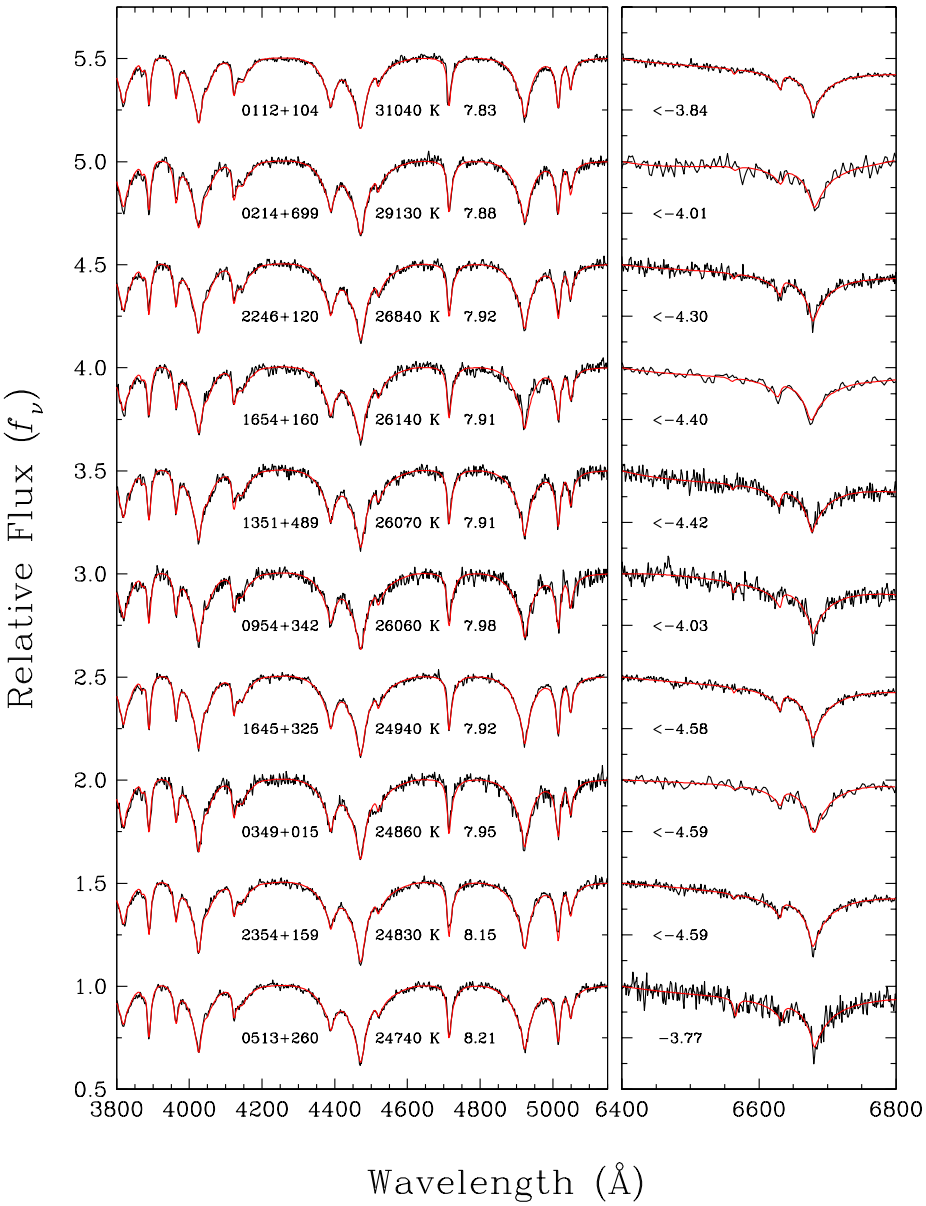

FIGURE A.1 – Spectroscopic fits for all DB and DBA stars in our sample, in order of decreasing effective temperature. The atmospheric parameters ($T_{\rm eff}$, $\log g$, $\log {\rm H/He}$) of each object are given in the figure. The region near Hα (right panel) is used to measure, or to constrain, the hydrogen abundance. In the case of DB stars, these spectra only provide *upper limits* on the hydrogen-to-helium abundance ratio.

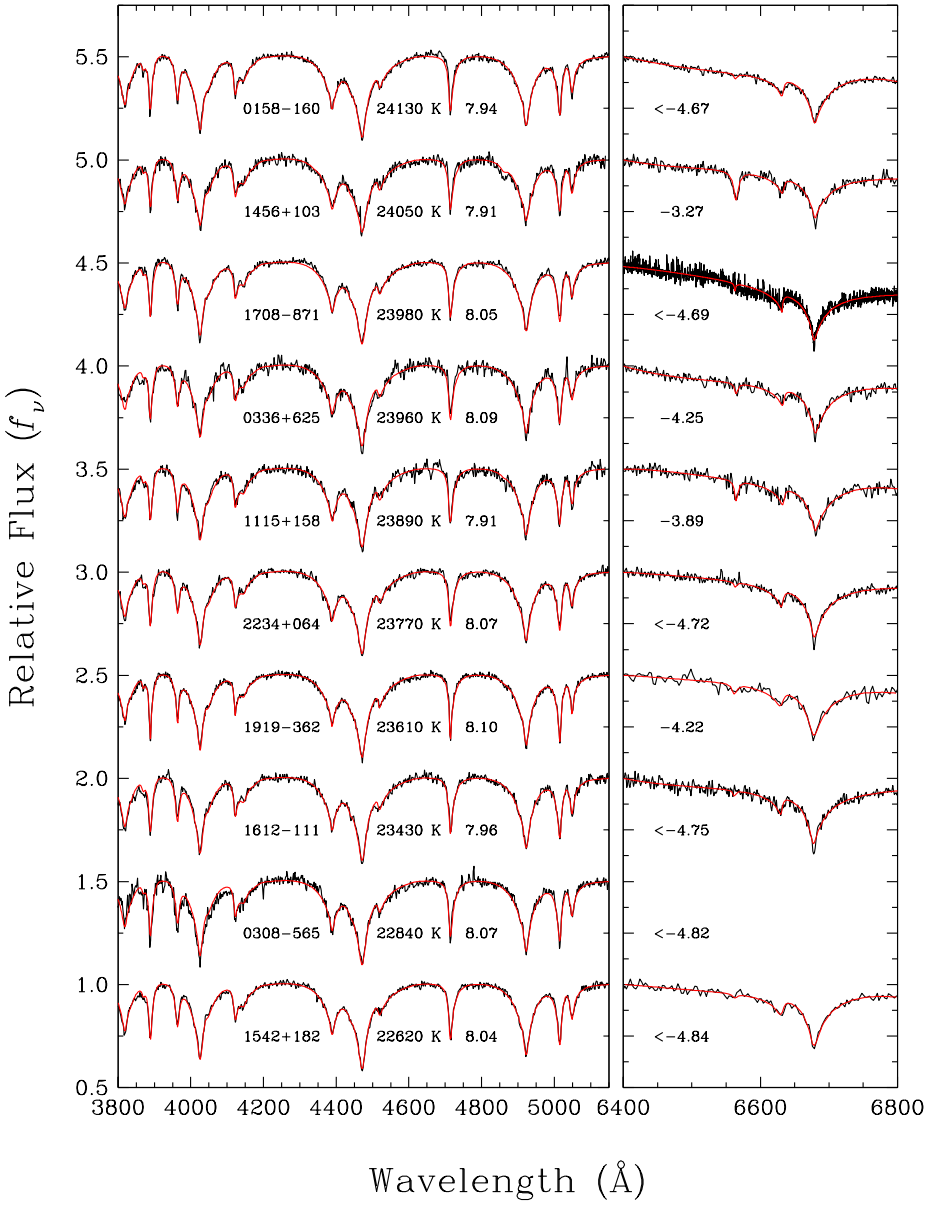

FIGURE A.1 – (Continued)

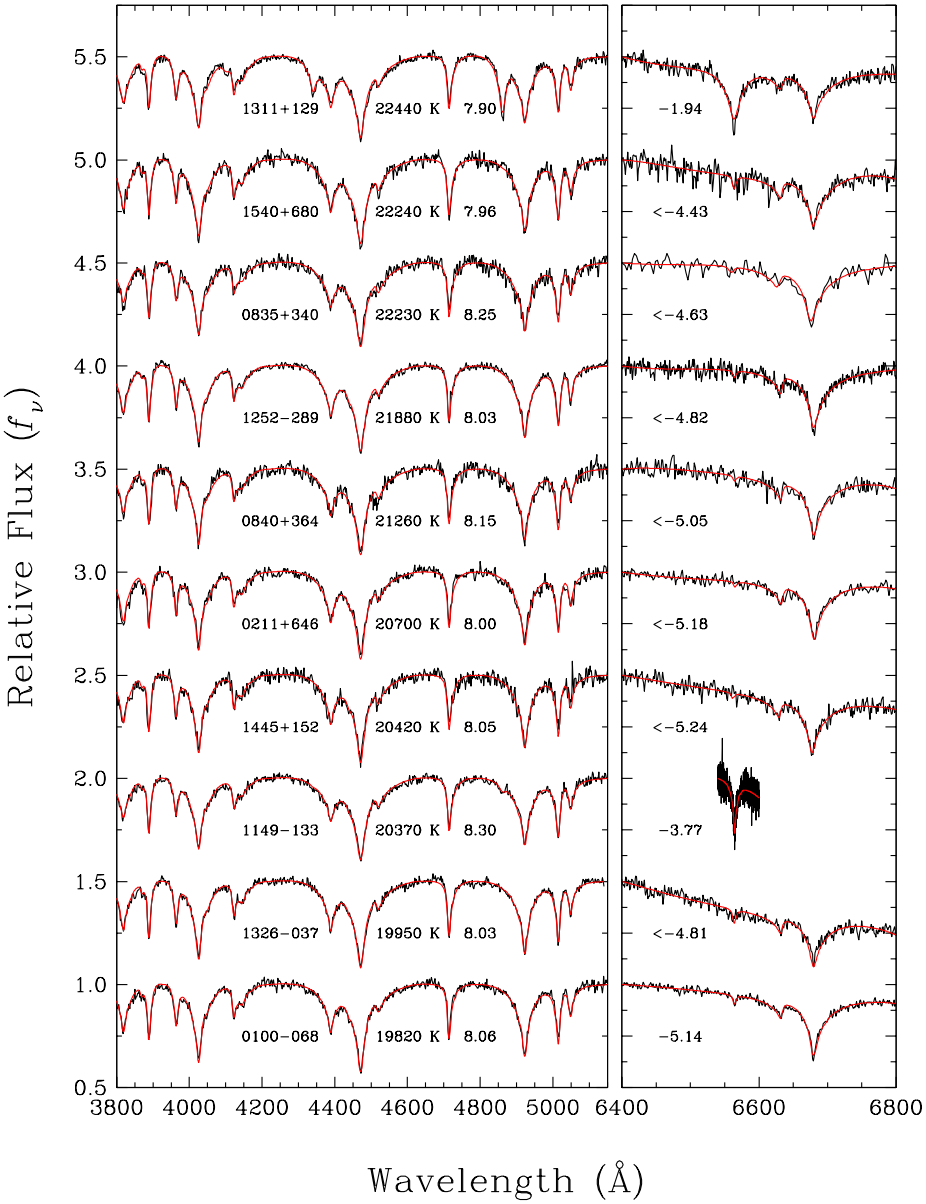

FIGURE A.1 – (Continued)

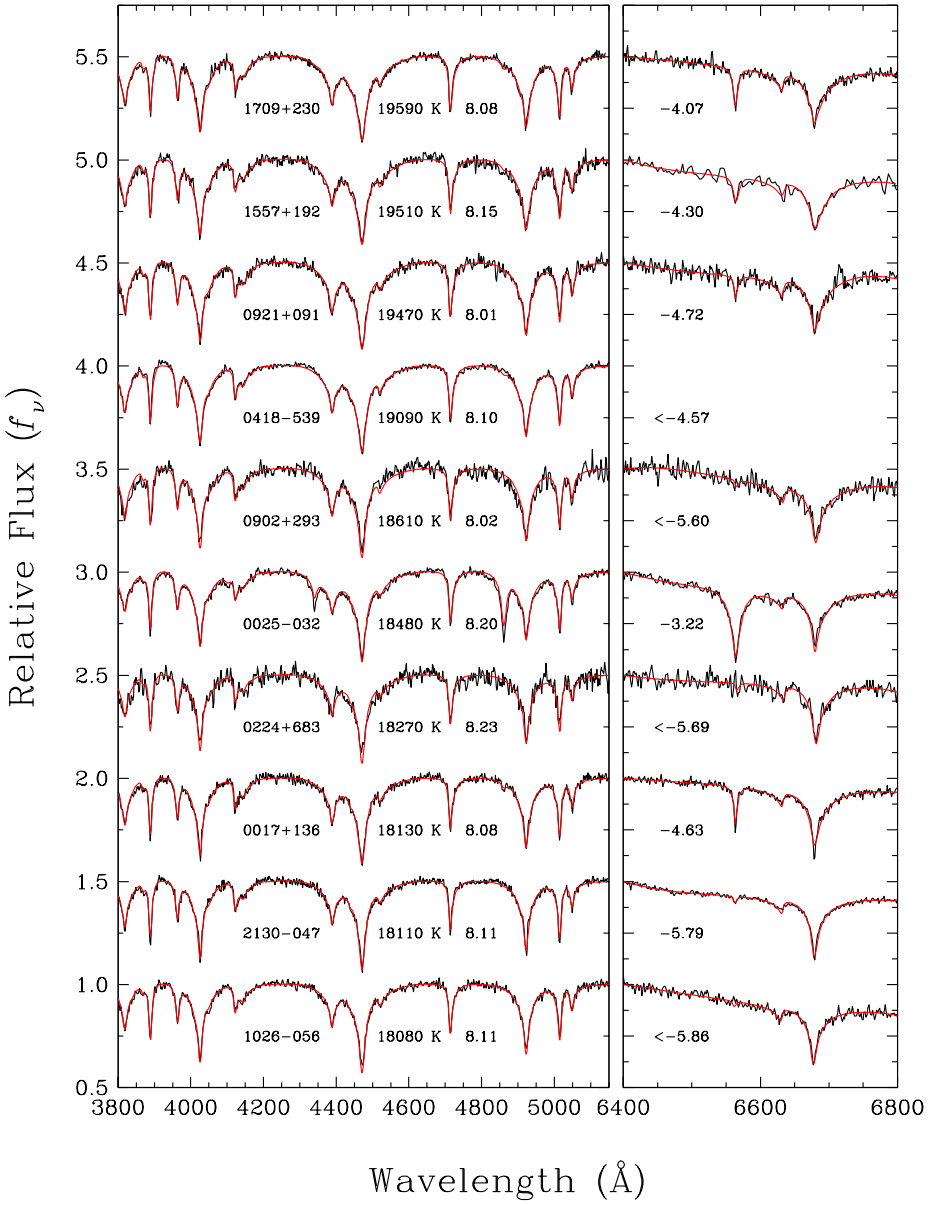

FIGURE A.1 – (Continued)

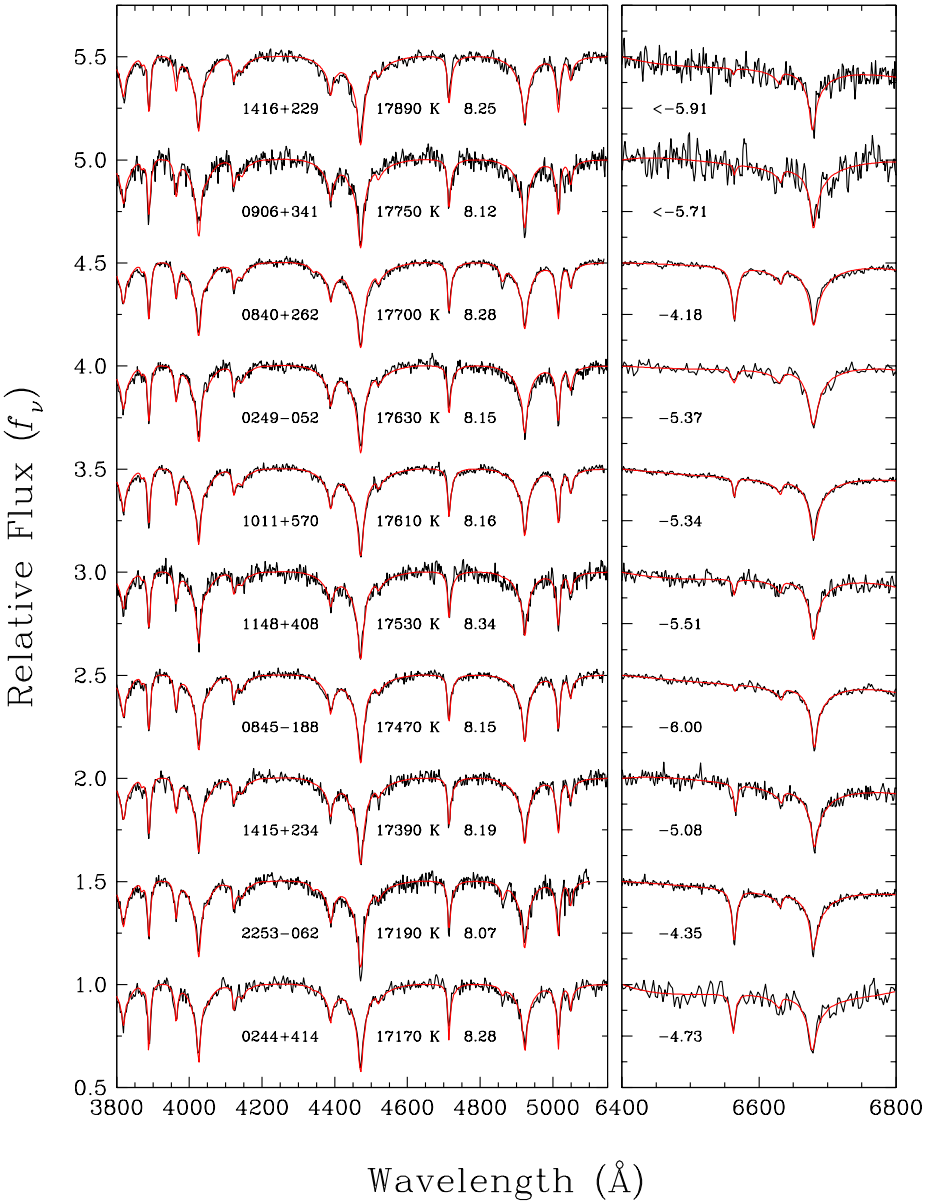

FIGURE A.1 – (Continued)

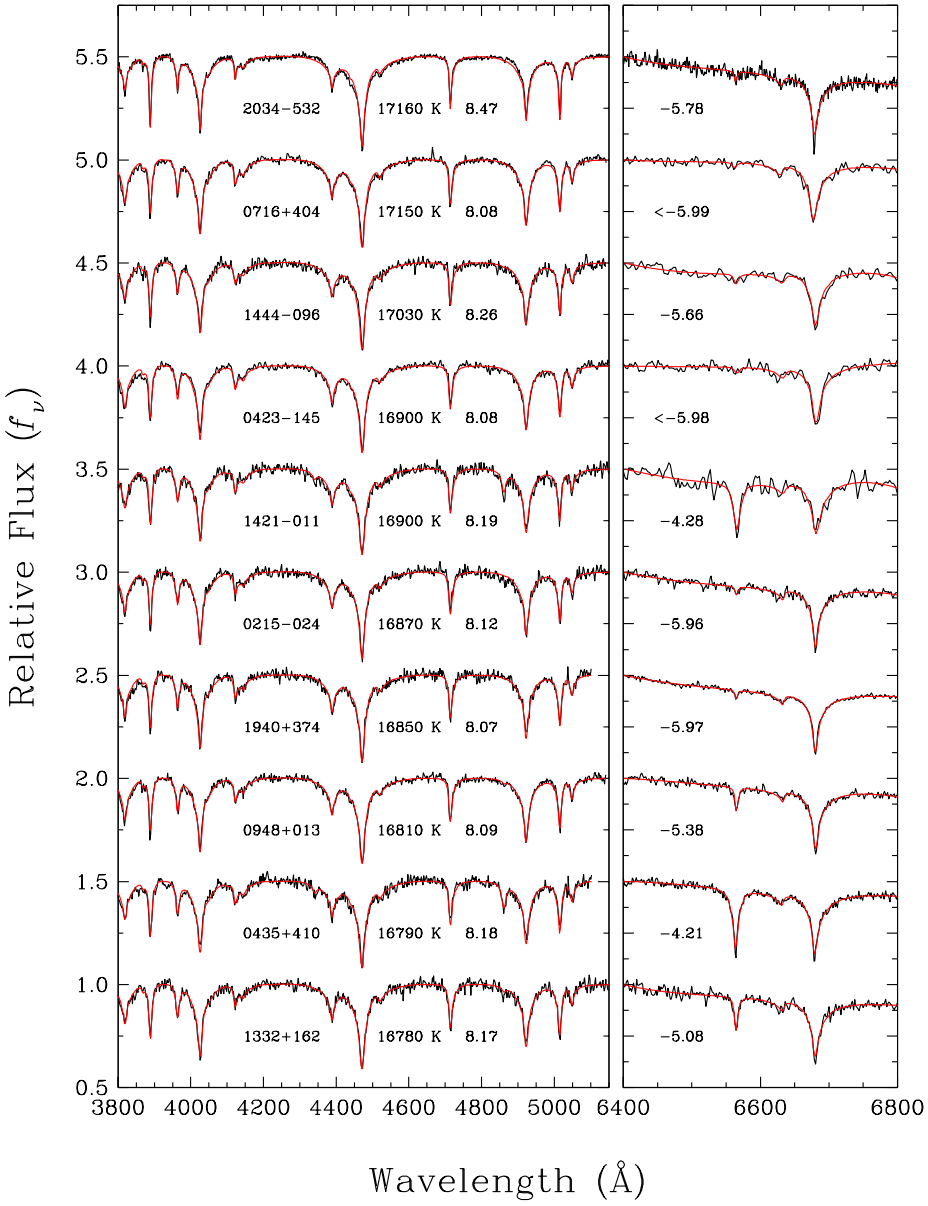

FIGURE A.1 – (Continued)

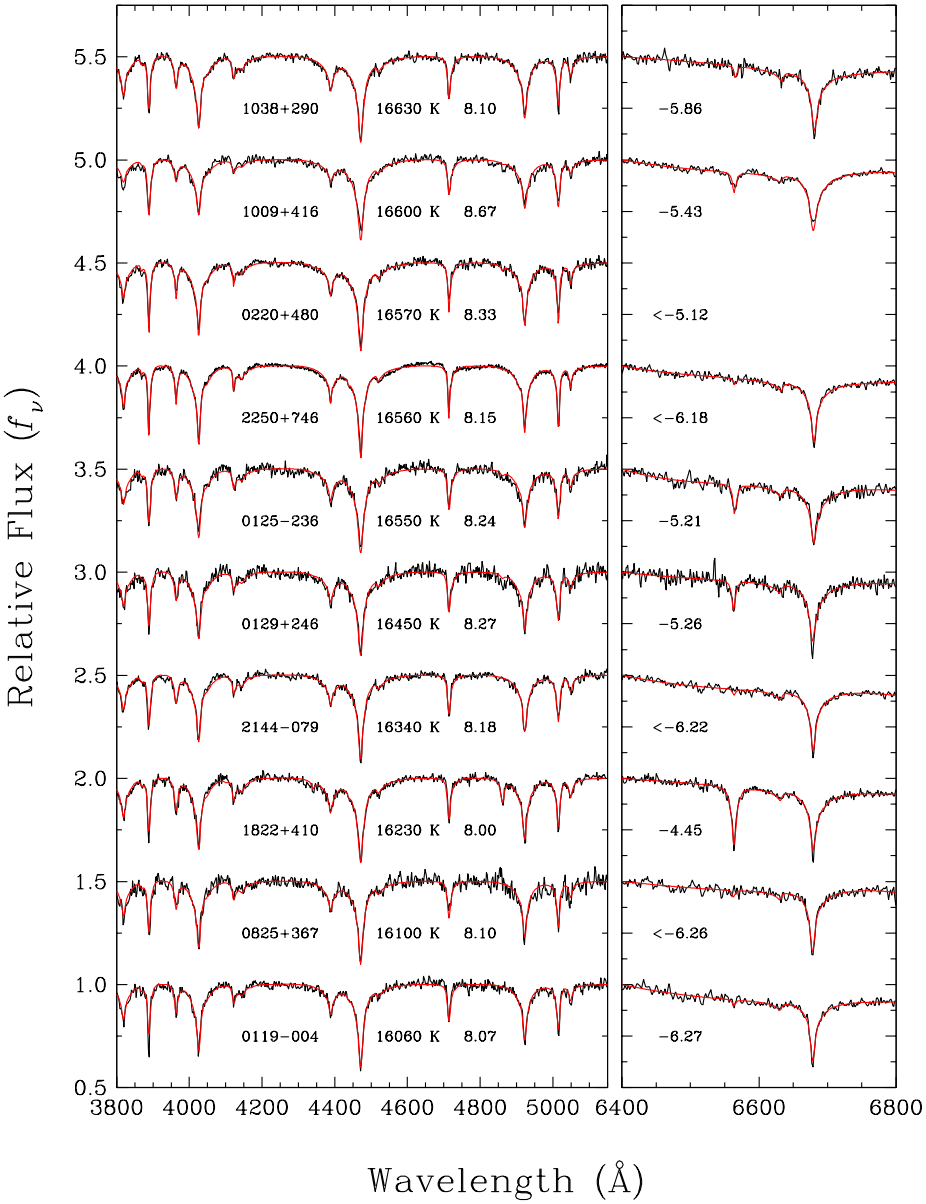

FIGURE A.1 – (Continued)

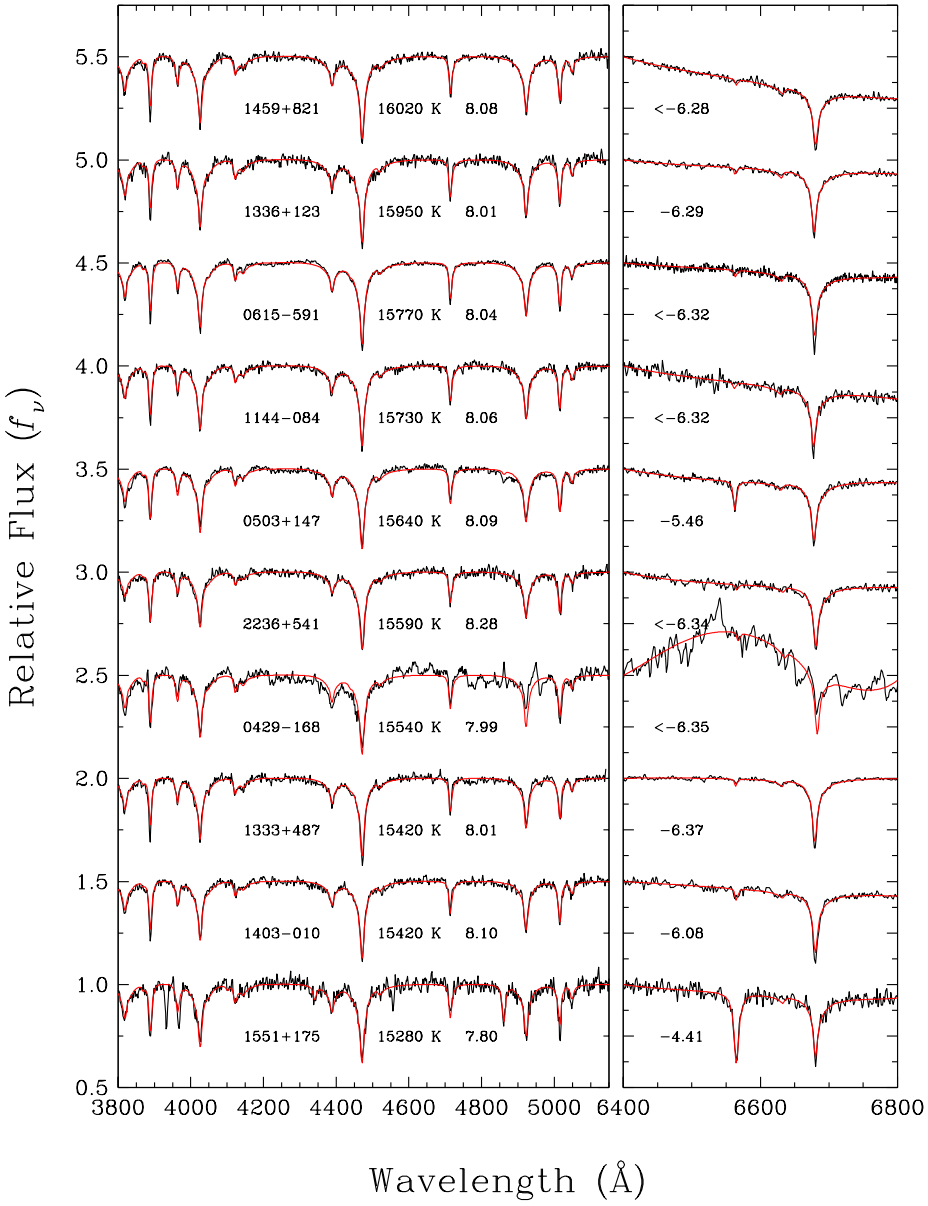

FIGURE A.1 – (Continued)

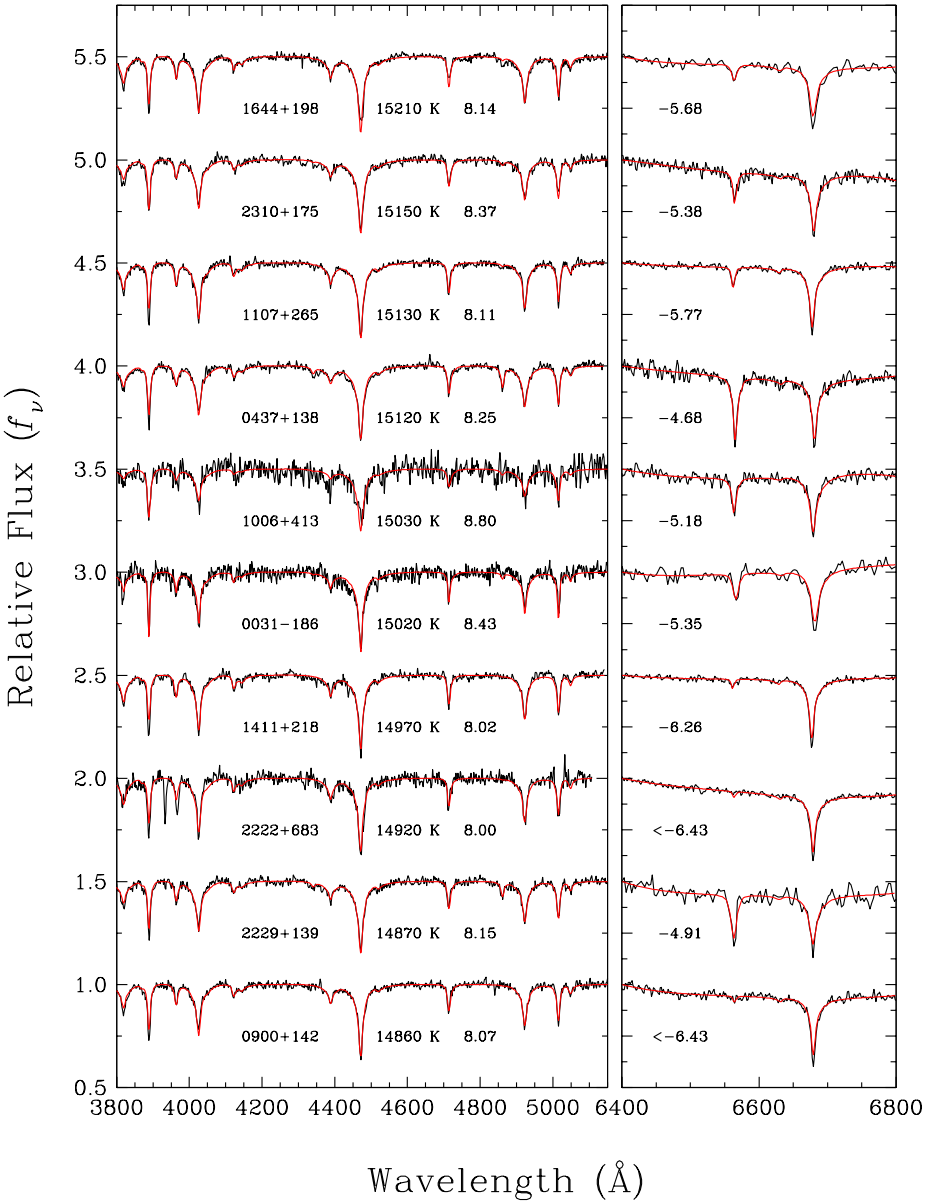

FIGURE A.1 – (Continued)

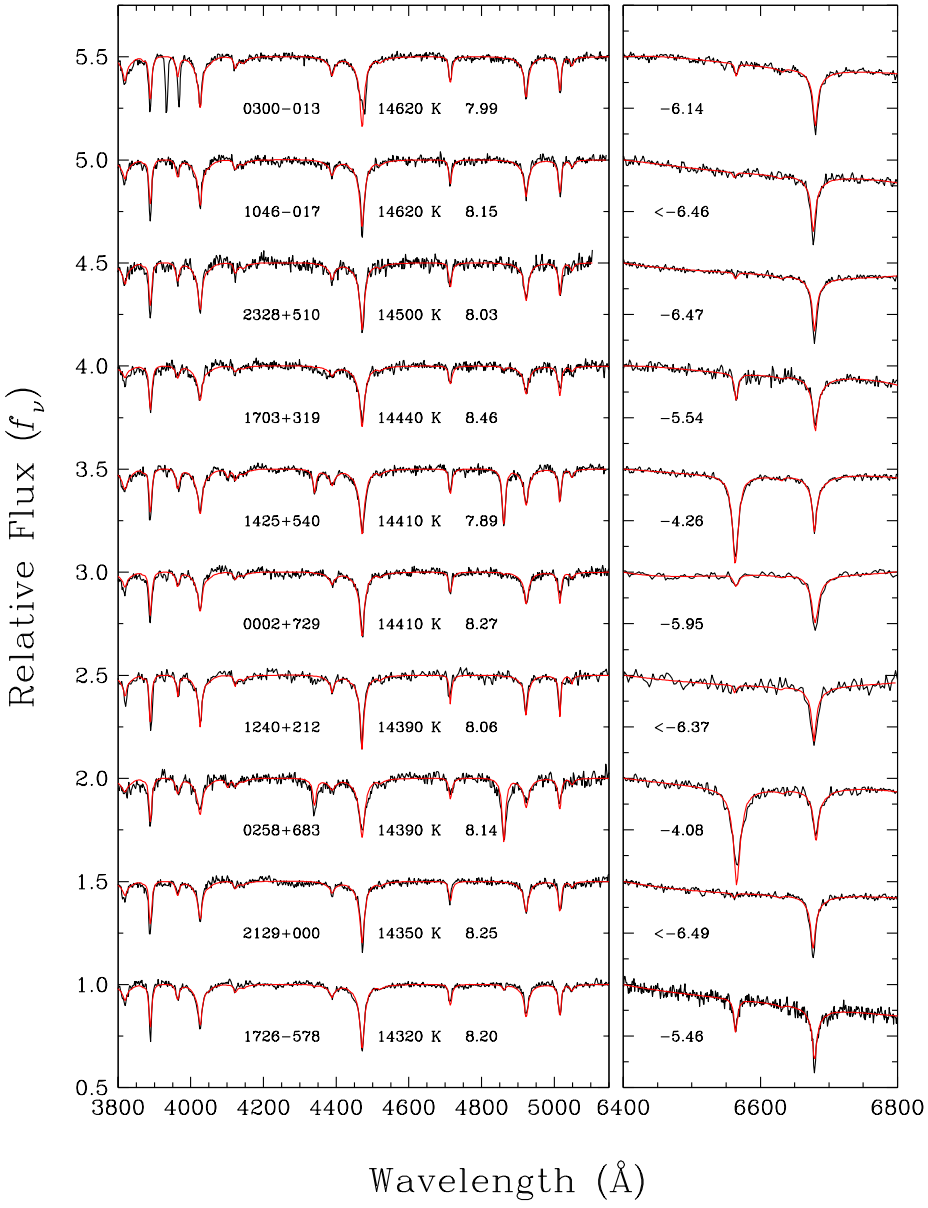

FIGURE A.1 – (Continued)

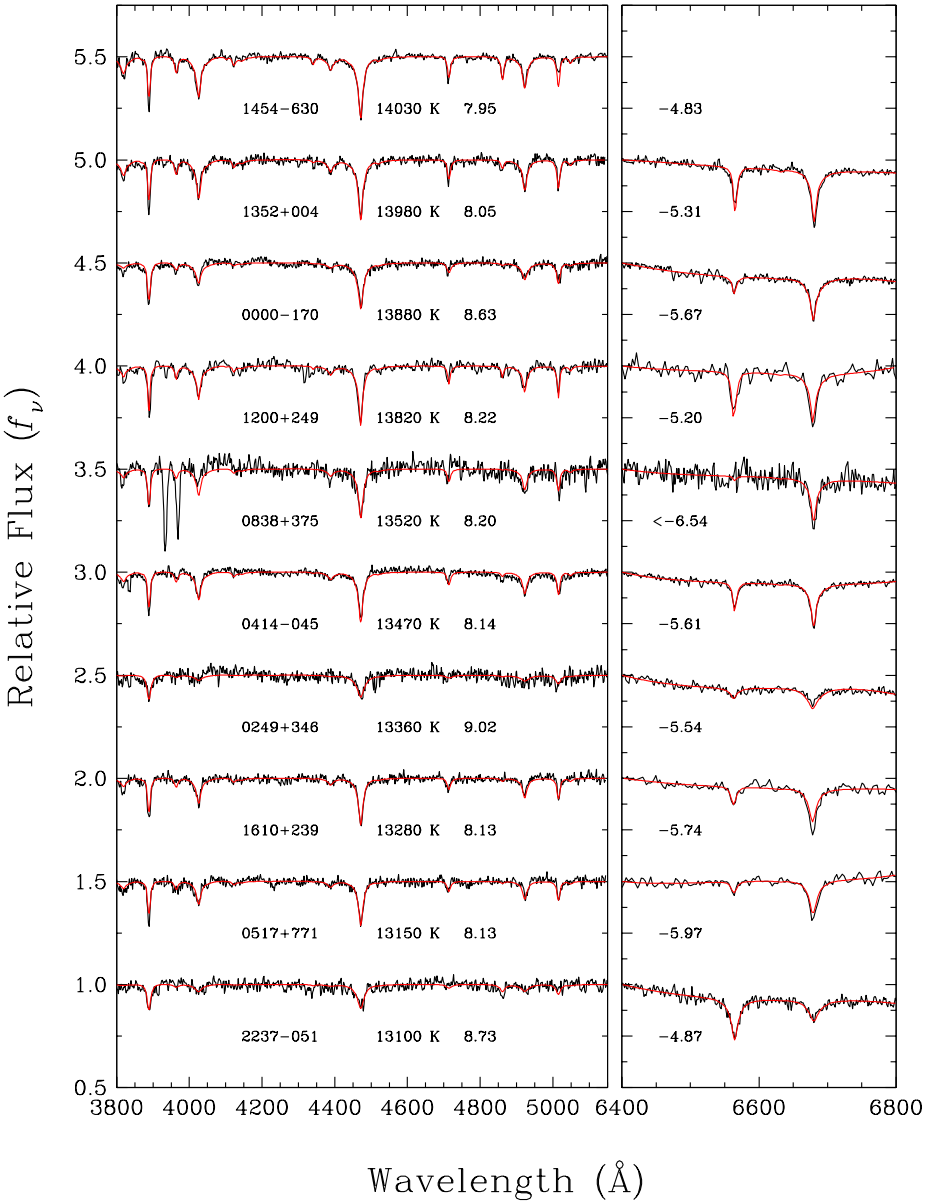

FIGURE A.1 – (Continued)

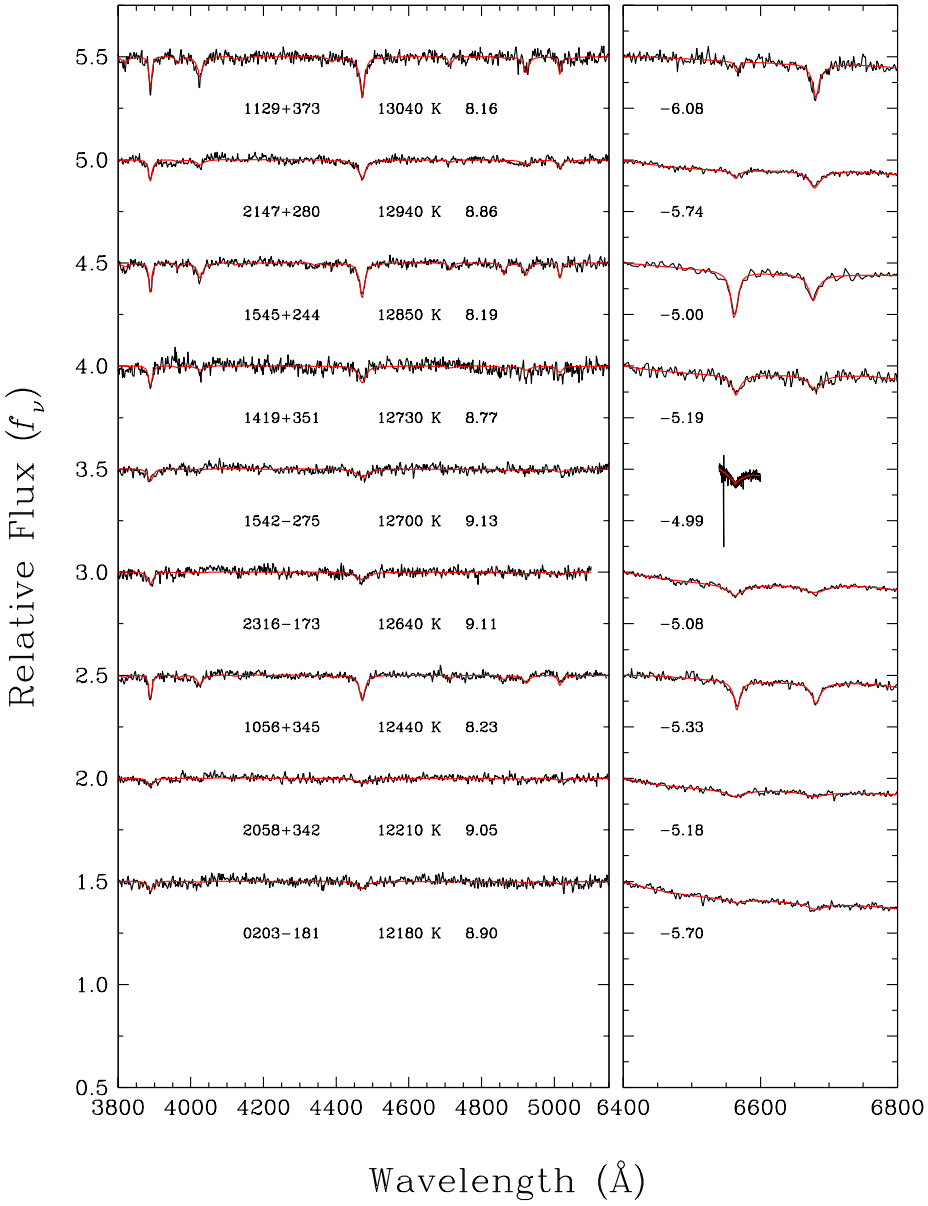

FIGURE A.1 – (Continued)

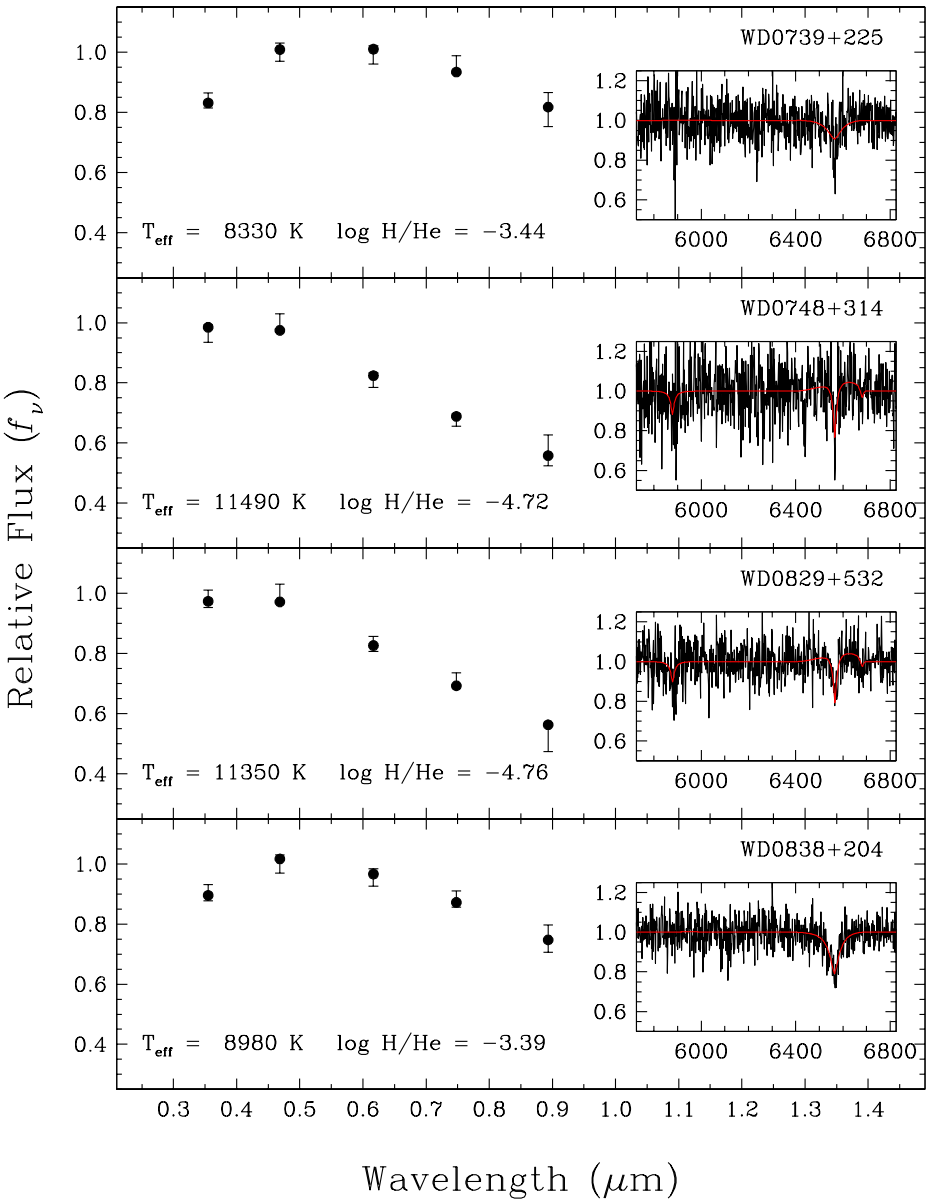

FIGURE A.2 – Fits obtained from the hybrid fitting method for cool, He-rich DA stars with homogeneous models at $\log g = 8$. The *ugriz* photometric observations are represented by error bars, while the model fluxes are shown by filled circles. The inset shows our fit to the spectrum near the Hα region, normalized to a continuum set to unity, which is used to measure the hydrogen abundance.

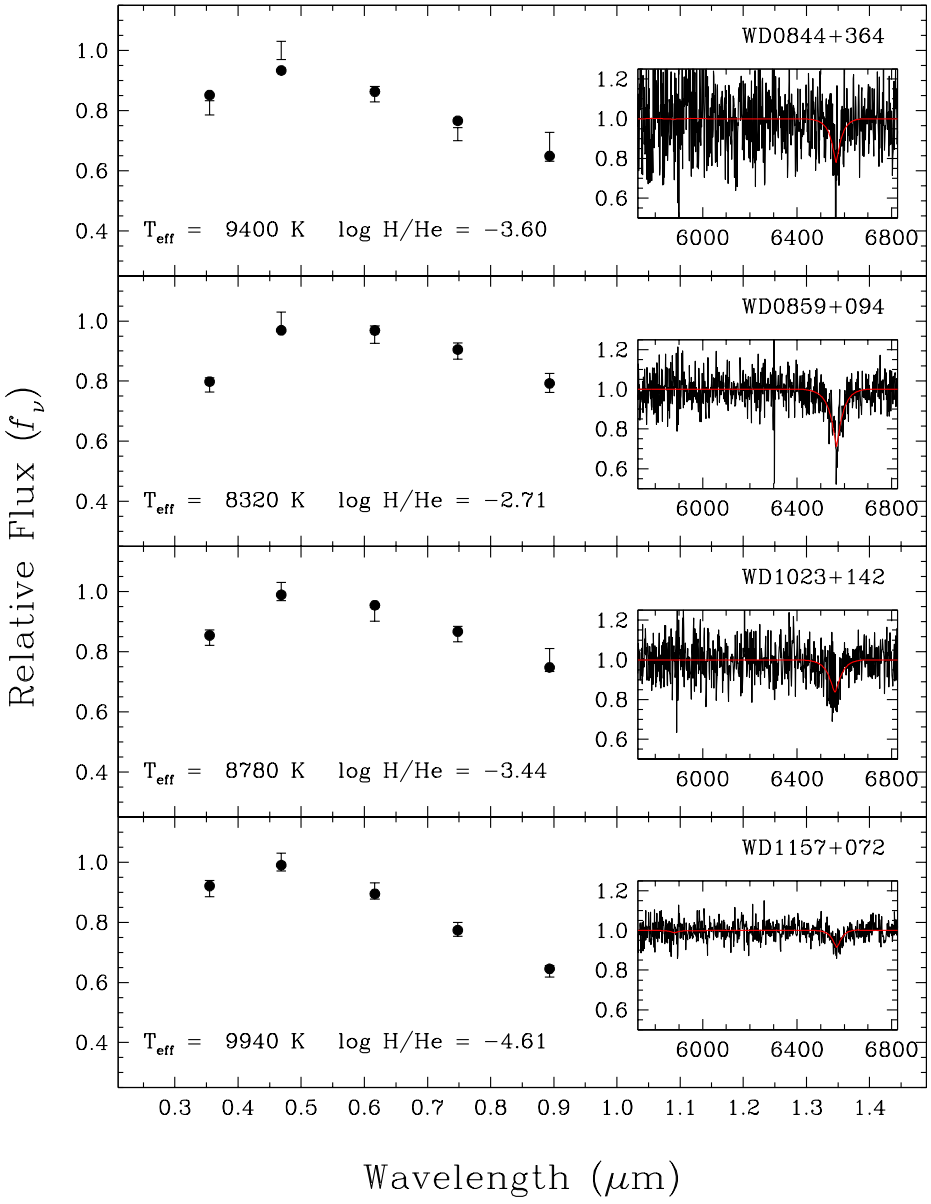

FIGURE A.2 – (Continued)

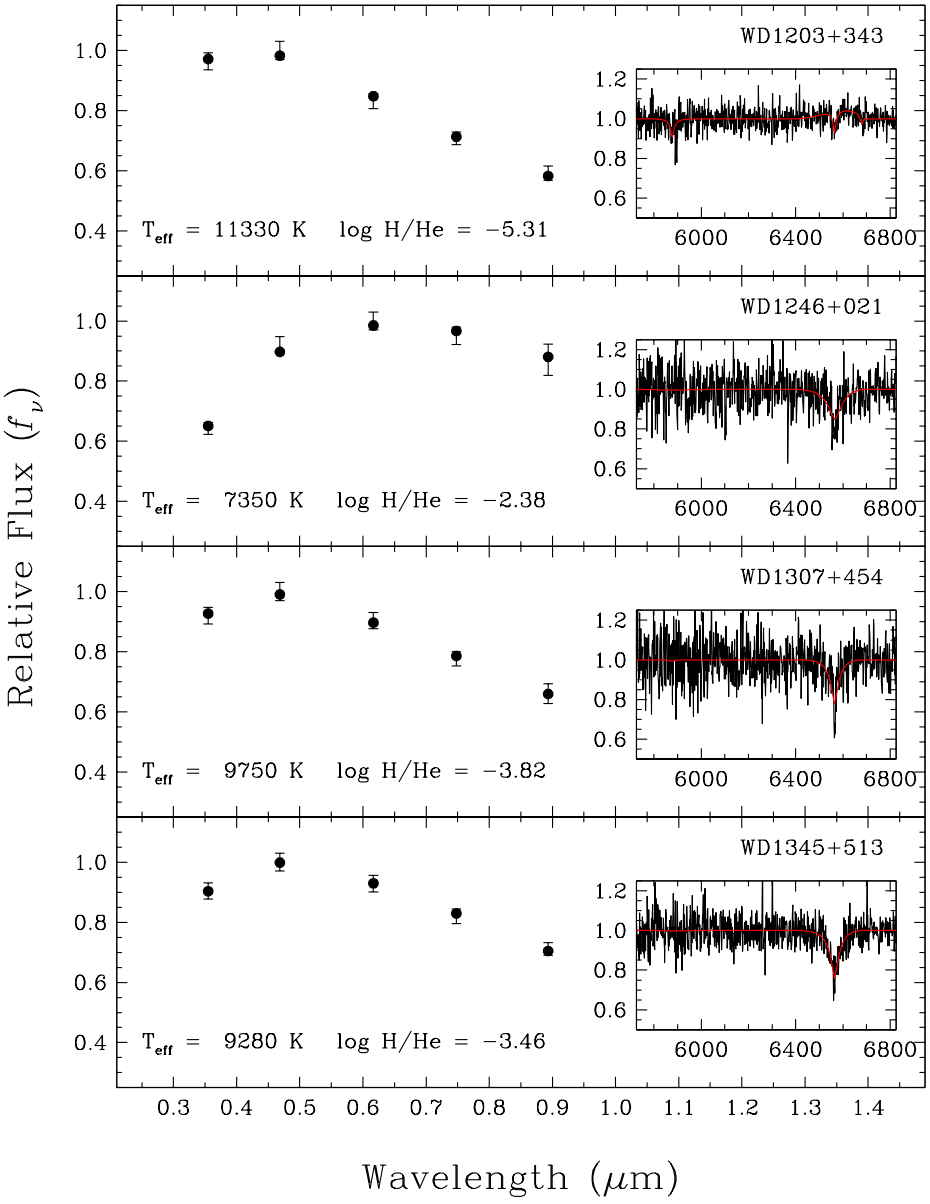

FIGURE A.2 – (Continued)

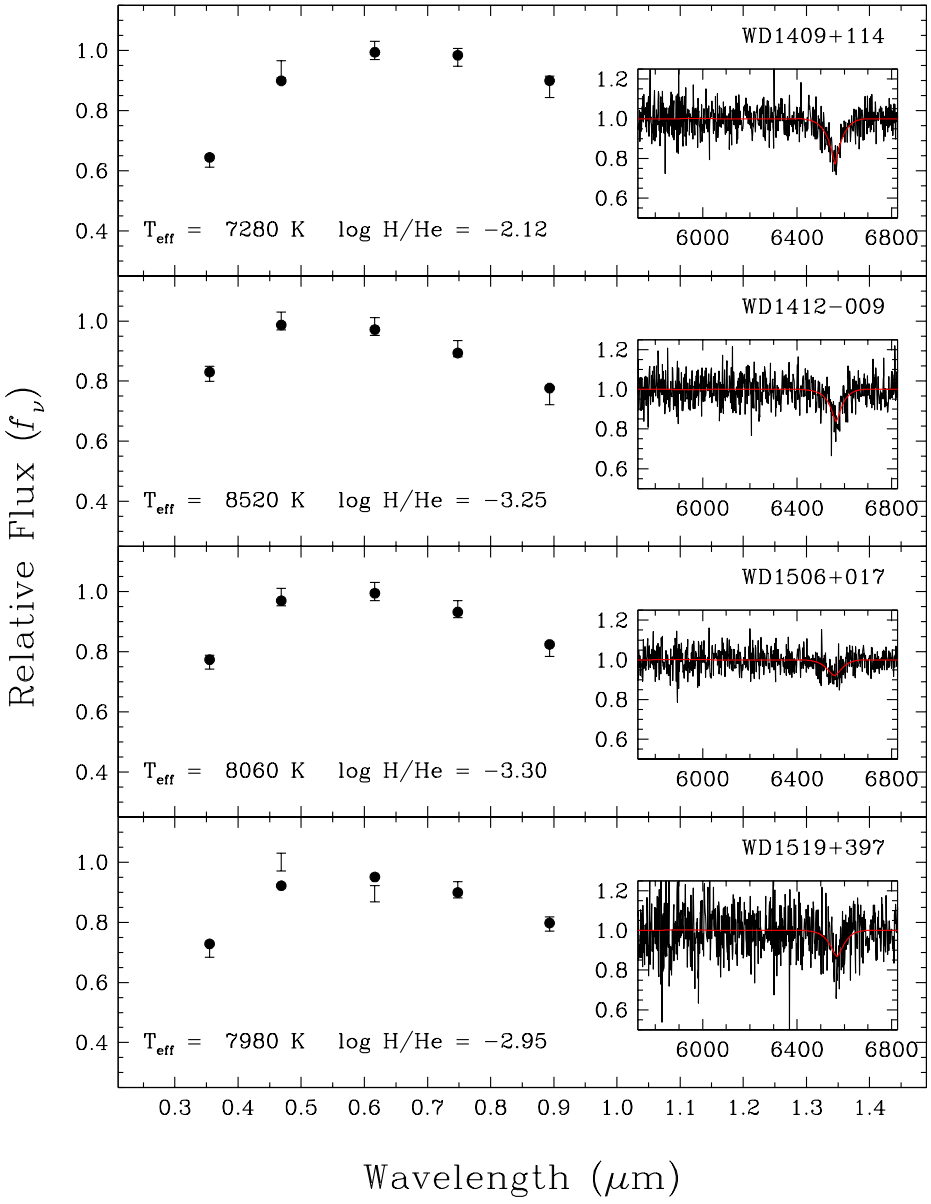

FIGURE A.2 – (Continued)

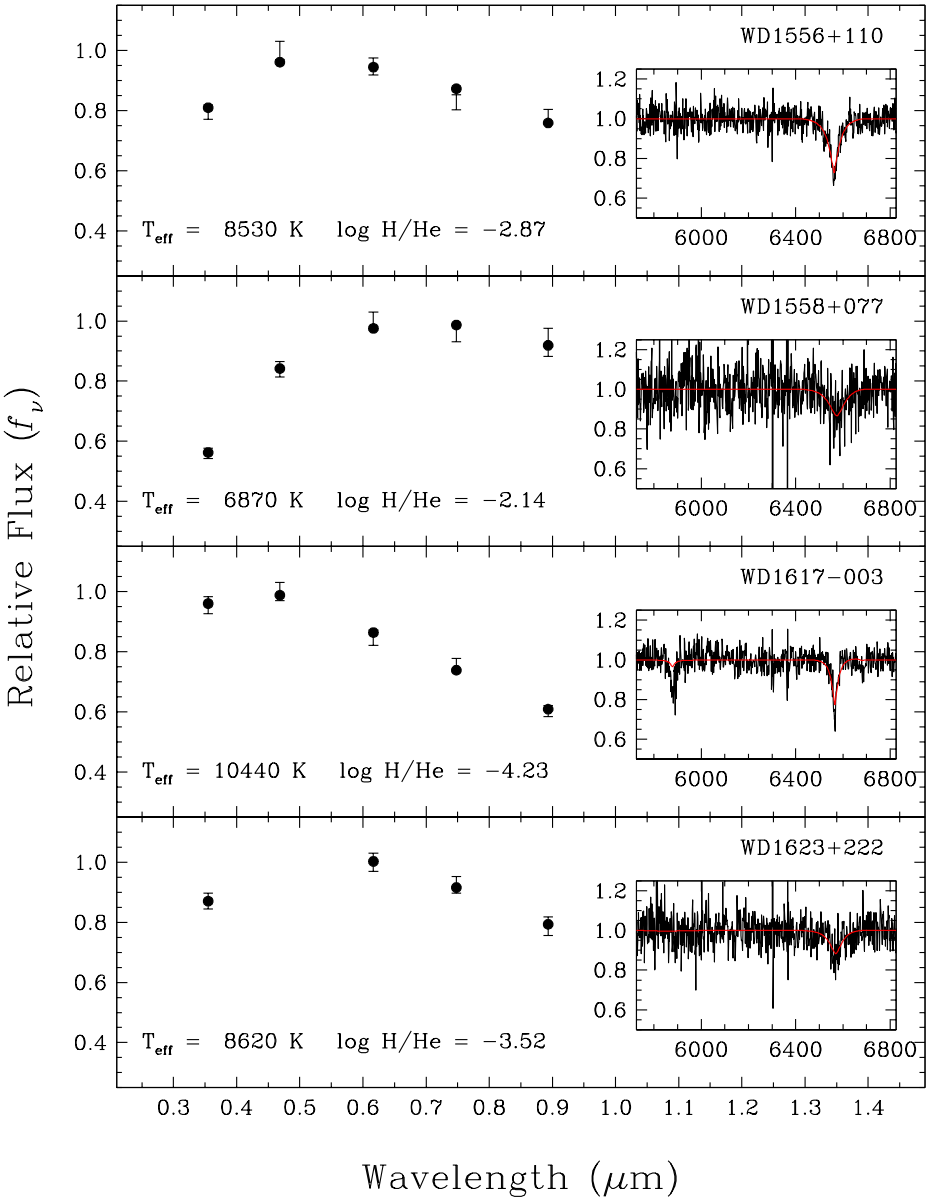

FIGURE A.2 – (Continued)

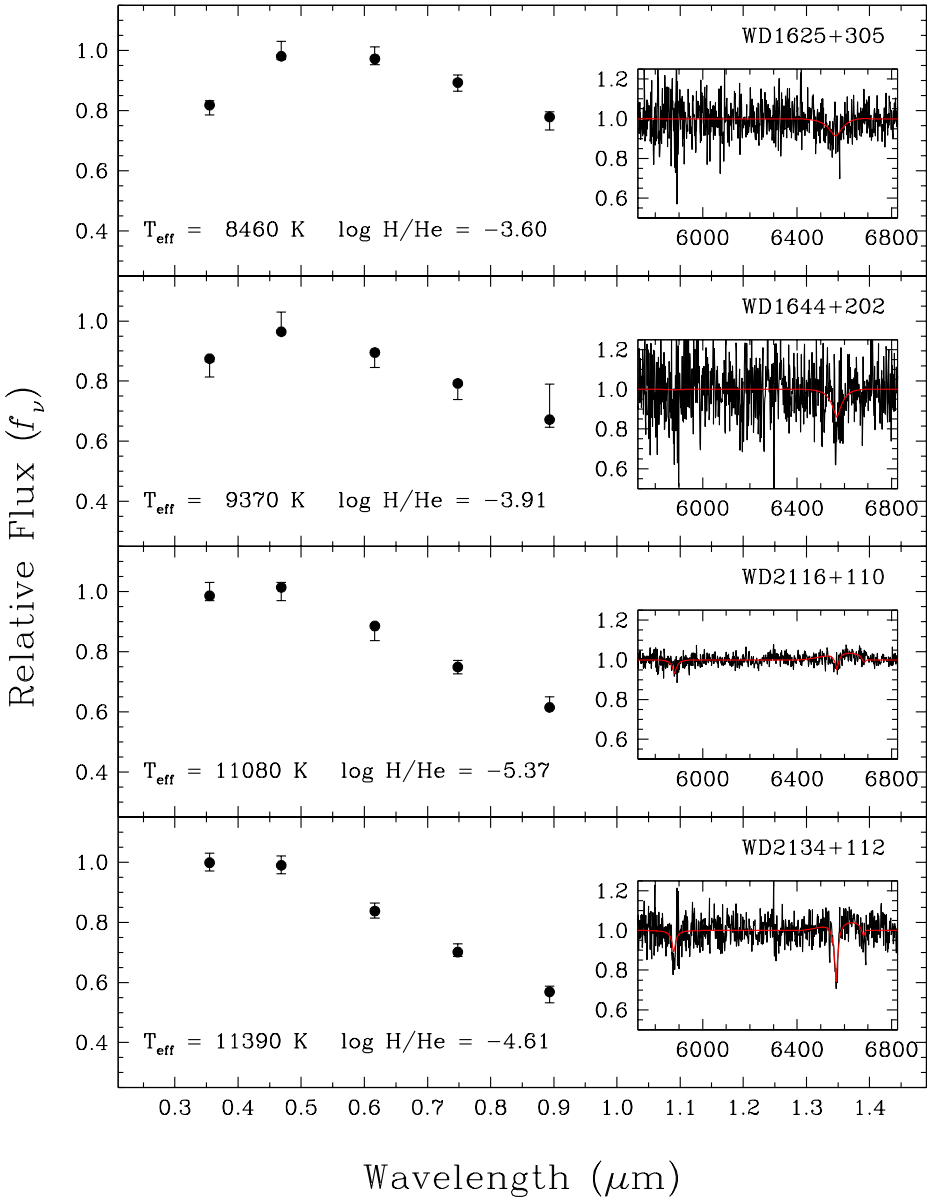

FIGURE A.2 – (Continued)

Annexe B

Calculs Supplémentaires (ML3)

En raison des contraintes d'espace imposées sur les publications dans *The Astrophysical Journal*, certaines figures de l'article présenté au Chapitre 3 sont absentes du corps du texte. Ces dernières seront fort probablement présentées sous format électronique par l'éditeur. À des fins de complétude, nous ajoutons cette annexe le résultat de tous les calculs effectués avec la version ML2/$\alpha = 2.0$ (ou ML3) de la théorie de la longueur de mélange.

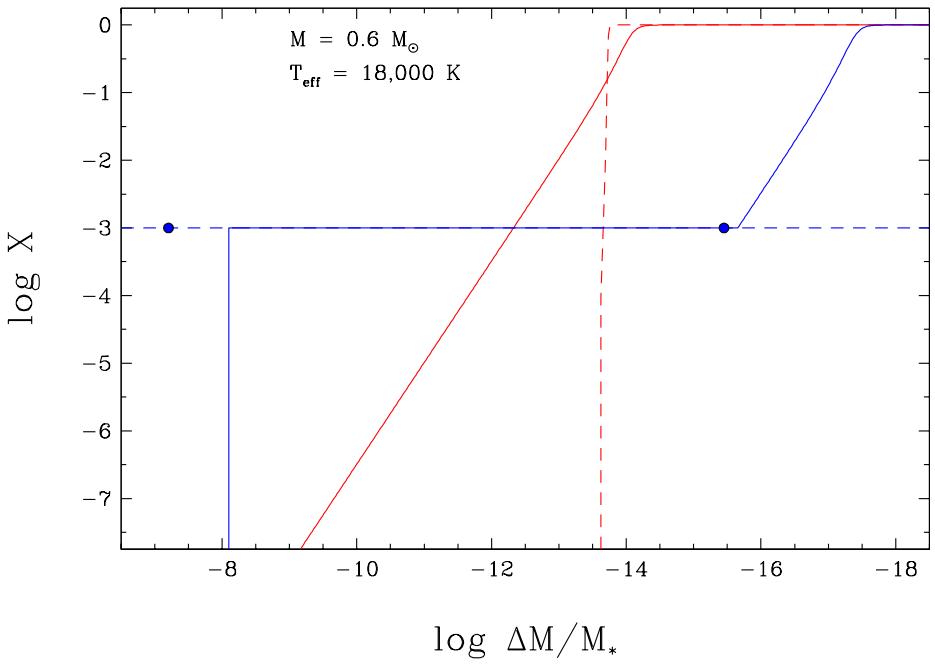

FIGURE B.1 – Hydrogen mass fraction as a function of depth, expressed as the fractional mass above the point of interest with respect to the total mass of the star, for various types of envelope structures at $T_{\rm eff} = 18,000$ K. Chemically stratified ($\log M_{\rm H}/M_\star = -13.77$) and mixed H/He models ($\log X = -3$) are shown in red and blue, respectively. Our approximate seed models (see text) are represented by dashed lines, while our improved structures are shown as solid lines. The extent of the convection zone in the seed mixed model is indicated with blue dots. All models have been calculated with the ML2/$\alpha = 2.0$ parameterization of the mixing-length theory.

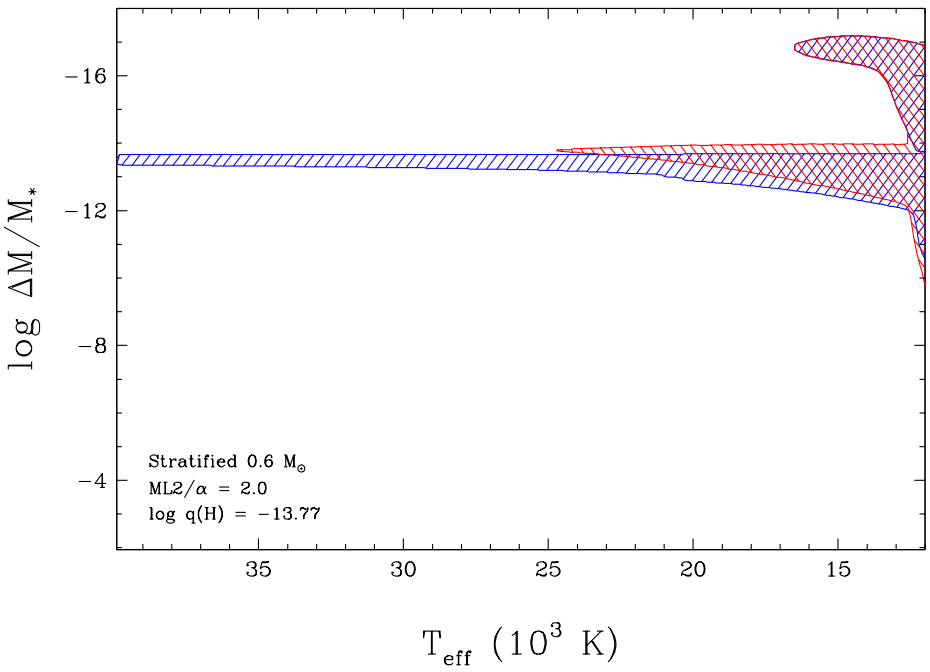

FIGURE B.2 – Examples of envelope structures for a 0.6 $M_{\odot}$ white dwarf with chemically stratified compositions. The extent of the convection zones are shown by the hatched regions. The models shown in blue correspond to the original calculations presented in RBF18, while those in red are obtained by solving the diffusion equation to compute the equilibrium H/He abundance profile (see also Figure 3.1).

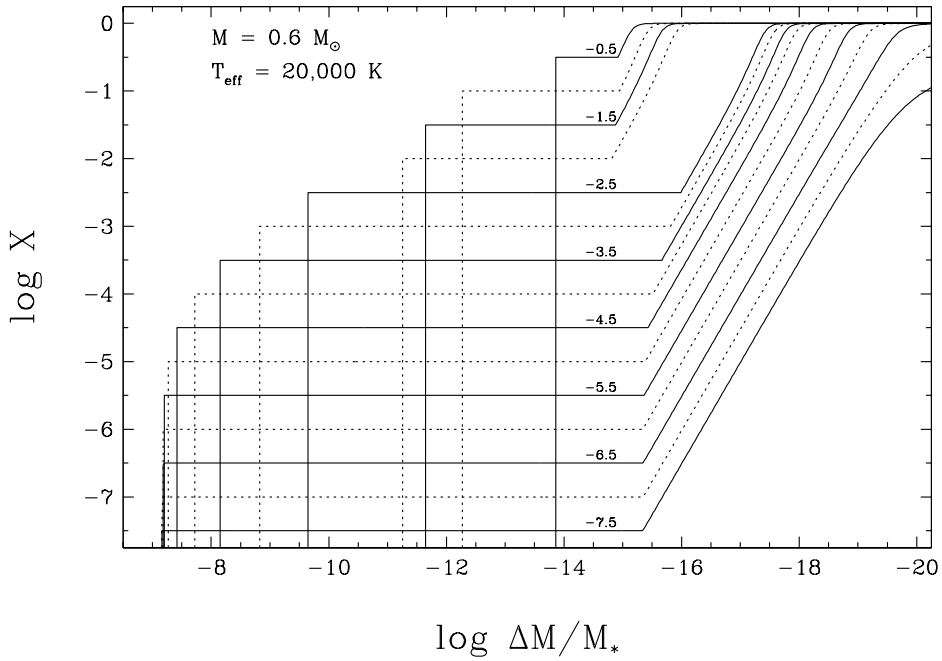

FIGURE B.3 – Hydrogen mass fraction as a function of depth for our new envelope models at 0.6 $M_{\odot}$, $T_{\rm eff} = 20,000$ K, and with various values of the hydrogen mass fraction in the mixed H/He convection zone ($\log X_{\rm cz}$), labeled in the figure.

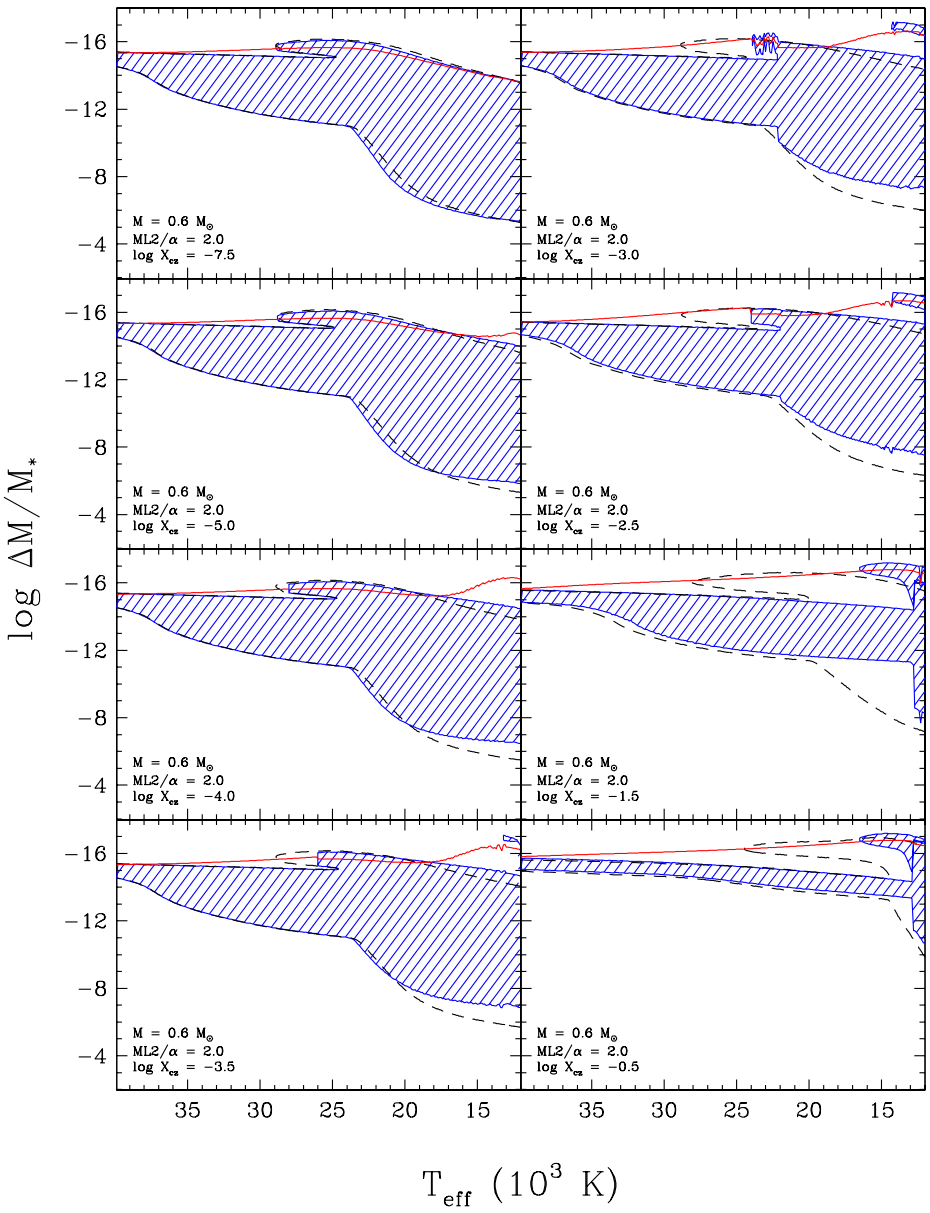

FIGURE B.4 – Examples of our new envelope models for white dwarf models at 0.6 $M_{\odot}$, and with increasing hydrogen mass fraction in the convection zone, $X_{\rm cz}$, from upper left to bottom right. The convection zones are shown by the hatched region, while the red solid line indicates the location of the photosphere. For comparison, the dashed lines indicate the extent of the convection zone for models with a homogeneous abundance profile throughout the stellar envelope.

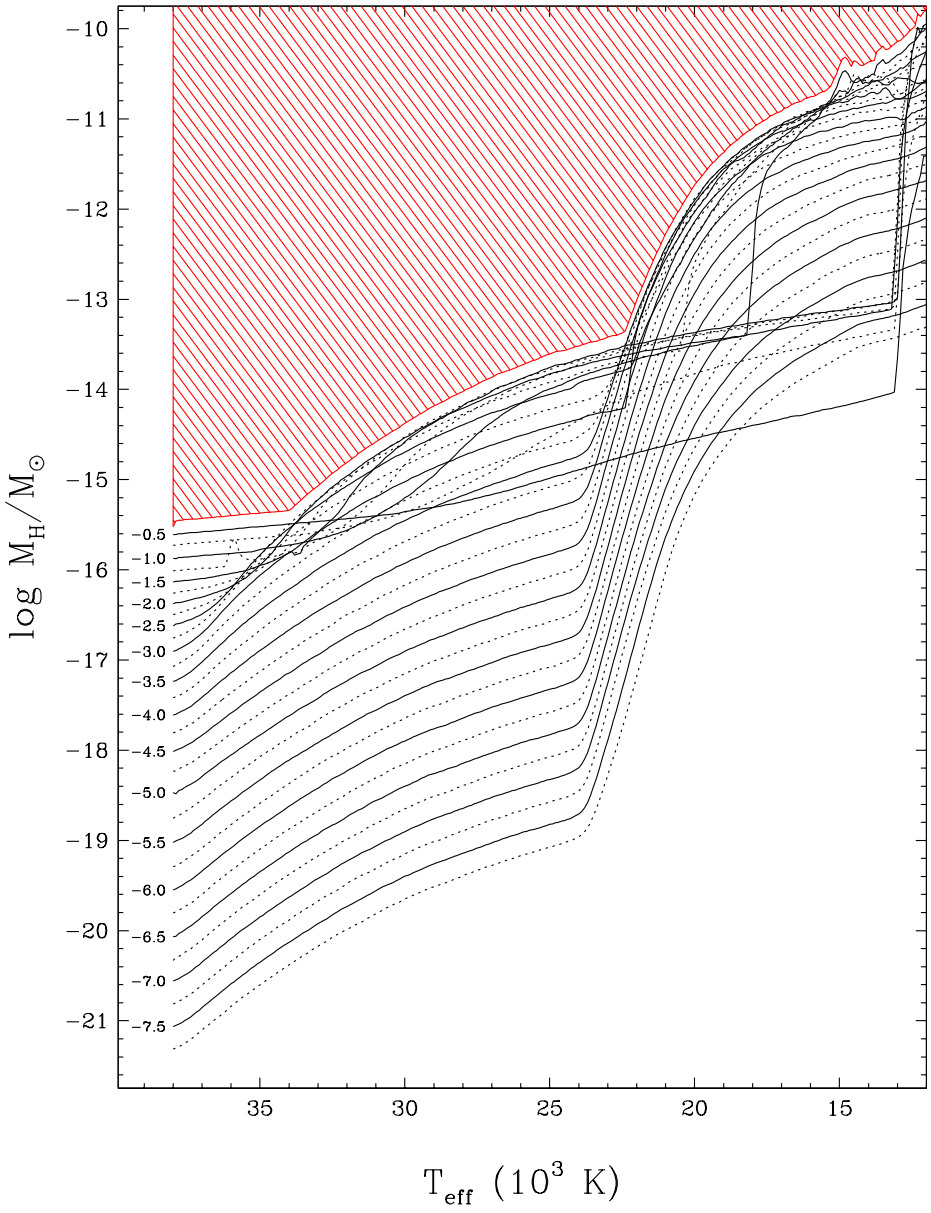

FIGURE B.5 – Total hydrogen mass, $M_{\rm H}$, in our improved envelope models at 0.6 $M_\odot$ as a function of effective temperature, and for various values of the hydrogen mass fraction in the convection zone, $X_{\rm cz}$, labeled on each curve. The region where white dwarfs should appear as DA stars is indicated by the red hatched area.

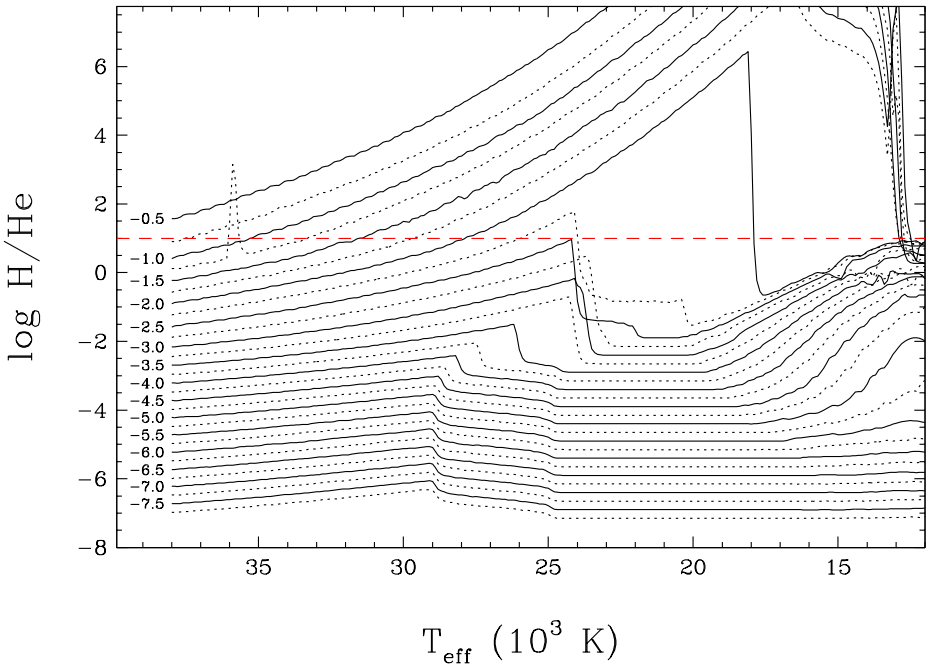

FIGURE B.6 – Hydrogen-to-helium abundance ratio measured at the photosphere ($\tau_R = 2/3$) of our 0.6 $M_\odot$ envelope models as a function of effective temperature. Each curve is labeled by the value of the hydrogen mass fraction in the convection zone, $\log X_{\rm cz}$. The limit above which an object is assumed to appear as a DA white dwarf is indicated by the red dashed line.

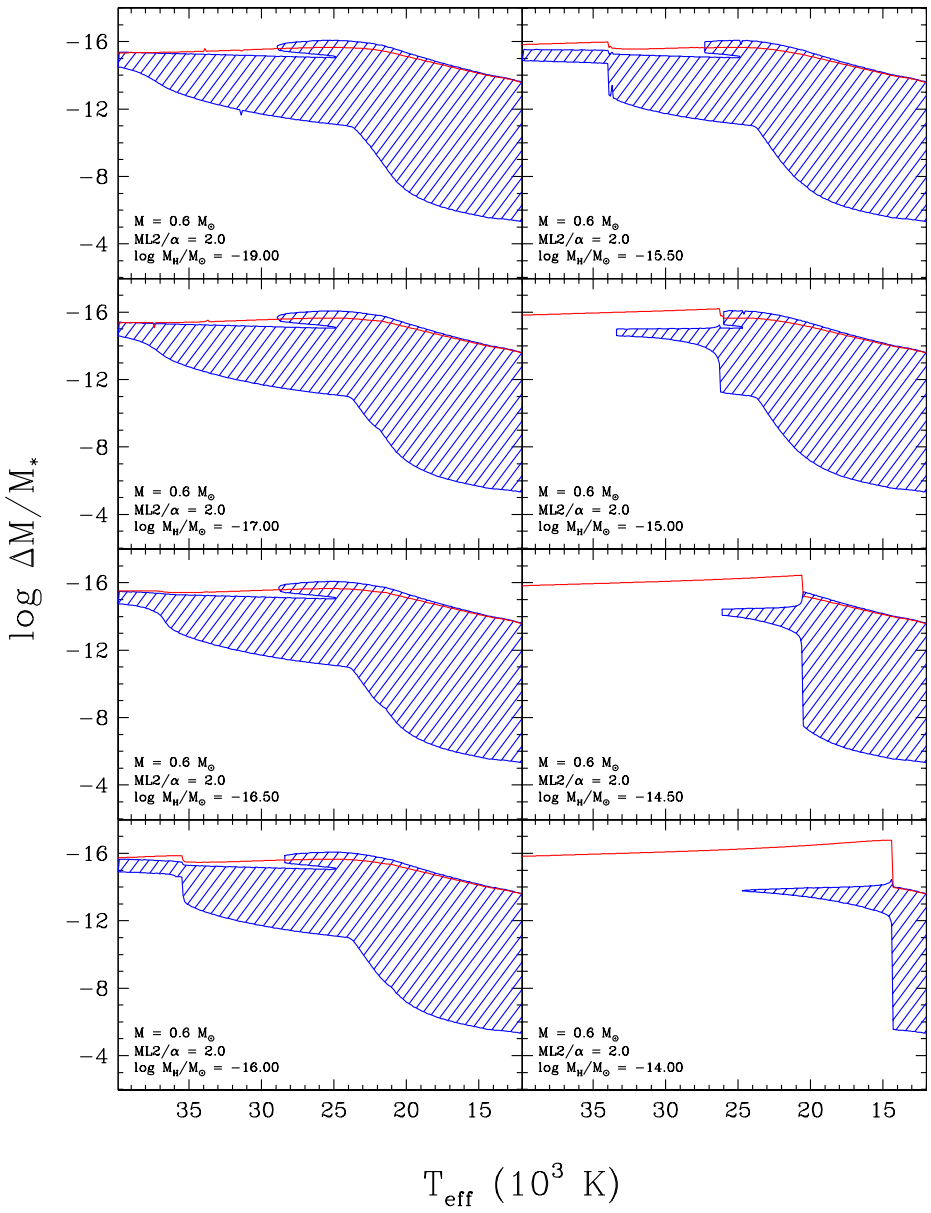

FIGURE B.7 – Examples of envelope structures for white dwarf models subject to a convective dilution process as a function of effective temperature. The depth is expressed as the fractional mass above the point of interest with respect to the total mass of the star. The red solid line corresponds to the location of the photosphere, and the convection zones are shown by the hatched region. The models illustrated here are (from upper left to bottom right) for 0.6 $M_{\odot}$ with increasing total hydrogen mass in the stellar envelope. The results shown here assume a ML2/α = 2.0 parameterization of the convective efficiency.

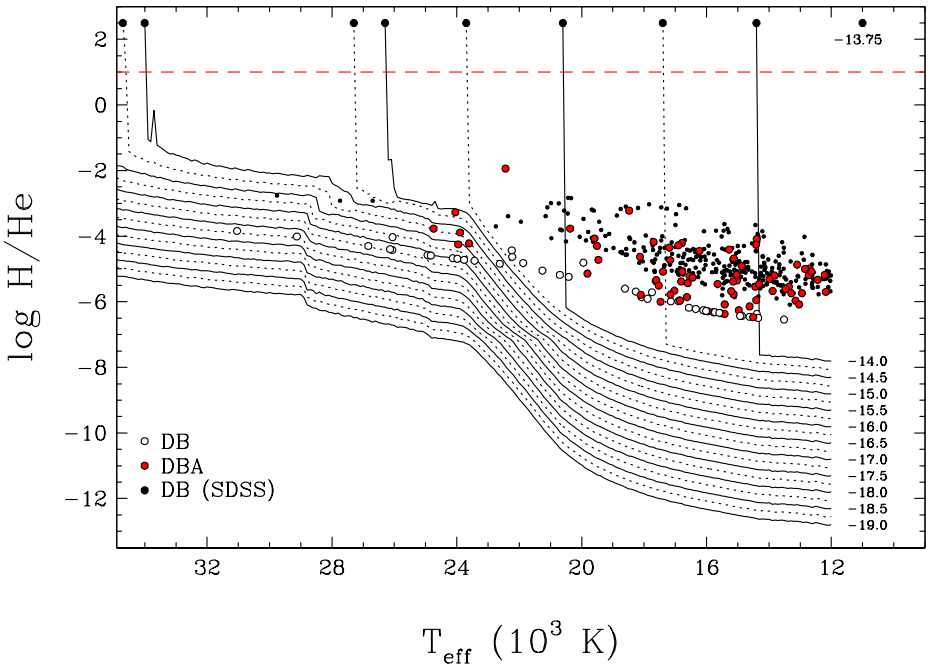

FIGURE B.8 – Results of our convective dilution simulations for models at 0.6 $M_{\odot}$ for the ML2/α = 2.0 version of the mixing-length theory. Each curve is labeled with the corresponding value of $\log M_{\rm H}/M_{\odot}$. The red dashed line indicates our empirical limit above which a white dwarf should appear as a DA star. Observed hydrogen abundances, or limits, for DB and DBA white dwarfs from RBF18 and Koester & Kepler (2015) are also reproduced.

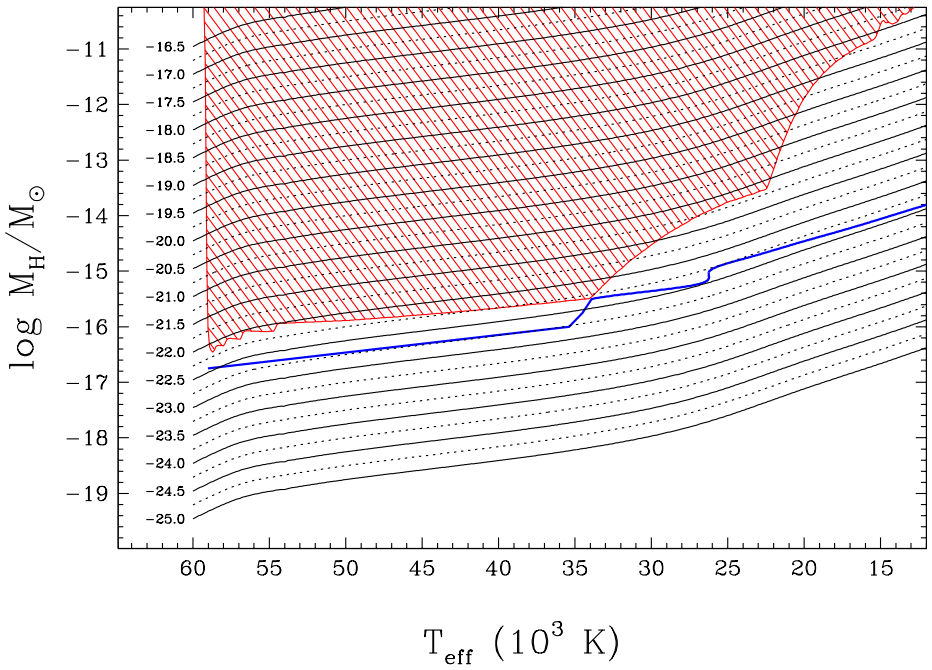

FIGURE B.9 – Total accreted mass of hydrogen onto a 0.6 $M_{\odot}$ pure helium-envelope white dwarf as a function of effective temperature and for various accretion rates. Each curve is labeled with the corresponding accretion rate in solar mass per year (on a logarithmic scale). The red hatched area represents the region where white dwarfs can only appear as chemically stratified DA stars. The hydrogen- to helium-atmosphere transition temperatures (see Table 3.1) is indicated by the blue line.

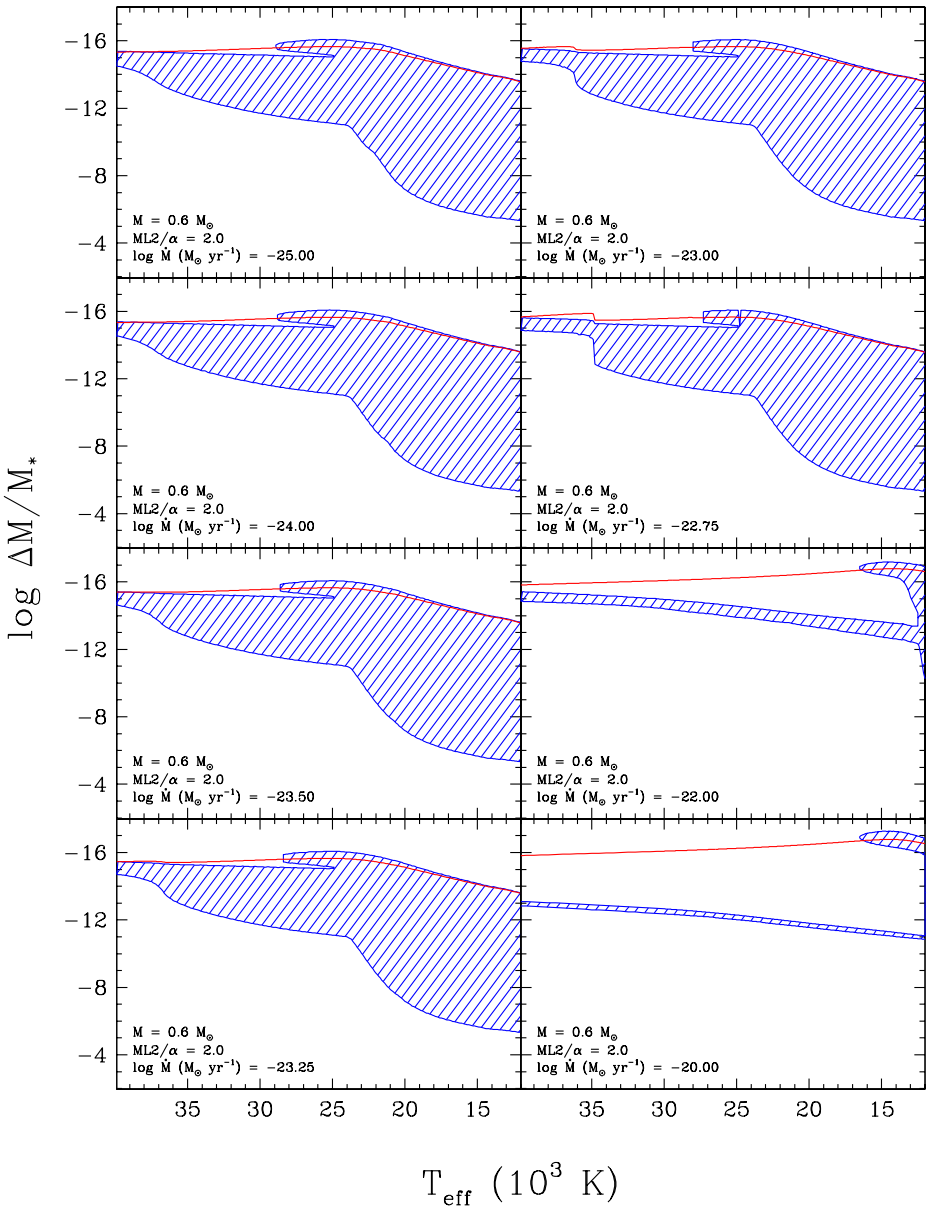

FIGURE B.10 – Examples of envelope structures for white dwarf models subject to a convective dilution process, similar to those shown in Figure B.8, but by also taking into account accretion from external sources of hydrogen. The models illustrated here are (from upper left to bottom right) for 0.6 $M_{\odot}$ with increasing hydrogen accretion rates expressed in solar masses per year.

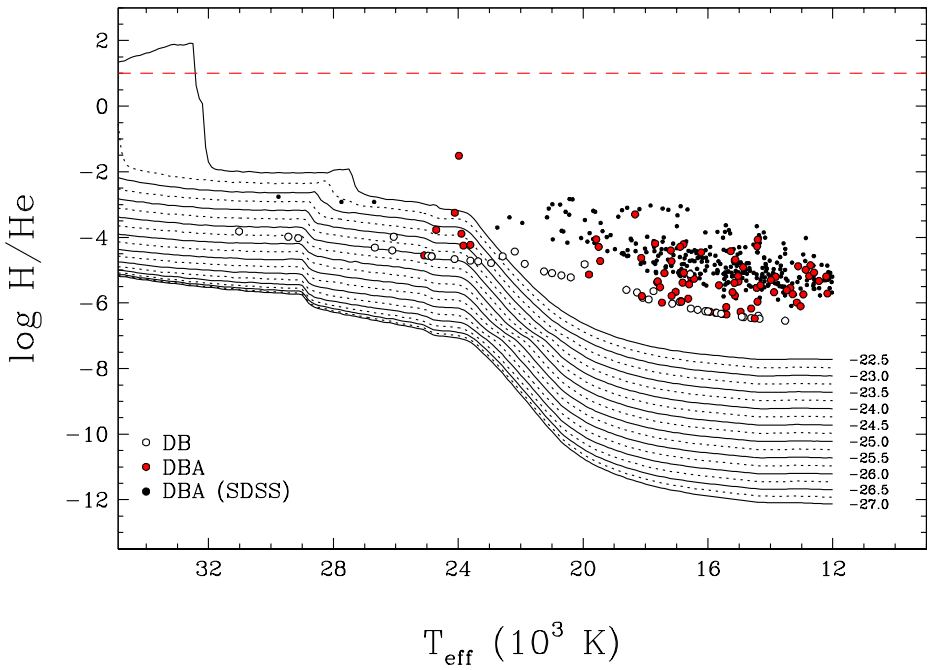

FIGURE B.11 – Same as Figure B.8, but for a 0.6 $M_{\odot}$ pure helium envelope white dwarf subject to accretion. Each curve is labeled with the corresponding accretion rate in solar mass per year (on a logarithmic scale).

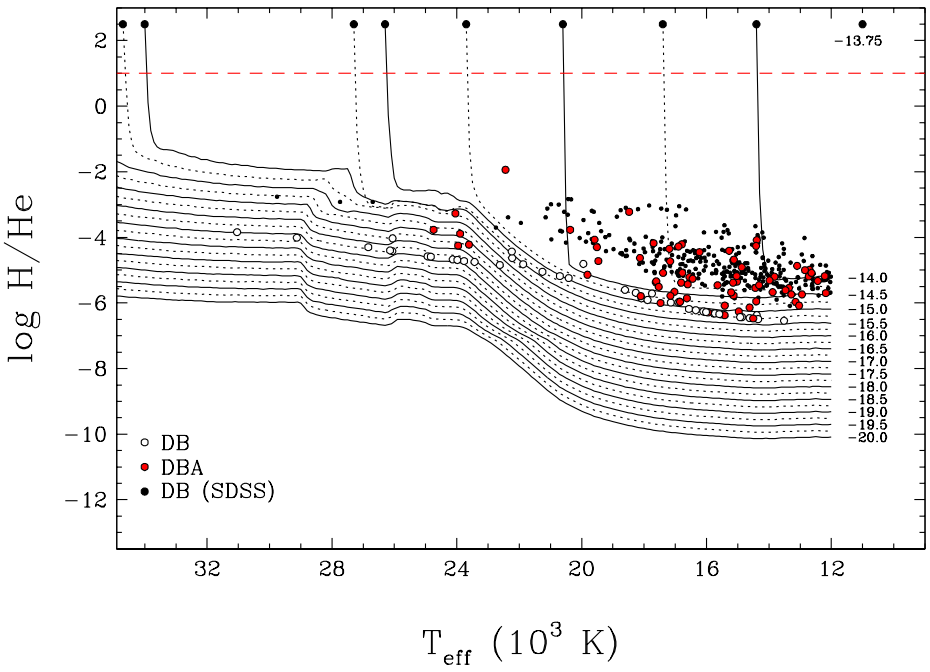

FIGURE B.12 – Same as Figure B.8, but for a 0.6 $M_\odot$ white dwarf undergoing convective dredge-up. Each curve is labeled with the corresponding initial hydrogen mass at the surface in solar mass (on a logarithmic scale).